Czech Technical University in Prague

Faculty of Electrical Engineering

Doctoral Thesis

April, 2024   *Jan Chvojka*

Czech Technical University in Prague

Faculty of Electrical Engineering

Department of Circuit Theory

THE SIGNIFICANCE OF HIGH-FREQUENCY OSCILLATIONS IN UNDERSTANDING ICTOGENESIS AND FUNCTIONAL ORGANIZATION OF EPILEPTOGENIC TISSUE

Doctoral Thesis

Jan Chvojka

Prague, April, 2024

Declaration

I hereby declare that I have written my dissertation thesis independently and consistently quoted the sources.

In Prague, April, 2024

Jan Chvojka

Acknowledgements

I would like to express my sincere gratitude to my co-supervisor, Roman Cmejla, for his valuable cooperation throughout my studies and particularly to my supervisor, Premysl Jiruska, for his deep encouragement, insightful guidance, and innovative research ideas. I am grateful for his unwavering patience and understanding, which were instrumental in the successful completion of my thesis.

I am also deeply indebted to my family for their unconditional love, encouragement, and unwavering support throughout my academic journey. I am particularly grateful to my almost wife Lenka, who was a constant source of inspiration, motivation, and belief in my abilities.

I would also like to acknowledge the stimulating discussions and intellectual contributions of my esteemed colleagues, Jakub Otahal, Jan Kudlacek, Antonin Posusta, David Kala, Jana Nguyen, Bohdana, Erika, Natalie, Monika, and others, whose diverse perspectives and invaluable insights have broadened my horizons and enriched both my non-academic and academic experience. Without their support, I would not have been able to overcome the challenges and frustrations that come with academic pursuits and gain the knowledge and skills necessary for my research.

Abstract

Pathological high-frequency oscillations (HFOs, 60-600 Hz) are cerebral oscillations that occur *de novo* in the epileptic brain. Past studies demonstrated that HFOs provide valuable information to localize the seizure onset zone and epileptogenic tissue, predict the future development of spontaneous seizures, or monitor disease activity. It is hypothesized that elucidation of the cellular and network mechanisms underlying HFO genesis can contribute to a better understanding of the functional organization of the epileptogenic tissues, its reorganization and to better understanding the mechanisms of seizure initiation. The central goal of the thesis was to explore the role of HFOs in seizure genesis and the functional organization of the neocortical epileptic networks. To address these questions, we utilized a range of research techniques ranging from in silico models of ictogenesis to acute seizure models *in vitro*, chronic focal epilepsy models, and human intracranial recordings. Spontaneous cellular and network activity was recorded using electrophysiological techniques from single-electrode to large-scale or multi-channel recording combined with electrical or optical stimulation. Obtained data were analyzed by traditional and advanced signal processing techniques, including semi-automatic detection algorithms, spectral analysis, methods from complex system dynamics, and a wide range of statistical approaches. Analysis of early warning signals of critical transition derived from the interictal HFO revealed a preictal loss of resilience accompanied by an increased sensitivity to perturbations ahead of seizures. The obtained results allowed us to formulate a new hypothesis about seizure genesis through the loss of brain stability and explain the dual role of interictal activity in ictogenesis. Identified dynamical principles of transition to seizure represented a substrate for developing an unsupervised technique estimating the epileptic brain state. Through the analysis of HFOs at the seizure onsets, we disclosed the dichotomy between the primary lesion and the main seizure onset zone in a model of non-lesional temporal lobe epilepsy. In a highly realistic model of neocortical epilepsy, we showed that the neocortex can generate a wide range of HFOs that co-localize with the primary lesion and seizure onset zone. Using optogenetics, we showed that mutated neocortical neurons are an integral part of the network, and their activation can initiate neocortical HFO and seizures. The thesis improved understanding of HFOs and seizure transition mechanisms, presenting diagnostic insights applicable to presurgical epilepsy evaluations. It contributed novel insights into neocortical HFOs and epileptic network organization, valuable for diagnosing and treating drug-resistant focal epilepsies.

Keywords: high-frequency oscillations; epilepsy; focal cortical dysplasia; seizures; dynamical system;

Abstrakt

Patologické vysokofrekvenční oscilace (VFO, 60-600 Hz) jsou mozkové oscilace, které se objevují *de novo* v epileptické tkáni. Předchozí studie prokázaly, že VFO přináší klinicky relevantní informace ohledně lokalizace zóny počátku záchvatu, či epileptogenní zóny. VFO jsou přítomny v časných fázích epilepsie a jejich výskyt předchází rovoji spontánních záchvatů. Zároveň lze VFO využít v monitorování aktivity onemocnění. Předpokládá se, že objasnění buněčných a síťových mechanizmů odpovědných za vznik VFO může zásadně přispět k lepšímu pochopení funkční organizace epileptogenní tkáně, mechanizmům epileptogenní přestavby mozku, či dějům odpovědných za vznik záchvatu. Cílem této práce bylo objasnit úlohu VFO v patofyziologii epilepsie a vzniku záchvatů. Za tímto účelem jsme využili řadu výzkumných technik sahající od počítačového modelování iktogeneze až po akutní modely záchvatů *in vitro*, chronické modely fokální epilepsie a analýzu lidské intrakraniální aktivity. Spontánní elektrická buněčná a síťová aktivita byla zaznamenána pomocí technik jednokanálového či vícekanálového záznamu lokálních potenciálů z mozku, jež byly kombinovány s elektrickou nebo optickou stimulací. Získaná data byla analyzována tradičními i pokročilými technikami zpracování signálů, včetně poloautomatických detekčních algoritmů, spektrální analýzy, metod z oblasti dynamiky složitých systémů a široké škály statistických přístupů. Analýzou časných varovných signálů kritického přechodu, odvozených z vlastností interiktálních VFO, jsme prokázali předzáchvatovou ztrátu resilience mozkové tkáně, jež se manifestovala zvýšenou citlivostí mozku k perturbacím. Získané výsledky nám umožnily formulovat novou hypotézu vzniku epileptických záchvatů, kdy přechod do záchvatu je spojený s postupnou ztrátou stability mozku. Zároveň nám pozorování umožnila vysvětlit duální úlohu interiktální aktivity v iktogenezi. Identifikované dynamické principy přechodu do záchvatu posloužily jako substrát pro vývoj techniky shlukové analýzy odhadující stav epileptického mozku. Analýzou VFO na počátku záchvatů jsme odhalili dichotomii mezi primární lézí a hlavní zónou počátku záchvatu v nelezionálním modelu epilepsie temporálního laloku. V modelu neokortikální epilepsie na podkladě fokální kortikální dysplázie jsme prokázali, že mozková kůra generuje široké spektrum VFO. Tyto VFO mají diagnostickou výpovědní hodnotu, neboť lokalizují primární lézi a zónu počátku záchvatu. Pomocí optogenetických metod jsme prokázali, že mutované neurony ve fokální kortikální dysplázii mohou generovat patologickou epileptiformní aktivitu, včetně VFO. Tato disertační práce přinesla nové poznatky o VFO a jejich úloze v patofyziologii epilepsie a záchvatů a využití VFO v předoperační diagnostice v rámci chirurgické léčby epilepsie. Práce poskytla nové poznatky o buněčných a síťových mechanizmech VFO, které jsou cenné pro diagnostiku a léčbu farmakorezistentních fokálních epilepsií.

Klíčová slova: vysokofrekvenční oscilace; epilepsie; fokální kortikální dysplázie; záchvat; dynamický systém;

List of Abbreviations

4AP 4-amino-piridine.

AMPA alpha-amino-3-hydroxy-5-methyl-4-isoxazolepropionic acid.

ASM anti-seizure medication.

ATP adenosine triphosphate.

CBX carbenoxolone.

CD cortical dysplasia.

d-APV D-2-Amino-5-phosphonovaleric acid.

DB depolarization block.

DC direct-current.

EEG electroencephalogram.

EPSPs excitatory postsynaptic potentials.

EZ epileptogenic zone.

FCD focal cortical dysplasia.

FS fast-spiking.

GABA gamma-aminobutyric acid.

GABAA gamma-aminobutyric acid type A receptor.

HFA high frequency activity.

HFOs high frequency oscillations.

HYP hypersynchronous.

IED interictal epileptiform discharge.

IPSPs inhibitory postsynaptic potentials.

IUE in utero electroporation.

KCC2 K-Cl cotransporter 2.

LVF low-voltage-fast.

NMDA N-methyl-D-aspartate.

pHFOs pathological high frequency oscillations.

PIN pathologically-interconnected neuron.

PTZ pentylenetetrazol.

PV+ parvalbumin positive interneuron.

SE status epilepticus.

SEM standard error of the mean.

sEPSCs spontaneous excitatory postsynaptic currents.

sIPSCs spontaneous inhibitory postsynaptic currents.

SOM+ somatostatin positive interneuron.

SOZ seizure onset zone.

SWRs sharp-wawe ripples.

TLE temporal lobe epilepsy.

TSC tuberous sclerosis complex.

Contents

1   Introduction

1.1   Epilepsy

Epilepsy is a neurological disorder affecting between 0.5 and 1 % of the population worldwide (Mula and Cock, 2015). It is characterized by an enduring predisposition to generate recurrent seizures. Seizures are transient episodes of excessive or hypersynchronous activity of neurons that are associated with a range of symptoms, from brief periods of confusion to violent, life-threatening convulsions (Engel et al., 2008). The symptoms of epilepsy can vary widely from person to person, depending on the type of epilepsy and the location of the brain where the epileptic neurons are located.

Symptoms   A person may experience altered states of consciousness, which can range from confusion lasting only a few seconds to complete loss of awareness. Some people with epilepsy may experience auras, such as visual disturbances, strange smells or tastes, amnesia, or a feeling of déjà vu. Other individuals may experience physical sensations like altered hearing, tingling, dizziness, nausea, staring, and chewing, or may encounter picking at clothing, wandering aimlessly, and other atypical behaviors (Engel et al., 2008; Fisher et al., 2017).

Duration   The length of seizures can vary widely. Some seizures may stop on their own, while others may require medical intervention. In general example, a focal seizure, which originates in a specific area of the brain, or a generalized tonic-clonic seizure, which involves the whole brain, can last from a few seconds to several minutes (Scharfman, 2007). Seizures that last longer than five minutes are referred to as status epilepticus (Trinka et al., 2015) and require immediate medical attention. Prolonged seizures can be dangerous and can lead to severe brain damage.

Disease onset   Epilepsy can occur at any age and can be caused by a variety of factors of genetic or acquired origin (brain injury, infection, ...). Genetic causes of epilepsy can arise from mutations in specific genes, either in the germline or somatic (occurring during embryonic de-

velopment or later in life). These mutations can affect ion channels, neurotransmitter receptors, or other proteins involved in the proper functioning of neurons or their migration or maturation during brain development. On the other hand, epilepsy can also emerge as a result of injury or insult to the brain, such as traumatic brain injury, stroke, brain infection, or tumors. These insults can cause changes in the brain that alter neuronal properties and connectivity between neurons, and epileptogenic tissue reorganization leading to abnormal excitability and spontaneous seizures emergence (Engel et al., 2008).

Adverse effects People with epilepsy may face a range of medical and social challenges, such as the fear about when and where their next seizure will occur, the risk of injury, medication side effects such as memory impairment, drowsiness, depression, psychiatric comorbidities, and social stigma, isolation, and others. Epilepsy can impose limitations on activities such as driving or working in certain professions, leading to social stigma and causing considerable stress and anxiety. Epilepsy is associated with loss of productivity (Baker et al., 1997) and significant direct and indirect health costs (Strzelczyk et al., 2008). With proper management and support, however, many people with epilepsy are able to lead fulfilling lives and achieve good seizure control (Baker et al., 1997; Löscher, 2020; Frauscher et al., 2017).

Treatment Seizures can be controlled in approximately two thirds of people, using currently available anti-seizure medication (ASM) that stabilizes neuronal excitability (Perucca et al., 2008) and prevents high-frequency firing. One third of patients have drug-refractory epilepsy. A small proportion with focal epilepsy can benefit from epilepsy surgery (Sisodiya, 2004; Frauscher et al., 2017); (Fig.1.1). Other available therapies include neurostimulation or ketogenic diet. The candidates for epilepsy surgery need to undergo a meticulous presurgical examination that includes a comprehensive analysis of video-electroencephalogram (EEG), magnetic resonance imaging (MRI), functional imaging (fMRI, PET, SPECT), and neuropsychology testing. The resection margin is delineated based on the synthesis of all measured data in the presurgical evaluation and the whole medical history of the patient (Marusic, 2018). Selected patients need to undergo long-term monitoring with intracranial electrodes to precisely delineate the resection margins. For epileptologists reviewing the presurgical EEG, the signals of interest are usually interictal spikes (IEDs) and high-frequency oscillations (HFOs), which are markers of the presence of epileptic neurons and endogenous epileptogenicity (Jiruska et al., 2017).

The significance of pHFOs HFOs were discovered two decades ago and since their discovery, they attracted the attention of clinical and experimental epileptologists. Oscillations of various frequencies have been observed in both humans and animals and even in both conditions - pathological and physiological. The pathological HFOs (pHFOs) are thought to play a role in

2
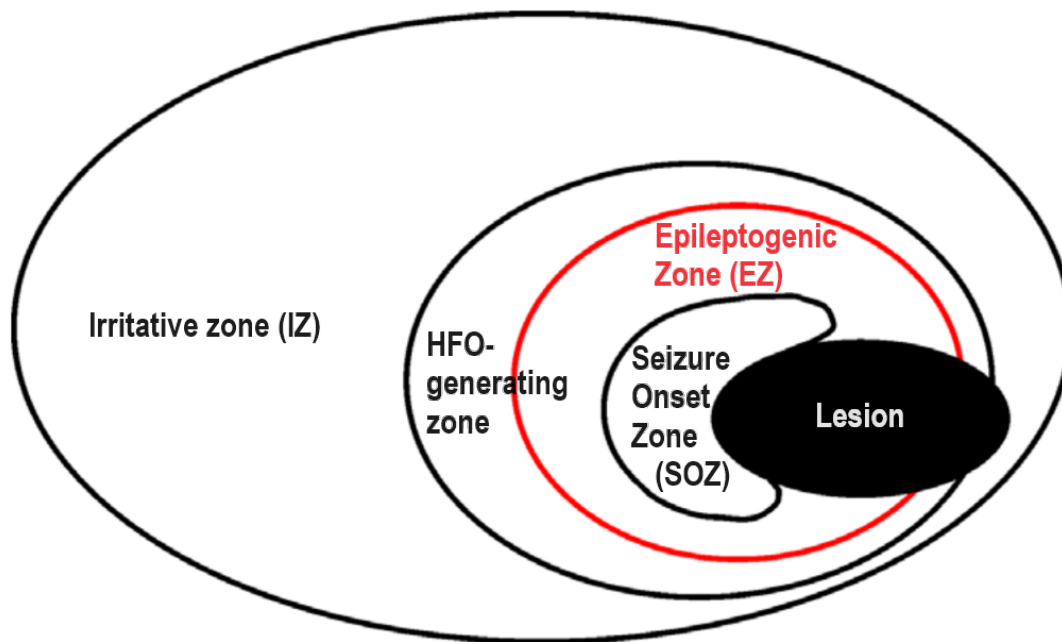
Figure 1.1: The concept of zones in epilepsy. Epileptogenic zone (EZ): The area of the brain that is necessary and sufficient to resect for seizures to disappear. In the Irritative zone, the interictal discharges are generated (image edited with approval of Jiruska, P.)

the initiation and propagation of seizures and mark epileptic tissue while the physiological ones are understood as a correlate of information processing in the brain (Jiruska, 2013). Compared to IEDs, pHFOs are thought to be a more specific biomarker of the seizure onset zone. HFOs mirror disease activity in patients with epilepsy (Zijlmans et al., 2009) and correlate positively with a lesion size (Cserpan et al., 2022). Including HFOs in the resection is associated with better surgical outcomes (Worrell and Gotman, 2011). pHFOs show a tighter link to seizure activity, reflecting disease severity over time in experimental works (Lévesque et al., 2011), and clinical studies (Zijlmans et al., 2009). pHFOs characterize epileptogenic networks in the SOZ (Jacobs et al., 2009; Bragin et al., 1999a) and their frequency is positively correlated with the specificity of detecting epileptogenic and seizure-generating regions (Brázdil et al., 2017). pHFOs serve as biomarkers of epileptogenesis and targets for surgical removal (Zijlmans et al., 2012). These features make HFOs clinically and experimentally attractive. However, the precise cellular and network mechanisms of HFOs remain elusive.

2 High frequency oscillations

2.1 Brain and oscillations

The empirical classification of oscillations into a series of frequency bands (δ, θ, α, β, γ) supported by statistical analysis of EEG spectrum (Lopes da Silva, 2011), has stood the test of time. Indeed, the brain is inherently predisposed to oscillate. Specific brain regions are more prone to generate oscillatory activity than others (Buzsáki, 1989). Various physiological oscillations are electrographic correlates of cognitive mechanisms. The inclination to oscillations is not merely a happenstance but rather a foundational aspect essential for proper brain functioning. A key part of information flow and thinking is orchestrated by synchronization and precisely coordinated neuronal firing rather than by structural anatomical connectivity (Fries, 2015). Across evolution, cerebral oscillations have become adapted to modulate communication and binding of distributed cell assemblies during complex cognitive acts like perception, memory, and motion (Cannon et al., 2014). Disruption of these rhythms compromises cognitive abilities and is associated with cognitive deficit (Buzsáki, 2015).

Oscillations are inherent to brain tissue. In both normal and epileptic tissue, one of the most captivating phenomena is high-frequency oscillations (HFOs). HFOs are transient oscillatory patterns in the EEG signals recorded directly from the brain, with at least four cycles and frequencies over 80 Hz (Zijlmans et al., 2019). Major subtypes include:

OSCILLATION TYPE	FREQUENCY RANGE
gamma oscillations	30-100 Hz
ripples	80-250 Hz
fast ripples	250-500 Hz
very high-frequency oscillations	>500 Hz

Table 2.1: High-frequency oscillation subtypes and their frequency ranges.

The precise frequency ranges of HFOs differ between authors (Jefferys et al., 2012; Zijlmans et al., 2019; Brázdil et al., 2017). However, the ranges should not be defined strictly as the frequencies of adjacent HFOs typically overlap. In the following sections, specific types of

HFOs will be described in detail.

2.2 Gamma oscillations

The brain is not just a passive, stimulus-driven organ. Instead, it actively creates meaning and predictions using top-down processing based on prior knowledge and expectations (Marusic, 2023). For example, when seeing a blurry object, top-down signals from higher-level cortical areas encode prior knowledge and expectations about common objects and can shape processing in early visual cortex to perceive the most likely interpretation even in the presence of noisy or incomplete sensory information. Similarly, when looking at a bistable image (that can be perceived in either of two possible ways), the grouping and synchrony between neurons encoding the image components will rearrange as your perception flips between the two interpretations (Engel et al., 2008).

Gamma oscillations refer to synchronous neural activity in the 30-80 Hz frequency range. They are most prominent in the superficial layers 2/3 of the neocortex and in the hippocampus (Wang, 2010). When attention is directed to a stimulus, gamma-band synchronization increases among neurons encoding that stimulus. This selective coherence enables the interaction between the receiving group and the attended group to be highly effective. Temporal binding refers to the process in which neurons encoding different components of the same object will synchronize their firing in the gamma band. This temporal coordination binds all the distributed neurons representing an object into a unified percept (Engel et al., 2001; Isaacson and Scanziani, 2011; Fries, 2005). The desynchronized activity would not allow distinct networks to "communicate" through shared timing. Gamma oscillations provide a common "language" for neural populations to bind their representations. Nevertheless, this portrayal is too simplistic as in reality rhythms can be even history-dependant (Cannon et al., 2014), exhibit cross-frequency coupling involving other frequency bands such as theta, or even facilitate signal gating and routing based on slightly different frequencies as has been demonstrated in rat auditory cortex (Ainsworth et al., 2011).

At the single neuron level, cortical "chattering cells" can intrinsically generate rhythmic bursting in the gamma band. This fast rhythmic bursting relies on the interplay between voltage-gated sodium channels and potassium channels, rather than slower calcium-dependent mechanisms. However, in most cases, gamma rhythms arise from reciprocally connected excitatory and inhibitory fast-spiking (FS) interneurons. Pyramidal cells provide excitatory drive to FS interneurons, which then rhythmically inhibit the pyramidal cells, constituting a feedback loop

(Isaacson and Scanziani, 2011). Experiments have shown that blocking either excitation or inhibition eliminates gamma oscillations. The frequency of the gamma oscillations is determined by the time constants of AMPA receptor-mediated excitation and GABAa receptor-mediated inhibition. In addition, electrical coupling through gap junctions among FS interneurons further aids their synchronization as shown in transgenic mice, the gamma power has been reduced after knocking out gap junction proteins (Wang, 2010).

2.3   Sharp wave and physiological ripples

Sharp waves are irregular large amplitude field potentials that reflect synchronous bursts of neuronal firing in the mammalian hippocampus. Sharp waves are thought to be initiated in the CA3 region of the hippocampus through recurrent connectivity between CA3 pyramidal neurons but are recorded mainly in the CA1 stratum radiatum (Buzsáki et al., 1983). The emergence of sharp wawes depends on the synchronization of tens of thousands of neurons, making them the most synchronous physiological events in the brain (Buzsáki, 2015; Buzsáki and Chrobak, 1995). Thalamocortical inputs affect the initiation of SWRs, demonstrating the interplay between hippocampal and neocortical activity. The deep depolarizations caused by sharp waves trigger high-frequency bursting of CA1 pyramidal neurons (Ylinen et al., 1995).

Physiological ripples are fast oscillations (200 Hz) riding on sharp waves. They are most prominent in the CA1 region of the hippocampus (Ylinen et al., 1995) and occur mainly during non-rapid eye movement (NREM) and immobile waking states (Buzsáki, 2015). Physiological ripples are involved in the process of forming declarative memory and in the reactivation of memory traces (O'Neill et al., 2006; O'Neill et al., 2010). Sharp waves together with ripples in the hippocampal circuit provide the necessary conditions for synaptic plasticity and memory consolidation by replaying memories formed during wakefulness (Buzsáki, 2015). The loss of the ability to generate these oscillations or the disruption of the mechanisms of their genesis results in cognitive deficits and neurological or psychiatric disorders (Uhlhaas and Singer, 2006). Physiological ripples appear to reflect summated synchronous inhibitory postsynaptic potentials (IPSPs) generated by subsets of interneurons that regulate the discharges of principal cells (Fig.2.1-E); (Ylinen et al., 1995). Pathologically, the same mechanism may be involved in low-amplitude fast activity ictal onset but usually with frequencies lower than ripples (Jiruska, 2013).

2.4 Pathological ripples and fast ripples
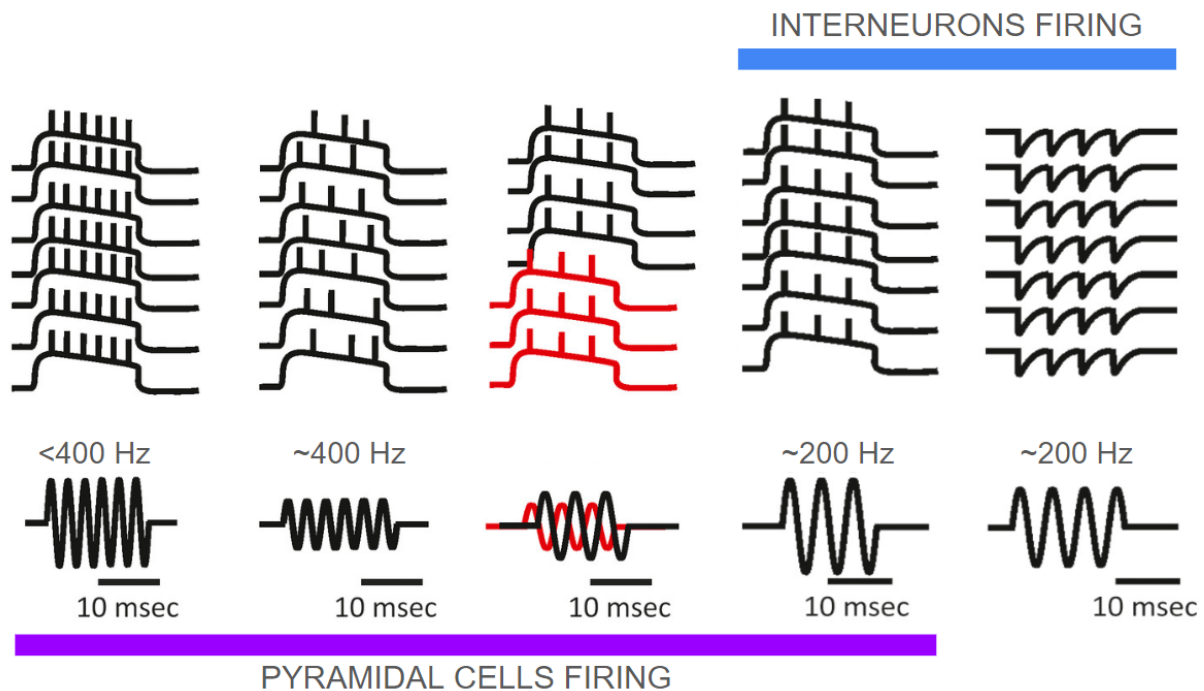
Figure 2.1: HFO mechanisms. A-D: HFOs generated by population spikes of pyramidal cell firing. A, D: Pure oscillations are the most synchronous. B: Asynchronous firing of highly active cells can manifest as ripples or fast ripples, although with lower amplitude. C: Emergent HFOs generated by out-of-phase firing of two or more populations due to various causes (cell loss, various lengths of axons, hub neurons, and local circuits). D: Pathologic ripples generated when interneurons gate action potentials of pyramidal cells. E: Physiological ripples resulting from IPSPs on the membrane of pyramidal cells. Mechanisms D and E depend on intact inhibition, unlike A-C (edited with approval of Jiruska, P.)

The hippocampus and surrounding mesial temporal lobe structures are known to be significant generators of pathological fast ripples and ripples. These structures are often involved in the initiation and propagation of seizures in temporal lobe epilepsy, one of the most common forms of epilepsy in adults. The hippocampus has a well-defined and relatively simple anatomical structure, making it easier to study in experimental conditions, such as *in vitro* electrophysiological or pharmacological studies. Therefore, the majority of knowledge about the mechanisms of HFOs relies on studies focused on these structures (Bragin et al., 1999b; Staba et al., 2002).

A pioneering study demonstrating the existence of pHFOs was focused on epileptogenesis in the kainate model of temporal lobe epilepsy (TLE) (Bragin et al., 1999b). Following the status epilepticus (SE) induced by kainate injection, HFOs within the 100-500 Hz range emerged, but only in the rats that later developed spontaneous seizures (Bragin et al., 2004). A recent study (Naggar et al., 2020) employing 64-electrode array recordings from rat hippocampal slices

demonstrated that ripples induced by perfusing slices with GABAA blockers or kainic acid were dependent on the intact AMPA receptor signaling, unlike NMDA. Gap junctions can increase neuronal firing but surprisingly, do not seem to be the main drivers in HFO synchronization. Also, the study showed CA3c is the main area of ripple generation.

HFOs are thought to be generated by distinct mechanisms involving multiple cell types such as interneurons and principal cells. All the mechanisms, however, share a common requirement - within the population of neurons, a sufficient number of neurons must engage in rapid firing, giving rise to synchronized high-frequency population spikes to be extracellularly recorded as an HFO event. Which cells are responsible for these oscillations?

Pathological 'pure' ripples   When principal cells get synchronized on a millisecond time scale, which can be achieved via fast synaptic transmission (Dzhala and Staley, 2004) or non-synaptic mechanisms like gap-junction coupling (Draguhn et al., 1998), so-called "pure" oscillations emerge (Ibarz et al., 2010); (Fig.2.1-A, D). Specific geometric organization, particularly tight cellular arrangement favors such precise synchronization. Therefore, this mechanism of oscillation is typical for several hippocampal regions and subiculum. Typically, only the pathological ripples are thought to be generated by such mechanism (Ibarz et al., 2010), because the physical properties of principal cells limit their rate of firing to achieve particularly high frequencies. Therefore, it is improbable for fast ripples to be generated by such a mechanism (Jiruska et al., 2017). Besides principal cells, there are FS granule cells capable of firing much faster. Again, it is unlikely for fast ripples to be generated by granule cells. The contribution to the extracellular field by such cells during fast ripple engagement is negligible as was demonstrated in a computer simulation (Fink et al., 2015). Although pathological ripples are not primarily generated by interneuronal firing, there is evidence that interneurons, particularly basket cells are highly involved. In an *in vitro* study employing a high-potassium model of seizures in the hippocampus, a substantial portion of interneurons increased firing during individual cycles of ripple oscillations (Morris et al., 2016). Therefore, pathological ripples seem to be generated by epileptic pyramidal cells controlled by inhibitory postsynaptic potentials of basket cells, regulating the firing of action potentials (Fig.2.1-D). This mechanism is dependent on intact perisomatic inhibition.

Do pathologic 'pure' fast ripples exist?   Research into the precise mechanisms has been limited by recording technology. Unlike interictal spikes, HFOs are low-voltage events. Also, fast ripples are thought to be generated by localized groups of cells on a very small scale, rather than broadly (Bragin et al., 2003). When an epileptic fast ripple is generated in the hippocampus, hundreds to thousands of cells are probably involved, far beyond the resolution provided by modern silicone arrays. Advancements in imaging techniques, such as voltage-sensitive dyes

and calcium imaging, have facilitated recordings from multiple cells concurrently. However, the temporal resolution, particularly concerning fast ripples, remains inadequate for capturing the rapid dynamics (Grewe et al., 2010). Fortunately, *in silico* experiments have been successful in studying ripple and fast ripple mechanisms. It turns out that HFOs may result from random coincidental firing of excited neuronal population (Fig.2.1-B). HFOs can be simply viewed as an emergent phenomenon of active networks. Using the same computational framework, it was shown that oscillations >250 Hz can not be generated by applying noisy IPSP output to principal cells (Fig.2.1-E). Interestingly, noise input applied to interneurons achieved higher frequencies. Although it was possible to elicit rhythms with fast ripple frequencies, such rhythms exhibited very low amplitude. The same was true for action potentials. Action potential waveforms were present but contributed very little to the local field potentials, due to basket cells' small size (Fink et al., 2015). Furthermore, pathological HFOs including fast ripples can be generated even in the absence of any network connectivity. HFOs may simply represent a marker of highly activated neurons, regardless of the underlying structure or mechanism (Stacey et al., 2009; Gliske et al., 2017). This finding is very important because it has the fewest assumptions and the experimental evidence, while not directly proving it, at least does not contradict it. For example, in low-calcium or high-potassium models of seizures *in vitro*, the coincidental firing of the cells can manifest as high-frequency activity in the ripple band (Jiruska et al., 2010). Also, the observation of simultaneous ripple activity with occasional fast ripples is a realistic consideration, as well as its relationship with epileptic spikes, which, on the other hand, are thought to represent electrographic correlation during the most synchronous state of the underlying network (Buzsáki, 2015). Regarding the frequency, the simulations in the study (Gliske et al., 2017) were conducted under a base firing frequency of 200 Hz, a rather conservative estimate of the maximum frequency of pyramidal cells as demonstrated by unit recordings in other studies. Juxtacellular recordings from stratum pyramidale of the CA1 region revealed a neuronal firing at 360 Hz (Ibarz et al., 2010) while in the subiculum, frequencies up to 250 Hz were reported (Alvarado-Rojas et al., 2015). The higher the frequency, however, the lower the amplitude of such oscillation, eventually it falls behind the noise floor. In conclusion, this mechanism is capable of safely explaining all the pathologic ripples and at least a part of the oscillations from the fast ripple band. Addressing pathologic fast ripples, it has been shown that FS GABAergic interneurons could also contribute (Cepeda et al., 2020) but the prevailing stance is that there are no 'pure' pathologic fast ripples.

Pathologic 'emergent' fast ripples When large groups of hyperexcitable, hyper synchronized pyramidal cells start to fire out of phase, 'emergent' oscillations are born (Foffani et al., 2007; Ibarz et al., 2010; Jiruska et al., 2017); (Fig.2.1-C). Out-of-phase firing between two neuronal populations manifests extracellularly in doubling of the frequency, as each of the two population oscillates at a lower frequency. This mechanism can explain fast ripple oscillations even of very high frequencies, previously unexplainable due to the physical constraints behind the

generation of action potential. Theoretically, the frequency limitations are not in place if we incorporate more than two cell populations. Rather two populations firing out of phase are currently thought of as realistic (Jiruska et al., 2017). The reasons why the two populations split may be asymmetric excitatory input due to various lengths of axons, various morphologic changes such as disrupted axonal sprouting, the presence of hub neurons or cell loss, and consequent weakened electrical coupling (Jiruska et al., 2017). Observations from temporal lobe epilepsy, where the rate of fast ripples in the hippocampus correlates positively with the severity of cell loss support this hypothesis (Staba et al., 2007). Computer simulation indicates that loss of interneurons favors fast ripple emergence. Precisely, the model demonstrated, that as more basket cell connections onto pyramidal cells were lost, the same input that had previously generated only sharp wave-ripple events began to produce fast ripples (Fink et al., 2015). Several computational and experimental studies indicate that fast ripples can emerge in the absence of fast inhibition (Jiruska et al., 2017). For example, after the injection of tetanus toxin - which blocks neurotransmitter release responsible for fast inhibition - the hippocampus was still able to generate fast ripples in a model of temporal lobe epilepsy (Ferecskó et al., 2015).

Relationship with seizures

Across different etiologies in patients with intractable focal epilepsy, DC shifts were observed prior to pHFOs. The DC shifts might be indicative of an altered ionic environment, particularly increased extracellular K+ levels, which can result from both neuronal and glial dysfunction. This altered ionic environment, potentially initiated by glial depolarization and impaired homeostasis, is proposed to create conditions conducive to the emergence of pHFOs (Kanazawa et al., 2015).

The ictal core - penumbra theory states, that the core occupies only a portion of the area in which ictal EEG waveforms are present while the "penumbra" is rapidly expanding surrounding area in which inhibitory currents try to restrict pyramidal cell firing. In this concept, the high gamma oscillations (80–150 Hz) mark the ictal core (Weiss et al., 2015) because the penumbra is not sufficiently synchronized to generate a high gamma signature.

pHFOs were observed in the context of hypersynchronous (HYP) onset seizures (Lévesque et al., 2012). HYP onset seizures are most common in limbic structures (Li et al., 2019). In an experimental study using pilocarpine-treated epileptic mice, pHFOs recorded in the dentate gyrus are generated by hypersynchronized action potentials of principal cells in the absence of basket cells firing (Bragin et al., 2011).

More specifically, the pHFOs are generated by pathologically interconnected neuron (PIN)

clusters. PIN clusters are hypothesized to generate pathological synchronous bursts of population spikes, recorded as ripples (80-200 Hz) and fast ripples (200-800 Hz). Fast ripples reflect out-of-phase firing of distinct clusters consisting primarily of excitatory principal cells. In the epileptic brain, after an initial insult, PIN clusters could form and through a kindling process, lead to widespread PIN clusters generating increasing HFO activity until seizures occur (Santana-Gomez et al., 2022). A transient reduction in inhibition causes the PIN clusters to increase in size and consolidate, leading to increased synchronization of the pHFOs. As the pHFOs become more synchronized and reach a critical mass, they can propagate as the hypersynchronous discharges characteristic of HYP seizure onsets. However, the role of inhibition in HYP onsets was not always clear. The current view is that a transient decrease, rather than increase, in inhibition onto the pHFO-generating PIN clusters may initiate HYP seizures, contrasting with the previous belief (Li et al., 2019).

Conclusion The above described studies provided insights into the candidate mechanisms of HFOs, relying on highly synchronized gap junction networks, desynchronous groups of cells, or even weakly synchronized cells. The results from human tissue (Alvarado-Rojas et al., 2015; Staba et al., 2007; Curot et al., 2023; Lévesque et al., 2012) support the localized nature (Curot et al., 2023) of fast ripples as well as the predictions from *in vitro* and computational models and favor rather the heterogeneous firing theory. Taken together, the most likely mechanisms explaining pathological fast ripples (of particularly high frequencies) are those depicted in (Fig.2.1-B, C).

From the clinical standpoint, despite their great successes, HFOs should not be the sole factor in determining the SOZ. Pathological and physiological HFO bands overlap. To date, there has been no reliable feature discovered that distinguishes any of the underlying conditions. The removal of all HFO-generating regions does not guarantee seizure freedom (Höller et al., 2015; Weiss et al., 2023).

Furthermore, it was demonstrated that physiological HFOs can transform into pathological HFOs under conditions of decreased inhibition, increased gap junction coupling, formation of recurrent synapses, and increased synaptic activity (Stacey et al., 2009; Stacey et al., 2011). These observations suggest that HFO frequency is inadequate in distinguishing the pathological or physiological nature of HOFs. Therefore, the use of spike-informed (Guth et al., 2021; Cai et al., 2021) HFOs or other feature combinations (such as ictal phase-locked high gamma) (Weiss et al., 2015) has recently gained attention as a means to obtain a more accurate biomarker for identifying epileptic tissue.

2.5 Neocortical physiological HFOs

Ripples The pioneering work (Grenier et al., 2001), relying on local field potential recordings and intracellular recordings in cats, showed physiological ripples in the neocortex emerge during the depolarizing phase of the slow oscillation. Fast-rhythmic-bursting and FS neurons showed the highest firing rates in synchrony with recorded ripples. Ripples could be generated independently in other structures, demonstrated by recordings from isolated cortical slabs, suggesting that intracortical networks alone are sufficient for their generation. The study suggests the most likely mechanisms are similar to the mechanisms observed in hippocampal ripples (Fig.2.1-D). The neocortical findings were observed under ketamine-xylazine anesthesia and in chronic experiments during natural sleep-wake cycles, suggesting the observed effects are attributable to low-level mechanisms independent of anesthetic agents or natural sleep states. In a clinical study on mixed pathologies, anesthesia, however, significantly affected the HFO properties (Weiss et al., 2021).

Fast ripples Fast ripples can be generated in the neocortex, in various regions like occipital, temporal, and frontal cortices during the visual memory task. According to intracranial recordings from 12 patients (Kucewicz et al., 2014), fast ripples seem to arise from the transient synchronized firing of neuronal populations in local circuits, with interneuron-pyramidal cell interactions. They may share similar neuronal networks and mechanisms as ripples. Interneurons firing before pyramidal cells in a specific phase relationship could coordinate the fast oscillations, similar to ripples. Apart from the neocortex, such oscillations were recorded simultaneously in limbic areas, indicating fast synchronization across distant areas (Kucewicz et al., 2014). Compared to physiological ripples, which are frequent in the eloquent cortex, physiological fast ripples recorded mainly from the occipital area were found very rarely in intracerebral stereoencephalographic recordings from humans (Frauscher et al., 2018).

2.6 Neocortical pathological HFOs

The neocortex is also capable of generating pathological HFOs. In a mouse model of hippocampal sclerosis induced by a kainate injection, pathological fast ripples originating in the neocortex - a remote region from the epileptic focus - were observed, while the neocortex itself was not epileptogenic. The authors suggest the slow oscillations originating from the hippocampus propagate to the frontal cortex and increase the likelihood of rapid firing, favoring the generation of fast ripples in the frontal cortex (Sheybani et al., 2019).

It is well known that neocortical slow oscillations (Steriade et al., 1993) coordinate activity across the neocortex, entorhinal cortex, subiculum, and hippocampus shortly after the down state of slow-wave sleep (Sirota et al., 2003; Sirota and Buzsáki, 2005). However, here the authors study hippocampal ripples and not the neocortical fast oscillations. Unfortunately, there is a minimum of studies focused on pathological neocortical HFOs as the research was hindered by the lack of relevant animal models of neocortical epilepsy. The knowledge about HFO mechanisms obtained from TLE models cannot be automatically applied to the pathophysiology of neocortical epilepsy and neocortical HFOs (Jiruska, 2013). In this section, we will explore the HFOs generated in the neocortex based on studies focusing on neocortical focal epilepsy.

Using intracellular recordings from cats during electrically stimulated seizures, it was demonstrated that pathological ripples have higher amplitude than physiological ones, and the mechanism is dependent on electrical coupling (Grenier et al., 2003). The vicious feedback loop in which very fast synchronous action potentials help generate and synchronize action potentials in adjacent neurons was formed through electrical interactions.

In focal neocortical epilepsy induced by tetanus toxin injection into the motor cortex (Louis et al., 1990), rats showed the emergence of pathological ripples (70-160 Hz) (Wykes et al., 2012). The study investigated layer 5 pyramidal cells, a type of neuron readily identifiable and accessible for manipulation. The cells exhibited increased excitability, which was demonstrated by increased resting membrane potential and the ability to exhibit rebound repetitive firing. The pathologies were partially counteracted by overexpression of the Kv1.1 potassium channel and optogenetic inhibition of the pyramidal cells (Wykes et al., 2012). The tetanus toxin model exhibits EEG features similar to those seen in chronic human focal neocortical epilepsy.

The recordings from awake, behaving mice induced with neocortical freezing lesions and acute cortical local field potential recordings from microelectrode arrays in anesthetized mice, suggest that inhibitory cells in the deep supragranular layer may play a role in generating pathological fast ripples (Williams and Sun, 2019). In the upper cortical layers of the malformed cortex, HFOs (300-800 Hz) phase-locked to the spike component were observed. However, the strongest spike coherence of isolated single units was found in the deeper supragranular and granular layers, specifically for fast ripple frequencies suggesting interneurons may be the driving substrate for ripple wave generation near the lesion. This challenges the traditional view of glutamatergic excitation as the sole driving force (Williams and Sun, 2019). In the follow-up study employing the same animal model, they described the excitation/inhibition balance in cortical regions proximal or distal to the lesion. The study found the onset of hyperexcitable burst is located not in the lesion but in the distal areas located in layer 2/3. The hyperexcitability was presumably caused by aberrant input from layer 5 and was controllable by enhancing dendritic

inputs from somatostatin interneurons using optogenetic stimulation. The perisomatic inhibition from PV+ interneurons, however, was not effective in suppressing the hypersynchronous bursts (Yang et al., 2020).

The tetanus toxin and freezing lesion models are considered as sub-optimal, but still useful. Fortunately, there is an increasing number of experimental studies employing much more realistic animal models, and also functional studies employing human tissue samples. Besides the lack of certain human-specific developmental events (e.g., cortical expansion and gyrification) - an obvious limitation of rodent models - there are several other shortcomings such as unspecificity in brain regions and cell types being affected, unsatisfactory electrophysiology correlate, or even premature death (Meikle et al., 2007; Uhlmann et al., 2002; Magri et al., 2011; White et al., 2020). Genetically induced models are thought to be the most advanced. Mutations in genes regulating mTORC1 signaling pathway (MTOR, RHEB, PIK3CA, PTEN, TSC1, TSC2, DEPDC5, NPRL2,3, and many others); (Perucca et al., 2020), lead to enhanced mTORC1 signaling and were shown to be underlying genetic cause of FCD type II. In transgenic models, the malformation across the cortex and other brain regions is usually diffuse and lacks focal localization (Kassai et al., 2014; Meikle et al., 2007). This unspecificity is partially addressed by animal models based on IUE. IUE models offer higher seizure frequency and longer life span (Hsieh et al., 2016; Lim et al., 2015).

In a mouse study (Breton et al., 2021), the deletion of the Wwox gene led to neocortical hyperexcitability, likely through imbalanced excitation/inhibition, along with hypomyelination, which could contribute but may not directly cause epilepsy. The neocortical circuitry turned hyperexcitable, manifested by seizures and HFO bursts, while the hippocampus maintained normal levels of excitability. The gene knockout probably affected the development of GABAergic interneurons and altered the expression of certain ion channels or receptors in pyramidal neurons. These changes manifested *in vitro* by decreased strength and frequency of IPSCs and increased presence of miniature excitatory postsynaptic currents (mEPSCs) and spontaneous excitatory postsynaptic currents (sEPSCs). This favors the classical excitatory-inhibitory imbalance theory. In addition, pharmacological manipulation of glutamatergic transmission using d-APV and CBX revealed that excitatory currents are likely mediated by NMDA receptors and the role of gap junctions in synchronizing the network activity (Breton et al., 2021).

There is evidence that GABAergic FS PV+ interneurons, play an important role in the generation of pHFOs in the neocortex. Modulation of GABA activity of such cells could have a surprisingly positive impact on patients. Besides mechanisms such as depolarizing GABA signaling, a pacemaker GABA activity and consequent synchronization of pyramidal cell firing was found to be crucial across different pathologies. The work by (Cepeda et al., 2020)

searched for differences between HFO generating and HFO silent tissue using patch-clamp recordings. The most interesting finding was that regardless of the different pathology (FCD I and II, TSC and non-CD cases), the GABA signaling of FS interneurons was significantly increased in HFO-generating tissue. Excitatory signaling did not differ between the sites, but there was a decrease in input resistance of pyramidal cells which might suggest an increased density of gap-junctions, enhancing the HFO synchronization (Cepeda et al., 2020).

The results are in line with previous studies, as HFO-generating areas in cortical tissue from pediatric epilepsy surgery patients correlated with increased spontaneous GABA synaptic activity (Cepeda et al., 2014). (Blauwblomme et al., 2019) found, that in slices from pediatric cortical dysplasia tissue with altered chloride cotransporter expression, GABA neurotransmission can depolarize pyramidal neurons and underlie spontaneous interictal discharges.

Other cellular and network abnormalities that would favor HFO genesis in the neocortex arise from the studies that explored neocortical icotgenesis. In the neocortex, seizures commonly originate through (low-voltage fast) LVF onset. LVF seizure onset refers to the gradual increase in activity above the beta range. The role of inhibition in LVF onsets is described as increased inhibitory interneuron activity preceding the LVF onset, which may be an initial protective reaction that then leads to rebound excitation and the LVF seizure pattern.

PV+ FS cells are critical in generating fast network oscillations like gamma, theta, and ripples in the neocortex. Their fast signaling properties arising from specialized molecular, structural, and electrophysiological adaptations allow them to provide temporally precise inhibition of pyramidal cells (Tremblay et al., 2016).

In the context of neocortical seizures, PV+ fast-spiking interneurons (and not SOM+ cells) are a major source of the inhibitory barrages that oppose ictal discharge propagation in 4AP or low Mg^{2+} model of seizures *in vitro* (Cammarota et al., 2013; Gnatkovsky et al., 2008) and also in acute pilocarpine-induced neocortical seizures *in vivo* (Magloire et al., 2019). The activity of PV+ cells might switch to pro-ictal through depolarizing GABA (Magloire et al., 2019).

Patch-clamp recordings from surgically resected cortical tissue samples of human subjects with FCD support disinhibition theory. The spontaneous EPSCs and IPSCs of FS interneurons were significantly reduced in the seizure onset zone (SOZ) compared to the non-SOZ group (Cheng et al., 2022). This suggests impaired excitatory and inhibitory synaptic inputs onto interneurons in the SOZ. For pyramidal cells, the sEPSCs were significantly increased while the sIPSCs were significantly reduced in the SOZ compared to non-SOZ groups. This indicates increased excitation and decreased inhibition of pyramidal cells in the SOZ. The density of PV+

interneurons was significantly lower in the SOZ compared to non-SOZ, with disrupted laminar organization. The dysfunction of fast-spiking PV+ interneurons leads to the disinhibition of pyramidal cells during the interictal period (Cheng et al., 2022). Higher involvement of PV+ interneurons in seizure onset and pre-onset seizure activity were also proved experimentally using optogenetics (Sohal et al., 2009; Shiri et al., 2016)

The current evidence suggests, that interplay between PV+ fast-spiking cells and pyramidal cells in the area of layer 2/3 and layer 5 are the most likely key components in the mechanisms underlying the generation of neocortical epileptiform phenomena, including HFOs (Breton et al., 2021; Yang et al., 2020; Cepeda et al., 2020). However, the cellular mechanisms, particularly with respect to fast ripples, are unclear and probably heterogeneous. Because fast ripples correlate with high GABA synaptic activity (Cepeda et al., 2020) which also play a role in neocortical seizures (Magloire et al., 2019) and IEDs (Blauwblomme et al., 2019), depolarizing GABA could play a role also in the mechanisms of fast ripples. Neocortical epilepsy and neocortical oscillations represent a challenge for future experimental epilepsy research, which will undoubtedly bring further insights into understanding the functional organization and dynamics of neocortical epileptic networks and mechanisms of neocortical seizure generation (Schevon et al., 2009).

2.7   Objectives

The central objective of this work was to investigate the complex role of HFOs in epilepsy, clarify the mechanisms behind HFOs, and provide experimental observations that could improve the diagnosis and treatment of epilepsy.

Objective 1 *Describe the HFO features in a highly realistic model of neocortical epilepsy due to focal cortical dysplasia type II.* Here, we investigated the role of gamma ripples and fast ripples as a biomarker of epileptogenic neocortical tissue. By employing a highly realistic mouse model of FCD type II, the research not only broadens our understanding of HFO mechanisms but also provides valuable insights into the clinical applications of HFOs in localizing epileptic lesions with higher specificity (Chvojka et al., 2024b). During the experimental work, we developed new hardware for the IUE to induce FCD (Prochazkova et al., 2024).

Objective 2 *Determine the impact of anti-seizure medication on physiological HFOs.* In this study, we examined the impact of two anti-seizure drugs on sharp-wave ripples, a common

physiological oscillation. This study not only contributed to our understanding of the drug effects but also suggested a novel and elegant method to distinguish between physiological and pathological HFOs, a pivotal unresolved question in epileptology (Kudlacek et al., 2017).

Objective 3 *Provide insights into the mechanisms responsible for pre-ictal changes in HFOs.* Using multiple experimental techniques and an interdisciplinary approach, we explored the intricate relationship between high-frequency activity and the loss of neuronal network resilience preceding seizures via a mechanism called critical slowing. By linking HFOs to dynamical stability and the ictogenic nature of interictal perturbations, the research contributed significantly to our understanding of seizure initiation. The implications extend beyond HFOs, offering insights into the broader dynamics of neuronal networks and their resilience (Chang et al., 2018). Understanding the nature of epileptic dynamical states allowed us to provide an explanation of the multifaceted role of interictal discharges in ictogenesis (Chvojka et al., 2021). Obtained results also allowed us to implement advanced computational techniques to perform unsupervised classification of dynamical states of the epileptic brain (Dallmer-Zerbe et al., 2023). The analysis of resilience in long-term recordings revealed that the loss resilience also precedes the onset of seizure clusters. In the following study, we explored the mechanisms that may be responsible for seizure clustering (Kudlacek et al., 2021). We have demonstrated that the nature of seizure represents a key factor that shapes the intra-cluster seizure profile, cluster termination, and duration of the subsequent period between clusters.

Objective 4 *Define spatial properties of hypersynchronous seizure onset in the model of temporal lobe epilepsy.* In this study, we described in detail the spatial features of hypersynchronous seizure onset with superimposed HFOs in the model of non-lesional temporal lobe epilepsy (Chvojka et al., 2024a). Through the analysis of seizure onsets, we have demonstrated a dichotomy between primary epileptogenic lesion and major seizure onset zones that point to the complex network organization of temporal lobe epilepsy networks.

3 Mouse model of focal cortical dysplasia type II generates a wide spectrum of high-frequency EEG activities

3.1 The contribution toward the progress of the field

The study provides several novel information.

Experimental model For the first time, it describes both spiking and oscillatory interictal activity in a mouse model of neocortical epilepsy in great detail. This is significant because theories about HFO mechanisms are mainly based on research on the hippocampus, and findings on temporal lobe epilepsy may not apply to the neocortex. Before, it was uncertain whether the neocortex could generate fast ripple HFOs, with only a few studies showing the ability to generate gamma or ripple band HFOs (Chvojka et al., 2024b).

Clinical confirmation This study enhances the clinical application of HFOs in neocortical epilepsies. The robustness of this argument is strengthened by the utilization of a highly realistic mouse animal model. In this study, we have examined key features and aspects of the FCD model, including disrupted cortical lamination, the presence of dysmorphic neurons, the presence of HFOs, and the occurrence of spontaneous seizures, which closely mirror the clinical manifestation of FCD-related epilepsy. We provide a compelling experimental basis for HFO utilization as an important diagnostic tool in this complex neurological condition.

The clinical application of HFOs is hampered by the presence of physiological HFOs that share frequency ranges with pathological HFOs. In this study, we focused on HFOs superimposed on IEDs and reported morphological differences between IEDs and HFOs in seizing and seizure-free groups. This additional context is important in the clinical utilization of HFOs. As the lag analysis of IED clusters revealed, a subpopulation of IEDs (and HFOs) originated in the

lesion and spread out of the lesion to the interconnected cortical areas of both hemispheres. Another subpopulation originated outside the lesion and propagated to the lesion. Animals that developed spontaneous seizures demonstrated the highest proportions of bi-hemispheric interplay. The callosal connections, which are the connections between the left and right hemispheres of the brain, may play a crucial role in the propagation of IEDs between the hemispheres.

HFO properties We demonstrated that our experimental FCD type II model generates a wide spectrum of HFOs that are able to localize the lesion with a higher specificity than traditional electrographic markers. Both gamma-ripples and fast ripples turned out to be superior to inter-ictal discharges in FCD lesion localization. Gamma-ripple power is particularly well correlated to the epileptogenicity of animals. The lowest power and incidence were found in non-seizing FCD animals, with higher power for non-seizing FCD animals while the seizing FCD animals exhibited the highest gamma-ripple power and rate. We not only analyzed spontaneous HFOs from chronic recordings but also aimed to elucidate the role of mutated neurons in the disease. Optogenetic stimulation of mutated neurons showed that they represent an active component of the FCD network, capable of recruiting other interconnected neurons and collectively generating IEDs with HFOs.

3.2   The author's contributions

The author was responsible for the experimental part of the project and data collection. The author was subsequently responsible for data recording and management, the experimental design, and the entire analysis of EEG recordings. The applied analytical approaches included visual labeling of artifact-free EEG periods, the pipeline for automated data processing, and statistical analysis. The author implemented a more advanced technique for the automated detection of HFOs. The author was involved in the literature review and manuscript preparation. The author presented the work at international conferences (EEC Geneva 2022, IEC Dublin 2023).
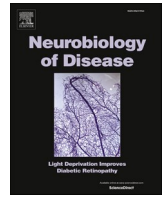
3.3   Compliance with the thesis objectives

The study is a core part of this thesis and complies with the thesis objectives in all aspects.

Mouse model of focal cortical dysplasia type II generates a wide spectrum of high-frequency activities

Jan Chvojka [a,b,1], Natalie Prochazkova [a,1], Monika Rehorova [a], Jan Kudlacek [a], Salome Kylarova [a], Michaela Kralikova [a], Peter Buran [c], Romana Weissova [c], Martin Balastik [c], John G.R. Jefferys [a], Ondrej Novak [a,2], Premysl Jiruska [a,*,2]

[a] Department of Physiology, Second Faculty of Medicine, Charles University, Prague, Czech Republic
[b] Department of Circuit Theory, Faculty of Electrical Engineering, Czech Technical University in Prague, Prague, Czech Republic
[c] Laboratory of Molecular Neurobiology, Institute of Physiology of the Czech Academy of Sciences, Prague, Czech Republic

ARTICLE INFO

ABSTRACT

High-frequency oscillations (HFOs) represent an electrographic biomarker of endogenous epileptogenicity and seizure-generating tissue that proved clinically useful in presurgical planning and delineating the resection area. In the neocortex, the clinical observations on HFOs are not sufficiently supported by experimental studies stemming from a lack of realistic neocortical epilepsy models that could provide an explanation of the pathophysiological substrates of neocortical HFOs. In this study, we explored pathological epileptiform network phenomena, particularly HFOs, in a highly realistic murine model of neocortical epilepsy due to focal cortical dysplasia (FCD) type II. FCD was induced in mice by the expression of the human pathogenic mTOR gene mutation during embryonic stages of brain development. Electrographic recordings from multiple cortical regions in freely moving animals with FCD and epilepsy demonstrated that the FCD lesion generates HFOs from all frequency ranges, i.e., gamma, ripples, and fast ripples up to 800 Hz. Gamma-ripples were recorded almost exclusively in FCD animals, while fast ripples occurred in controls as well, although at a lower rate. Gamma-ripple activity is particularly valuable for localizing the FCD lesion, surpassing the utility of fast ripples that were also observed in control animals, although at significantly lower rates. Propagating HFOs occurred outside the FCD, and the contralateral cortex also generated HFOs independently of the FCD, pointing to a wider FCD network dysfunction. Optogenetic activation of neurons carrying mTOR mutation and expressing Channelrhodopsin-2 evoked fast ripple oscillations that displayed spectral and morphological profiles analogous to spontaneous oscillations. This study brings experimental evidence that FCD type II generates pathological HFOs across all frequency bands and provides information about the spatiotemporal properties of each HFO subtype in FCD. The study shows that mutated neurons represent a functionally interconnected and active component of the FCD network, as they can induce interictal epileptiform phenomena and HFOs.

1. Introduction

The discovery of high-frequency oscillations (HFOs) and research into their cellular and network mechanisms substantially contributed to understanding of the organization of epileptogenic tissue and how pathological epileptic activity is generated (Bragin et al., 1999; Jefferys et al., 2012; Jiruska et al., 2017; Staba et al., 2002). Seminal experimental and clinical studies demonstrated a close relationship between HFOs and epileptogenic tissue, which led to HFOs being considered as an electrographic biomarker of seizure onset zone and epileptogenic zone (Bragin et al., 2002; Bragin et al., 2004; Bragin et al., 2000; Staba et al., 2002). In early studies, the clinical significance of HFOs was demonstrated in animal models and in patients with temporal lobe epilepsy (TLE). Later studies explored the clinical significance of

HFOs in localizing seizure onset zone and epileptogenic tissue in cases of neocortical epilepsy (Jacobs et al., 2009). Retrospective studies (Frauscher et al., 2017) and subsequent meta-analysis (Höller et al., 2015) demonstrated the benefits of resecting HFO-generating tissue for good surgical outcomes.

In TLE, experimental and clinical studies were mutually supportive and contributed to a better understanding of mechanistic, functional, and clinical characteristics of the HFOs (Jefferys et al., 2012; Jiruska et al., 2017). The interpretation of HFOs in neocortical epilepsy substantially lags behind TLE studies primarily due to the absence of clinically relevant models of neocortical epilepsy and a limited number of studies. A persisting controversy questions whether the neocortex (whether normal or epileptic) has an endogenous capacity to generate HFOs, especially in the fast ripple bands (Jiruska et al., 2017). The ability of the neocortex to generate gamma or ripple oscillations is well documented (Grenier et al., 2003; Wykes et al., 2012; Bragin et al., 2016; Reid et al., 2016). On the contrary, neocortical fast ripples were recorded only in the traumatic brain injury model (Li et al., 2022) and the kainate model of TLE (Sheybani et al., 2018). Clinical observations on neocortical HFOs still need underpinning by experimental studies to identify what kinds of HFOs the neocortex can generate and how they are related to endogenous epileptogenicity of neocortical tissue and its capacity to generate seizures.

In this study, we examine HFOs coupled with interictal epileptiform discharges (IEDs) generated in a highly realistic murine model of epilepsy due to focal cortical dysplasia (FCD) type II. We provide seminal observations that the FCD generates a whole spectrum of interictal activities ranging from IEDs to HFOs from gamma, ripple, and fast ripple bands. We show that the gamma oscillations, ripples, and fast ripples mark the FCD lesion. HFOs can propagate outside the FCD lesion to the interconnected cortical areas of both hemispheres, and a small HFO proportion is generated independently of the FCD. From the cellular perspective, we show that neurons carrying mTOR mutation represent an integral component of the FCD network capable of inducing HFOs, namely fast ripples.

2. Materials and methods

2.1. Animals

All experiments were performed under the Animal Care and Animal Protection Law of the Czech Republic, fully compatible with the guidelines of the European Union directive 2010/63/EU. The protocol was approved by the Ethics Committees of the Second Faculty of Medicine (Project License No. MSMT-31765/2019–4). Animals were housed in groups under standard conditions in a room with a controlled temperature ($22 \pm 1\,°C$) and a 12/12 h light/dark cycle. Experimental animals were offspring of SST-IRES-Cre (Jackson Laboratory cat. Number #018973) or PV-P2A-Cre (Jackson Laboratory cat. Number #012358) mice crossed with flex-tdTomato mice (Jackson Laboratory cat. Number #007909) since after the electrophysiological experiments, they were used for another study related to neuronal morphology. One mouse line were offspring of (C57BL/6 x 129S4/SvJae) F1 VIP-IRES-Cre (Jackson Laboratory number #010908) and C57BL/6S flex-tdTomato mice (Jackson Laboratory cat. Number #007909). There were 3 male and 5 female animals in the FCD group and 3 male and 1 female animals in the control group. Experimenters were not blinded to the treatment of the mice.

2.2. FCD induction

The FCD lesion was induced by *in utero* electroporation (Lim et al., 2015). Pregnant mice (day 14.5 ± 0.5 post-fertilization) were anesthetized with isoflurane. Uterine horns were exposed by midline laparotomy, and the left lateral ventricle of each embryo was injected with a mixture of plasmids diluted in 2 μg/ml Fast Green (F7252, Sigma, USA),

using pulled and beveled glass capillaries. In FCD animals, the plasmid mixture contained 3 μg/μl mutant mTOR (p.Leu2427Pro, SoVarGen Co., Ltd., Korea) coexpressing mAmetrine and 1.5 μg/μl pCAG-GFP to visualize the lesion. Control animals were electroporated with 1.5 μg/μl pCAG-GFP only. After injection, forceps-type electrodes (3 mm, CUY650P3, Nepagene) were positioned on the head of each embryo, and electroporation of plasmids was elicited by a custom–made high-resolution electroporator with a 40 mA current limiter, delivering five 35–45 V 50 ms pulses with 950 ms interpulse intervals.

2.3. Electrode implantation and EEG recording

Mice were implanted with EEG electrodes at 8–10 weeks of age. Prior to implantation, custom EEG implants were prepared by soldering coated silver wires (127 μm in diameter, AM Systems, Inc., USA, cat. no. 786000) to prefabricated connectors (TME Electronic Components, Poland, cat. no. DS1065-03-2*6S8BV). Mice were anesthetized with isoflurane, a small area of skin on the head was removed to expose the frontal and parietal bones of the skull, and fluorescence screening was performed to determine the exact position of the FCD or GFP lesion. Seven holes, adjusted to the position of the lesion, were drilled through the skull. Two electrodes were placed in the parietal bone in the center and on the margin of the lesion (lesion, "L" and peri-lesion, "P"). Three additional electrodes were implanted, one contralaterally homotopic to the lesional electrode (contralateral, "C") and two over the frontal cortices (front left, "FL" and front right "FR"). Two holes were drilled above the cerebellum for grounding/reference electrodes. The electrodes were positioned on the surface of the dura mater and the holes were covered with bone wax (SMI, Belgium, cat. no. Z046). The electrodes together with the connector were attached to the skull using cyanoacrylate glue (Loctite, USA, cat. no. 1363589).

2.4. EEG recording and analysis

Following a five-day recovery period, the animals were individually video-EEG monitored continuously for four weeks. Recordings were through wires plugged into the headmount connected to the recording device through counterbalanced slip rings. The spontaneous electrographic activity was amplified, band-pass filtered (0.1 Hz–1.6 kHz), and sampled at 5 kHz using a 32-channel headstage amplifier with AD converter (Intan Technologies, USA, cat. no. RHD2132) and Spike2 software (Spike2 software (Cambridge Electronic Design, Cambridge, UK). EEG was analyzed using custom-made scripts in Matlab 2019b computing environment (Mathworks Inc., USA). Seizures were identified by manual review of the signals whereas spikes and HFOs were detected automatically, see below.

2.5. Optogenetic neuronal activation

For optogenetic studies, the FCD model was generated by electroporation of C57B/6 J mice with mTOR p.Leu2427Pro (pCAG-mTOR pL2427P-IRES-mAmetrine-Cre) and GFP plasmids. Mice positive for GFP fluorescence were implanted with epidural electrodes into the lesion and contralateral sites at the age of eight weeks. During the surgery, AAV virus (AAV9-EF1a-double floxed-hChR2(H134R)-mCherry; Addgene, USA) at the concentration vg $8*10^{11}$ was injected into the lesion (350 μm below the dura, 4x60nl) to induce expression of Channelrhodopsin-2 (ChR2) in the mutated neurons. The mice were subjected to video-EEG monitoring one week after the surgery. Light stimulation was performed two to three weeks after viral transduction. Blue LED diode ThorLabs, Inc., USA) light pulses (470 nm; pulse width 1 ms) were used to activate ChR2 and depolarize the mutated neurons. During optogenetic experiments, the EEG signal was amplified (1000×, A-M Systems amplifier, Model 3000, USA), band-pass filtered (0.1 Hz–3 kHz), and sampled at 20 kHz using Micro 1401 and Spike2 software (Cambridge Electronic Design, Cambridge, UK). The position and shape of lesions of

experimental animals were determined by Lightsheet Z.1 microscopy (ZEISS, Germany) after the end of optogenetic experiments.

2.6. HFO detection

Artifact-free periods of EEG of slow-wave sleep were manually selected from two-hour epochs extracted at around noon from every other day of the recording. The artifact-free EEG data were subjected to automated detection of spikes (putative IEDs) based on statistical modeling of signal envelope distributions (Janca et al., 2015). HFOs were identified in the detected spikes using the modified root mean square (RMS) based approach (Supplementary Fig. 1) (Kudlacek et al., 2017; Staba et al., 2002). Only 200 ms segments of EEG in the vicinity of detected spikes (IEDs) were subjected to HFO detection. This study focused on IED-coupled HFOs. HFOs independent of IEDs were not analyzed. Because of the observed spectral properties, we decided to merge gamma and ripple oscillations together and analyzed HFOs in two frequency bands – gamma-ripples and fast ripples. The signal was band-pass filtered in the frequency domain (pass-band frequencies 45–250 Hz for gamma-ripples and 300–800 Hz for fast ripples). The filters' frequency responses were flat with wide gaussian roll-offs with half maximum bandwidths 35–300 Hz for gamma-ripples and 250–900 Hz for fast ripples in order to minimize ringing artifacts. An RMS of the filtered signal was computed in 5 ms or 3 ms sliding windows for gamma-ripple and fast ripple band, respectively. Putative detections were created by thresholding the RMS signal by a multiple of its standard deviation (2.2 for gamma-ripples and 3 for fast-ripples). In the gamma-ripple detection, only segments of at least 18 ms in duration and with at least 9 peaks in its autocorrelation function were selected. Events <15 ms apart were treated as a single event. For fast ripple detection, only segments of at least 4 ms in duration and with at least 13 peaks in its autocorrelation function were selected. Events closer than 3 ms were treated as a single event. For the HFO detection to be accepted, the second peak of the autocorrelation function had to have a minimum amplitude of 25% of the first peak.

2.7. HFO and IED analysis

Power spectral density (PSD) was estimated by Welch method from 1 s segments centered around the detected spike and weighted by Hanning window. The HFO frequency was determined from the distance between the first and the second peak of the autocorrelation function calculated from a $20\times$ oversampled signal to increase the resolution. For the statistical analysis, we labelled each electrode (and the electrographic events recorded from it) as "lesional" or "non-lesional" based on the presence of the GFP fluorescence below the given electrode. Then, the features of interest for both the IEDs and HFOs were computed per each animal for "lesional" and "non-lesional" sites. To assess IED-coupled HFO propagation, we first clustered all detected IEDs into five groups according to spatial profile and the time lag between the IEDs across EEG channels (Supplementary Fig. 2). Clusters with a time lag <1.5 ms between IEDs were marked as "inconclusive" and excluded from the analysis. Then, we filtered IED-related HFO events to assess HFO propagation. Events where HFOs were localized to the brain regions outside the lesion or propagated from the non-lesional brain areas were classified as independent HFOs.

2.8. Morphological analysis of the FCD model

At the end of the experiments, the animals were overdosed with ketamine/xylazine and transcardially perfused. Brains were extracted and postfixed overnight in 4% paraformaldehyde. To quantify the spatial extent of the FCD lesion, the post-fixed brains were photographed against a graticule, GFP signal intensity was thresholded to define clear boundaries of the FCD lesion, and the area of the lesion was determined using ImageJ software (National Institutes of Health and the Laboratory

for Optical and Computational Instrumentation). To obtain approximate lesion volume, the lesion area was multiplied by the cortical thickness in a given anatomical area as stated in the Allen Mouse Brain Atlas. In control animals, GFP lesion size was determined in brains that were cleared using the CUBIC protocol (Susaki et al., 2014). The GFP-positive areas were scanned in three-dimensional space using the Lightsheet Z.1 microscope (ZEISS, Germany), and images of the brains were processed using Imaris software (Oxford Instruments, United Kingdom). Subsequently, a section of each brain was scanned in high resolution on a custom-made two-photon microscope.

2.9. Statistical analysis

All results and graphs are shown as mean $\pm$ s.e.m. (median) unless otherwise stated. Statistical analysis was performed using Matlab. Mann-Whitney-Wilcoxon *U* test was used for analysis between animal groups and between lesional and non-lesional sites. The Kolmogorov-Smirnov test was used to determine the difference between the histograms and power spectra. The confidence intervals for the median of power spectral density were computed by the distribution-free method (Hogg and Tanis, 2010). The non-parametric confidence interval for the median was obtained by selecting the k-th lowest and the k-th highest value from the sample. Recorded data and analytical tools used in this study are available from the corresponding author upon request.

3. Results

3.1. Morphological features of FCD lesion

We generated FCD in eight mice using *in utero* electroporation of a plasmid containing a mutated mTOR gene and a plasmid with a GFP reporter. Four control animals were electroporated with GFP reporter only to confirm that the mutated mTOR was responsible for FCD and the associated epilepsy. In control animals ($n = 4$), the area of GFP fluorescence was designated as the lesion; its size was 4 ± 1 (5) mm³ (Fig. 1A). In mutated-mTOR electroporated (FCD) animals ($n = 8$), the lesion is the FCD (Fig. 1B, C). In 5/8 FCD animals, the lesion was unilateral (Fig. 1B) and bilateral in 3/8 FCD animals (Fig. 1C). The FCD lesion size was 16 ± 2 (14) mm³. Imaging in controls demonstrated that GFP-positive cells migrated to layers II and III of the neocortex (Fig. 1D) and the neuronal morphology was normal (Fig. 1E, F). The FCD lesion displayed morphological features that agreed with those originally described (Fig. 1G-I) (Lim et al., 2015). Neuronal migration was altered in all FCD animals, with cells present in the white matter (Fig. 1G). Moreover, dysmorphic neurons with large cell bodies and extensive dendritic arborization were observed (Fig. 1H, I). Lightsheet imaging demonstrated the presence of GFP-positive axonal fibers emerging from the unilateral FCD and terminating in the contralateral homotopic cortex (Fig. 1J) which is indicative of the existence of interconnectivity between FCD and the contralateral brain areas.

3.2. Seizures and interictal activity in FCD-related epilepsy

Chronic EEG recording was performed in eight animals with FCD and four control animals. Seizures were observed in 4/8 FCD animals and in none of the control animals (Fig. 2A). Seizure onsets were characterized by repetitive low-amplitude spikes, which progressively increased in amplitude and decreased in frequency (Fig. 2A). The cross-correlation technique (Supplementary Fig. 3) demonstrated that FCD lesion represented the primary seizure onset zone in 95 ± 2 (95) % of analyzed seizures ($n = 134$ seizures, 4 animals). The average seizure frequency was 5 ± 2 (4) seizures per day, and seizure duration was 90 ± 30 (60) s. The first seizure occurred on 76 ± 9 (70) postnatal day. In all FCD animals, the EEG contained pathological interictal epileptiform phenomena, including IEDs (Fig. 2 B; Supplementary Fig. 4), rhythmic bursts of polyspikes, and a wide spectrum of HFOs (Fig. 2C, D; Supplementary
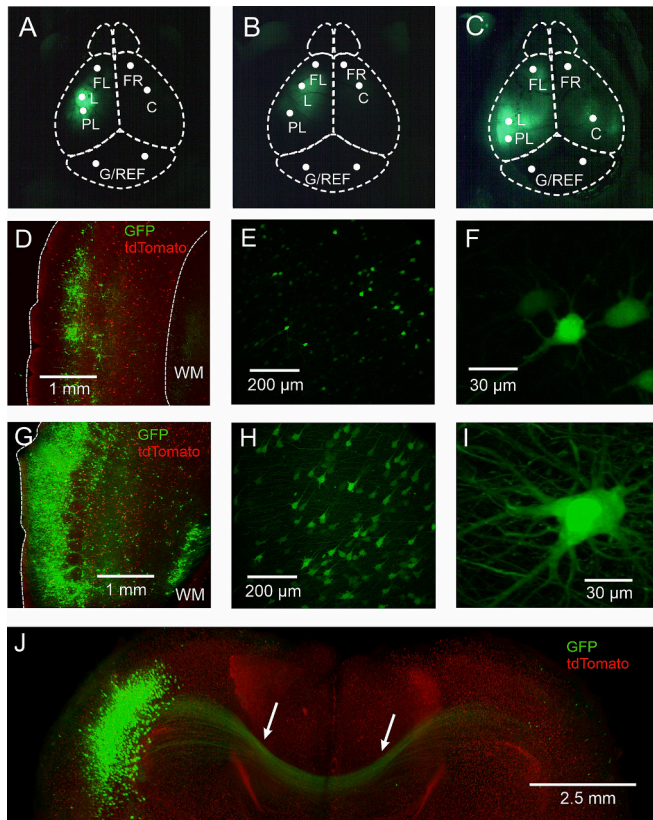
Fig. 1. Morphological features of the FCD type II model. (A) Macroscopic image of GFP-positive areas in the control brain and in animals with unilateral (B) and bilateral (C) FCD lesions. Images also demonstrate the approach to the electrode positioning with respect to the GFP or FCD lesion (C-contralateral, FL-frontal left, FR-frontal right, L-lesional, PL-perilesional). (D) GFP fluorescence in control animal electroporated with GFP plasmid only. Two-photon imaging of the cortical structure showed electroporated neurons neatly organized in layers II and III. Interneurons are expressing red tdTomato. (E) Pyramidal neurons in the control brain displayed normal morphology. (F) The morphology of principal cells in detail. No morphologically abnormal neurons are present. (G) Altered migration in FCD model. Neurons dispersed along the cortex and white matter (WM) indicate disrupted neuronal migration during cortical development. (H) FCD lesion is characterized by the presence of abnormal neuronal phenotypes, namely large dysmorphic neurons. (I) Dysmorphic cells have an abnormal shape, massive dendritic branching, and large size bodies compared to control neurons. The presence of dysmorphic cells is a marker of altered cell maturation (J). FCD lesion is connected to the homotopic contralateral areas. The coronal section through the brain shows the FCD lesion and GFP-positive callosal projections (arrows) originating inside the FCD and terminating in the contralateral cortex. Abbreviations: PL – perilesional, C – contralateral, FR – frontal right, FL – frontal left, L – lesion. (For interpretation of the references to colour in this figure legend, the reader is referred to the web version of this article.)

Fig. 4).

3.3. FCD, IEDs and HFOs

We applied the envelope spike detector (Janca et al., 2015) to the artifact-free recordings in control and FCD animals. It detected 87,356 spikes (putative IEDs) in FCD animals, and 9703 spikes in controls (Supplementary Fig. 5 A-E). The width of detected spikes was 15.8 ± 0.4 (15.8) ms in controls and 11.8 ± 0.8 (11.3) ms in FCD animals (Fig. 3A). The detection rate was 1.3 ± 0.2 (1.4) spikes/min in controls and 4 ± 2 (2) spikes/min in FCD animals. The spike rates did not differ between experimental groups (Fig. 3B, $p = 0.8$, Wilcoxon signed-rank test), nor between inside and outside the FCD lesion (Fig. 3C, $p = 0.55$, Wilcoxon
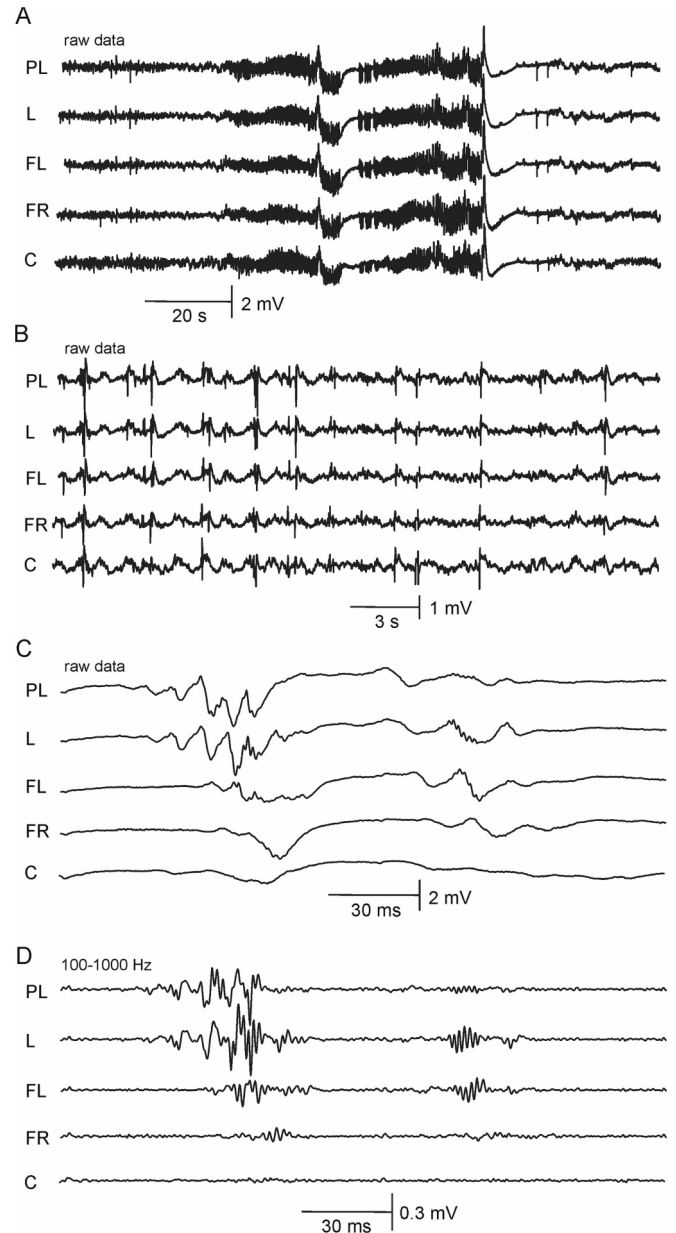
Fig. 2. Electrographic features of the FCD type II model. (A) An example of ictal activity in an animal with a localized FCD lesion. The seizure quickly spreads over the large areas of both hemispheres. (B) Interictal activity during sleep is characterized by the presence of interictal epileptiform activity of various morphologies, ranging from interictal discharges to repetitive spikes and HFOs. (C, D) An example of interictal discharges with superimposed HFOs from gamma to ripples and fast ripples. Note the presence of time delay and propagation of the interictal activity between the electrodes positioned in the lesion and other brain areas of the ipsilateral and contralateral hemispheres. Abbreviations: PL – perilesional, C – contralateral, FR – frontal right, FL – frontal left, L – lesion.

rank sum test). The frequency spectrum profile of detected events in FCD animals demonstrated the presence of peaks in HFO frequency bands greater than in controls (Fig. 3D-F). The difference with respect to control spectral profiles was most prominent in gamma-ripple and fast ripple bands (Fig. 3E, F). Visual review of recorded EEG and detected spikes confirmed the presence of HFOs of various frequency bands in all animals from both groups (Fig. 4, Supplementary Fig. 5 A-E). The HFOs were clearly visible in unfiltered signal (Fig. 4A) and manifested as a stand-alone oscillation in time-frequency plot (Fig. 4B). The various
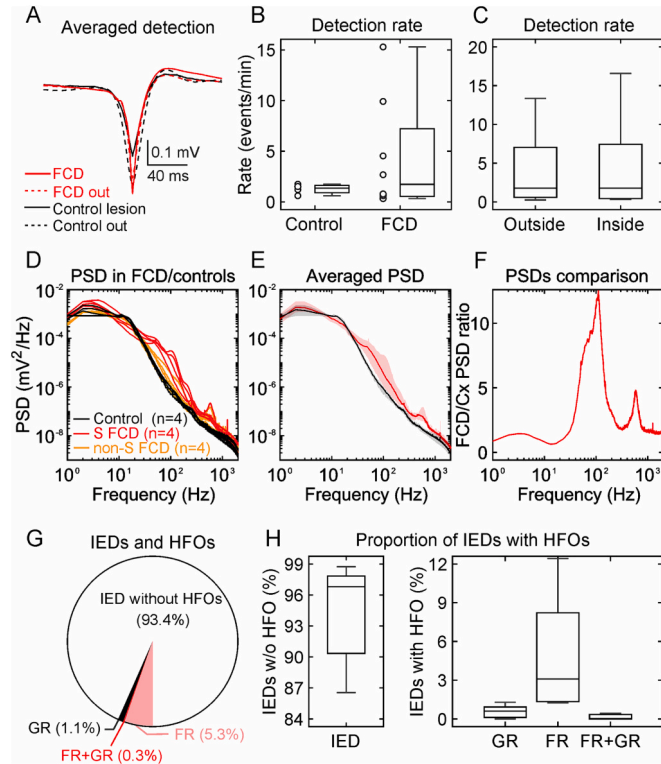
Fig. 3. Properties of the detected spikes and IEDs. (A) Average normalized waveforms of detected events in FCD and controls. In controls, the detected events displayed a longer duration in comparison to detections in FCD animals. (B) The rate of detection does not differ between both study groups. (C) In FCD animals, the detection rate (IED rate) doesn't differ between the lesion and the areas outside the lesion. (D) Average spectral density of detected spikes in controls and FCD (E) Median of power spectral density of detected events in FCD and control animals. The shaded areas for mutated and control animals represent 93% and 87.5% confidence intervals, respectively. Power in gamma-ripple and fast ripple bands are significantly higher in FCD animals which is indicative of the presence of HFOs. (F) The ratio of power spectral densities shows peaks in both HFO bands. (G) A proportion of FCD-related IEDs with superimposed gamma-ripple, fast ripple or both types of oscillations. (H) Proportions of IEDs without HFOs and with HFOs in FCD animals. IED – interictal epileptiform discharge, GR – gamma-ripples, FR – fast ripples.

subtypes of HFOs occurred either isolated or coincident (Fig. 4C-G). These features contributed to a high variety and complex morphology of IEDs and HFOs. In FCD, 6.6% of spike detections were associated with HFOs. If expressed per FCD animal, 0.6 ± 0.2 (0.6) % of IEDs were associated with gamma-ripples, 5 ± 2 (3) % with fast ripples, and 0.15 ± 0.07 (0.03) % were accompanied by both gamma-ripples and fast ripples (Fig. 3G, H).

3.4. FCD and gamma-ripple oscillations

In total, we detected 1143 gamma-ripple events in FCD animals. In controls, the gamma-ripples were nearly absent (3 events). On average, we detected 100 ± 100 (38) gamma-ripple events in FCD animals. The average processed EEG signal length in FCD animals was 560 ± 90 (620) minutes and 500 ± 300 (388) minutes in control animals. In clinical studies, the rate is considered the most relevant diagnostic HFO feature that localizes the epileptogenic tissue. In this study, we similarly found that the rate of gamma-ripple was significantly higher inside the FCD lesion 0.08 ± 0.04 (0.02) events/min compared to the neocortex outside the lesion 0.02 ± 0.01 (0.003) events/min ($p = 0.015$, Wilcoxon rank sum test, Fig. 5B, C). The mean frequency of gamma-ripples in FCD was 79 ± 7 (72) Hz (Fig. 5D). The visual inspection of the frequency of
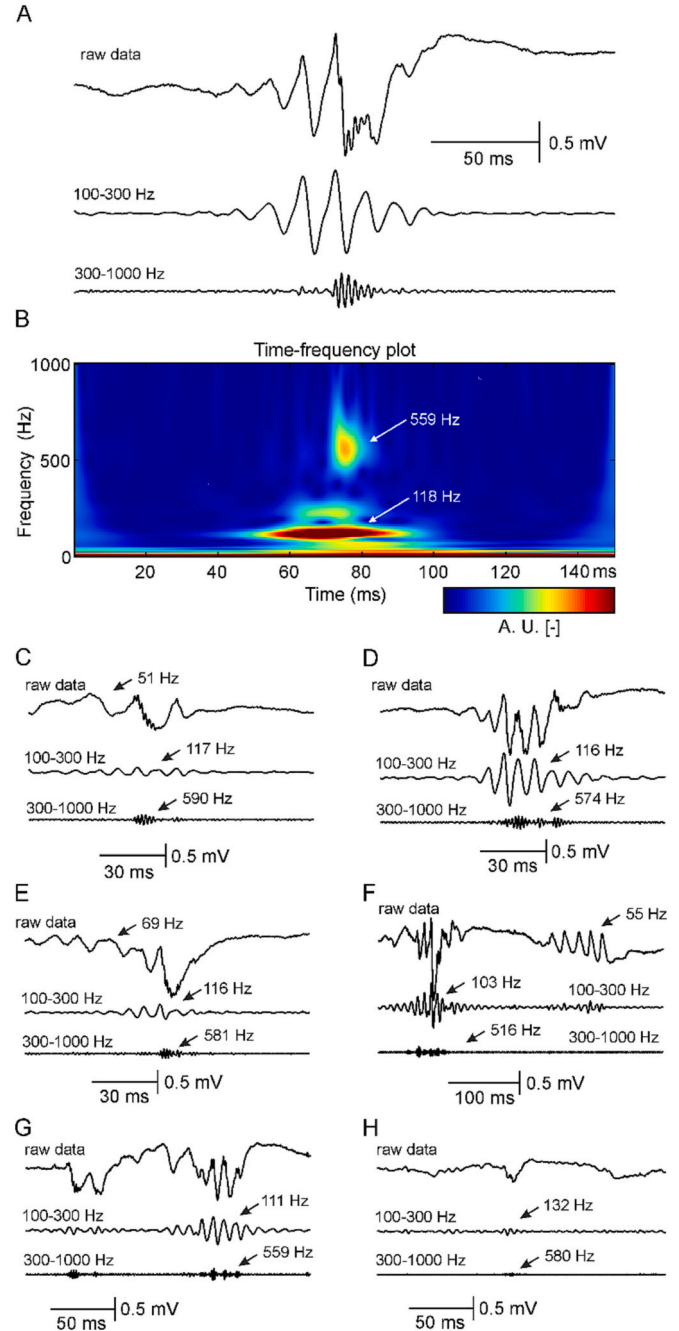
Fig. 4. HFOs in murine FCD type II model. (A) An example of a complex interictal discharge with superimposed HFO activity from gamma-ripple and fast ripple bands. The HFOs from various frequency bands can be present isolated or co-occur together. (B) The corresponding time-frequency map demonstrates the presence of clear 'blobs' in gamma-ripple and fast ripple bands (arrows). (C-G) Examples of various shapes of interictal epileptiform discharges and HFOs. Note the complex nature of the discharges with a broad spectrum of superimposed HFOs. (H) The fast ripple oscillation detected in the control animal.

individual events, however, showed a bimodal distribution of gamma-ripple frequencies, with peaks in gamma (54.1 ± 0.3 Hz) and fast gamma (105.7 ± 0.7 Hz) band (Fig. 5E). We did not observe any difference in gamma-ripple frequency inside and outside the FCD lesion (Fig. 5F, G; $p = 0.31$, Wilcoxon rank sum test). The mean frequency of gamma-ripples was 79 ± 7 (72) Hz in FCD and 54 ± 3 (54) Hz in non-lesional sites. The parameter of the proportion of IEDs with gamma-ripples marked the FCD lesion. The proportion was 0.9 ± 0.3 (1.0) %
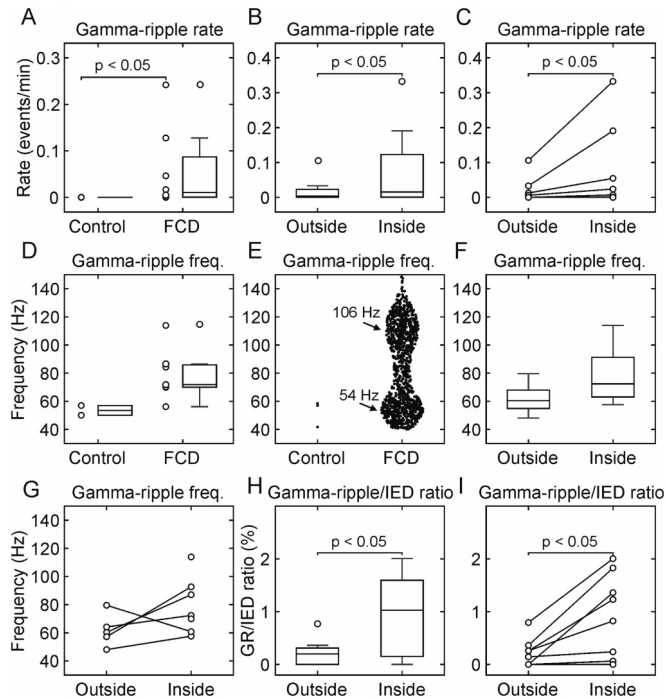
Fig. 5. Properties of gamma-ripples in FCD type II model. (A) Gamma-ripples occurred nearly exclusively in FCD animals. (B) The gamma-ripple rate was significantly greater inside the lesion compared to the areas outside the FCD lesion. (C) The gamma-ripple rate difference between the FCD lesion and non-lesional cortical areas was observable across all FCD animals. (D) The frequency profile of gamma-ripples in control animals and FCD ones. (E) In FCD animals, the frequency profile of gamma-ripples had bimodal distribution with two peaks at 54.1 ± 0.3 Hz and 105.7 ± 0.7 Hz. (F, G) The ripple frequency did not differ between the FCD lesion and non-lesional cortex. (H, I) The proportion of IEDs with superimposed gamma-ripple HFOs did not differ inside and outside the FCD lesion.
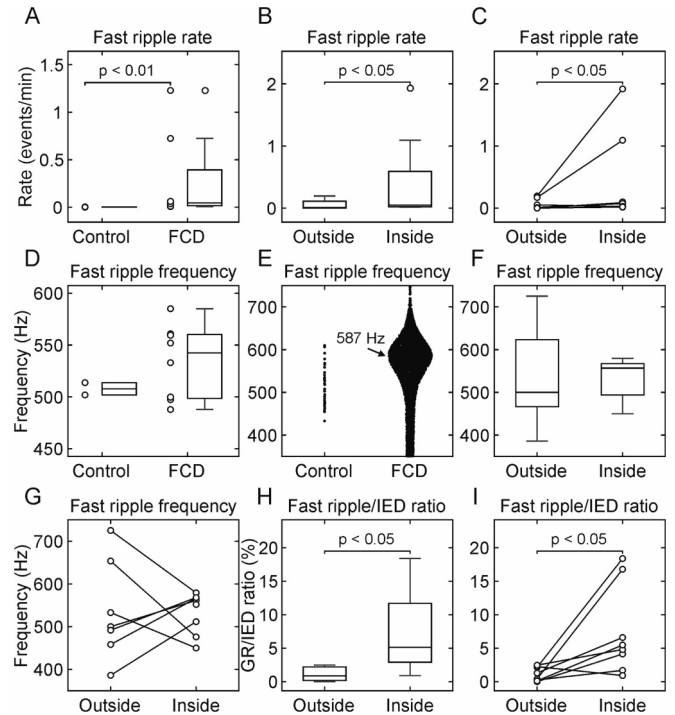

Fig. 6. Fast ripple features in FCD type II model. (A) Fast ripples were detected in both the control and FCD animals. However, the fast ripple rate was significantly higher in FCD. (B) The rate of fast ripples was significantly higher in the FCD lesion. (C) The spatial difference of fast ripple rate was preserved in all but one FCD. (D) The fast ripple frequency did not differ between experimental groups. (E) In FCD, the distribution of frequency of fast ripple events displayed a single peak at 586.5 ± 0.7 Hz. (F, G) The fast ripple frequency profile was the same inside and outside the lesion. (H, I) The proportion of IEDs with superimposed fast ripple was significantly greater inside the FCD lesion in all but one animal.

in the lesion and 0.23 ± 0.09 (0.20) % outside (Fig. 5H, I; p = 0.015, Wilcoxon rank sum test).

3.5. FCD and fast ripple oscillations

In contrast to gamma-ripples, fast ripple oscillations were present not only in FCD animals (4872 total events, 600 ± 300 (98) events per animal, Fig. 4C-G), but also in controls (37 total events, 9 ± 7 (4) events per animal, Fig. 4H, Supplementary Fig. 5). The fast ripple rate was significantly higher in FCD animals 0.3 ± 0.2 (0.0) events/min in respect to control animals 0.002 ± 0.001 (0.002) events/min (p = 0.004, Wilcoxon signed rank test; Fig. 6A). The fast ripple rate was also higher inside the lesion (0.4 ± 0.3 (0.1) events/min) compared to the non-lesional sites 0.06 ± 0.03 (0.01) events/min, p = 0.039, Wilcoxon rank sum test; Fig. 6B, C). This spatial difference was observable in all but one FCD animal (Fig. 6B). The average frequency of fast ripples was 508 ± 6 (508) Hz in controls and 530 ± 10 (542) Hz in FCD animals (p = 0.7, Wilcoxon signed rank test; Fig. 6D). Fast ripple frequency in FCD displayed a single peak distribution with mode of 586.5 ± 0.7 Hz (Fig. 6E). The fast ripple frequency was not significantly different between FCD lesion (530 ± 20 (557) Hz) and non-lesional sites (540 ± 40 (500) Hz) (p = 0.8, Wilcoxon rank sum test; Fig. 6F, G). The FCD lesion displayed a higher proportion of IEDs with superimposed fast ripples (7 ± 2 (5) %) compared to non-lesional regions (1.1 ± 0.4 (0.8) %, p < 0.015, Wilcoxon rank sum test; Fig. 6G, H).

3.6. Propagating and independent HFOs

The results showed that the cortex outside the FCD lesion also

generated HFOs (Fig. 7). We examined whether the non-lesional HFOs represented propagating HFOs (Fig. 7B) or whether they were generated independently outside the FCD lesion. We estimated the time delay between IEDs with superimposed HFOs (Fig. 7C, D). From the total number of detected HFOs, 90.1% of HFOs were generated only in the FCD, 2.8% propagated from the FCD, and 7.1% were generated independently outside FCD (Fig. 7F). The proportion varied across animals. The mean proportion of propagating HFOs was 1.7 ± 0.7 (1.9) %. Propagating gamma-ripple comprised 0.6 ± 0.3 (0.5) % of all gamma-ripples and occurred at the rate 0.004 ± 0.003 (0.003) events/min. The proportion of propagating fast ripples was 3 ± 1 (3) % and their rate was 0.05 ± 0.04 (0.02) events/min. The mean proportion of HFOs generated independently in non-lesional areas was 17 ± 9 (11) %. From all gamma-ripples, 12 ± 3 (13) % originated from non-lesional areas at the rate of 0.06 ± 0.04 (0.04) events/min (Fig. 7G). The proportion of independent fast ripples was 20 ± 20 (6) % and their rate was 0.12 ± 0.04 (0.13) events/min (Fig. 7H). The average time delay of HFOs propagating from the lesion was 7.6 ± 0.9 (7.3) ms, while the conduction time of HFOs generated in non-lesional areas was 7 ± 1 (5) ms.

3.7. Mutated neurons and HFOs

Mutated neurons play a central role in the pathogenesis of FCD and FCD-related epilepsy. Using optogenetic approach, we examined whether mutated neurons contribute to IEDs and HFOs generated by the FCD. We activated neurons carrying the mTOR mutation and expressing ChR2 (Fig. 8A, B) by brief light pulses. In 3/6 animals, the FCD illumination evoked spikes with superimposed HFOs, mainly from the fast ripple band (Fig. 8C). The IED and HFO detection algorithms were
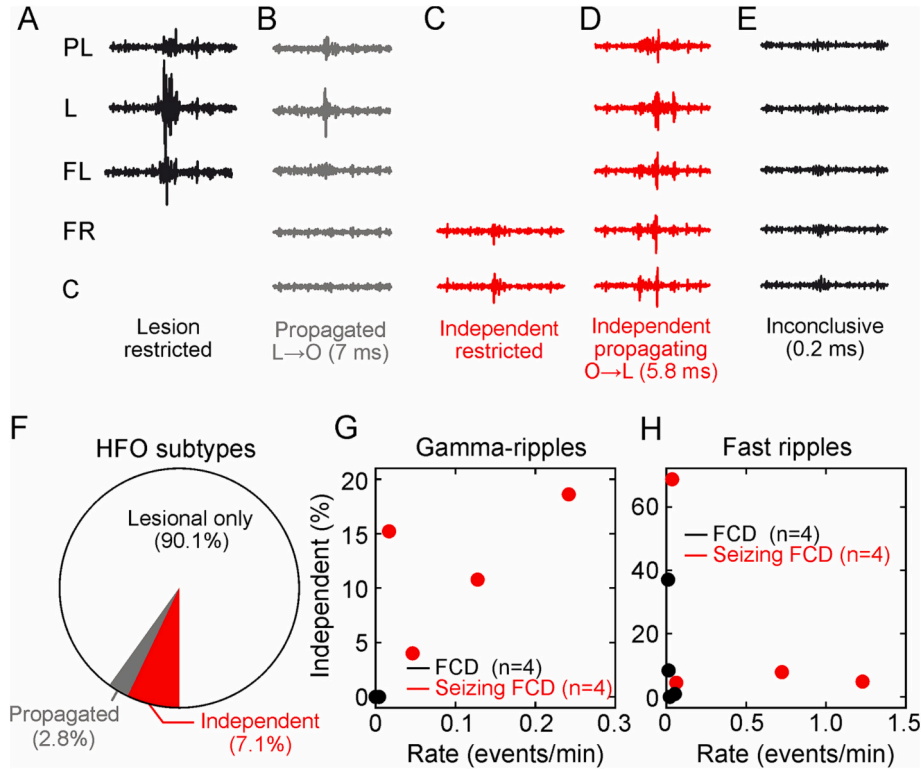
Fig. 7. Propagating and independent HFOs. (A) Example of HFO localized to the lesion. (B) HFO propagating from the lesion (L) to the ipsilateral and contralateral cortex outside the lesion (O) with a time delay of 7 ms. (C) HFOs generated independently outside the lesion and with the propagation to the lesion with a delay of 5.8 ms (D). (E) An example of inconclusive HFO in which the propagation cannot be determined. (F) The vast majority of HFOs are spatially restricted to the FCD lesion. From all detected HFOs, 2.8% fulfilled the criteria of HFOs propagating from the lesion, and 7.1% of HFOs were generated independently outside the lesion. (G) The rate and proportion of independent gamma-ripple in individual FCD animals. (H) Independent fast ripple rate and proportion of independent fast ripple in each animal with FCD.
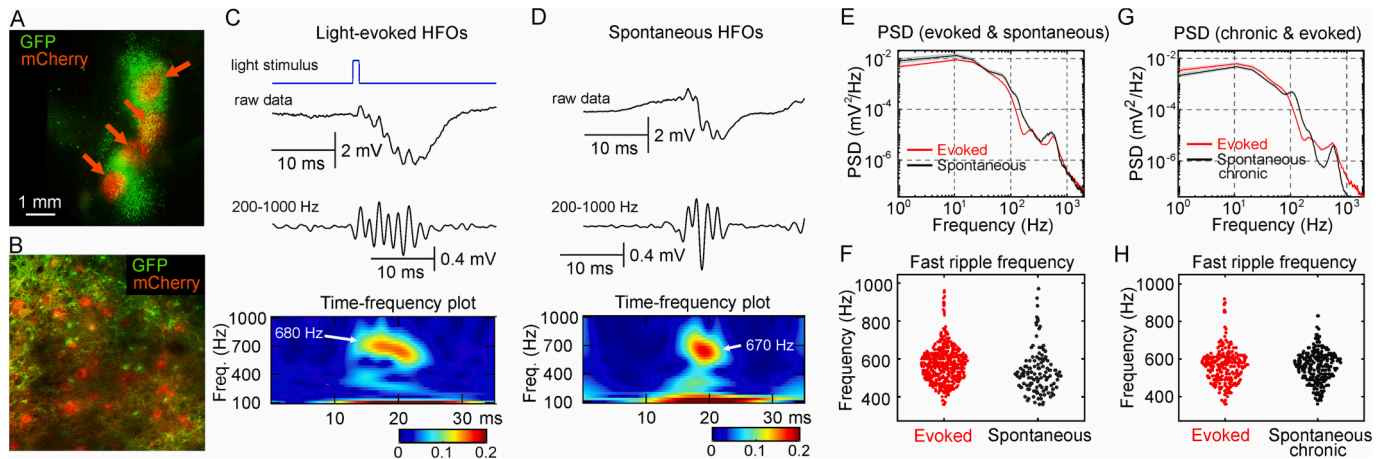
Fig. 8. Involvement of mutated neurons in HFOs genesis. (A) Light-sheet microscopy of the FCD lesion (GFP) and four injection sites with mutated neurons expressing Channelrhodopsin-2 (ChR2) and red fluorescent protein mCherry (red arrows). (B) Two-photon image of the mutated neurons expressing mCherry protein. (C) Blue light stimulation triggered spike with superimposed fast ripple with mean frequency of 680 Hz. Raw data, filtered signal, and corresponding time-frequency decomposition of the signal are shown. (D) Spontaneous fast ripple event with a frequency of 670 Hz in the same animal. (E) Mean power spectral density (PSD) of spontaneous and evoked HFOs in the same animal. (F) Frequency of individual evoked and spontaneous fast ripples in the same animal. (G) Mean power spectral density of evoked responses from three FCD animals and randomly selected HFOs from three chronically recorded animals. (H) Frequency of individual evoked HFO events and randomly selected spontaneous HFO events from the chronic experiments. (For interpretation of the references to colour in this figure legend, the reader is referred to the web version of this article.)

applied to evoked EEG signals (3 animals) and evoked HFO properties were compared with HFOs from the chronic experiments. Estimated PSD of optogenetically evoked ($n = 270$ events, 3 animals) and chronic spontaneous HFOs ($n = 270$ events, 3 animals) demonstrated the presence of prominent peaks in the fast ripple band (Fig. 8G). The average frequency of evoked fast ripples was 571 ± 7 (570) Hz, while the frequency of spontaneous fast ripples was 565 ± 6 (570) Hz ($p = 0.54$; Two sampled *t*-test; Fig. 8H). These data show that mutated

neurons are capable of triggering HFO events.

4. Discussion

In this study, we present evidence that experimental FCD can generate a wide range of IED-coupled HFOs, including gamma, ripples, and fast ripples. Most of our knowledge about HFOs in epilepsy comes from studies on hippocampal epilepsy (Engel Jr et al., 2009; Ibarz et al., 2010; Jiruska et al., 2010; Lévesque et al., 2011; Staba et al., 2002), and less emphasis has been given to extra-hippocampal structures. Understanding whether the pathophysiological principles observed in the hippocampus are applicable to HFOs of neocortical origin is crucial for epilepsy and HFO research (Engel Jr et al., 2009; Ibarz et al., 2010; Jiruska et al., 2010; Lévesque et al., 2011; Staba et al., 2002). Previous studies on TLE models have demonstrated the presence of HFOs in various parts of the limbic system, including the entorhinal cortex, which shares anatomical similarities with the neocortex (Bragin et al., 1999). Neocortical HFOs were investigated in a rat model of traumatic brain injury, where HFOs with frequencies ranging from 80 to 300 Hz were observed in the center and surrounding tissue of the traumatic lesion (Bragin et al., 2016). These neocortical HFOs displayed similar characteristics to those observed in the kainic acid TLE model. The study also identified repetitive HFOs (rHFOs) superimposed on bursts of spikes with a frequency of 10–16 Hz, which displayed the same spatial distribution as isolated HFOs (Bragin et al., 2016; Reid et al., 2016). Recently, fast ripples were identified in the TBI model, where fast ripples proved to be a reliable biomarker of the future development of spontaneous seizures (Li et al., 2022). Tetanus toxin injection into the neocortex, mimicking neocortical epilepsy, has also been reported to generate HFOs in the 70–160 Hz range (Wykes et al., 2012). Furthermore, ictal and interictal neocortical ripples with a frequency of 100–130 Hz have been observed in epileptic cats (Grenier et al., 2003). Cellular dynamics analysis revealed that the firing of principal neurons and interneurons was phase-locked with the ripple cycles. While principal cells fired during the late phase of the ripple cycle, interneurons fired during the initial phases (Grenier et al., 2003). Sheybani et al. used a large-scale recording of scalp EEG activity combined with micro-array recording from the hippocampus to explore the network properties of interictal activity generated in the murine model of TLE (Sheybani et al., 2018). In their study, they detected neocortical interictal discharges with superimposed fast ripples that were coupled with discharges and fast ripples generated in the hippocampus. During the advanced stages of chronic epilepsy, neocortical fast ripples independent of the hippocampal epileptic focus were recorded. HFOs act as a robust biomarker that identifies epileptogenicity independently of the lesion character (Frauscher et al., 2017; Zijlmans et al., 2012). However, multiple clinical observations suggested that the diagnostic significance of HFOs may vary depending on the nature of the epileptogenic lesion and its endogenous epileptogenicity. HFOs have been observed in various epilepsy cases caused by different lesion types such as hippocampal sclerosis, tumors, nodular heterotopias, and FCD (Akiyama et al., 2011; Brázdil et al., 2010; Cho et al., 2014; Thomas et al., 2023) and the specific lesion can generate HFOs at varying rates. For instance, mesiotemporal lobe sclerosis, FCD, and nodular heterotopia exhibit higher HFO rates than lesions like polymicrogyria or tuberous sclerosis (Ferrari-Marinho et al., 2015). In FCD cases, FCD type II generates higher rates of ripples and fast ripples than FCD type I, correlating with a higher seizure rate (Kerber et al., 2013). Spatial distribution analysis of HFOs in FCD reveals higher rates in perilesional tissue than in the lesion itself (Ferrari-Marinho et al., 2015). Furthermore, FCD type II exhibits very high HFOs in addition to ripples and fast ripples (Brázdil et al., 2010; Brázdil et al., 2017). Our study supports clinical observations, demonstrating that the experimental FCD can generate a wide spectrum of HFO subtypes ranging from gamma to ripples and fast ripples. Several detected fast ripple events could even fall into the category of very high HFOs. In this study, we combined non-seizing FCD animals and animals that developed FCD-related epilepsy. The results showed that in both groups of FCD animals, HFOs distinguish FCD animals from controls and serve as a biomarker for localizing the FCD lesion. In seizing animals, the HFO rates localize the seizure onset zone.

The presence and rate of HFOs serve as crucial diagnostic features for localizing epileptogenic or seizure-generating tissue. In clinical epileptology and particularly in epilepsy surgery, the identification of a close spatial association between the location of HFOs and the epileptogenic zone and/or the seizure onset zone has led to the incorporation of measurements of HFO properties into presurgical examinations (Jacobs et al., 2012; Frauscher et al., 2017). From the diagnostic perspective, HFOs are more specific markers of seizure onset zone than IEDs. Fast ripples display the highest sensitivity to mark the seizure onset zone, followed by ripples and IEDs (Jacobs et al., 2012). Our results agree with these clinical observations. In the FCD model, the HFO parameters differentiate lesional areas from non-lesional and mark the seizure onset zone. Compared to clinical observations in epilepsy surgery cases, gamma-ripples prove to be a more exclusive marker of FCD and seizure onset zone than fast ripples due to the presence of fast ripples in control animals. It is important to stress that in our study, we focused on only IED-coupled HFOs. HFOs display a close link with IEDs, and HFOs independent or superimposed on IEDs are well documented in animal models of TLE and humans (Levesque et al., 2022). In human studies, 64% of ripples and 86% of fast ripples occurred with IEDs (Urrestarazu et al., 2007). IED-coupled HFOs provide diagnostic information, and, for example, IED-coupled ripples were more closely related to the seizure onset zone than ripples alone (Goncharova et al., 2016).

HFOs are not spatially limited to seizure onset or epileptogenic zones due to their propagation to distant brain regions *via* synaptic mechanisms or independent generation of HFOs in distant regions (Jacobs et al., 2008; Jiruska et al., 2010; Gonzalez Otarula et al., 2019). In our study, HFO propagation can be observed in non-lesional areas, namely in the contralateral neocortex. Independent generation of HFOs in those areas is also detected. Should these areas be considered potentially epileptogenic? HFOs outside the epileptogenic zone are typically generated at much lower rates, both in temporal and neocortical epilepsy. In chronic TLE, the distant areas may become actively involved in the epileptogenic process, leading to the generation of independent interictal epileptiform activity and, eventually, seizures through structural and functional reorganization. HFOs can contribute to the recruitment of these distant regions, reminiscent of the kindling phenomenon (Bragin et al., 2000; Weiss et al., 2022; Jiruska et al., 2023). Similarly, chronic neocortical epileptic foci can induce alterations in projection areas, increasing local neuronal excitability and promoting synchronized network activity (Brener et al., 1991; Jiruska et al., 2023). In FCD, the involvement of distant areas in epileptiform activity is particularly pronounced. This can be attributed to the underlying mTORopathy, leading to enhanced axonal connectivity, abnormal synaptic terminals, increased response to synaptic stimulation, and heightened neuronal excitability in distant regions (Lim et al., 2015; Proietti Onori et al., 2021). Increased recruitment of distant sites may result from intense synaptic epileptiform activity, kindling effects, and other forms of intercellular communication, such as exosome exchange (Budnik et al., 2016; Koh et al., 2021; Proietti Onori et al., 2021). Apart from HFO rates, analysis of the HFO initiation sites (sources) and their propagation patterns seems to increase the diagnostic yield of HFOs. By applying of network perspective to HFO analysis, Otarula et al. showed that the HFO sources co-localized with the seizure onset zone, and their resection was associated with favorable surgical outcomes (Gonzalez Otarula et al., 2019).

Dysmorphic neurons carrying the mTOR mutation are hallmark of FCD type II. Although these neurons represent only a small fraction of neurons in FCD they play a central role in the pathogenesis of FCD and associated epilepsy. They express abnormal ion channels and synaptic receptors (Cepeda et al., 2020; Hsieh et al., 2020) that predispose them to pathological firing. Treatment with rapalogs reducing the increased

mTOR signalling leads to seizure cessation (Lim et al., 2015). Although mutated neurons play a central role in epileptogenesis, seizure, and interictal activity genesis may be attributed to non-mutated neurons in the FCD, transition cortex between dysplastic and normal neocortex, or contralateral neocortex (Koh et al., 2021; Proietti Onori et al., 2021). Our results suggest that mutated neurons represent an active component of the FCD network that can be involved in HFO and IED genesis and trigger these network events, which may recruit inter-connected neurons (Ibarz et al., 2010; Jiruska et al., 2017).

The presence of sharp transients and HFOs in control animals could represent physiological as well as pathological activity (Jefferys et al., 2012; Jiruska et al., 2017). It is well established that the normal (non-epileptic) neocortex generates a wide spectrum of physiological HFOs involved in cognitive functions (Buzsaki and Lopes da Silva, 2012; Frauscher et al., 2017). The significance of gamma, fast gamma, ripples, and even fast ripples in cognition is well documented in experimental conditions and in humans (Buzsaki and Lopes da Silva, 2012). Fast ripples and their propagation through the brain networks were described during visual task processing (Kucewicz et al., 2014) or in response to sensory stimulation (Curio, 2000; Baker et al., 2003). The amplitude and rate of physiological fast ripples are much lower than for pathological fast ripples. It has been hypothesized that physiological ripples probably reflect the firing of single cells rather than compound network fast oscillatory activity generated by the epileptic tissues (Jiruska et al., 2017). From the clinical perspective, the frequency overlap between physiological and pathological HFOs hinders their utilization as a diagnostic marker in epilepsy surgery cases (Frauscher et al., 2017; 2018). In our study, gamma-ripples associated with IEDs were detected nearly exclusively in FCD animals, while fast ripples were also observed in controls (although less frequently).

Sharp transients, morphologically similar to IEDs, can occur in the non-epileptic neocortex. Sharp transients were detected in patients with intractable chronic facial pain implanted with intracranial electrodes for experimental brain stimulation treatment (Janca et al., 2015). Physiological sharp transients also occur in human scalp EEG recordings, for example, benign epileptiform transients of sleep, wicket spikes, "14-" and "6-" Hz positive spikes, and others. Neocortical sharp transients reminiscent of IEDs were reported in wild-type mice but at a much lower rate than in our control animals (Purtell et al., 2018). Because our control animals underwent *in utero* electroporation, it is probable that observed sharp transients and HFOs represent pathological events. The injection of the plasmids into the ventricle through a glass pipette is an invasive procedure considering the size of the embryonic brain, and it can damage the brain tissue. Also, the expression of GFP or other proteins can be cytotoxic and induce cell damage or even cell death (Ansari et al., 2016). Therefore, sharp transients and fast ripples observed in control animals can reflect epileptogenic tissue remodeling because of cytotoxic damage or traumatic brain injury during the early stages of brain development (Bragin et al., 2016).

5. Conclusion

Our results highlight the significance of HFOs in the pathophysiology and functional organization of neocortical epileptic foci. We demonstrate that FCD and neocortex (although morphologically abnormal) can generate a wide spectrum of HFOs. Besides its pathophysiological relevance, the results support the clinical observations about the HFO's role in the identification and differentiation of epileptogenic and seizure onset zones in neocortical epilepsy. Finally, we provide novel observations about the putative central and direct role of mutated neurons in FCD-related interictal and HFO phenomena.

Funding

Author contributions

P.J. and O.N. contributed to the conception and design of the study; J.C., N.P., M.R., S.K., J.K., M.K., R.W., P.B., M.B, J.G.R.J, O.N., and P.J. contributed to experimental work or data analysis. J.C., N.P., J.K., S.K., M.K., J.G.R.J., O.N., and P.J. contributed to drafting the text or preparing the figures.

CRediT authorship contribution statement

Jan Chvojka: Data curation, Formal analysis, Methodology, Writing – original draft, Writing – review & editing. **Natalie Prochazkova:** Data curation, Formal analysis, Methodology, Writing – original draft, Writing – review & editing. **Monika Rehorova:** Data curation, Investigation, Methodology. **Jan Kudlacek:** Data curation, Formal analysis, Investigation, Methodology, Supervision, Writing – original draft, Writing – review & editing. **Salome Kylarova:** Data curation, Formal analysis, Investigation, Methodology. **Michaela Kralikova:** Data curation, Formal analysis, Investigation, Methodology. **Peter Buran:** Methodology. **Romana Weissova:** Methodology. **Martin Balastik:** Funding acquisition, Methodology, Supervision. **John G.R. Jefferys:** Data curation, Formal analysis, Methodology, Supervision, Writing – original draft, Writing – review & editing. **Ondrej Novak:** Conceptualization, Investigation, Methodology, Writing – original draft, Writing – review & editing. **Premysl Jiruska:** Conceptualization, Formal analysis, Funding acquisition, Project administration, Supervision, Writing – original draft, Writing – review & editing.

Declaration of Competing Interest

No conflicts of interest to disclose.

Data availability

Recorded data and analytical tools used in this study are available from the corresponding author upon request.

Appendix A. Supplementary data

Supplementary data to this article can be found online at https://doi.org/10.1016/j.nbd.2023.106383.

References

Akiyama, T., McCoy, B., Go, C.Y., Ochi, A., Elliott, I.M., Akiyama, M., Donner, E.J., Weiss, S.K., Snead III, O.C., Rutka, J.T., others, 2011. Focal resection of fast ripples on extraoperative intracranial EEG improves seizure outcome in pediatric epilepsy. Epilepsia 52 (10), 1802–1811.

Ansari, A.M., Ahmed, A.K., Matsangos, A.E., Lay, F., Born, L.J., Marti, G., Harmon, J.W., Sun, Z., 2016. Cellular GFP Toxicity and Immunogenicity: Potential Confounders in in Vivo Cell Tracking Experiments. Stem. Cell. Rev. Rep. 2 (5), 553–559.

Baker, S.N., Curio, G., Lemon, R.N., 2003. EEG oscillations at 600 Hz are macroscopic markers for cortical spike bursts. J. Physiol. 550 (Pt 2), 529–534.

Bragin, A., Engel Jr., J., Wilson, C.L., Vizentin, E., Mathern, G.W., 1999. Electrophysiologic analysis of a chronic seizure model after unilateral hippocampal KA injection. Epilepsia 40 (9), 1210–1221.

Bragin, A., Wilson, C.L., Engel Jr., J., 2000. Chronic epileptogenesis requires development of a network of pathologically interconnected neuron clusters: a hypothesis. Epilepsia 41, 144–152.

Bragin, A., Mody, I., Wilson, C.L., Engel, J., 2002. Local generation of fast ripples in epileptic brain. J. Neurosci. 22 (5), 2012–2021.

Bragin, A., Wilson, C.L., Almajano, J., Mody, I., Engel Jr., J., 2004. High-frequency oscillations after status epilepticus: epileptogenesis and seizure genesis. Epilepsia 45 (9), 1017–1023.

9

Bragin, A., Li, L., Almajano, J., Alvarado-Rojas, C., Reid, A.Y., Staba, R.J., Engel Jr., J., 2016. Pathologic electrographic changes after experimental traumatic brain injury. Epilepsia 57 (5), 735–745.

Brázdil, M., Halámek, J., Jurák, P., Daniel, P., Kuba, R., Christina, J., Novák, Z., Rektor, I., 2010. Interictal high-frequency oscillations indicate seizure onset zone in patients with focal cortical dysplasia. Epilepsy Res. 90 (1–2), 28–32.

Brázdil, M., Pail, M., Halámek, J., Plešinger, F., Cimbálník, J., Roman, R., Klimeš, P., Daniel, P., Christina, J., Brichtová, E., 2017. Very high-frequency oscillations: novel biomarkers of the epileptogenic zone. Ann. Neurol. 82 (2), 299–310.

Brener, K., Amitai, Y., Jefferys, J.G.R., Gutnick, M.J., 1991. Chronic epileptic foci in neocortex: in vivo and in vitro effects of tetanus toxin. Eur. J. Neurosci. 3 (1), 47–54.

Budnik, V., Ruiz-Cañada, C., Wendler, F., 2016. Extracellular vesicles round off communication in the nervous system. Nat. Rev. Neurosci. 17 (3), 160–172.

Buzsaki, G., Lopes da Silva, F., 2012. High frequency oscillations in the intact brain. Prog. Neurobiol. 98 (3), 241–249.

Cepeda, C., Levinson, S., Nariai, H., Yazon, V.-W., Tran, C., Barry, J., Oikonomou, K.D., Vinters, H.V., Fallah, A., Mathern, G.W., others, 2020. Pathological high-frequency oscillations associate with increased GABA synaptic activity in pediatric epilepsy surgery patients. Neurobiol. Dis. 134, 104618.

Cho, J.R., Koo, D.L., Joo, E.Y., Seo, D.W., Hong, S.-C., Jiruska, P., Hong, S.B., 2014. Resection of individually identified high-rate high-frequency oscillations region is associated with favorable outcome in neocortical epilepsy. Epilepsia 55 (11), 1872–1883.

Curio, G., 2000. Linking 600-Hz "spikelike" EEG/MEG wavelets ("sigma-bursts") to cellular substrates: concepts and caveats. J. Clin. Neurophysiol. 17 (4), 377–396. Jul.

Engel Jr., J., Bragin, A., Staba, R., Mody, I., 2009. High-frequency oscillations: what is normal and what is not? Epilepsia 50 (4), 598–604.

Ferrari-Marinho, T., Perucca, P., Mok, K., Olivier, A., Hall, J., Dubeau, F., Gotman, J., 2015. Pathologic substrates of focal epilepsy influence the generation of high-frequency oscillations. Epilepsia 56 (4), 592–598.

Frauscher, B., Bartolomei, F., Kobayashi, K., Cimbalnik, J., Klooster, M., Rampp, S., Otsubo, H., Höller, Y., Wu, J., Asano, E., Engel, J., Kahane, P., Jacobs, J., Gotman, J., 2017. High-frequency oscillations: the state of clinical research. Epilepsia 58 (8), 1316–1329.

Frauscher, B., von Ellenrieder, N., Zelmann, R., Rogers, C., Nguyen, D.K., Kahane, P., Dubeau, F., Gotman, J., 2018. High-frequency oscillations in the Normal human brain. Ann. Neurol. 84 (3), 374–385.

Goncharova, I.I., Alkawadri, R., Gaspard, N., Duckrow, R.B., Spencer, D.D., Hirsch, L.J., Spencer, S.S., Zaveri, H.P., 2016. The relationship between seizures, interictal spikes and antiepileptic drugs. Clin. Neurophysiol. 127 (9), 3180–3186.

Gonzalez Otarula, K.A., von Ellenrieder, N., Cuello-Oderiz, C., Dubeau, F., Gotman, J., 2019. High-frequency oscillation networks and surgical outcome in adult focal epilepsy. Ann. Neurol. 85 (4), 485–494.

Grenier, F., Timofeev, I., Steriade, M., 2003. Neocortical very fast oscillations (ripples, 80–200 Hz) during seizures: intracellular correlates. J. Neurophysiol. 89 (2), 841–852.

Hogg, R.V., Tanis, E.A., 2010. Probability and Statistical Inference. Prentice Hall, Upper Saddle River, NJ.

Höller, Y., Kutil, R., Klaffenböck, L., Thomschewski, A., Höller, P.M., Bathke, A.C., Jacobs, J., Taylor, A.C., Nardone, R., Trinka, E., 2015. High-frequency oscillations in epilepsy and surgical outcome. A meta-analysis. Front. Hum. Neurosci. 9, 574.

Hsieh, L.S., Wen, J.H., Nguyen, L.H., Zhang, L., Getz, S.A., Torres-Reveron, J., Wang, Y., Spencer, D.D., Bordey, A., 2020. Ectopic HCN4 expression drives mTOR-dependent epilepsy in mice. Sci. Transl. Med. 12 (570).

Ibarz, J.M., Foffani, G., Cid, E., Inostroza, M., de la Prida, L.M., 2010. Emergent dynamics of fast ripples in the epileptic hippocampus. J. Neurosci. 30 (48), 16249–16261.

Jacobs, J., LeVan, P., Chander, R., Hall, J., Dubeau, F., Gotman, J., 2008. Interictal high-frequency oscillations (80–500 Hz) are an indicator of seizure onset areas independent of spikes in the human epileptic brain. Epilepsia 49 (11), 1893–1907.

Jacobs, J., LeVan, P., Châtilon, C.-É., Olivier, A., Dubeau, F., Gotman, J., 2009. High frequency oscillations in intracranial EEGs mark epileptogenicity rather than lesion type. Brain 132 (4), 1022–1037.

Jacobs, J., Staba, R., Asano, E., Otsubo, H., Wu, J.Y., Zijlmans, M., Mohamed, I., Kahane, P., Dubeau, F., Navarro, V., Gotman, J., 2012. High-frequency oscillations (HFOs) in clinical epilepsy. Prog. Neurobiol. 98 (3), 302–315.

Janca, R., Jezdik, P., Cmejla, R., Tomasek, M., Worrell, G.A., Stead, M., Wagenaar, J., Jefferys, J.G.R., Krsek, P., Komarek, V., 2015. Detection of interictal epileptiform discharges using signal envelope distribution modelling: application to epileptic and non-epileptic intracranial recordings. Brain Topogr. 28, 172–183.

Jefferys, J.G.R., De La Prida, L.M., Wendling, F., Bragin, A., Avoli, M., Timofeev, I., da Silva, F.H.L., 2012. Mechanisms of physiological and epileptic HFO generation. Prog. Neurobiol. 98 (3), 250–264.

Jiruska, P., Finnerty, G.T., Powell, A.D., Lofti, N., Cmejla, R., Jefferys, J.G.R., 2010. Epileptic high-frequency network activity in a model of non-lesional temporal lobe epilepsy. Brain 133 (5), 1380–1390.

Jiruska, P., Alvarado-Rojas, C., Schevon, C.A., Staba, R., Stacey, W., Wendling, F., Avoli, M., 2017. Update on the mechanisms and roles of high-frequency oscillations in seizures and epileptic disorders. Epilepsia 58 (8), 1330–1339.

Jiruska, P., Freestone, D., Gnatkovsky, V., Wang, Y., 2023. An update on the seizures beget seizures theory. doi: 10.1111/epi.17721. Epub ahead of print. (accepted).

Kerber, K., LeVan, P., Dümpelmann, M., Fauser, S., Korinthenberg, R., Schulze-Bonhage, A., Jacobs, J., 2013. High frequency oscillations mirror disease activity in patients with focal cortical dysplasia. Epilepsia 54 (8), 1428–1436.

Koh, H.Y., Jang, J., Ju, S.H., Kim, R., Cho, G.B., Kim, D.S., Sohn, J.W., Paik, S.B., Lee, J. H., 2021. Non-cell autonomous epileptogenesis in focal cortical dysplasia. Ann. Neurol. 90 (2), 285–299.

Kucewicz, M.T., Cimbalnik, J., Matsumoto, J.Y., Brinkmann, B.H., Bower, M.R., Vasoli, V., Sulc, V., Meyer, F., Marsh, W.R., Stead, S.M., Worrell, G.A., 2014. High frequency oscillations are associated with cognitive processing in human recognition memory. Brain 137 (8), 2231–2244. https://doi.org/10.1093/brain/awu149.

Kudlacek, J., Chvojka, J., Posusta, A., Kovacova, L., Hong, S.B., Weiss, S., Volna, K., Marusic, P., Otahal, J., Jiruska, P., 2017. Lacosamide and levetiracetam have no effect on sharp-wave ripple rate. Front. Neurol. 8, 687.

Lévesque, M., Bortel, A., Gotman, J., Avoli, M., 2011. High-frequency (80–500 Hz) oscillations and epileptogenesis in temporal lobe epilepsy. Neurobiol. Dis. 42 (3), 231–241. https://doi.org/10.1016/j.nbd.2011.01.007.

Levesque, M., Wang, S., Etter, G., Williams, S., Avoli, M., 2022. Bilateral optogenetic activation of inhibitory cells favors ictogenesis. Neurobiol. Dis. 171, 105794.

Li, L., Kumar, U., You, J., Zhou, Y., Weiss, S.A., Engel, J., Bragin, A., 2022. Spatial and temporal profile of high-frequency oscillations in posttraumatic epileptogenesis. Neurobiol. Dis. 161, 105544.

Lim, J.S., Kim, W.I., Kang, H.C., Kim, S.H., Park, A.H., Park, E.K., Cho, Y.W., Kim, S.W., Kim, H.M., Kim, J.A., 2015. Brain somatic mutations in MTOR cause focal cortical dysplasia type II leading to intractable epilepsy. Nat. Med. 21 (4), 395–400.

Proietti Onori, M., Koene, L.M.C., Schäfer, C.B., Nellist, M., De Brito Van Velze, M., Gao, Z., Elgersma, Y., Van Woerden, G.M., 2021. RHEB/mTOR hyperactivity causes cortical malformations and epileptic seizures through increased axonal connectivity. PLoS Biol. 19 (5), e3001279.

Purtell, H., Dhamne, S.C., Gurnani, S., Bainbridge, E., Modi, M.E., Lammers, S.H.T., Super, C.E., Hameed, M.Q., Johnson, E.L., Sahin, M., Rotenberg, A., 2018. Electrographic spikes are common in wildtype mice. Epilepsy Behav. 89, 94–98.

Reid, A.Y., Bragin, A., Giza, C.C., Staba, R.J., Engel Jr., J., 2016. The progression of electrophysiologic abnormalities during epileptogenesis after experimental traumatic brain injury. Epilepsia 57 (10), 1558–1567.

Sheybani, L., Birot, G., Contestabile, A., Seeck, M., Kiss, J.Z., Schaller, K., Michel, C.M., Quairiaux, C., 2018. Electrophysiological evidence for the development of a self-sustained large-scale epileptic network in the Kainate mouse model of temporal lobe epilepsy. J. Neurosci. 38 (15), 3776–3791.

Staba, R.J., Wilson, C.L., Bragin, A., Fried, I., Engel Jr., J., 2002. Quantitative analysis of high-frequency oscillations (80–500 Hz) recorded in human epileptic hippocampus and entorhinal cortex. J. Neurophysiol. 88 (4), 1743–1752.

Susaki, E.A., Tainaka, K., Perrin, D., Kishino, F., Tawara, T., Watanabe, T.M., Yokoyama, C., Onoe, H., Eguchi, M., Yamaguchi, S., 2014. Whole-brain imaging with single-cell resolution using chemical cocktails and computational analysis. Cell 157 (3), 726–739.

Thomas, J., Kahane, P., Abdallah, C., Avigdor, T., Zweiphenning, W.J.E.M., Chabardes, S., Jaber, K., Latreille, V., Minotti, L., Hall, J., 2023. A subpopulation of spikes predicts successful epilepsy surgery outcome. Ann. Neurol. 93 (3), 522–535.

Urrestarazu, E., Chander, R., Dubeau, F., Gotman, J., 2007. Interictal high-frequency oscillations (100-500 Hz) in the intracerebral EEG of epileptic patients. Brain 130, 2354–2366.

Weiss, S.A., Sheybani, L., Seenarine, N., Fried, I., Wu, C., Sharan, A., Engel Jr., J., Sperling, M.R., Nir, Y., Staba, R.J., 2022. Delta oscillation coupled propagating fast ripples precede epileptiform discharges in patients with focal epilepsy. Neurobiol. Dis. 175, 105928.

Wykes, R.C., Heeroma, J.H., Mantoan, L., Zheng, K., MacDonald, D.C., Deisseroth, K., Hashemi, K.S., Walker, M.C., Schorge, S., Kullmann, D.M., 2012. Optogenetic and potassium channel gene therapy in a rodent model of focal neocortical epilepsy. Sci. Transl. Med. 4 (161) (161–152).

Zijlmans, M., Jiruska, P., Zelmann, R., Leijten, F.S.S., Jefferys, J.G.R., Gotman, J., 2012. High-frequency oscillations as a new biomarker in epilepsy. Ann. Neurol. 71 (2), 169–178.

4 Lacosamide and Levetiracetam Have No Effect on Sharp-Wave Ripple Rate

4.1 The contributions toward the progress of the field

Based on the evidence from both the experimental and human studies (Zijlmans et al., 2009; Behr et al., 2015), anti-seizure medication (ASM) decreases the HFO rate among individuals with epilepsy. In this experimental study conducted on healthy subjects, the authors explored whether physiological HFOs of hippocampal origin respond to ASM treatment. Levetiracetam and lacosamide, two commonly used ASMs, do not reduce the rate of physiological HFOs. These findings, together, offer a new tool for epilepsy diagnosis. Monitoring the change in HFO rate in response to changes in AED treatment has two novel applications.

Marker of epileptogenic tissue A significant change in the HFO rate can help identify epileptogenic tissue, while no change indicates healthy tissue. Such tests could be introduced toward the end of invasive exploration, guiding resection planning, and ultimately resulting in better surgical outcomes.

Personalization of treatment The quantification of changes in the rate of HFOs and gamma-ripple activity in response to ASM treatment or withdrawal can effectively serve as a subject-specific parameter. This parameter can be utilized to personalize HFO detection algorithms or any other method that currently lacks knowledge about the individual's specific epilepsy features.

4.2   The author's contributions

The author was responsible for running the experiment including animal welfare, conducting video-EEG monitoring, data collection and management, and subsequent analysis. The author labeled the artifact-free EEG and video, implemented techniques of automated HFO detection, visually reviewed and quantified the HFOs, and contributed to the manuscript writing. The author presented the work at several conferences.

4.3   Compliance with the thesis objectives

The outcomes of the study not only provide an important insight into the field of HFO research but most importantly, have a direct application to epilepsy diagnosis.

Lacosamide and Levetiracetam Have No Effect on Sharp-Wave Ripple Rate

Jan Kudlacek[1,2], Jan Chvojka[1,2], Antonin Posusta[1], Lubica Kovacova[1], Seung Bong Hong[3,4], Shennan Weiss[5], Kamila Volna[6], Petr Marusic[6], Jakub Otahal[1†] and Premysl Jiruska[1*†]

[1]Department of Developmental Epileptology, Institute of Physiology, The Czech Academy of Sciences, Prague, Czechia, [2]Department of Circuit Theory, Faculty of Electrical Engineering, Czech Technical University in Prague, Prague, Czechia, [3]Department of Neurology, Samsung Medical Center, Samsung Advanced Institute for Health Sciences & Technology (SAIHST), Sungkyunkwan University School of Medicine, Seoul, South Korea, [4]Samsung Biomedical Research Institute, Seoul, South Korea, [5]Department of Neurology, Thomas Jefferson University, Philadelphia, PA, United States, [6]Department of Neurology, 2nd Faculty of Medicine, Charles University and Motol University Hospital, Prague, Czechia

Pathological high-frequency oscillations are a novel marker used to improve the delineation of epileptogenic tissue and, hence, the outcome of epilepsy surgery. Their practical clinical utilization is curtailed by the inability to discriminate them from physiological oscillations due to frequency overlap. Although it is well documented that pathological HFOs are suppressed by antiepileptic drugs (AEDs), the effect of AEDs on normal HFOs is not well known. In this experimental study, we have explored whether physiological HFOs (sharp-wave ripples) of hippocampal origin respond to AED treatment. The results show that application of a single dose of levetiracetam or lacosamide does not reduce the rate of sharp-wave ripples. In addition, it seems that these new generation drugs do not negatively affect the cellular and network mechanisms involved in sharp-wave ripple generation, which may provide a plausible explanation for the absence of significant negative effects on cognitive functions of these drugs, particularly on memory.

Keywords: high-frequency oscillations, sharp-wave ripples, levetiracetam, lacosamide, antiepileptic drugs, hippocampus, ripples, *in vivo*

HIGHLIGHTS

- Pathological high-frequency oscillations (pHFOs) represent electrographic biomarker of epileptogenic tissue.
- Current approaches are not able to distinguish pathological HFOs from physiological ones in intracranial recordings.
- Antiepileptic drugs decrease the rate of pHFOs.
- Levetiracetam or lacosamide do not decrease the rate of sharp-wave ripples—a representative of physiological HFOs.
- Pharmacological testing could be used to discriminate pathological and physiological HFOs.

INTRODUCTION

Pathological high-frequency oscillations (pHFOs) represent a new electrographic marker of epileptogenic tissue. Early after their discovery, pHFO analysis was introduced into the presurgical evaluation to better delineate the resection margin and to improve the outcome of surgery. pHFOs are classified according to their frequency into two main groups—ripples (80–250 Hz) and fast ripples (250–600 Hz) (1, 2). Although fast ripples are considered more specific for epileptogenic tissue than ripples, both types of pHFO can localize the epileptogenic zone or seizure onset areas in humans

who undergo exploration with invasive electrodes (1, 2). Several studies have demonstrated the beneficial effect of complete resection of the pHFO generating areas on surgical outcome (3–5). The practical utilization of pHFOs in presurgical evaluation is substantially hindered by the inability to differentiate them from physiological high-frequency oscillations, such as hippocampal sharp-wave ripples (SWRs) as they display substantial frequency overlap (2, 6, 7). Currently, we do not have any effective tools, which can reliably discriminate between them. Identification of an approach to reliably discriminate between normal and pathological HFOs is a complex, but essential, issue to address if the properties of pHFOs are to be fully utilized in clinical practice.

One of the features of pHFOs is their responsiveness to antiepileptic drugs (AEDs). In the chronic pilocarpine model of temporal lobe epilepsy, pHFOs and seizure rate decrease after treatment with levetiracetam (8) or lacosamide (9). In humans, withdrawal of AEDs is associated with increased rate of pHFOs (10). A pharmacological test using AEDs could be a plausible strategy to discriminate physiological oscillations from pathological ones, providing rate of physiological HFOs is not decreased by AEDs.

In this proof-of-principle study, we explored the impact of a single dose of lacosamide or levetiracetam on the rate of SWRs—a hippocampal representative of physiological HFOs (11). SWRs play a crucial role in the process of coordinated memory reactivation and formation of long-term memory (12). We have tested the hypothesis that the application of a single therapeutic dose of levetiracetam or lacosamide does not affect SWR rate.

MATERIALS AND METHODS

Electrode Implantation and EEG Recording

All experiments were performed under the Animal Care and Animal Protection Law of the Czech Republic fully compatible with the guidelines of the European Union directive 2010/63/EU. The protocol was approved by the Ethics Committee of The Czech Academy of Sciences (Project License No. 71/2016). Animals were housed in groups under standard conditions in a room with controlled temperature ($22 \pm 1°C$) and 12/12 h light/dark cycle. Eleven adult male Wistar rats weighing between 350 and 430 g were used in this study. The surgical preparation was performed under isoflurane anesthesia. The animals were implanted with bipolar twisted silver electrodes (120 µm in diameter, AM Systems, Inc., USA) bilaterally in the stratum pyramidale (AP: −4.1, L: 2.2, D: 2.5) and stratum radiatum (AP: −4.6, L: 2.6, D: 2.6) of the dorsal CA1 according to the stereotaxic atlas (13). The two contacts of each electrode were 0.5 mm apart. Two ground/reference jeweler's screws were placed over the cerebellum. Following a 5-day recovery period, animals were individually video-EEG monitored for 4 weeks continuously. Spontaneous electrographic activity was amplified, band-pass filtered (0.1 Hz–1.6 kHz), and digitized at 5 kHz using a RHD2132 32-channel amplifier chip (Intan Technologies, USA). After the end of the experiment, animals were humanely euthanized by an overdose of urethane, brains extracted, and processed to verify the positions of electrodes (**Figure 1E**).

AED Treatment

Each animal received sequential intraperitoneal injections of levetiracetam (Keppra®, UCB, S.A., Brussels, Belgium), saline (control solution) of equal volume, lacosamide (Vimpat®, UCB, S.A., Brussels, Belgium), and saline of equal volume. Additionally, three of the animals received diazepam (Apaurin®, Krka, d. d., Novo Mesto, Slovenia) and saline of equal volume.
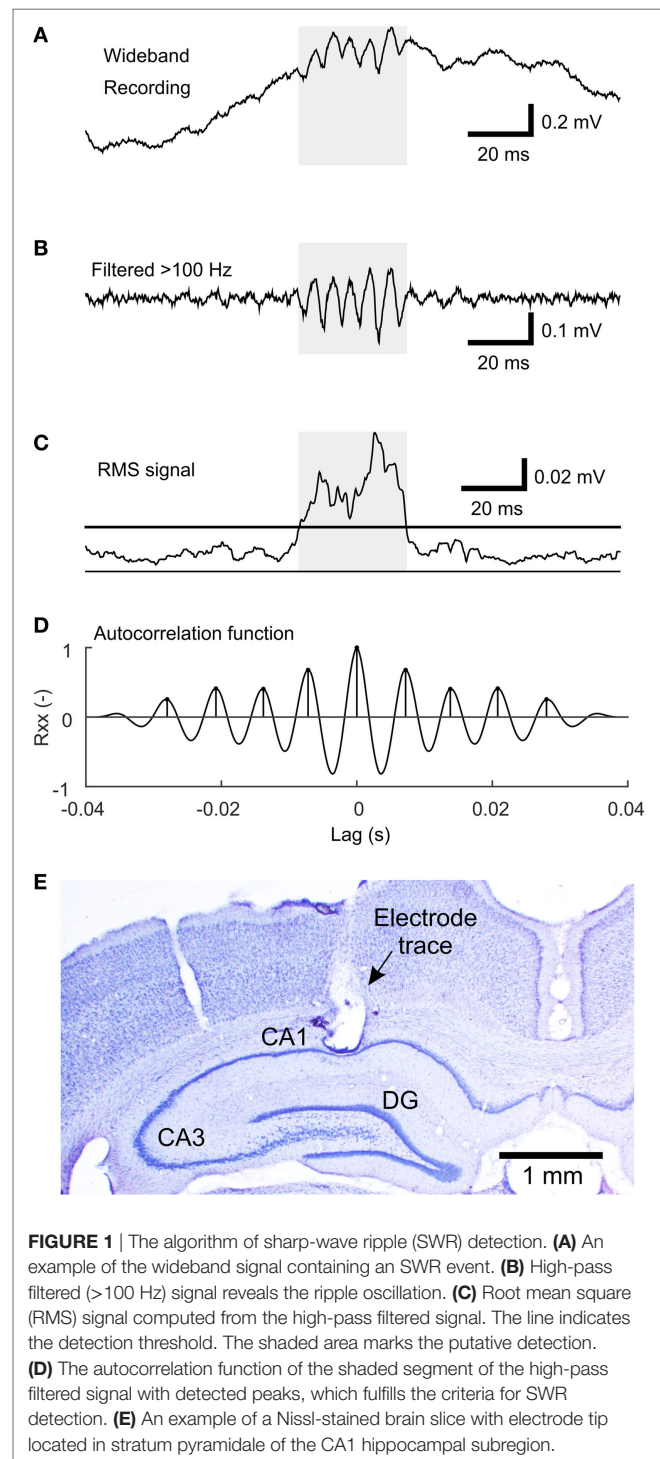
FIGURE 1 | The algorithm of sharp-wave ripple (SWR) detection. **(A)** An example of the wideband signal containing an SWR event. **(B)** High-pass filtered (>100 Hz) signal reveals the ripple oscillation. **(C)** Root mean square (RMS) signal computed from the high-pass filtered signal. The line indicates the detection threshold. The shaded area marks the putative detection. **(D)** The autocorrelation function of the shaded segment of the high-pass filtered signal with detected peaks, which fulfills the criteria for SWR detection. **(E)** An example of a Nissl-stained brain slice with electrode tip located in stratum pyramidale of the CA1 hippocampal subregion.

Diazepam acted as a positive control since it was shown to decrease the SWR rate *in vivo* (14). The interval after each injection, whether it was an AED or saline, was 3 days to allow maximal elimination of the drug from the body based on the known pharmacokinetics (14–16). The doses for levetiracetam and lacosamide were 80 and 30 mg/kg, respectively. At comparable doses, these drugs were shown to effectively suppress pHFOs (8, 9). The dose of diazepam was 1 mg/kg which was shown to reduce or even suppress the SWR rate (14, 17). The sequence of injections was randomized between animals. In a given rat, every injection was administered at the same time of the day (10:30 a.m. or 2:00 p.m.).

EEG Analysis

EEGs were analyzed using custom made scripts in Matlab 2015a computing environment (Mathworks Inc., Natick, MA, USA). Two animals were removed from the analysis due to extremely noisy EEG signals. In one animal, the experiment was terminated prematurely due to the loss of the head cap prior to lacosamide injection. Therefore, the total number of animals used in the evaluation of the three drugs was nine for levetiracetam, eight for lacosamide, and three for diazepam. In each animal, SWRs were analyzed only in the channel in which SWRs displayed the highest amplitude. Correct positions of these electrodes in the hippocampal CA1 were verified histologically. We analyzed two epochs each lasting 2 h. The first epoch was from 0.5 to 2.5 h after the injection and the second one was from 4.5 to 6.5 h after the injection. To determine the SWR rate during the same brain state, we extracted episodes of slow-wave sleep only, from each epoch, based on the presence of slow waves in the EEG and verified behaviorally in video recordings.

SWR Detection

Sharp-wave ripples were detected using the modified root mean square (RMS)-based approach (18). The signal was band-pass filtered (passband 100–200 Hz) using a FIR filter with a 40-Hz wide transition band and stopband attenuation at 80 dB. RMS value was calculated in 4 ms sliding windows. Only segments of at least 18 ms in duration with an RMS value >1.5 SD above the RMS mean were selected as putative SWRs. Events closer than 10 ms were treated as a single event. The next step of the detection procedure included estimation of the autocorrelation function in high-pass filtered segments (>100 Hz, otherwise the same parameters). Detections with at least seven peaks in the autocorrelation function with a lag corresponding to the SWR frequency band (100–200 Hz) and with the second peak of at least 25% of magnitude were selected. The main steps of the detection procedure are visualized in **Figures 1A–D**.

To evaluate the detector's performance, 24 randomly selected epochs of slow-wave sleep were labeled by an expert. Automatic detections were compared to the expert's labels. A true positive (TP) detection was defined as the one overlapping with an expert's label by at least 50% of the detection's duration. A false positive (FP) detection was a detection not fulfilling the criteria for TP detection. The number of false negatives (FN) was defined as the number of expert's labels, which had no overlap with any of the TP detections. Finally, sensitivity and positive predictive value (PPV) of the detector was calculated using the following equations:

$$\text{sensitivity} = \frac{TP}{TP + FN}$$

$$PPV = \frac{TP}{TP + FP}.$$

Sensitivity and PPV of the detector was 57 and 80%, respectively. Detector's settings were optimized to achieve mainly high PPV to detect only true SWRs, omit ambiguous SWRs, and to minimize the risk of FP detections.

Statistical Evaluation

In this study, the primary hypothesis tested was that injections of selected AEDs do not affect SWR rates. This is in contrast to the vast majority of drug studies, which examine and test for the presence of an effect of the drug on specific phenomena, including HFOs. Thus, we had to implement an appropriate statistical method that tests equality and not an effect. In this study, we adopted the method recommended by Piaggio et al. (19). For each rat, each injection and each time after the injection we calculated average SWR rate during the slow-wave sleep epochs. Then, for each rat, each drug and each time after the injection, we calculated the ratio of SWR rate after AED injection to SWR rate after the corresponding saline injection. Since the data did not display normal distribution, we used a non-parametric approach. For each drug and each time after the injection, median of the ratios and its non-parametric confidence interval was calculated. The non-parametric confidence interval for the median is obtained as the *k*-th lowest and the *k*-th highest value from the sample. *k* is determined so that the true population median lies within that interval with confidence equal or higher than required. In our study, we required at least 90% confidence. For sample sizes nine and eight we took *k* = 2 which gives confidences of 96 and 93%, respectively. For the three diazepam animals, we took the first and the last value as the confidence interval (widest possible), which gives up to 75% confidence (20). We obtained confidence intervals for all three drugs and two time windows after the injections. These six confidence intervals were compared to equality margins, which were set to 0.75 and 1.25. If the confidence interval did not cross the equality margins, the AED was considered to have no effect on SWR rate.

Following equality testing, we performed statistical analysis to evaluate the possible presence of a statistically significant effect of AEDs on the SWR rate. In this step, we used the Wilcoxon signed-rank test on each set of the ratios. Before applying the test, the ratios were transformed by subtracting 1 so that a decrease in the SWR rate resulted in a negative number and *vice versa*. In the case of a non-significant result, *post hoc* power of the Wilcoxon signed-rank test was determined using SD of the data and location shift equal to the equality margin, i.e., 0.25 (21, 22).

RESULTS

In total 43,011 SWRs were detected with 4,779 ± 3,125 events per animal. The average SWR rate was 16.0 events/min, which

34

is congruent with studies focused on SWR *in vivo* (11, 23–25). SWR rates of all animals, after each injection, in both analyzed time windows, are shown in **Figure 2**. The data revealed the presence of individual variability in the SWR rate and response to the tested drugs. The crucial parameter for examination of the effect of an AED is the ratio between the SWR rate after AED injection and the SWR rate after control saline injection (**Figure 3**). The median ratio of the SWR rate between levetiracetam and

the control was 0.91 and 0.98 for 30 min and 4.5 h after the injection, respectively ($n = 9$ animals). For levetiracetam, the ratios' confidence intervals did not cross the equality margins 30 min and 4.5 h after injection (**Figure 4**). Therefore, SWR rates after levetiracetam and saline treatment can be considered equal within the equality margins. The Wilcoxon signed-rank test for ratios was non-significant for 30 min ($p = 0.30$) and 4.5 h after the injection ($p = 0.57$), with a *post hoc* power of 88%. For lacosamide, the median ratio of the SWR rate was 1.14 and 1.22 for each time epoch ($n = 8$ animals). The confidence intervals of the SWR rate ratios crossed the equality margins in both time windows. The Wilcoxon signed-rank test demonstrated a significant increase in SWR rate ratio 30 min after injection of lacosamide ($p = 0.039$). After 4.5 h the effect of lacosamide was non-significant (Wilcoxon signed-rank test; $p = 0.11$; power = 85%). Diazepam, which was used as a positive control, reduced the SWR rate compared to the equivalent volume of saline in all rats by >50% with a median ratio of 0.46 and 0.70 for each time window (**Figure 4**). However, statistical significance could not be reached due to the small number of rats ($n = 3$ animals; Wilcoxon signed-rank test; $p = 0.25$; power = 46%).

DISCUSSION

We have shown that a single dose of levetiracetam and lacosamide does not reduce the rate of SWRs—a representative of physiological HFOs. The ability to reliably differentiate between pathological and physiological HFOs represents a crucial step
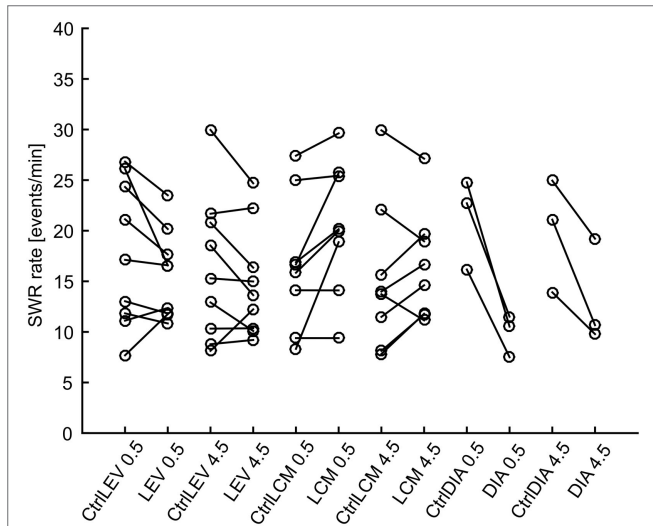
FIGURE 2 | Sharp-wave ripple (SWR) rates after various treatments. Lines connect data points from individual animals. LEV, levetiracetam; LCM, lacosamide; DIA, diazepam; CtrlXXX, injection of equivalent volume of saline; 0.5, half an hour after injection, 4.5, four and half hours after injection.
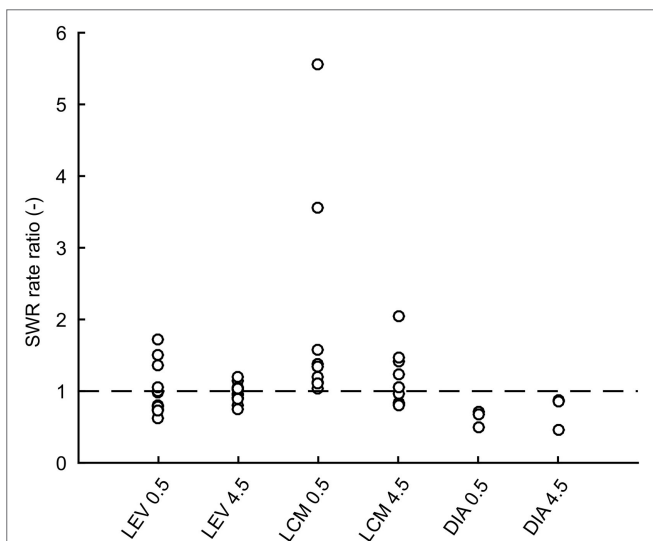
FIGURE 3 | Ratios of sharp-wave ripple (SWR) rates after drug treatment to rates after saline treatment for individual rats. Dashed line is at value 1 which constitutes no effect. LEV, levetiracetam; LCM, lacosamide; DIA, diazepam; CtrlXXX, injection of an equivalent volume of saline; 0.5, half an hour after injection; 4.5, four and half hours after injection.
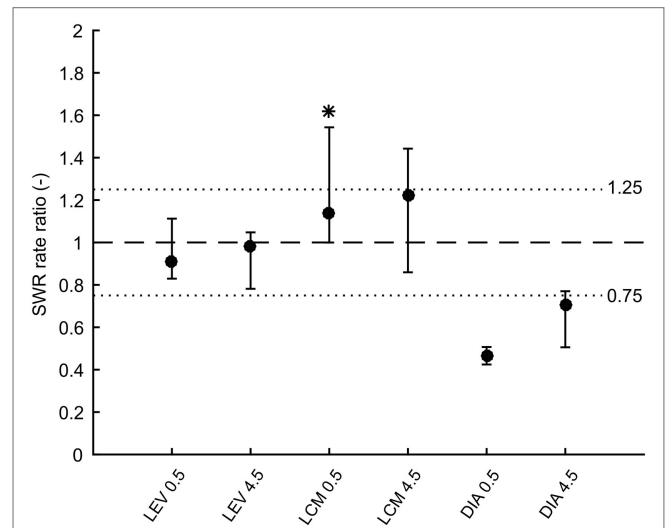
FIGURE 4 | Medians of ratios of sharp-wave ripple (SWR) rates after drug injection to rates after corresponding saline injection. Error bars represent non-parametric confidence intervals of the medians. Dashed line is at value 1 which constitutes no effect. Dotted lines at values 0.75 and 1.25 represent equality margins. LEV confidence intervals are at 96% confidence and do not cross the equality margins. LCM significantly increases SWR rate 0.5 h after administration, but 4.5 h after administration the effect dissipates. Confidence intervals are 93%. DIA markedly reduces SWR rate 0.5 h after administration and 4.5 h after administration the effect slowly dissipates. Confidence intervals are 75%. LEV, levetiracetam; LCM, lacosamide; DIA, diazepam.

toward the clinical utilization of pHFOs as biomarkers of the epileptogenic zone (2, 7). Epileptic pHFOs display a spectral overlap with physiological HFOs such as SWRs or fast gamma activity. Fast ripples are considered to be exclusively of epileptic origin, but physiological activity with a frequency around ~600 Hz has been described in the neocortex. Matsumoto and colleagues described features, which discriminated task-related physiological HFOs from pathological ones (26). Pathological HFOs were characterized by a higher spectral mean, longer duration, and lower mean frequency. Other studies tried to discriminate HFOs according to their spatial distribution, relationship with sleep phases (27), background activity (28), phase relationship with slow waves (29), or using cognitive tasks (30). However, the practical implementation of these criteria is challenging. Experimental treatment with levetiracetam or lacosamide has been shown to reduce the both ripples and fast ripples in the pilocarpine model of temporal lobe epilepsy, even though the effects were region specific (8, 9). In this *in vivo* study, we demonstrate that levetiracetam does not decrease the rate of hippocampal SWRs. The confidence intervals were set to tolerate a 25% change in SWR rate after the treatment. Studies which explored the effect of levetiracetam and lacosamide on pHFOs showed that these drugs reduced the pathological ripple rate in hippocampal structures by an average of 57% for levetiracetam and by 43% for lacosamide (8, 9). Although we studied the effect of these AEDs only on specific subtype of physiological HFOs, these experimental results suggest that the procedure of pharmacological testing can be a plausible approach to facilitate discrimination between physiological and pathological HFOs. Both drugs are used very frequently and their withdrawal and subsequent introduction is a very common procedure in patients undergoing invasive explorations. As an alternative, the introduction of AEDs could be replaced by an intravenous application of levetiracetam at the end of monitoring. HFOs that are not altered by AEDs can be considered to be physiological HFOs.

The absence of a major effect of the AEDs on the rate of SWRs and suppression of pHFOs can be explained by the currently known mechanisms of action of the drugs and cellular mechanisms of HFOs (31, 32). SWRs are oscillations that reflect the activation of large neuronal ensembles in the hippocampal CA1 region, particularly during sleep. On the cellular level, the oscillation depends on the precise interaction between pyramidal cells and inhibitory interneurons. The fast inhibitory postsynaptic potentials on the membrane of principal neurons play a key role in the coordination of principal cell firing (11). Pyramidal cells fire heterogeneously during the SWR; some cells can fire during every successive event, while other cells can fire only occasionally (17, 33). The sequence of neuronal activity during SWRs replays the sequence of neuronal activation during behavioral tasks, and it is considered to represent a mechanism of memory reactivation and long-term memory formation (12, 34). The cellular dynamics of pHFOs in both ripple and fast ripple bands differs and is more uniform (31, 32). During each pHFO, a large population of cells generates a burst of high-frequency action potentials superimposed on a large depolarizing envelope (35–37). While high-frequency spiking depends mainly on fast sodium channel kinetics, the depolarizing envelope is associated with an increase

in intracellular calcium *via* the opening of voltage-gated calcium channels or activation of non-NMDA and NMDA receptors. Lacosamide modifies voltage-gated sodium channel kinetics required for fast action potential firing, and it affects only neurons which are active or depolarized for prolonged periods of time and thus spares physiological functions (38). Therefore, pathological pHFOs are more susceptible to its effects than SWRs. The levetiracetam binds to SV2A, which is involved in trafficking and fusion of synaptic vesicles (39). It seems that levetiracetam reduces the vesicle release that is important for synaptic neurotransmission (40). It also partially blocks N-type calcium channels (41). However, the exact mechanisms of its actions are not well known, but we can assume that levetiracetam is capable of interfering with cellular processes involved in intense neuronal firing and pHFOs.

The absence of the effect of levetiracetam and lacosamide on the mechanisms of SWRs, in general, can also be deduced indirectly from the lack of their negative effect on cognitive functions including memory. It is well established that any drug or procedure, which has the capacity to interfere with the cellular mechanisms underlying the genesis of SWRs, also has the capacity to induce a memory deficit (42, 43). Levetiracetam is currently the drug of first choice, and lacosamide has also shown its therapeutic benefits as add-on therapy early after its introduction into epilepsy therapy. Both drugs are well tolerated by patients and demonstrate low adverse effects and an absence of a significant impact on cognition and memory (44–47). From electrophysiological perspective, these observations are supported by our experimental study, which demonstrates the absence of any suppressive effect of these drugs on the SWR generation. Moreover, lacosamide was shown to increase the speed of complex visual information processing (48), which may be in agreement with the transiently increased SWR rate observed in this study.

A possible limitation of this study is the single-dose scheme of drug administration. We might have missed the time period of SWR suppression by the drug. However, based on the known pharmacokinetics and mechanism of action of these drugs this seems unlikely (15, 16, 38, 49). Another possibility is that the drug was cleared from the body before its concentration in the brain could have reached sufficient intrathecal levels to influence the SWR rate. However, we used the same dose that was administered daily in studies exploring the effect of lacosamide and levetiracetam on pHFOs (8, 9) and pharmacokinetic studies showed that these drugs reach maximal brain concentration within 2 h after application (15, 16). Another weakness of the study is the single-dose application. We cannot exclude that prolonged or chronic application of these drugs may induce long-term changes, which would affect the properties of SWRs.

In conclusion, we have shown that levetiracetam does not change the rate of SWRs and lacosamide transiently increases it. Hence, these drugs can be considered for pharmacological testing to distinguish physiological versus pHFOs. Levetiracetam or lacosamide could be introduced toward the end of invasive exploration, and the response of HFOs to the drug introduction could be used to determine whether the HFOs are pathological or physiological. Moreover, our results are congruent with studies showing no negative effect of these drugs on cognition.

ETHICS STATEMENT

AUTHOR CONTRIBUTIONS

Conceived and designed the experiments: PJ, JO, PM, and SH. Performed the experiments: JC, JK, and LK. Analyzed the data: JC, JK, LK, AP, PJ, and JO. Wrote the paper: JC, JK, PJ, KV, SW, PM, JO, and SH.

ACKNOWLEDGMENTS

REFERENCES

1. Zijlmans M, Jiruska P, Zelmann R, Leijten FS, Jefferys JG, Gotman J. High-frequency oscillations as a new biomarker in epilepsy. *Ann Neurol* (2012) 71:169–78. doi:10.1002/ana.22548

2. Frauscher B, Bartolomei F, Kobayashi K, Cimbalnik J, van 't Klooster MA, Rampp S, et al. High-frequency oscillations: the state of clinical research. *Epilepsia* (2017) 58:1316–29. doi:10.1111/epi.13829.

3. Jacobs J, Zijlmans M, Zelmann R, Chatillon CE, Hall J, Olivier A, et al. High-frequency electroencephalographic oscillations correlate with outcome of epilepsy surgery. *Ann Neurol* (2010) 67:209–20. doi:10.1002/ana.21847

4. Cho JR, Koo DL, Joo EY, Seo DW, Hong SC, Jiruska P, et al. Resection of individually identified high-rate high-frequency oscillations region is associated with favorable outcome in neocortical epilepsy. *Epilepsia* (2014) 55:1872–83. doi:10.1111/epi.12808

5. Holler Y, Kutil R, Klaffenbock L, Thomschewski A, Holler PM, Bathke AC, et al. High-frequency oscillations in epilepsy and surgical outcome. A meta-analysis. *Front Hum Neurosci* (2015) 9:574. doi:10.3389/fnhum.2015.00574

6. Engel J Jr, Bragin A, Staba R, Mody I. High-frequency oscillations: what is normal and what is not? *Epilepsia* (2009) 50:598–604. doi:10.1111/j.1528-1167.2008.01917.x

7. Cimbalnik J, Kucewicz MT, Worrell G. Interictal high-frequency oscillations in focal human epilepsy. *Curr Opin Neurol* (2016) 29:175–81. doi:10.1097/WCO.0000000000000302

8. Levesque M, Behr C, Avoli M. The anti-ictogenic effects of levetiracetam are mirrored by interictal spiking and high-frequency oscillation changes in a model of temporal lobe epilepsy. *Seizure* (2015) 25:18–25. doi:10.1016/j.seizure.2014.11.008

9. Behr C, Levesque M, Ragsdale D, Avoli M. Lacosamide modulates interictal spiking and high-frequency oscillations in a model of mesial temporal lobe epilepsy. *Epilepsy Res* (2015) 115:8–16. doi:10.1016/j.eplepsyres.2015.05.006

10. Zijlmans M, Jacobs J, Zelmann R, Dubeau F, Gotman J. High-frequency oscillations mirror disease activity in patients with epilepsy. *Neurology* (2009) 72:979–86. doi:10.1212/01.wnl.0000344402.20334.81

11. Ylinen A, Bragin A, Nadasdy Z, Jando G, Szabo I, Sik A, et al. Sharp wave-associated high-frequency oscillation (200 Hz) in the intact hippocampus: network and intracellular mechanisms. *J Neurosci* (1995) 15:30–46.

12. Buzsáki G. Hippocampal sharp wave-ripple: a cognitive biomarker for episodic memory and planning. *Hippocampus* (2015) 25:1073–188. doi:10.1002/hipo.22488

13. Paxinos G, Watson C. The rat brain. 4th ed. *The Rat Brain in Stereotaxic Coordinates*. San Diego, CA: Academic Press, Inc (1998). 474 p.

14. Ponomarenko AA, Korotkova TM, Sergeeva OA, Haas HL. Multiple GABAA receptor subtypes regulate hippocampal ripple oscillations. *Eur J Neurosci* (2004) 20:2141–8. doi:10.1111/j.1460-9568.2004.03685.x

15. Tong X, Patsalos PN. A microdialysis study of the novel antiepileptic drug levetiracetam: extracellular pharmacokinetics and effect on taurine in rat brain. *Br J Pharmacol* (2001) 133:867–74. doi:10.1038/sj.bjp.0704141

16. Koo TS, Kim SJ, Ha DJ, Baek M, Moon H. Pharmacokinetics, brain distribution, and plasma protein binding of the antiepileptic drug lacosamide in rats. *Arch Pharm Res* (2011) 34:2059–64. doi:10.1007/s12272-011-1208-7

17. Buzsaki G, Horvath Z, Urioste R, Hetke J, Wise K. High-frequency network oscillation in the hippocampus. *Science* (1992) 256:1025–7. doi:10.1126/science.1589772

18. Staba RJ, Wilson CL, Bragin A, Fried I, Engel J Jr. Quantitative analysis of high-frequency oscillations (80–500 Hz) recorded in human epileptic hippocampus and entorhinal cortex. *J Neurophysiol* (2002) 88:1743–52. doi:10.1152/jn.00322.2002

19. Piaggio G, Elbourne DR, Pocock SJ, Evans SJ, Altman DG, CONSORT Group. Reporting of noninferiority and equivalence randomized trials: extension of the CONSORT 2010 statement. *JAMA* (2012) 308:2594–604. doi:10.1001/jama.2012.87802

20. Hogg RV, Tanis EA. *Probability and Statistical Inference*. New Jersey: Prentice Hall (2006).

21. Lehmann EL. *Nonparametrics: Statistical Methods Based on Ranks*. San Francisco: Holden-day, Inc. (1975).

22. Shieh G, Jan S-L, Randles RH. Power and sample size determinations for the Wilcoxon signed-rank test. *J Stat Comput Simul* (2007) 77:717–24. doi:10.1080/10629360600635245

23. Csicsvari J, Hirase H, Czurko A, Mamiya A, Buzsaki G. Fast network oscillations in the hippocampal CA1 region of the behaving rat. *J Neurosci* (1999) 19:Rc20.

24. Eschenko O, Ramadan W, Mölle M, Born J, Sara SJ. Sustained increase in hippocampal sharp-wave ripple activity during slow-wave sleep after learning. *Learn Mem* (2008) 15:222–8. doi:10.1101/lm.726008

25. Cheng S, Frank LM. New experiences enhance coordinated neural activity in the hippocampus. *Neuron* (2008) 57:303–13. doi:10.1016/j.neuron.2007.11.035

26. Matsumoto A, Brinkmann BH, Matthew Stead S, Matsumoto J, Kucewicz MT, Marsh WR, et al. Pathological and physiological high-frequency oscillations in focal human epilepsy. *J Neurophysiol* (2013) 110:1958–64. doi:10.1152/jn.00341.2013

27. Frauscher B, von Ellenrieder N, Dubeau F, Gotman J. EEG desynchronization during phasic REM sleep suppresses interictal epileptic activity in humans. *Epilepsia* (2016) 57:879–88. doi:10.1111/epi.13389

28. Kerber K, Dumpelmann M, Schelter B, Le Van P, Korinthenberg R, Schulze-Bonhage A, et al. Differentiation of specific ripple patterns helps to identify epileptogenic areas for surgical procedures. *Neurophysiol Clin* (2014) 125:1339–45. doi:10.1016/j.clinph.2013.11.030

29. von Ellenrieder N, Frauscher B, Dubeau F, Gotman J. Interaction with slow waves during sleep improves discrimination of physiologic and pathologic high-frequency oscillations (80–500 Hz). *Epilepsia* (2016) 57:869–78. doi:10.1111/epi.13380

30. Axmacher N, Elger CE, Fell J. Ripples in the medial temporal lobe are relevant for human memory consolidation. *Brain* (2008) 131:1806–17. doi:10.1093/brain/awn103

31. Jefferys JG, Menendez de la PL, Wendling F, Bragin A, Avoli M, Timofeev I, et al. Mechanisms of physiological and epileptic HFO generation. *Prog Neurobiol* (2012) 98:250–64. doi:10.1016/j.pneurobio.2012.02.005

37

32. Jiruska P, Alvarado-Rojas C, Schevon CA, Staba R, Stacey W, Wendling F, et al. Update on the mechanisms and roles of high-frequency oscillations in seizures and epileptic disorders. *Epilepsia* (2017) 58:1330–9. doi:10.1111/epi.13830

33. Csicsvari J, Hirase H, Czurko A, Mamiya A, Buzsaki G. Oscillatory coupling of hippocampal pyramidal cells and interneurons in the behaving rat. *J Neurosci* (1999) 19:274–87.

34. Csicsvari J, O'Neill J, Allen K, Senior T. Place-selective firing contributes to the reverse-order reactivation of CA1 pyramidal cells during sharp waves in open-field exploration. *Eur J Neurosci* (2007) 26:704–16. doi:10.1111/j.1460-9568.2007.05684.x

35. Bragin A, Wilson CL, Engel J Jr. Chronic epileptogenesis requires development of a network of pathologically interconnected neuron clusters: a hypothesis. *Epilepsia* (2000) 41(Suppl 6):S144–52. doi:10.1111/j.1528-1157.2000.tb01573.x

36. Foffani G, Uzcategui YG, Gal B, Menendez de la PL. Reduced spike-timing reliability correlates with the emergence of fast ripples in the rat epileptic hippocampus. *Neuron* (2007) 55:930–41. doi:10.1016/j.neuron.2007.07.040

37. Ibarz JM, Foffani G, Cid E, Inostroza M, Menendez de la PL. Emergent dynamics of fast ripples in the epileptic hippocampus. *J Neurosci* (2010) 30:16249–61. doi:10.1523/JNEUROSCI.3357-10.2010

38. Rogawski MA, Tofighy A, White HS, Matagne A, Wolff C. Current understanding of the mechanism of action of the antiepileptic drug lacosamide. *Epilepsy Res* (2015) 110:189–205. doi:10.1016/j.eplepsyres.2014.11.021

39. Lynch BA, Lambeng N, Nocka K, Kensel-Hammes P, Bajjalieh SM, Matagne A, et al. The synaptic vesicle protein SV2A is the binding site for the antiepileptic drug levetiracetam. *Proc Natl Acad Sci U S A* (2004) 101:9861–6. doi:10.1073/pnas.0308208101

40. Yang XF, Weisenfeld A, Rothman SM. Prolonged exposure to levetiracetam reveals a presynaptic effect on neurotransmission. *Epilepsia* (2007) 48:1861–9. doi:10.1111/j.1528-1167.2006.01132.x

41. Lukyanetz EA, Shkryl VM, Kostyuk PG. Selective blockade of N-type calcium channels by levetiracetam. *Epilepsia* (2002) 43:9–18. doi:10.1046/j.1528-1157.2002.24501.x

42. Girardeau G, Benchenane K, Wiener SI, Buzsaki G, Zugaro MB. Selective suppression of hippocampal ripples impairs spatial memory. *Nat Neurosci* (2009) 12:1222–3. doi:10.1038/nn.2384

43. Ego-Stengel V, Wilson MA. Disruption of ripple-associated hippocampal activity during rest impairs spatial learning in the rat. *Hippocampus* (2010) 20:1–10. doi:10.1002/hipo.20707

44. Lopez-Gongora M, Martinez-Domeno A, Garcia C, Escartin A. Effect of levetiracetam on cognitive functions and quality of life: a one-year follow-up study. *Epileptic Disord* (2008) 10:297–305. doi:10.1684/epd.2008.0227

45. Javed A, Cohen B, Detyniecki K, Hirsch LJ, Legge A, Chen B, et al. Rates and predictors of patient-reported cognitive side effects of antiepileptic drugs: an extended follow-up. *Seizure* (2015) 29:34–40. doi:10.1016/j.seizure.2015.03.013

46. Lancman ME, Fertig EJ, Trobliger RW, Perrine K, Myers L, Iyengar SS, et al. The effects of lacosamide on cognition, quality-of-life measures, and quality of life in patients with refractory partial epilepsy. *Epilepsy Behav* (2016) 61:27–33. doi:10.1016/j.yebeh.2016.04.049

47. Schoenberg MR, Rum RS, Osborn KE, Werz MA. A randomized, double-blind, placebo-controlled crossover study of the effects of levetiracetam on cognition, mood, and balance in healthy older adults. *Epilepsia* (2017) 58:1566–74. doi:10.1111/epi.13849

48. IJff DM, van Veenendaal TM, Majoie HJ, de Louw AJ, Jansen JF, Aldenkamp AP. Cognitive effects of lacosamide as adjunctive therapy in refractory epilepsy. *Acta Neurol Scand* (2015) 131:347–54. doi:10.1111/ane.12372

49. Deshpande LS, Delorenzo RJ. Mechanisms of levetiracetam in the control of status epilepticus and epilepsy. *Front Neurol* (2014) 5:11. doi:10.3389/fneur.2014.00011

38

5 Loss of neuronal network resilience precedes seizures and determines the ictogenic nature of interictal synaptic perturbations

5.1 The contributions toward the progress of the field

Seizure initiation is a sudden and dramatic change in brain function. However, the transition to seizure is rather a slow process that happens over time. During that process, the brain becomes less and less stable as it gets closer to having a seizure and displays features of critical slowing. Scientists have also found that interictal epileptiform discharges (IEDs) can either help prevent a seizure or make it more likely to happen. IEDs can act pro-ictally or anti-ictally, depending on what is happening in the brain at the time of the IED occurrence. By combining *in silico*, *in vitro*, and *in vivo* approaches and analysis of human intracranial recordings, the authors demonstrated that the transition to seizure occurs through the loss of dynamic stability and resilience.

***In vitro* study**   The authors used hippocampal slice preparations to model acute ictogenesis. Seizures were induced by perfusing the slices with artificial cerebrospinal fluid with an elevated concentration of potassium. Brief electrical stimulations were used to mimic IED activity. The authors measured the electrical activity in the brain slices exhibiting spontaneous recurrent seizure-like events. To examine the nature of the transition to seizure, several measures indicative of a progressive loss of resilience and an approaching transition to a different dynamic regime were applied to interictal HFOs. These measures included variance, frequency, autocorrelation, and spatial correlation. In complex dynamics theory, they are called early warning signals. The results demonstrated that the transition to seizure happens via critical slowing accompanied by the loss of dynamic resilience.

Repeated stimulations were used to actively perturb the hippocampal slices to determine the dynamical state and resilience and evaluate the state-dependent impact of IEDs on seizure genesis. Hippocampal slices without IEDs generated seizure-like events more often than the slices generating IEDs, suggesting anti-ictal effect. IEDs could also act pro-ictally as they were able to initiate the seizure featuring a hypersynchronous seizure onset pattern. To validate the hypothesis about the state-dependent effect of IEDs, we delivered single pulse stimulation of predetermined intensity either closely after the seizure-like activity or, in other cases, closely before the expected onset of the seizure. Surprisingly, even low intensities of stimulation were able to trigger the seizure when delivered before the expected seizure, but even the strongest stimuli were unable to trigger the seizure when delivered closely after the seizure. Furthermore, a pulse train delivered after the seizure had the capacity to prolong the time to the next seizure. These experiments confirmed the state-dependent effect of IEDs on ictogenesis when the pro-ictal or anti-ital effect is determined by the level of resilience at the time of the IED occurrence.

In silico **study** The experimental observations and theories were explored in a mathematical model of a dynamical system that replicated seizure dynamics and predicted the specific paths to reach the seizure onset. The seizure onset is a sudden drastic change in brain activity that can be understood as a bifurcation in a dynamical system. Different types of seizures might arise from different types of bifurcations. The specific bifurcation involved can reveal information about the cellular and network mechanisms responsible for seizure initiation. Without these mathematical models, we wouldn't be able to provide an explanation of how the subtle, nearly unnoticeable gradual changes in underlying slow processes could make the brain fragile and prone to seizures. The authors developed a mathematical model that used ordinary differential equations to represent the interaction between slow and fast variables, with the slow variable representing changes in population excitability and the fast variable representing the population firing rate. The mathematical model was repeatedly simulated with specific settings to study the effect of perturbations on the transition to seizure. The perturbations were modeled as brief increases in the population firing rate with various densities and amplitude to study their effect. The simulations revealed complex nonlinear effects of perturbations on the transition to seizure. The effects ranged from complete suppression of seizures to a substantial increase in seizure frequency. These effects were dependent on amplitude, frequency, and the timing of the perturbations with respect to the dynamical state of the system.

In vivo **experimental study** The authors analyzed long-term recordings in the tetanus toxin model of temporal lobe epilepsy and found that the period between seizure clusters is characterized by a loss of stability with the approaching cluster. The loss of stability was associated with increased duration, incidence, line length, and enhanced propagation of brief spike-oscillatory events called 'epileptic bursts'. The presence of several early warning signals in the analysis of

'epileptic bursts' supported the hypothesis of critical slowing. However, in other features also indicative of critical slowing such as autocorrelation and variance, no changes were found.

Human retrospective clinical study   The authors aimed to find evidence of critical slowing ahead of seizure in long-term intracranial electrographic recordings from chronically implanted epileptic patients. The results were mixed as out of twelve patients, only two supported the hypothesis while four patients showed completely opposite outcomes. The authors also searched for evidence of the pro-ictal effect of IEDs by template-matching IEDs that preceded a high-amplitude discharge that was considered the beginning of the seizure. The evidence for IED triggering a seizure in the high susceptible time period before the seizure was found in four patients.

Although the evidence of critical slowing varied across the studied domains, the critical slowing and the state-dependent effect of perturbations are plausible mechanisms that shape the dynamics of the transition to seizure. Critical slowing does not have to be the only dynamic pathway leading to seizure. Merging complex information about dynamical processes at multiple spatial and temporal scales can bring us closer to understanding the principles of seizure initiation, and possibly to a unified theory of ictogenesis to explain the existence of the various seizure classes (dynamotypes) and transitions to seizure.

5.2   The author's contributions

The author mastered the technique of preparation and measurement of electrical activity *in vitro* from rat and mouse brain slices. The author was responsible for the *in vitro* part of the study, particularly, the experiments focused on testing the effect of a single pulse and repetitive stimulation on an ongoing spontaneous seizure-like activity and the analysis of HFA and slow wave LFP fluctuations. The author was responsible for establishing the experimental method, the design, conducting, running, and analyzing such experiments. The author was also involved in the design and implementation of *in silico* models. The author contributed to manuscript preparation and covered part of the literature review about the relationship between seizures and spikes from a dynamic perspective. The author presented the work at several local and international conferences.

5.3 Compliance with the thesis objectives

In the context of the thesis, the part of the study that holds significant results for studying HFOs is the *in vitro* slice experiments. The interictal measurements, where the analysis of high-frequency activity (HFA, 100-300 Hz) was conducted, are particularly important for understanding the complex nature of HFOs. The HFA activity showed properties that are similar to HFOs, such as their high frequency and time-frequency representation. Periods between seizures were characterized by the presence of HFA with a frequency of 190 Hz. The progressive increase in high-frequency power with approaching seizure further supports the notion that HFOs may be involved in seizure initiation and propagation. HFOs represent a form of neuronal network synchronization, wherein groups of neurons fire in a highly coordinated manner. The presence of HFOs during interictal periods could be attributed to increased synchronization among neurons in the hippocampus and the interactions between excitatory and inhibitory neurons. Further experiments could be designed to investigate the role of specific synaptic mechanisms in the generation and propagation of these oscillations.

Loss of neuronal network resilience precedes seizures and determines the ictogenic nature of interictal synaptic perturbations

Wei-Chih Chang [1,11,13], Jan Kudlacek[2,3,13], Jaroslav Hlinka [4], Jan Chvojka[2,3], Michal Hadrava[4,5], Vojtech Kumpost[2], Andrew D. Powell[1,12], Radek Janca [3,6,7], Matias I. Maturana[8], Philippa J. Karoly[8,9], Dean R. Freestone[8], Mark J. Cook [8], Milan Palus [4], Jakub Otahal[2], John G. R. Jefferys [1,10,14]* and Premysl Jiruska [2,14]*

The mechanism of seizure emergence and the role of brief interictal epileptiform discharges (IEDs) in seizure generation are two of the most important unresolved issues in modern epilepsy research. We found that the transition to seizure is not a sudden phenomenon, but is instead a slow process that is characterized by the progressive loss of neuronal network resilience. From a dynamical perspective, the slow transition is governed by the principles of critical slowing, a robust natural phenomenon that is observable in systems characterized by transitions between dynamical regimes. In epilepsy, this process is modulated by synchronous synaptic input from IEDs. IEDs are external perturbations that produce phasic changes in the slow transition process and exert opposing effects on the dynamics of a seizure-generating network, causing either anti-seizure or pro-seizure effects. We found that the multifaceted nature of IEDs is defined by the dynamical state of the network at the moment of the discharge occurrence.

Epilepsy is the most common chronic neurological disorder, affecting approximately 0.5% of the population in developed countries. It is characterized by the enduring propensity of the affected area of brain to generate spontaneous and repeated seizures[1]. A seizure is a marked shift in brain dynamics that occurs when a large neuronal population becomes excessively active and synchronized[2]. The seizure state is naturally inherent to the brain[3]. However, the dynamical route to seizure initiation varies, and several possible pathways have been proposed[3,4]. In a normal brain, an acute symptomatic seizure can emerge under extreme stochastic circumstances, such as systemic intoxication, metabolic disturbances, or in association with a documented brain insult[5]. By contrast, seizures in epilepsy recur spontaneously and are unprovoked. Their seemingly unpredictable and random occurrence is the major debilitating factor. The actual mechanisms and dynamical principles responsible for seizure emergence in the epileptic brain remain enigmatic. Theoretical and modeling studies have proposed several dynamical pathways governing the transition to seizure[6,7]. Experimental verification and identification of the neurobiological mechanisms governing their dynamics is a crucial prerequisite for our understanding of epilepsy and seizure genesis.

During interictal periods (that is, between seizures), the presence of pathologically interconnected neurons manifests as brief and transient episodes of synchronous activity known as interictal epileptiform dicharges (IEDs)[8]. The role of IEDs in the transition to seizure is still a matter of intense debate, and available theories appear to be mutually exclusive[9]. Studies have demonstrated that IEDs can be either seizure preventing[10,11] or seizure facilitating[12,13]. Such dichotomy is currently explained by the existence of distinct cellular, synaptic, and network mechanisms that underlie the genesis of different forms of IEDs[9].

We sought to address these crucial and unresolved aspects of seizure genesis. First, how do seizures emerge from neural networks and what dynamical trajectories do they follow? Second, what is the role of IEDs in seizure genesis? We found that the transition to seizure was associated with a progressive loss of neural network stability and a slow, but inevitable, shift toward the seizure[7,14,15]. This process displayed features of critical slowing[15], a dynamic phenomenon that has gained increasing attention across various research fields, as it is able to capture the essence of the dynamics of a wide range of natural systems characterized by alternations between dynamical regimes (ranging from cell signaling to ecosystems and climate)[16]. Notably, elucidation of the governing dynamical principles of the transition to seizure can explain the observed dichotomy of the complex role of IEDs on seizure genesis and allows unification of antagonizing

[1]Neuronal Networks Group, School of Clinical and Experimental Medicine, University of Birmingham, Birmingham, UK. [2]Department of Developmental Epileptology, Institute of Physiology of the Czech Academy of Sciences, Prague, Czech Republic. [3]Department of Circuit Theory, Faculty of Electrical Engineering, Czech Technical University in Prague, Prague, Czech Republic. [4]Department of Complex Systems, Institute of Computer Science of the Czech Academy of Sciences, Prague, Czech Republic. [5]Department of Cybernetics, Faculty of Electrical Engineering, Czech Technical University in Prague, Prague, Czech Republic. [6]Department of Neurology, Second Faculty of Medicine, Charles University and Motol University Hospital, Prague, Czech Republic. [7]Department of Pediatric Neurology, Second Faculty of Medicine, Charles University and Motol University Hospital, Prague, Czech Republic. [8]The Graeme Clark Institute & Department of Medicine St. Vincent's Hospital, The University of Melbourne, Melbourne, Australia. [9]Department of Biomedical Engineering, The University of Melbourne, Melbourne, Australia. [10]Department of Pharmacology, University of Oxford, Oxford, UK. [11]Present address: Faculty of Veterinary Medicine and Neuroscience Center, University of Helsinki, Helsinki, Finland. [12]Present address: Department of Life Science, School of Health Sciences, Birmingham City University, Birmingham, UK. [13]These authors contributed equally: Wei-Chih Chang, Jan Kudlacek. [14]These authors jointly supervised to this work: John G. R. Jefferys, Premysl Jiruska. *e-mail: john.jefferys@pharm.ox.ac.uk; jiruskapremysl@gmail.com
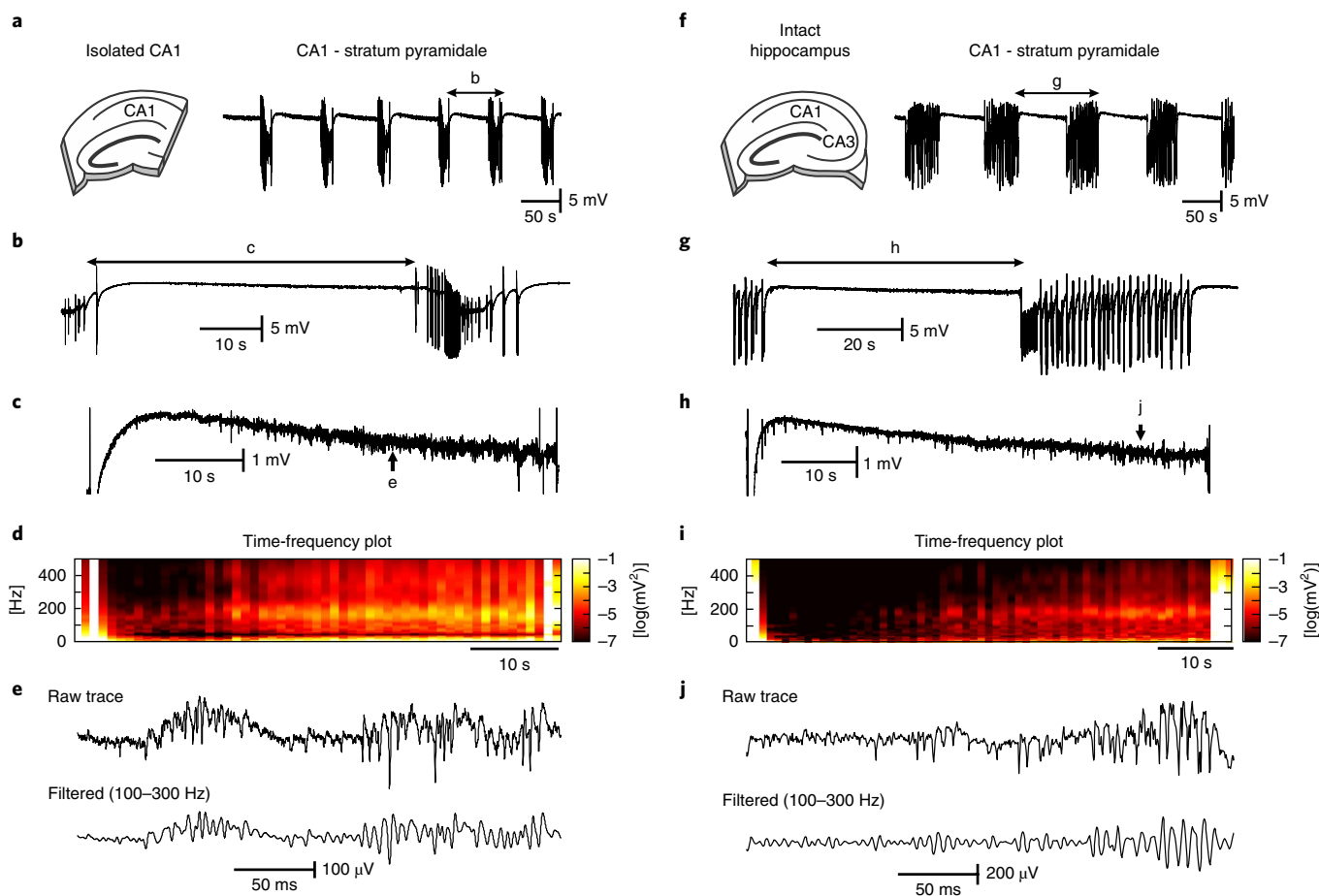
Fig. 1 | Seizures and interictal activity in the high-potassium model. a, In the isolated CA1, perfusion of ACSF with a potassium concentration of 8–10 mM led to the development of spontaneous and repeated seizure-like episodes ($n = 114/17$ seizures/slices). **b,c**, Periods between seizures were characterized by the presence of HFA ~190 Hz with superimposed unit activity. These electrographic phenomena were accompanied by decreasing DC shift ($n = 27/9$ interictal periods/slices). **d**, Time-frequency map showing the progressive increase in power in a high-frequency band with approaching seizure ($n = 114/17$ seizures/slices). **e**, Detail of interictal HFA. **f**, In intact hippocampal slices, seizures were also generated in the CA1 region ($n = 83/15$ seizures/slices). **g–i**, Interictal periods in the intact hippocampus were characterized by an increase in the amplitude and power of HFA ($n = 83/15$ interictal periods/slices), a negative shift in DC potential ($n = 24/8$ interictal periods/slices), and by the presence of interictal discharges. **j**, Example of interictal HFA in intact hippocampal preparation.

theories and observations. On the basis of our results, we propose a new theory explaining the multifaceted nature of IED.

Results

Seizures and interictal activity in the isolated CA1 and intact hippocampal slices. We analyzed 67 intact hippocampal slices and 73 isolated CA1 slices. Perfusion of isolated CA1 slices, with the CA3 region resected, with artificial cerebral spinal fluid (ACSF) containing 8–10 mM potassium resulted in spontaneous and recurrent electrographic seizures (Fig. 1a,b). The average duration of the seizures was 14.3 ± 0.8 s ($n = 114/17$ seizures/slices) and the periods between seizures (that is, the interictal periods) lasted for 50.3 ± 2.4 s ($n = 114/17$ interictal periods/slices). Interictal periods were characterized by the presence of high-frequency activity (HFA), with an average peak frequency of 191.2 ± 6.5 Hz ($n = 17$ slices) and an amplitude of 82.6 ± 4.8 μV with superimposed multiunit activity (Fig. 1c–e). HFA occurred early after the perfusion of the slice with high potassium and preceded the development of seizures.

Similar electrographic activity was observed in intact hippocampal slices with preserved CA3-CA1 connectivity (Fig. 1f–j). In this slice preparation, seizure duration was 44.4 ± 1.3 s ($n = 83/15$ seizures/slices) and the periods between seizures lasted for 69.8 ± 2.1 s

($n = 83/15$ interictal periods/slices; Fig. 1f). Seizures were characterized by an initial tonic phase followed by clonic discharges (Fig. 1g). Between seizures, the CA1 generated HFA, which had a frequency of 176.9 ± 5.8 Hz and an amplitude of 167.8 ± 40.7 μV ($n = 15$ slices; Fig. 1h–j).

In isolated CA1, the analysis of current source density profiles has suggested that individual HFA cycles are a result of action potential firing of neurons (Supplementary Fig. 1a–d). Tetrode recordings, phase analysis of cellular firing, and estimation of the strength of firing modulation using z score revealed that the negative phase of the HFA cycle was accompanied by significant increases in the probability of all pyramidal cell firing ($n = 47/4$ cells/slices, Kolmogorov–Smirnov test, $P < 0.05$; Fig. 2a,c). The activity of interneurons was not uniform during the HFA cycle, and the phase relationship of individual interneurons with the HFA cycle displayed increased phase firing variability ($n = 9/4$ cells/slices, Kolmogorov–Smirnov test, $P < 0.05$; Fig. 2b,c). Spatially, the HFA was present across the entire CA1 region ($n = 50$ slices; Supplementary Fig. 2b). Application of NMDA (AP5 25 μM, $n = 9$ slices) or non-NMDA (NBQX, 20 μM, $n = 10$ slices) antagonists did not block the HFA. In intact hippocampus, the HFA had a morphology, spatial properties (Supplementary Fig. 1e–h), and pharmacological profile that

44

a Isolated CA1
Firing probability
Principal cells
10 µV
Probability (%) 0.06 0.03 0.00
Phase (rad) −π 0 π

b Firing probability
Interneurons
10 µV
Probability (%) 0.14 0.07 0
Phase (rad) −π 0 π

c z score
Principal cells Interneurons
10 µV
z score (−) 25 12.5 0
Phase (rad) −π 0 π

d Intact hippocampus
Firing probability
Principal cells
20 µV
Probability (%) 0.3 0.15 0.0
Phase (rad) −π 0 π

e Firing probability
Interneurons
20 µV
Probability (%) 0.5 0.25 0
Phase (rad) −π 0 π

f z score
Principal cells Interneurons
20 µV
z score (−) 20 30 0
Phase (rad) −π 0 π

Fig. 2 | Cellular properties during cycles that comprise interictal HFA.
a, In the isolated CA1, the HFA cycle lasts around 5 ms (Supplementary Fig. 1). The cycle is characterized by an increased firing probability of principal cells during HFA troughs ($n = 47/4$ cells/slices, Kolmogorov–Smirnov test, $P < 0.05$). **b**, An average phase histogram of interneuronal activity in the isolated CA1 ($n = 9/4$ cells/slices, Kolmogorov–Smirnov test, $P < 0.05$). **c**, z values for individual neuron types and the timing of peak firing probability of individual cells. **d**,**e**, The firing probability of (**d**) principal cells ($n = 72/13$ cells/slices, Kolmogorov–Smirnov test, $P < 0.05$) and (**e**) interneurons ($n = 35/13$ cells/slices, Kolmogorov–Smirnov test, $P < 0.05$) was significantly modulated with the maximum probability around the trough of a HFA cycle. **f**, z values of phase histogram distribution for each cell. Circles and error bars represent mean and s.e.m., respectively.

was similar to that of HFA observed in isolated CA1 preparations. The action potential firing of all principal cells displayed a significant increase during the trough of the HFA cycle ($n = 72/13$ cells/slices, Kolmogorov–Smirnov test, $P < 0.05$; Fig. 2d,f). However, we observed a greater trough-coupled action potential firing in a subpopulation of interneurons ($n = 35/13$ cells/slices, Kolmogorov–Smirnov test, $P < 0.05$; Fig. 2e,f) than in the interneuronal profiles recorded in isolated CA1 preparations.

These data, supported by previous findings[17,18], suggest that HFA represents low-amplitude population spikes that result from the co-firing of a small number of pyramidal cells with a moderate interneuronal contribution.

Interictal HFA dynamics display features of early warning signals. The observed HFA did not remain uniform in its properties; it displayed dynamic changes as the seizure approached (Fig. 1c,h). To examine these changes, we applied several measures, which are indicative of a progressive loss of resilience and an approaching transition to a different dynamic regime[16]. These measures included variance, frequency, autocorrelation, and spatial correlation; in complex dynamics theory, they are called early warning signals. In isolated CA1 preparations, the spatiotemporal profile of HFA was characterized by a progressive increase in signal variance ($n = 76/17$

interictal periods/slices, one-way ANOVA, $F_{(1,7500)} = 154$, $P = 0.000$; Fig. 3a). The temporal evolution of the frequency profile of HFA was characterized by the progressive slowing of the first moment of power spectra in the 100–500-Hz band ($n = 76/17$ interictal periods/slices, one-way ANOVA, $F_{(1,7500)} = 336$, $P = 0.000$; Fig. 3b) and an increase in autocorrelation ($n = 76/17$ interictal periods/slices, one-way ANOVA, $F_{(1,7500)} = 1,821$, $P = 0.000$; Fig. 3c). On the spatial scale, cross-correlation analysis demonstrated the gradual spatial expansion of HFA with the approaching seizure ($n = 8/2$ interictal periods/slices, one-way ANOVA, $F_{(1,700)} = 206$, $P = 0.000$; Fig. 3d). At the cellular level, we observed an overall increase in neuronal firing (isolated CA1: $n = 56/4$ cells/slices, one-way ANOVA, $F_{(1,3900)} = 51$, $P = 0.000$; Fig. 3e), which combined the increase, decrease, or no change in firing of individual neurons. In intact hippocampal slices, the spatiotemporal profile of variance ($n = 57/15$ interictal periods/slices, one-way ANOVA, $F_{(1,5600)} = 307$, $P = 0.000$), first moment ($n = 57/15$ interictal periods/slices, one-way ANOVA, $F_{(1,5600)} = 1,830$, $P = 0.000$), autocorrelation ($n = 57/15$ interictal periods/slices, one-way ANOVA, $F_{(1,5600)} = 1,726$, $P = 0.000$), spatial correlation ($n = 40/11$ interictal periods/slices, one-way ANOVA, $F_{(1,3900)} = 127$, $P = 0.000$), and neuronal activity ($n = 107/13$ cells/slices, one-way ANOVA, $F_{(1,4100)} = 9$, $P = 0.012$) displayed a similar dynamical evolution as the seizure approached (Fig. 3a–e). In both slice preparations, the changes in early warning signals were accompanied by a negative DC shift ($n = 24/8$ interictal periods/slices, one-way ANOVA, $F_{(1,2399)} = 35$, $P = 0.000$ for intact hippocampal slice; $n = 27/9$ interictal periods/slices, one-way ANOVA, $F_{(1,2699)} = 13$, $P = 0.000$ for isolated CA1; Fig. 3f). Apart from the early warning signals, the loss of a system's stability is characterized by increased sensitivity to perturbations and a delayed recovery from them. The dynamical stability can be evaluated by actively delivering the perturbation[19,20]. In isolated CA1 sections, we examined the stability from the response of the system to stimulation of the Schaffer collaterals. The response was quantified using line length of the signal, which combines both measures, that is, changes in duration and amplitude respectively (Supplementary Fig. 3). With the approaching seizure, the response to perturbation of constant intensity progressively increased ($n = 24/8$ interictal periods/slices, one-way ANOVA, $F_{(1,2399)} = 2$, $P = 0.000$; Fig. 3g).

The presence of early warning signals of an impending critical transition derived from the properties of HFA, suggest that, with an upcoming seizure, the CA1 becomes less resilient and progressively approaches the critical point (critical bifurcation) beyond which the dynamics in the CA1 enter the seizure regime. In intact hippocampal slices, however, this process of critical transition was substantially modified by the synchronous synaptic input incoming from the IEDs originating in the CA3 region.

The impact of CA3 synaptic input on the critical transition to seizure. In an intact hippocampal slice, CA3 (predominantly the CA3b region) generated spontaneous and repeated IEDs with a duration of 68.9 ± 2.6 ms and an amplitude of 1.7 ± 0.2 mV ($n = 17$ slices; Fig. 4a,b). IEDs occurred approximately periodically with a mean frequency of 1.2 ± 0.1 Hz, and they were dependent on intact glutamatergic transmission ($n = 12$ slices). Spatially, they propagated to the entire CA1 with an average propagation time of 6.4 ± 0.5 ms ($n = 12$ slices). In the CA1, propagated IEDs represented a population of excitatory postsynaptic potentials with an amplitude of 0.4 ± 0.1 mV ($n = 17$ slices; Supplementary Fig. 4). In the CA1, IEDs interfered in a phasic manner with the pre-seizure dynamics of HFA and the process of critical transition. During each discharge, the probability of HFA occurrence transiently increased, and HFA amplitude increased to 224.5 ± 53.2 µV ($n = 17$ slices; Fig. 4a–c). The discharge was then followed by the suppression or absence of HFA and neuronal firing for >300 ms (Fig. 4a,c). Following this, HFA and neuronal activity progressively increased until the next IED.

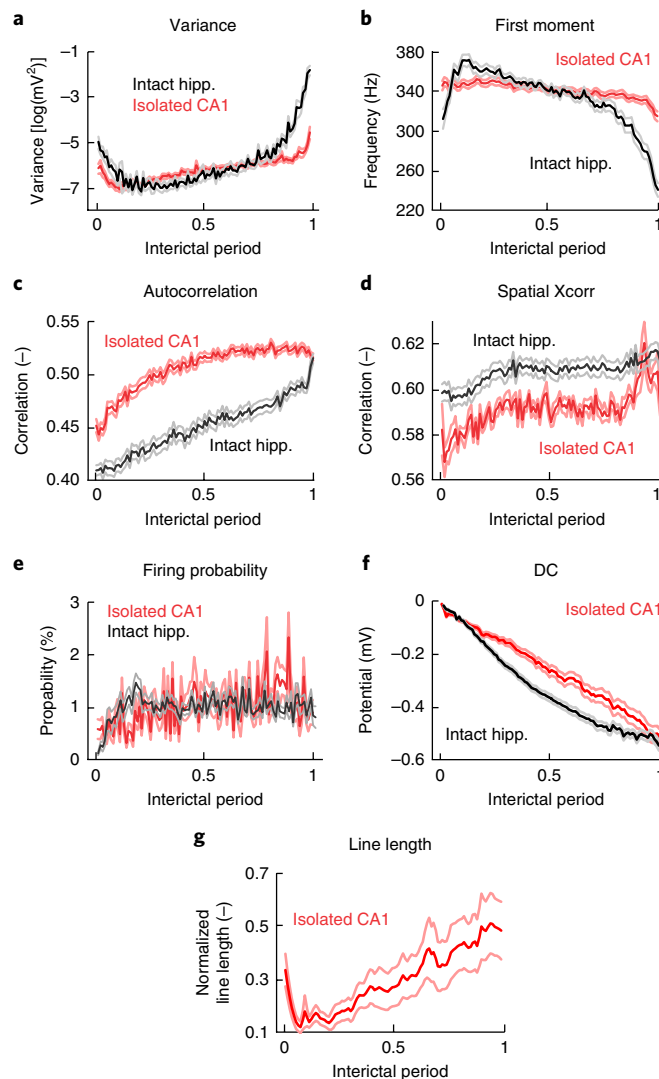**Fig. 3 | Interictal changes in HFA properties display features of early warning signals of the critical transition to seizure. a**, In both slice preparations, seizures were preceded by a significant increase in HFA amplitude variance (isolated CA1: $n = 76/17$ interictal periods/slices, one-way ANOVA, $F_{(1,7500)} = 154$, $P = 0.000$; intact hippocampus (hipp.): $n = 57/15$ interictal periods/slices, one-way ANOVA, $F_{(1,5600)} = 307$, $P = 0.000$). The duration of interictal periods was normalized from 0 to 1. **b**, Seizures were preceded by frequency slowing, which manifested as a progressive decrease of the first moment of power spectra (isolated CA1: $n = 76/17$ interictal periods/slices, one-way ANOVA, $F_{(1,7500)} = 336$, $P = 0.000$; intact hippocampus: $n = 57/15$ interictal periods/slices, one-way ANOVA, $F_{(1,5600)} = 1,830$, $P = 0.000$). **c,d**, Both autocorrelation (**c**; lag = 5 ms; isolated CA1: $n = 76/17$ interictal periods/slices, one-way ANOVA, $F_{(1,7500)} = 1,821$, $P = 0.000$; intact hippocampus: $n = 57/15$ interictal periods/slices, one-way ANOVA, $F_{(1,5600)} = 1,726$, $P = 0.000$) and spatial correlation (**d**; isolated CA1: $n = 8/2$ interictal periods/slices, one-way ANOVA, $F_{(1,700)} = 206$, $P = 0.000$; intact hippocampus: $n = 40/11$ interictal periods/slices, one-way ANOVA, $F_{(1,3900)} = 127$, $P = 0.000$) increase in advance of seizures. **e**, At the single-cell level, the seizures were predominantly preceded by an increase in cell firing (isolated CA1: $n = 56/4$ cells/slices, one-way ANOVA, $F_{(1,3900)} = 51$, $P = 0.000$; intact hippocampus: $n = 107/13$ cells/slices, one-way ANOVA, $F_{(1,4100)} = 9$, $P = 0.012$). **f**, In both preparations, the early warning signals were accompanied by a negative DC shift (isolated CA1: $n = 27/9$ interictal periods/slices, one-way ANOVA, $F_{(1,2699)} = 13$, $P = 0.000$; intact hippocampus: $n = 24/8$ interictal periods/slices, one-way ANOVA, $F_{(1,2399)} = 35$, $P = 0.000$). **g**, In the isolated CA1, seizures were preceded by progressively increasing the amplitude and duration of the response evoked by stimulations of Schaffer's collaterals ($n = 24/8$ interictal periods/slices, one-way ANOVA, $F_{(1,2399)} = 2$, $P = 0.000$). The responses were quantified using line-length measurement. Lines and shaded lines represent mean and s.e.m., respectively.

In summary, the presence of discharges induced phasic changes in HFA, which were superimposed on the slow changes in the properties of HFA described above. This phasic profile of HFA was maintained for the entire interictal period ($n = 17$ slices; Fig. 4d).

To explore the IED capacity to delay the onset of seizures, we examined the duration of periods between seizures in individual preparations. In the isolated CA1, the duration of the interictal period was 50.3 ± 2.4 s ($n = 114/17$ interictal periods/slice), whereas the period between seizures lasted 69.8 ± 2.1 s in intact slices ($n = 83/15$ interictal periods/slice, two-sided Mann–Whitney–Wilcoxon U test, $U = 1577$, $P = 0.000$; Fig. 4e). Pharmacological blockade of IEDs in intact slices with NBQX and AP5 led to a shortening of the interictal period from 53.6 ± 2.1 ($n = 27/5$ interictal periods/slices) to 41.4 ± 2.3 s ($42/5$ interictal periods/slices, two-sided Mann–Whitney–Wilcoxon U test, $U = 188$, $P = 0.000$; Fig. 4f).

The discharges also influenced seizure onset and its pattern. In isolated CA1 slices, the seizure onset was characterized by the spontaneous emergence of low-amplitude rhythmic activity from a single-recording channel, which gradually increased in amplitude and progressively spread across the CA1 with an average time delay of 639.3 ± 63.2 ms between adjacent electrodes ($n = 86/7$ seizures/slices; Fig. 4g,i). In intact slices, synchronous excitatory synaptic input from CA3 was able to trigger a seizure and change its onset pattern to a high-amplitude heralding discharge that occurred synchronously across the entire or large parts of the CA1 with an average delay of 10.4 ± 2.1 ms ($n = 49/9$ seizures/slices; Fig. 4h,i).

Our data suggest that the CA3 input perturbs the slow process of the transition to seizure in the CA1 region and that the response to this perturbation is determined by the dynamical state of the CA1 area. During the interictal period, the transient phasic suppression of HFA after IED may have a stabilizing (anti-seizure) effect and the capacity to delay the seizure onset. However, when the CA1 dynamics are close to seizure initiation (critical bifurcation), the transient fast increase in excitation or neuronal firing resulting from the incoming IED may have a destabilizing (pro-seizure) effect that is capable of prematurely shifting the CA1 dynamics into the seizure and rapidly synchronizing seizure initiation over large spatial scales.

Modeling of cyclic dynamical shifts and the impact of interictal perturbations. To evaluate in detail the effect of CA3 synaptic perturbations on CA1 dynamics, we implemented a model of the slow-fast process[14,21] that simulates the cyclic dynamical shifts to seizure that are characteristic of in vitro models of seizures. In this model, the excitability represents the slowly changing variable, whereas the population-firing rate represents the fast variable. For small values of excitability, the system has a single dynamic equilibrium (stable fixed point) corresponding to a low-firing state between seizures (Supplementary Fig. 5a). For high excitability values, the system has a single equilibrium at a high-firing state, that is, seizure. For intermediate excitability values, the system is characterized by the existence of two stable states and the curve describing the response of the system to external perturbations has the feature of a fold catastrophe separated by an unstable equilibrium (unstable fixed points; Supplementary Fig. 5a). This system has two catastrophic fold bifurcations (F_1, F_2), when an infinitesimally small change in a control parameter induces large changes in the system dynamics by shifting it to the contrasting dynamical regime (for F_1 interictal→seizure and for F_2 seizure→interictal). If the slow-fast process is driven by dynamical changes in excitability, its dynamics have the character
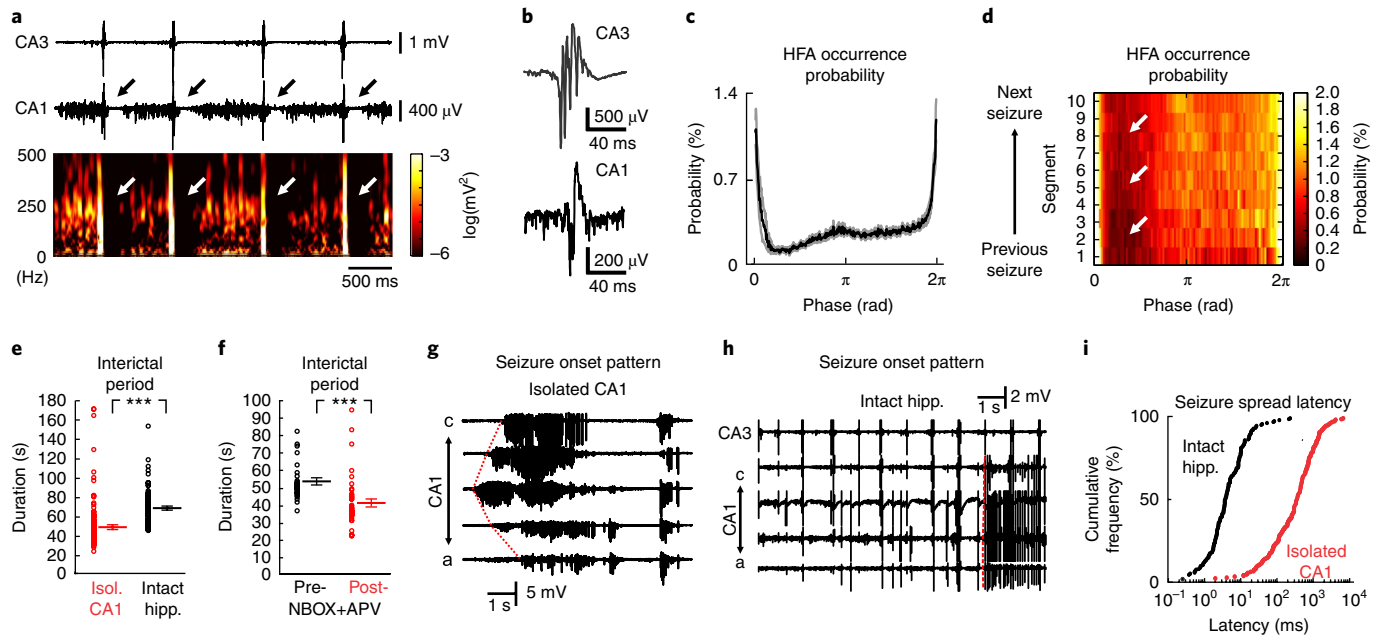
Fig. 4 | The effect of IEDs on the transition to seizure. a, IEDs interfere with the slow process of transition to seizure and HFA. The raw data and corresponding time-frequency plot revealed the suppression of HFA after each discharge. **b**, Details of IEDs generated in the CA3 and propagating to the CA1. **c**, The average phase histogram revealed that the probability of HFA occurrence substantially increased during the peak of the discharge. It was followed by transient HFA suppression and then gradually increased until the next IED ($n = 15$ slices). **d**, Post-discharge suppression of HFA persisted throughout the course of entire period between seizures. **e**, Periods between seizures in intact hippocampi ($n = 83/15$ interictal periods/slice) had longer duration than in isolated (isol.) CA1 preparations, where the IEDs were absent ($n = 114/17$ interictal periods/slice; two-sided Mann–Whitney–Wilcoxon U test, $U = 1,577$, $P = 0.000$). **f**, Block of IEDs by NBQX and AP5 also shortened the interictal period (baseline recording: $n = 27/5$ interictal periods/slices; post-NBQX+AP5: 42/5 interictal periods/slices, two-sided Mann–Whitney–Wilcoxon U test, $U = 188$, $P = 0.000$). **g**, IEDs modified the seizure initiation pattern. In isolated CA1 preparations, seizures were characterized by focal initiation and the slow spread of seizure activity to the rest of the CA1. **h**, In intact slices, seizures initiated instantaneously across either large areas or the entire CA1 as a result of incoming IEDs from the CA3. **i**, A cumulative histogram of the seizure spread velocity in the intact hippocampus and isolated CA1 slices revealed that the seizure spread is nearly two orders faster than in the intact slice. Line and error bars represent mean and s.e.m., respectively; ***$P \leq 0.001$.

of a limit cycle (Supplementary Fig. 5b), periodically switching between seizure and interictal state (Supplementary Fig. 5b,c and Supplementary Video 1), mimicking the dynamics observed in isolated CA1 slices. In such a scenario, the system will always slowly, but inevitably, shift toward seizure.

In a dynamically changing system, we explored the effect of IEDs on the transition to seizure. The perturbations were represented as approximately periodic transient increases in the population firing rate. Perturbation, which did not increase the firing rate beyond the unstable fixed point, shifted the system to the left, to a more stable state with lower excitability, before recovering from the perturbation (Fig. 5a,c,e and Supplementary Video 2). It mimics the 'refractory period' observed after each IED. As a result, the IED increases the distance from the catastrophic bifurcation and slows down the transition to seizure. If the perturbation is capable of crossing the unstable point, then the dynamics of the system shift to a seizure and the perturbation has a destabilizing pro-seizure effect (Fig. 5a–d). However, these effects are dependent on the timing of the perturbation. If the system dynamics are approaching the catastrophic bifurcation to seizure, then even weak interictal perturbations are capable of shifting the system dynamics prematurely into a seizure (Fig. 5a,b and Supplementary Video 2). Large-amplitude perturbations have a stronger seizure-inducing capacity, and they can initiate seizures far in advance of the catastrophic bifurcation (Fig. 5c,d and Supplementary Video 3). We performed multiple iterations in which we systematically varied the most important model parameters, that is, the amplitude of the perturbation and its occurrence probability. The simulations revealed complex nonlinear effects of IEDs on the transition to seizure, which emerged directly from interactions

between the perturbation amplitude, frequency, and the timing of the discharge occurrence with respect to the dynamical state of the system (Fig. 5g). The seizure-delaying effect increased with the increased number of perturbations and with the amplitude of perturbation and could result in the complete abolition of seizures (Fig. 5e–g and Supplementary Video 4). However, sparse large-amplitude perturbations had the capacity to substantially increase the seizure frequency (Fig. 5c,d,g).

The model of the slow-fast process is able to capture the basic complexity of the transition between interictal state and seizure. However, it neglects the faster dynamics of local field potentials, that is, seizure discharges. To determine whether the inclusion of local field potential dynamics is essential for explaining the multifaceted nature of interictal perturbation, we ran the simulations with a more biologically realistic model, the Epileptor (Supplementary Fig. 6)[3]. In the modified version of the Epileptor, we were able to replicate all of the state-dependent effects of interictal perturbation on ictogenesis, ranging from an increased probability of transition to seizure prevention.

State-dependent effect of interictal perturbations. To explore theoretical predictions derived from the numerical simulations, we performed a set of experiments in which interictal perturbations were mimicked using stimulation of Schaffer collaterals in isolated CA1 preparations. First, the CA1 network was perturbed with regularly delivered stimuli with a frequency of 1 Hz. The stimulation was initiated after the end of the seizure (Fig. 6a). The duration of the interictal period with stimulation was compared with the nearest control interictal period. We found that the early onset stimulation

had the capacity to delay seizure onset by increasing the duration of the interictal period ($n = 213/8$ stimulations/slices, two-sided Mann-Whitney-Wilcoxon U test, $U = 2180$, $P = 0.000$; Fig. 6a–d). Prolongation of interictal period positively correlated with the duration of the stimulation (Fig. 6c,d). To evaluate the observation that the pro-seizure effect of IED occurs when the neural networks are unstable and close to the bifurcation point, we delivered single stimuli early after the previous seizure (before 25% of the time of the expected interictal period) and before the next seizure (after 75% of the time of the expected interictal period, $n = 3$ slices). Only 38% of stimulations with an intensity of 300 µA were able to induce seizure ($n = 3/8$ stimulations; Fig. 6e,g) if they were delivered during the early part of the interictal period. Simultaneously, all of the stimulations delivered before the seizure were able to trigger seizures. Stimulation with the lowest intensity, 100 µA, triggered a seizure in 36% of cases ($n = 3/8$ stimulations; Fig. 6f,g). Stimulation with an intensity of either 200 µA and 300 µA induced seizure in all cases (6/6 and 4/4 stimulations, respectively; Fig. 6g).

Loss of resilience in a chronic model of temporal lobe epilepsy.
To ascertain whether the dynamical path characterized by the loss of resilience can be observed in vivo, we analyzed long-term recordings in the tetanus toxin model of temporal lobe epilepsy. In this model, we observed changes in network stability over longer time scales. In the tetanus toxin model, seizures tend to cluster in time[22], separated by seizure-free periods lasting 2.7 ± 0.2 h ($n = 6/6$ intercluster periods/animal). Between seizures and clusters is a specific type of pathological activity known as an epileptic burst[22]. Bursts are characterized by an initial high-amplitude discharge followed by a burst of rhythmic activity. They have an origin in the injected hippocampus and they are distinct from IEDs (Supplementary Fig. 7)[22,23]. The analysis of the properties of the burst ($1,041.3 \pm 149.2$ bursts per cluster) from the perspective of critical slowing suggested that the period between clusters is characterized by a loss of the stability with the approaching cluster. The temporal profile of burst duration ($n = 6/6$ intercluster periods/animals, one-way ANOVA, $F_{(1,53)} = 2.751$, $P = 0.012$; Fig. 7a) and line length ($n = 6/6$ intercluster periods/animals, one-way ANOVA, $F_{(1,53)} = 3.347$, $P = 0.003$; Fig. 7b) increased, which suggested that the brain displays a delayed recovery from the perturbation. Recent results from a network model demonstrated that the approaching critical transition to seizure can manifest as an increasing rate of interictal activity[19], which would correspond to the increased rate of epileptic bursts that we observed ($n = 6/6$ intercluster periods/animals, one-way ANOVA, $F_{(1,59)} = 3.105$, $P = 0.005$; Fig. 7c). Spatial correlation of the bursts progressively increased ($n = 6/6$ intercluster periods/animals, one-way ANOVA, $F_{(1,53)} = 7.792$, $P = 0.001$; Fig. 7d) as a result of the enhanced propagation of bursts outside the right hippocampus to the left hippocampus and motor cortices of both hemispheres (Supplementary Fig. 7b–d). We did not observe significant changes in autocorrelation ($n = 6/6$ intercluster periods/animals, one-way ANOVA, $F_{(1,53)} = 0.57$, $P = 0.928$; Fig. 7e), variance ($n = 6/6$ intercluster periods/animals, one-way ANOVA, $F_{(1,53)} = 0.4$, $P = 0.814$; Fig. 7f), or the first spectral moment of bursts ($n = 6/6$ intercluster periods/animals, one-way ANOVA, $F_{(1,53)} = 1.659$, $P = 0.128$; Fig. 7g).

Loss of resilience and state-dependent effect of IEDs in humans.
Next, we explored whether the transition to seizure via critical slowing can be observed in humans. We analyzed long-term intracranial recordings obtained from patients implanted with seizure prediction devices ($n = 12$ patients)[24]. The average number of recorded seizures per patient was 157.5 ± 32.1 ($n = 12$ patients). In these recordings, we examined the temporal evolution of the lag-1 autocorrelation coefficient 30 min before the seizure. In total, we analyzed 1,890 pre-ictal periods. In 4 of 12 patients, we observed a statistically significant increase in lag-1 autocorrelation before the
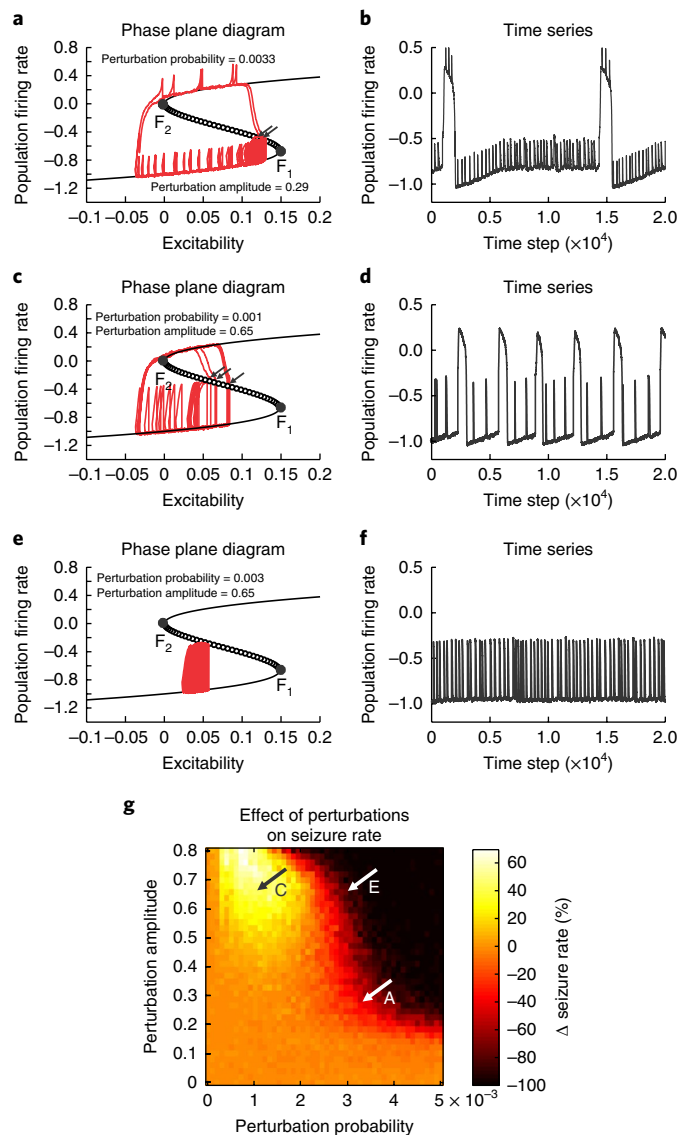
Fig. 5 | The complex effect of interictal perturbations on the transition to seizure. a, Approximately periodic perturbations interfered with the slow-fast process, and frequent low-amplitude perturbations had an ambiguous effect on the transition to seizure. If the perturbation occurred at the moment when the system was far from the unstable fixed point (tipping point), it led to a transient increase in firing followed by a shift in the system's dynamics back toward the more stable state (less excitable state). Such a perturbation has an anti-seizure property and prolongs the interictal period. In contrast, if the system was approaching the tipping point, then even small perturbations, which increase the excitability or firing rate, were able to shift the system over the unstable fixed point and prematurely initiate the seizure (arrow). **b**, The corresponding time series. **c,d**, Rare high-amplitude perturbations had the capacity to cross the unstable fixed (tipping) point (arrows) far in advance of catastrophic bifurcation F₁ and substantially increase the seizure rate. The pro-seizure effect of the perturbation outperformed the anti-seizure effect and was also dependent on the instantaneous dynamical state of the system. **e,f**, Frequent high-amplitude perturbations were able to completely abolish the seizure by locking the system dynamics far from the tipping point and preventing the system from crossing the unstable region into seizure. **g**, The probability of occurrence and amplitude of perturbations were systematically varied. Our results demonstrate that all of the currently known effects on the transition to seizure—that is, no change, increase, decrease in seizure frequency, or the complete abolition of seizures—can be reliably replicated. Animations of the selected transitions can be found as Supplementary Videos 2–4.

48
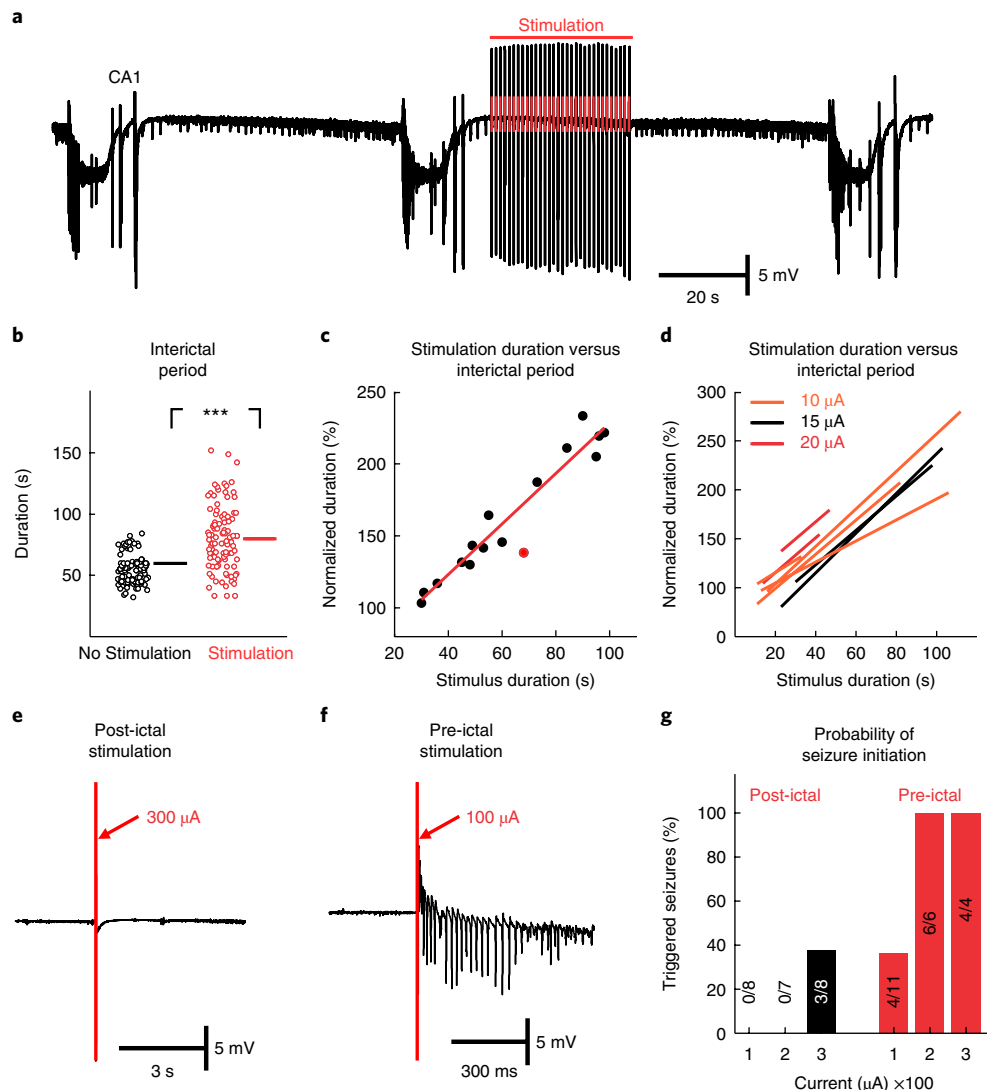
Fig. 6 | State-dependent effect of interictal perturbations. a, Seizures and interictal period without stimulation was followed by the interictal period when the train of Schaffer collateral stimulations (1 Hz) was delivered during the early stages of the interictal period. The stimulation extended the duration of the interictal period. **b**, The duration of interictal periods with and without early stimulations ($n = 213/8$ stimulations/slices; two-sided Mann–Whitney–Wilcoxon U test, $U = 2180$, $P = 0.000$). **c**, Example of an individual slice that was stimulated with an intensity of 15 μA. The duration of the interictal period increased with the duration of stimulation. Data were fitted with a regression curve. The red dot marks a stimulation, which was associated with a seizure. **d**, Regression curves for individual slices and current intensities of the stimulation revealed the seizure-delaying effect of interictal perturbations. **e**, A single stimulus of stronger intensity (300 μA) delivered during the early stage of interictal period failed to induce seizures. **f**, A stimulus of lower intensity (100 μA) delivered during the late phase of the interictal period had the capacity to initiate a seizure. **g**, The probability of a seizure-initiating effect of the stimulations delivered during the early and late stages of the interictal period ($n = 3$ slices). During the early stages (black bars), only strong stimulations were capable of initiating seizures. During the later stage of the interictal period (red bars), both weak and strong stimulations had a higher probability to initiate seizure. Lines and error bars represent mean and s.e.m., respectively; ***$P \leq 0.001$.

onset of their habitual seizures, which were consistent within each patient (Fig. 8a). In 2 of 12 patients, we observed a simultaneous increase in signal variance (Supplementary Fig. 8). In 4 of 12 cases, the autocorrelation and variance significantly decreased (Fig. 8a). One patient demonstrated only a decrease in variance. In 3 of 12 patients, the preictal changes were not significant. These results suggest that, at least for specific populations of patients, critical slowing is evident in the lead up to seizures.

Next, we explored the plausibility of the state-dependent effect of IEDs by testing the hypothesis based on in vitro and numerical observations, that is, that the seizure-triggering spike (heralding spike) at the onset of seizure is an IED occurring during a highly unstable state of brain dynamics and capable of triggering a seizure.

We compared heralding spikes to IEDs with respect to their morphology and spatial distribution using a template-matching algorithm. We identified 37 seizures initiating with a heralding spike in 13 patients. In four patients, we found a total of eight heralding spikes that displayed a >98% morphological match to IEDs far in advance of the seizure, which did not have the capacity to trigger the seizure (Fig. 8b–f).

Discussion

Seizure initiation marks the onset of a sudden and dramatic change in brain function, which represents the bifurcation of a dynamical system[3,6,7]. The seizure can initiate through several bifurcation types, including Hopf, saddle-node, and fold bifurcations[25,26]. The nature

of a bifurcation can be inherent to specific seizure types (generalized tonic-clonic, absence, or focal seizures with distinct seizure onset patterns), as well as reflect the involvement of specific cellular and network mechanisms responsible for seizure initiation[3,25,27]. To understand seizures and the enduring predisposition of the brain to generate seizures, it is crucial to elucidate the dynamical pathways through which the brain reaches the bifurcation point. Results from computational modeling replicating seizure dynamics have predicted the existence of specific pathways to ictal bifurcation[7,28]. One of the key concepts assumes the existence of bistable or multistable brain dynamics[7,26], where there is an initial separation between seizure and interictal state, and random perturbations do not have the capacity to reach the critical threshold to induce seizure. However, the distance between these dynamical regimes may progressively decrease as a result of slow changes in critical unstable parameters and manifest as a loss in the brain's resilience as the seizure approaches[7,15,19,29]. In medicine, catastrophic transition has been shown to drive seizure termination[30], asthmatic attacks, cardiac arrhythmia, and the onset or termination of depression[16,31].

In this study, we numerically, experimentally, and clinically inferred that the transition to focal seizure follows this dynamical route and that the slow process displays dynamical features of critical slowing that mark the progressive loss of neural network stability[16,21]. Early warning signals derived from the properties of field potentials reflect the underlying discrete changes in the stability of neuronal networks and the increased susceptibility to a seizure[18,32]. Further evidence of decreasing resilience can be derived from the response to active probing[20] or from the response to spontaneous perturbation[19]. The observed increasing probability of a pro-seizure effect of interictal synaptic perturbations with the approaching seizure, the progressively increasing sensitivity of the network to electric stimulation[18], or increased rate of bursts can therefore be indicative of weakening brain resilience. The idea that the brain becomes fragile in a barely visible or invisible way because of very subtle changes in a slow underlying process is the most counterintuitive aspect of critical slowing[16,29]. Whenever a large transition occurs, the causative event is intuitively sought in close vicinity to the transition and may result in the formulation of false causal relationships[29]. Various cellular and network processes have been identified and postulated to have a crucial role in seizure genesis[33]. However, the majority of these processes may represent only stochastic perturbations that initiate a seizure in a neural network whose dynamics are already approaching the catastrophic bifurcation via critical slowing.

We found that insights into the dynamics of seizure emergence were a crucial prerequisite for clarifying the role of IEDs in seizure genesis, an unresolved issue that has attracted the attention of generations of epileptologists[9]. Evidence from experimental and clinical studies has revealed that IEDs have both pro-seizure and anti-seizure effects[10,12,13]. Disconnection of seizure-generating networks from brain regions generating IEDs or pharmacological block of IEDs lead to increased seizure frequency[10,34], whereas electrical pacing mimicking IEDs can abolish seizures[10,34]. On the other hand, IEDs also have a well-documented capacity to induce seizures[12,13]. Studies examining changes in IED properties before seizures have found that IED frequency can both increase and decrease in advance of a seizure[11,35]. Finally, it has been claimed that IEDs have no relationship to ictogenesis at all[35]. Such complex behavior of IEDs is currently explained by the existence of different underlying cellular mechanisms[36]. The first type of discharges are represented by glutamatergic ones, which can display pro-seizure[13] and anti-seizure effects[10,34]. In these types of discharges, the transient increase in excitation is usually curtailed by a subsequent suppression of the neuronal activity as a result of intrinsic neuronal mechanisms, inhibitory synaptic feedback, changes in the extracellular environment, etc.[8,37,38]. The second class of IEDs depend purely on
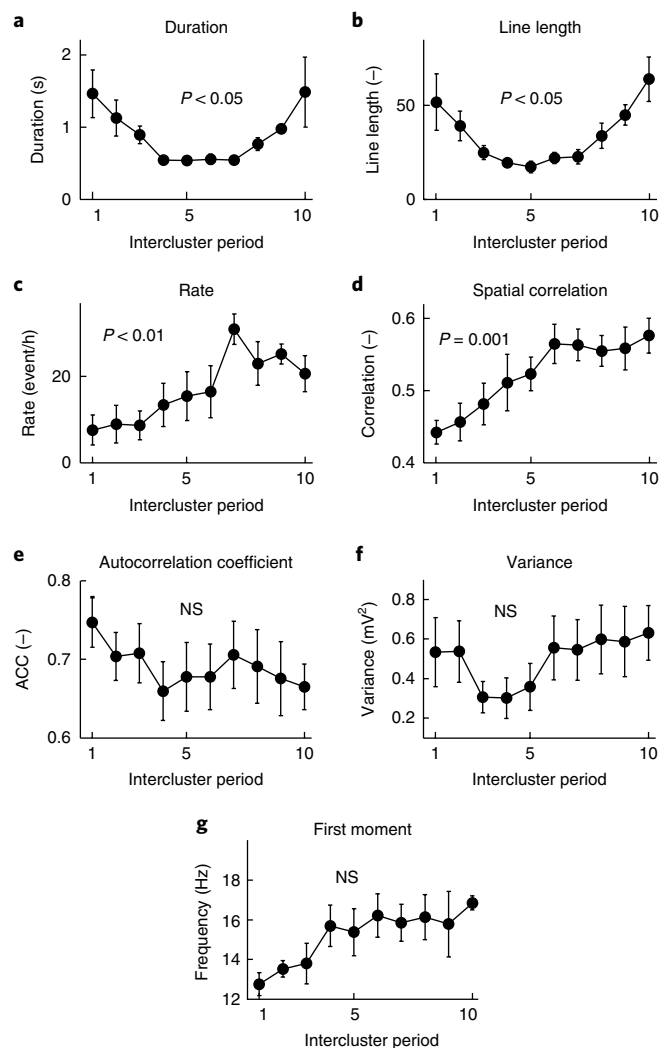
Fig. 7 | Changes in the properties of epileptic bursts between clusters of seizures. a,b, With the approaching cluster, the duration of the bursts increased (**a**; $n = 6/6$ intercluster periods/animals, one-way ANOVA, $F_{(1,53)} = 2.751$, $P = 0.012$), as did the line-length parameter (**b**; $n = 6/6$ intercluster periods/animals, one-way ANOVA, $F_{(1,53)} = 3.347$, $P = 0.003$). **c**, The proximity to critical transition was also marked by the increasing rate of epileptic bursts ($n = 6/6$ intercluster periods/animals, one-way ANOVA, $F_{(1,59)} = 3.105$, $P = 0.005$). **d**, Increase in spatial correlation reflects enhanced propagation of bursts to the hippocampus and motor cortex ($n = 6/6$ intercluster periods/animals, one-way ANOVA, $F_{(1,53)} = 7.792$, $P = 0.001$). **e–g**, The autocorrelation (**e**; $n = 6/6$ intercluster periods/animals, one-way ANOVA, $F_{(1,53)} = 0.57$, $P = 0.928$), signal variance (**f**; $n = 6/6$ intercluster periods/animals, one-way ANOVA, $F_{(1,53)} = 0.4$, $P = 0.814$), and the first spectral moment (**g**; $n = 6/6$ intercluster periods/animals, one-way ANOVA, $F_{(1,53)} = 1.659$, $P = 0.128$) did not show significant changes with the approaching cluster. The significance of changes in temporal profiles was analyzed using one-way ANOVA. Circles and error bars represent mean and s.e.m., respectively. NS, nonsignificant.

GABAergic transmission[39]. They are accompanied by potassium transients and have been linked primarily with pro-seizure effects. IEDs in our study were of glutamatergic origin and, throughout the course of the period between seizures, were always followed by a transient suppression of neuronal and network activity. These synaptic perturbations induced phasic changes, which interfered with the slow process of critical slowing, and the discharges possessed both pro-seizure and anti-seizure effects. Combining experimental

50
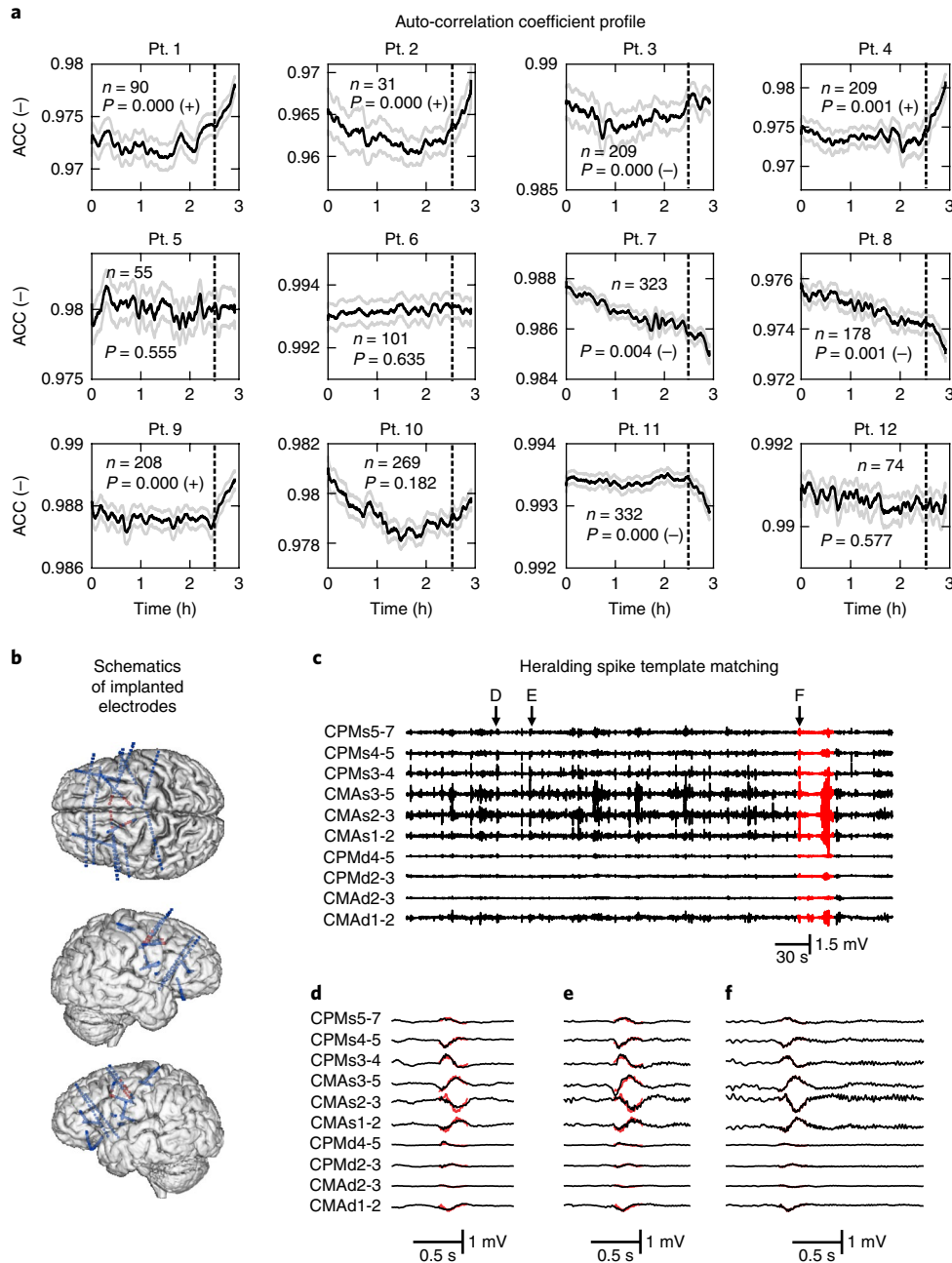
Fig. 8 | The loss of resilience and state-dependent effect of IEDs in humans. a, Temporal profile of the autocorrelation coefficient (ACC) derived from intracranial recordings in 12 patients. The temporal profile 3 h before a seizure is shown. The dashed line marks the 30 min before the seizure during which the ACC profile was analyzed. In four patients, the ACC increased before the seizure. In four patients, ACC significantly decreased. n denotes the number of recorded seizures in each patient. P values were measured by the Wilcoxon sign-rank test. The sign after the P value indicates whether the right-tailed (+) or left-tailed (−) Wilcoxon sign-rank tests were significant. Lines and shaded lines represent mean and s.e.m., respectively. **b**, Schematics of depth electrode implantation in a patient with refractory epilepsy. The signals from red contacts are shown. **c**, An example of spontaneous activity recorded 5 min before and during the seizure (red). **d**,**e**, Examples of the IEDs. Their waveforms and patterns of spatial distribution displayed a >98% match with the superimposed template of the heralding spike (red). **f**, Heralding spike at the onset of a habitual seizure.

observations with modeling revealed that the complex effect of IEDs depends on when they occur, how often they occur, and how strong the perturbations are with respect to the instantaneous dynamical state of the seizure-generating network and with respect to the character of the dynamical process that governs the slow transition to seizure. The combination of these factors could explain all of the currently known effects of IEDs on seizure genesis and explain why their effects can vary in time. The anti-seizure effect is achieved via a subsequent suppression of neuronal activity, which shifts the neural

network dynamics back to the more stable/resilient state. If the network is close to the tipping point, transient excitation/synchronization acts as a destabilizing perturbation, which acts across large spatial scales. It then rapidly shifts the critical neuronal mass into a seizure in advance of the catastrophic bifurcation in which the seizure would have occurred spontaneously[18,40].

The implemented phenomenological model of the slow-fast process is a widely accepted model in nonlinear dynamics research[14,21,29], including applications in neuroscience and epilepsy

modeling proper[41]. Despite being a very simplified model, it is able to capture and explain the rich and complex dynamical phenomena that we observed. The identified principles also operate in the more advanced model of the Epileptor[3], which can replicate epileptiform phenomena in greater detail and which also depends on the presence of basic slow-fast dynamics of switching between seizure and non-seizure state. Other models of epileptic dynamics have been proposed to provide an explanation of the principles of seizure onset. Apart from the interictal perturbations, phenomena such as the various types of instabilities[6], the role of network structure and network effects[42], slow variations in global excitability[43], seizure spread[44], and the balance between excitation and inhibition[25] shape the seizure. However, experimental evidence points to the crucial role of the slowly changing variable of the slow process, which determines the dynamical trajectory of the epileptic brain, the probability of the transition to seizure, and complex response to interictal perturbation. Numerical simulations and understanding the governing dynamical principles can be beneficial in the search for candidate mechanisms that underlie this slow process and for the design of dynamics-based control strategies[29]. In addition, a slowly changing process and loss of resilience have the potential to be better controlled than the random occurrence of stochastic perturbations initiating seizure. In the high-potassium model, seizures tend to occur after dozens of minutes when the CA1 network enters the bi-stable state, which suggests that ictal events depend on more complex processes than just a change in membrane potential. The transition to seizure is associated with a DC shift, which reflects slow progressive neuronal and glial membrane depolarization, which is closely, but not ultimately, associated with the accumulation of potassium in the extracellular space between seizures[45,46]. The slowly changing process may include a vicious circle of multiple cellular and network changes ranging from an alteration in the KCC2 co-transporter to increased intracellular load of chloride, erosion of inhibition, ectopic action potential generation, and the involvement of non-synaptic interactions, etc.[33]. The exact mechanisms underlying the slow process in humans or in vivo remain to be elucidated.

Our results suggest that the progressive loss of resilience of epileptic tissue may characterize the transition to both experimental and clinical seizures. In a complex system such as a human or rat brain, the loss of resilience, critical slowing, and the dynamical path of the transition to seizure can be substantially influenced by other parameters and processes such as the progressive nature of epileptogenesis[47], long-term fluctuations in the brain's predisposition to seize[48], and seizure clustering[47]. Critical slowing will be difficult to observe if the seizure occurs prematurely as a result of a large external perturbation, which may be the case for some human subjects. Furthermore, critical slowing does not have to be the only dynamical pathway leading to seizure[3,7,49], and trajectories leading to seizure can vary inter-individually, that is, between patients, as well as intra-individually, that is, within each patient[48–50]. Recent theoretical work suggests that merging complex information about dynamical processes at multiple spatial and temporal scales can bring us much closer to understanding the principles of seizure emergence and initiation, and possibly to a unified theory of ictogenesis in the epileptic brain to explain the existence of the various classes of seizure type and transitions to them[49].

Online content

Any methods, additional references, Nature Research reporting summaries, source data, statements of data availability and associated accession codes are available at https://doi.org/10.1038/s41593-018-0278-y.

References

1. Fisher, R. S. et al. ILAE official report: a practical clinical definition of epilepsy. *Epilepsia* **55**, 475–482 (2014).
2. Jiruska, P. et al. Synchronization and desynchronization in epilepsy: controversies and hypotheses. *J. Physiol. (Lond.)* **591**, 787–797 (2013).
3. Jirsa, V. K., Stacey, W. C., Quilichini, P. P., Ivanov, A. I. & Bernard, C. On the nature of seizure dynamics. *Brain* **137**, 2210–2230 (2014).
4. Lopes da Silva, F. Epilepsy as a disease of the dynamics of neuronal networks: models and predictions. In *Seizure Prediction in Epilepsy: From Basic Mechanisms to Clinical Applications* (eds. Schelter, B., Timmer, J. & Schulze-Bonhage, A.) 97–107 (Wiley-VCH, Weinheim, Germany, 2008).
5. Beghi, E. et al. Recommendation for a definition of acute symptomatic seizure. *Epilepsia* **51**, 671–675 (2010).
6. Breakspear, M. et al. A unifying explanation of primary generalized seizures through nonlinear brain modeling and bifurcation analysis. *Cereb. Cortex* **16**, 1296–1313 (2006).
7. Lopes da Silva, F. et al. Epilepsies as dynamical diseases of brain systems: basic models of the transition between normal and epileptic activity. *Epilepsia* **44** (Suppl 12), 72–83 (2003).
8. de Curtis, M. & Avanzini, G. Interictal spikes in focal epileptogenesis. *Prog. Neurobiol.* **63**, 541–567 (2001).
9. Avoli, M., de Curtis, M. & Köhling, R. Does interictal synchronization influence ictogenesis? *Neuropharmacology* **69**, 37–44 (2013).
10. Barbarosie, M. & Avoli, M. CA3-driven hippocampal-entorhinal loop controls rather than sustains in vitro limbic seizures. *J. Neurosci.* **17**, 9308–9314 (1997).
11. Karoly, P. J. et al. Interictal spikes and epileptic seizures: their relationship and underlying rhythmicity. *Brain* **139**, 1066–1078 (2016).
12. Avoli, M. & de Curtis, M. GABAergic synchronization in the limbic system and its role in the generation of epileptiform activity. *Prog. Neurobiol.* **95**, 104–132 (2011).
13. Huberfeld, G. et al. Glutamatergic pre-ictal discharges emerge at the transition to seizure in human epilepsy. *Nat. Neurosci.* **14**, 627–634 (2011).
14. Rinaldi, S. & Scheffer, M. Geometric analysis of ecological models with slow and fast processes. *Ecosystems* **3**, 507–521 (2000).
15. Scheffer, M. et al. Anticipating critical transitions. *Science* **338**, 344–348 (2012).
16. Scheffer, M. et al. Early-warning signals for critical transitions. *Nature* **461**, 53–59 (2009).
17. Draguhn, A., Traub, R. D., Schmitz, D. & Jefferys, J. G. Electrical coupling underlies high-frequency oscillations in the hippocampus in vitro. *Nature* **394**, 189–192 (1998).
18. Jiruska, P. et al. High-frequency network activity, global increase in neuronal activity, and synchrony expansion precede epileptic seizures in vitro. *J. Neurosci.* **30**, 5690–5701 (2010).
19. Lopes, M. A., Lee, K. E. & Goltsev, A. V. Neuronal network model of interictal and recurrent ictal activity. *Phys. Rev. E* **96**, 062412 (2017).
20. Kalitzin, S., Velis, D., Suffczynski, P., Parra, J. & da Silva, F. L. Electrical brain-stimulation paradigm for estimating the seizure onset site and the time to ictal transition in temporal lobe epilepsy. *Clin. Neurophysiol.* **116**, 718–728 (2005).
21. Scheffer, M. & Carpenter, S. R. Catastrophic regime shifts in ecosystems: linking theory to observation. *Trends Ecol. Evol.* **18**, 648–656 (2003).
22. Hawkins, C. A. & Mellanby, J. H. Limbic epilepsy induced by tetanus toxin: a longitudinal electroencephalographic study. *Epilepsia* **28**, 431–444 (1987).
23. Jiruska, P. et al. Epileptic high-frequency network activity in a model of non-lesional temporal lobe epilepsy. *Brain* **133**, 1380–1390 (2010).
24. Cook, M. J. et al. Prediction of seizure likelihood with a long-term, implanted seizure advisory system in patients with drug-resistant epilepsy: a first-in-man study. *Lancet Neurol.* **12**, 563–571 (2013).
25. Wendling, F., Bartolomei, F., Bellanger, J. J. & Chauvel, P. Epileptic fast activity can be explained by a model of impaired GABAergic dendritic inhibition. *Eur. J. Neurosci.* **15**, 1499–1508 (2002).
26. Fröhlich, F., Sejnowski, T. J. & Bazhenov, M. Network bistability mediates spontaneous transitions between normal and pathological brain states. *J. Neurosci.* **30**, 10734–10743 (2010).
27. de Curtis, M. & Avoli, M. Initiation, Propagation, and Termination of Partial (Focal) Seizures. *Cold Spring Harb. Perspect. Med.* **5**, a022368 (2015).
28. Suffczynski, P. et al. Dynamics of epileptic phenomena determined from statistics of ictal transitions. *IEEE Trans. Biomed. Eng.* **53**, 524–532 (2006).
29. Scheffer, M. *Critical Transitions in Nature and Society* (Princeton University Press, Princeton, NJ, USA, 2009).
30. Kramer, M. A. et al. Human seizures self-terminate across spatial scales via a critical transition. *Proc. Natl. Acad. Sci. USA* **109**, 21116–21121 (2012).
31. van de Leemput, I. A. et al. Critical slowing down as early warning for the onset and termination of depression. *Proc. Natl. Acad. Sci. USA* **111**, 87–92 (2014).
32. Jiruska, P., Mormann, F. & Jefferys, J.G.R. Neuronal and network dynamics preceding experimental seizures. in *Recent Advances in Predicting and Preventing Epileptic Seizures* (eds. Tetzlaff, R. & Elger, C.E.) 16–29 (2013).

33. Blauwblomme, T., Jiruska, P. & Huberfeld, G. Mechanisms of ictogenesis. *Int. Rev. Neurobiol.* **114**, 155–185 (2014).

34. Jensen, M. S. & Yaari, Y. The relationship between interictal and ictal paroxysms in an in vitro model of focal hippocampal epilepsy. *Ann. Neurol.* **24**, 591–598 (1988).

35. Gotman, J. & Marciani, M. G. Electroencephalographic spiking activity, drug levels, and seizure occurrence in epileptic patients. *Ann. Neurol.* **17**, 597–603 (1985).

36. Avoli, M. et al. Specific imbalance of excitatory/inhibitory signaling establishes seizure onset pattern in temporal lobe epilepsy. *J. Neurophysiol.* **115**, 3229–3237 (2016).

37. de Curtis, M., Librizzi, L. & Biella, G. Discharge threshold is enhanced for several seconds after a single interictal spike in a model of focal epileptogenesis. *Eur. J. Neurosci.* **14**, 174–178 (2001).

38. Muldoon, S. F. et al. GABAergic inhibition shapes interictal dynamics in awake epileptic mice. *Brain* **138**, 2875–2890 (2015).

39. Avoli, M. et al. Synchronous GABA-mediated potentials and epileptiform discharges in the rat limbic system in vitro. *J. Neurosci.* **16**, 3912–3924 (1996).

40. Bikson, M., Fox, J. E. & Jefferys, J. G. Neuronal aggregate formation underlies spatiotemporal dynamics of nonsynaptic seizure initiation. *J. Neurophysiol.* **89**, 2330–2333 (2003).

41. Suffczynski, P., Kalitzin, S. & Lopes Da Silva, F. H. Dynamics of non-convulsive epileptic phenomena modeled by a bistable neuronal network. *Neuroscience* **126**, 467–484 (2004).

42. Benjamin, O. et al. A phenomenological model of seizure initiation suggests network structure may explain seizure frequency in idiopathic generalised epilepsy. *J. Math. Neurosci.* **2**, 1 (2012).

43. Naze, S., Bernard, C. & Jirsa, V. Computational modeling of seizure dynamics using coupled neuronal networks: factors shaping epileptiform activity. *PLoS Comput. Biol.* **11**, e1004209 (2015).

44. Kim, J. W., Roberts, J. A. & Robinson, P. A. Dynamics of epileptic seizures: evolution, spreading, and suppression. *J. Theor. Biol.* **257**, 527–532 (2009).

45. Jensen, M. S. & Yaari, Y. Role of intrinsic burst firing, potassium accumulation, and electrical coupling in the elevated potassium model of hippocampal epilepsy. *J. Neurophysiol.* **77**, 1224–1233 (1997).

46. Traynelis, S. F. & Dingledine, R. Potassium-induced spontaneous electrographic seizures in the rat hippocampal slice. *J. Neurophysiol.* **59**, 259–276 (1988).

47. Williams, P. A. et al. Development of spontaneous recurrent seizures after kainate-induced status epilepticus. *J. Neurosci.* **29**, 2103–2112 (2009).

48. Baud, M. O. et al. Multi-day rhythms modulate seizure risk in epilepsy. *Nat. Commun.* **9**, 88 (2018).

49. Saggio, M. L., Spiegler, A., Bernard, C. & Jirsa, V. K. Fast-slow bursters in the unfolding of a high codimension singularity and the ultra-slow transitions of classes. *J. Math. Neurosci.* **7**, 7 (2017).

50. Cook, M. J. et al. Human focal seizures are characterized by populations of fixed duration and interval. *Epilepsia* **57**, 359–368 (2016).

Author contributions

P.J., J.G.R.J., W.-C.C., J.C., J.H., and M.J.C. conceived the study and designed the experiments. A.D.P., W.-C.C., P.J., J.K., J.O., J.H., J.C., M.I.M., M.J.C., P.J.K., and D.R.F. performed the experiments. W.-C.C., P.J., J.O., M.P., V.K., J.K., J.H., R.J., R.C., A.D.P., J.G.R.J., M.I.M., M.J.C., P.J.K., and D.R.F. analyzed the data. W.-C.C., P.J., J.G.R.J., J.H., and J.K. wrote the manuscript.

Competing interests

The authors declare no competing interests.

Additional information

Supplementary information is available for this paper at https://doi.org/10.1038/s41593-018-0278-y.

Reprints and permissions information is available at www.nature.com/reprints.

Correspondence and requests for materials should be addressed to J.G.R.J. or P.J.

Publisher's note: Springer Nature remains neutral with regard to jurisdictional claims in published maps and institutional affiliations.

6   The role of interictal discharges in icto-genesis — A dynamical perspective

6.1   The contributions toward the progress of the field

Based on the evidence from Chang et al. (2018), there exists a plausible explanation for why previous studies have reported a wide spectrum of effects of IEDs, ranging from pro-seizure, anti-seizure effect, to no impact of IEDs on ictogenesis. We propose that the impact of IEDs on seizure is determined by the dynamical state of the brain at the moment of IED discharge occurrence, which explains the existing dichotomy. This study is important also from a clinical perspective. It is not clear whether the complete cessation of IEDs is a reliable marker of epilepsy remission and whether IED-free EEG or the cessation of seizures but persistence of IEDs should be considered as a therapeutic success. The review also highlights the direct therapeutic application of the findings (Chang et al., 2018), which may be highly relevant for the optimization of therapeutic neurostimulation to stabilize the epileptic brain and prevent seizure emergence. Stimulation delivered during the stable states may display seizure delaying and stabilizing effect effect whereas stimulation applied during an unstable state may increase the probability of seizure occurrence.

6.2   The author's contributions

The author was responsible for the literature review and manuscript writing.

6.3   Compliance with the thesis objectives

Thinking of the brain as a dynamic system that exhibits stable states of varying degrees is very important in studying HFOs. As we have previously shown, (Chang et al., 2018) the oscillatory nature of HFO is closely related to the degree of dynamical stability and may serve as a biomarker in diagnostics.
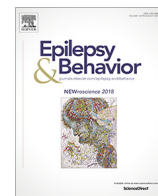
Review

The role of interictal discharges in ictogenesis — A dynamical perspective

Jan Chvojka [a,b,c], Jan Kudlacek [a,b,c], Wei-Chih Chang [d], Ondrej Novak [a], Filip Tomaska [a], Jakub Otahal [b], John G.R. Jefferys [a,e], Premysl Jiruska [a,b,*]

[a] Department of Physiology, Second Faculty of Medicine, Charles University, Prague, Czech Republic
[b] Department of Developmental Epileptology, Institute of Physiology of the Czech Academy of Sciences, Prague, Czech Republic
[c] Department of Circuit Theory, Faculty of Electrical Engineering, Czech Technical University in Prague, Prague, Czech Republic
[d] Faculty of Veterinary Medicine and Neuroscience Center, University of Helsinki, Helsinki 00014, Finland
[e] Department of Pharmacology, University of Oxford, Mansfield Road, Oxford OX1 3QT, United Kingdom

ARTICLE INFO

ABSTRACT

Interictal epileptiform discharge (IED) is a traditional hallmark of epileptic tissue that is generated by the synchronous activity of a population of neurons. Interictal epileptiform discharges represent a heterogeneous group of pathological activities that differ in shape, duration, spatiotemporal distribution, underlying cellular and network mechanisms, and their relationship to seizure genesis. The exact role of IEDs in epilepsy is still not well understood, and there remains a persistent dichotomy about the impact on IEDs on seizures. Proseizure, antiseizure, and no impact on ictogenesis have all been described in previous studies. In this article, we review the existing knowledge on the role of interictal discharges in seizure genesis, and we discuss how dynamical approaches to ictogenesis can explain the existing dichotomy about the multifaceted role of IEDs in ictogenesis.
This article is part of the Special Issue "NEWroscience 2018"

© 2019 Elsevier Inc. All rights reserved.

1. Introduction

Interictal epileptiform discharge (IED) is a traditional electrographic hallmark of the presence of epileptic tissue in the brain [1]. Its significance was identified early after the introduction of electroencephalography into the clinical practice [2]. Since then, IEDs are considered an electrographic biomarker of epileptic tissue, and their presence in electroencephalogram (EEG) is used to diagnose epilepsy. In a patient with diagnosed epilepsy, IEDs and their properties are utilized to monitor the disease activity, determine the response to the antiepileptic drug treatment, and define the epilepsy remission [1]. The spatial distribution of IEDs helps to localize the epileptic focus, and it is extensively used in presurgical examination in candidates of epilepsy surgery [3], where IEDs define the irritative zone [3,4]. Additional information derived from IED morphology, rate, time delay, spread etc. help to stratify irritative zone in greater detail and differentiate areas of IED origin from areas of IED propagation [4,5]. Some of these features are more closely associated with endogenous epileptogenicity and discriminate regions of the irritative zone that colocalize with seizure onset or epileptogenic zone — area of the brain necessary to remove or disconnect to achieve seizure freedom. Unfortunately, the information that can be extracted

from IEDs is not always clear, and multiple ambiguities about the clinical significance of IEDs exist. It is not clear whether the complete cessation of IEDs is a reliable marker of epilepsy remission and whether IED-free EEG should represent the main therapeutic goal. Key questions include whether changes in IED rates are a good marker of antiepileptic drug efficacy or whether the cessation of seizures but persistence of IEDs should be considered as a therapeutic success. These clinical ambiguities can be attributed to the incomplete knowledge about the cellular and network mechanisms of IEDs and their role in epilepsy and seizures. It is well established now that IEDs are not a uniform phenomenon. They rather represent a group of heterogeneous epileptiform activities that may share similar morphological features in EEG, but they may substantially differ in the underlying network mechanisms and their involvement in seizure genesis and epileptogenesis.

2. Cellular and network mechanisms of IED

Traditionally, textbooks describe IED as a field potential (e.g., EEG) correlate of the synchronous activation of a large population of principal neurons [6]. At the cellular level, it is characterized by a large depolarizing envelope due to giant excitatory postsynaptic potential — paroxysmal depolarization shift [7]. Alternatively, the depolarization envelope can result from the opening of calcium channels [8] although other currents like impaired potassium currents or enhanced Na^+-K^+ (h) currents are involved, too [9–11]. This depolarizing component

and synchronous activation largely depend on glutamatergic transmission; pharmacological blockage of both α-amino-3-hydroxy-5-methyl-4-isoxazolepropionic acid (AMPA) and N-methyl-D-aspartate (NMDA) receptors suppresses or attenuates IEDs [12,13]. The IED is a network phenomenon, and therefore, the cellular dynamics during IED is very heterogeneous [14]. Early studies have shown that the depolarization shift is accompanied by a burst of action potentials of principal cells [14]. Similarly, later studies showed that the shift is also observed in interneurons. For example, soma-targeting (parvalbumin positive) interneurons and axon-targeting interneurons were observed to fire ahead of principal neurons, but then rapidly entered into depolarization block [14]. The failure of soma-targeting inhibition allows principal neurons to burst unlimitedly on the top of IED [14].

The depolarizing part of IED has a brief duration of 80–200 ms. It is terminated by a hyperpolarizing event that can have intrinsic component due to the outward currents (potassium, calcium-induced potassium currents) or a network component. In the latter, the hyperpolarization is induced by feedforward and feedback inhibition originating from interneurons recovered from the depolarization block [14].

The second major group of interictal discharges is dependent on gamma-aminobutyric acid (GABA) transmission and $GABA_A$ receptor-associated conductance. It was identified in the 4-aminopyridine model of acute seizure in entorhinal cortex [15,16]. These discharges are less frequent and of longer duration. They can be blocked by perfusing slices with GABA receptor inhibitor, and they persist if both non-NMDA and NMDA receptors are blocked [17]. It is assumed that these discharges can have proseizure impact. The slow IED is associated with moderate elevation of extracellular potassium due to upregulated potassium chloride cotransporter (KCC2) activity [18,19]. If the brain is balancing on the verge of transition to the seizure, then this potassium transient can tip the balance towards the seizure initiation (see below) [15,16].

Recently, the interictal epileptiform activity was explored in detail in human epileptic slices. In this elegant study, two types of discharges were identified [20]. Interictal discharges that occurred widely distributed across large areas of the limbic system. Their occurrence was spatially random; they had smaller amplitude and low velocity of propagation. Their onset was preceded by interneuronal firing, and they depended on both glutamatergic and GABAergic transmission, respectively. A specific type of preictal discharges was observed in subiculum where seizures also originated. These discharges were of glutamatergic origin, had high amplitude, and were preceded by principal cell firing. They occurred several seconds in advance of an approaching seizure. Their close spatial relationship with seizure onset zone was examined using electrical stimulation. While the repeated stimulation of subiculum induced preictal discharges and seizures, it was unable to induce these phenomena in the areas of preictal discharge propagation pointing to endogenous epileptogenicity of subiculum.

When considering the functional impact of IEDs and their potential effect on seizures and disease activity, it is essential to recognize that the cellular mechanisms of IEDs can differ in the areas where IEDs are generated from the areas to which they propagate. In the site of IED origin, neurons generate a typical depolarization envelope [7,21] with intense high-frequency action potential firing. In contrast, neurons in areas surrounding the epileptic focus and areas of IED propagation demonstrate cellular behavior characterized by a sequence of excitatory and inhibitory postsynaptic potentials [22,23], with increased action potential firing only in a minority of principal cells [24,25]. This difference can be attributed to the inhibitory mechanisms and activity of interneurons.

Recent studies demonstrate that interneurons display very rich behavior during IEDs. Using calcium imaging in awake animals, Muldoon et al. demonstrated that interictal discharge was associated with dramatic activation of interneuronal populations [26]. Although interneurons may play a role in IED initiation, they play a crucial role in shaping the morphology, propagation, spatial extent, and the effect of IEDs on seizures [26,27]. It is well documented now that all these phenomena are substantially modified by the activity of interneuronal network, and each interneuronal subtype have specific role interictal activity. Interneurons are recruited into epileptic activity via feedback and feedforward activation, through interneuronal syncytia, or by long-range neuronal and interneuronal connections [26–29].

3. The epileptogenic and ictogenic potential of IEDs

Interictal epileptiform discharges represent an electrographic marker of the epileptic brain. They occur during early stages of epileptogenesis and precede the occurrence of spontaneous seizures [30–32]. Neuronal processes involved in the genesis of IEDs also have epileptogenic and ictogenic potential. It has been shown that they promote the sprouting of axon collaterals and induce molecular reorganization and changes in the expression of ligand- and voltage-gated ion channels [30,31]. These changes enhance the synaptic efficiency and tissue excitability that lead to an increased endogenous propensity to generate seizures. In particular, IEDs with superimposed pathological high-frequency oscillations are considered to be highly epileptogenic as they spatially correlate with epileptogenic brain areas [33–36], and they can promote epileptogenic conversion via kindling mechanisms. Also, mechanisms that are involved in high-frequency oscillations seem to be similar to the mechanisms responsible for seizure initiation [37]. It is well established that IEDs interfere with the occurrence of seizures. Specific types of IEDs have proictal effects and induce seizures, for example, by increasing extracellular potassium concentration or enhancing glutamatergic transmission [13,16,20]. Other studies demonstrate that the presence of IEDs is beneficial as they can display antiictogenic effect [38,39].

Seminal work of Jensen and Yaari in a high-potassium model of seizures in hippocampal slices in vitro showed that discharges generated in CA3 and propagating to CA1 have the capacity to delay the onset of seizures, which are primarily produced in CA1 [40]. In this preparation, IED events were dependent on intact glutamatergic transmission as they were blocked by AMPA and NMDA receptor antagonists [13,40]. If IEDs were pharmacologically blocked or CA3-disconnected from CA1, seizure frequency increased [13,40]. The seizure frequency returned to baseline if the IEDs were replaced by repeated electrical stimulation of Schaffer collaterals. Electrical stimulation could even lead to a complete cessation of seizures [40]. A similar observation was described in hippocampal–entorhinal preparation exposed to 4-aminopyridine [13,39]. Here, seizures were generated primarily in the entorhinal cortex and transition to seizure is controlled by the IEDs from CA3. After Shaffer collateral cut, IEDs disappeared from entorhinal cortex, CA1, and DG, and seizure frequency increased. These studies suggest that at least in the limbic system preparations, IEDs represent a phenomenon that can display an antiictogenic effect. Negative correlation between IEDs generated in piriform cortex and seizures originating in entorhinal cortex and hippocampal were observed also in isolated guinea pig brain exposed to bicuculline [41]. From this perspective, the therapeutic suppression of IEDs could be a counterproductive approach that could increase seizure propensity. Convincing studies or similar observations in vivo humans are lacking both in experiment rodents and in humans.

Other studies suggest that interictal discharges are proictogenic, i.e., they can directly trigger a seizure, or their presence reflects a preictal state and the imminence of seizure. Specific seizure onset types are characterized by the presence of large-amplitude discharge so-called heralding spike, which shares morphology and spatial distribution with IEDs (Fig. 3) [13,35,42,43]. Moreover, they can also share a high-frequency component. Specifically, hypersynchronous seizure onset is characterized by the initial IED-like discharge superimposed with a high-frequency oscillation that has similar morphology and spectral profile as an oscillation superimposed on IEDs between seizures [35]. It is assumed that because of these similarities, the cellular mechanism behind IEDs and high-frequency oscillation is also involved in

seizure initiation, and on this occasion, they have a proictal or seizure-triggering effect. Intracellularly recorded large depolarization accompanying GABAergic interictal discharges was also recorded during the onset of ictal discharge in entorhinal cortex. Preictal discharges identified by Huberfeld et al. immediately preceded the seizure onset in human epileptic subiculum [20]. Neurophysiologists tend to explain the proictogenic or antiictogenic potential of IEDs predominantly by the existence of the specific network, cellular and pharmacological features of IEDs [38]. Another parameter of IEDs that was explored in greater detail, especially in seizure warning (prediction) studies, was IED rate. Here, it was expected that changes in IED rate could predict the approaching seizure, and it could also be informative about the network changes responsible for the transition to seizure [44]. While specific studies demonstrated that IED rate increased ahead of seizures, other studies showed rather a decrease or absence of changes in IED rate ahead of seizure. Karoly et al. analyzed the relationship of IEDs and seizures in patients with a chronically implanted recording device [45,46]. They did not find any correlation between the patient's average IED rate and seizure rate. When looking at possible preictal changes, in 9/15 patients, they discovered IED rate change before a seizure, where in 6/9 patients, IED rate was decreased and in 3/9 patients, it was increased. Is there any possibility how the multifaceted role of IEDs in seizure genesis and existing (often antagonistic) theories about their functional effect on the epileptic network activity could be explained? This question could be addressed by studies that approach epilepsy and seizures as dynamic phenomena [13,47–49].

4. Ictogenesis from a dynamical perspective

The brain can be conceptualized as a dynamical system that exists in two states, interictal and seizure, respectively (Fig. 1A). Seizure initiation and termination are viewed as a bifurcation. In the dynamics of complex systems, bifurcation occurs when a small change of specific parameter (the bifurcation parameters) of a system causes a sudden and dramatic 'qualitative' shift in the system's behavior [48,49]. Various pathways were identified how the brain could reach the bifurcation and enter the seizure state [48,50–52]. The healthy brain operates in the dynamical regime characterized by high stability and strong resilience to internal or external perturbations. To shift its dynamics to seizure and to reach the bifurcation requires the occurrence of a significant and very strong perturbation (Fig. 1B). Such transition process is typical for acute seizures, which emerge in normal brain after severe traumatic brain injury, stroke, or intoxication, etc.

In contrast to the healthy brain, the epileptic brain is characterized by enduring predisposition to generate seizures, i.e., it is bistable. Its dynamics is characterized by repeated switching between interictal and ictal states. Such transition can easily occur in a brain that is very unstable with its dynamics operating very close to the tipping point (bifurcation) separating interictal state and a seizure [48,49]. Such a system has very low resilience to perturbations when even very weak perturbation can tip the dynamics to the ictal regime (Fig. 1C). Because the brain is constantly exposed to stochastic perturbations, seizures in the unstable brain will occur randomly, and they cannot be predicted. It is assumed that this type of transition to seizure is characteristic for generalized epilepsies.

A second major route for the epileptic brain to enter the seizure state is characterized by gradual changes in system's stability due to changes in a specific critical parameter, which slowly and inevitably shifts the brain dynamics towards the tipping point (Fig. 1D) [48,50,53,54]. This route is characterized by a progressively decreasing brain resilience and increasing sensitivity to internal or external perturbations with approaching seizure. Close to the tipping point, the system becomes highly unstable, and any weak perturbation can flip the dynamics to the contrasting regime. This dynamical pathway was observed in focal epilepsies [13,55]. The exact cellular mechanisms that drive the system slowly but inevitably to the seizure are not known. One of the most
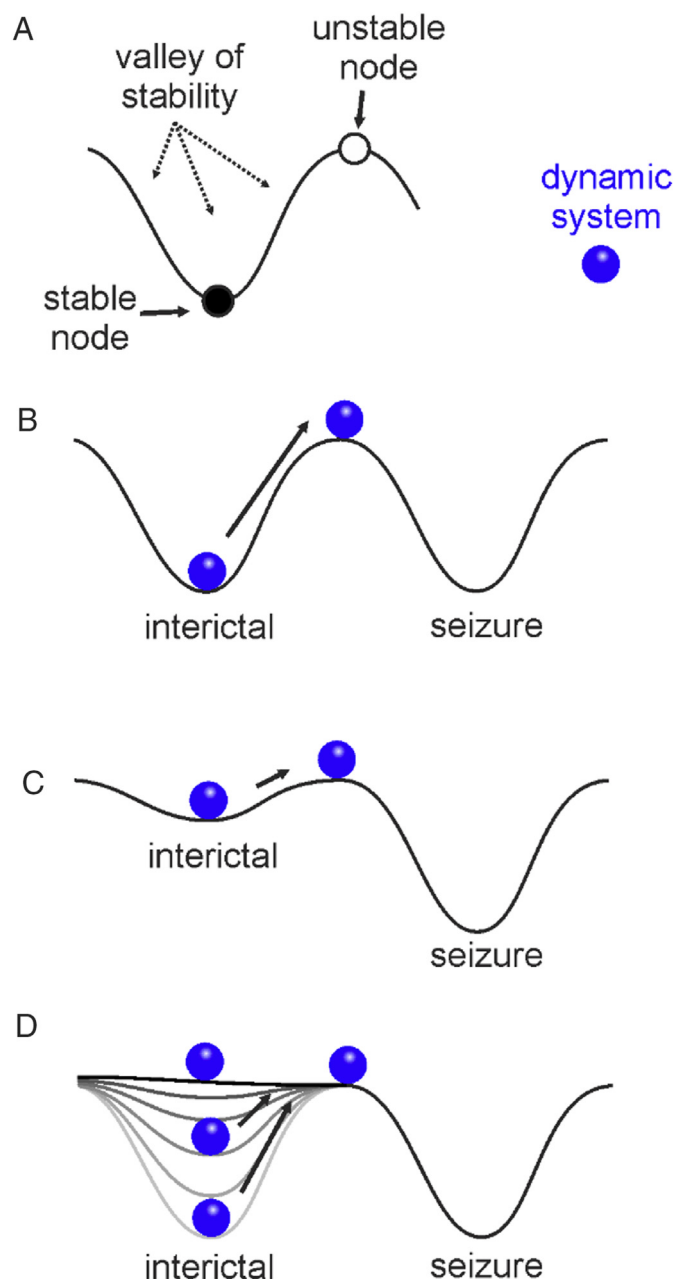
Fig. 1. A dynamical approach to ictogenesis. A: The brain can be conceptualized as a dynamic system that can exist in the interictal or seizure state. Each state can be described by the valley of stability with its stable node at the bottom of the valley to which the system is attracted. Both states are separated by the unstable node (tipping point) where bifurcation occurs. B: Seizure emerging from stable brain dynamics requires significant perturbation to shift to seizure. C: Generalized epilepsies are characterized by low stability and low resilience to perturbation when even weak stochastic disruptions can easily initiate seizure. D: The transition to seizure via critical slowing occurs when the system progressively loses stability and resilience. It manifests by increasing sensitivity to perturbation and delayed recovery from the perturbation with approaching seizure.

commonly cited candidate mechanisms is a vicious circle of intense neuronal activity, increased neuronal depolarization, an increase in extracellular potassium, alteration in the KCC2 cotransporter, shifts in the direction of the ion transport, etc. The consequent increased intracellular load of chloride and an increase in extracellular potassium can be further aggravated by active inhibition, which hampers the increased cellular and network activity [13,55]. In slice preparations, pharmacological manipulations aiming at slow processes like extracellular potassium transients, altered chloride shift, or the depolarizing effect of GABA

can effectively suppress seizures. As the resilience and stability deteriorate other pathological phenomena like ectopic action potential generation, conversion of neurons to burst firing and increased nonsynaptic interactions can come into action and contribute to a vicious circle.

The nature of this transition and the progressive decrease in resilience can be monitored. The most effective tool to explore the system's stability and resilience represents active perturbation using electrical stimulation [13,55–57]. It has been shown that with approaching seizure, the response to electrical stimulation (orthodromic, antidromic, or applied external fields) is characterized by delayed recovery from the stimulation and increased sensitivity to the stimulus intensity [13,55]. Because of increasing delay from recovery, the process of how the brain loses resilience is called critical slowing [58,59]. Because any system is continuously challenged by internal or external perturbation, the delayed recovery from the perturbations can be derived by passively observing the system's behavior. The features that characterize the slowing of recovery are denoted as an early warning signal of critical transition [60]. The representative signals are frequency slowing down, increase in autocorrelation, flickering, increase in variance, spatial expansion, etc. The second route was shown to be involved in both transition to seizure [13,55,59] and seizure termination [51,61]. It is important to note that even in the system characterized by a dramatic decrease in its resilience, the early warning signals of critical slowing could be very discrete or difficult to observe. The early warning signals may also be absent in a dynamic scenario where the velocity towards which the system evolves to a bifurcation is very fast.

## 5. IED effect depends on the dynamical state of the epileptic brain

From a dynamical perspective, IED can be viewed as a perturbation of the epileptic brain dynamics [13]. The dynamical state of the brain then determines how the brain will respond to the perturbation and what will be the functional effect of interictal discharges. In the brain that undergoes a change in brain resilience, incoming interictal discharge acts as an external perturbation, which displaces the system close to the tipping point. If the system rests in a stable state with high resilience, IED, even of high amplitude, is not able to reach the tipping point of bifurcation, and the system quickly recovers from IED (Fig. 2B). Only extremely strong IEDs can cross the tipping point and shift the dynamics to seizure. In this scenario, IED can have a beneficial effect, and it can move the brain dynamics even to a more stable state (Fig. 2B). Such a 'positive' impact of a perturbation of the system behavior is well described in various dynamical systems, and refractory period after IED could be a major contributor [13,62,63]. It has been shown experimentally in silico and in vitro that if the IED is mimicked by electrical stimulation, then the stimulation delivered during early parts of the interictal period characterized by high resilience can have stabilizing seizure delaying effect [13]. In contrary, if the system is becoming less stable and rests close to the tipping point (bifurcation), then exactly the same perturbation has proictal nature, and even weaker perturbation can prematurely shift the brain to seizure (Fig. 2B). In silico modeling showed that the functional effect depends on the dynamical state, amplitude, and rate of the perturbation. The combination of all the parameters could replicate all the known features of IED, i.e., from increasing the rate of seizures to seizure suppression or no effect on seizures [13]. Here, it is important to note that the perturbation character remains constant and does not change its properties. If applied to neurophysiology, it suggests that the cellular and network mechanisms of IED remain consistent throughout the entire interictal period. The only change is the response to the IEDs in the brain undergoing the loss of resilience.

So far, we have discussed the scenario in which IED was generated outside the seizure onset zone, for example, in the slice preparation where CA3 is the irritative zone that generates IEDs that propagate to CA1 region, which generates seizures. Similar principles can be applied to the scenario when IEDs are generated directly within the seizure
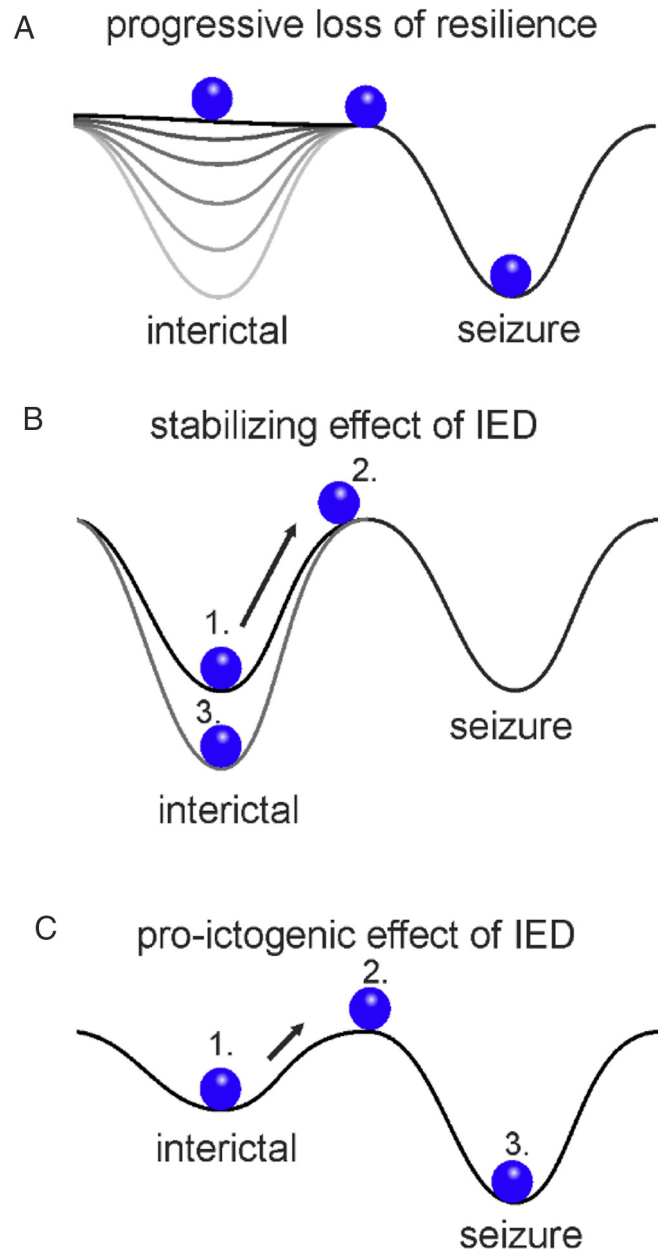
Fig. 2. The impact of IEDs on ictogenesis. A: Changes in slow parameter result in progressive loss of resilience, which will end up in a spontaneous transition to seizure. B: The IED perturbs the interictal dynamics and displaces the system (brain). During the stable state, even large perturbation is insufficient to shift the dynamic regime to seizure and system rapidly recovers back. The perturbation may paradoxically stabilize the system. Such IED has an antiictogenic effect. C: Similar IED perturbation that occurs during the low-resilience state can have proictogenic effect and trigger seizure prematurely.

onset zone. Here, the process of critical slowing can also be accompanied by changes in IED properties [64]. Numerical simulations suggested that as the epileptic brain is approaching bifurcation, the loss of resilience manifests by the occurrence of interictal like spikes and their increasing rate in the vicinity of the seizure [64]. It is explained by a progressively decreasing threshold to IEDs, which can emerge spontaneously or be evoked using stimulation. The impending seizure and loss of resilience can also manifest by delayed recovery from the interictal discharge. Increased rate of preictal discharges was observed by Huberfeld et al. in advance of seizures [20]. Changes in the rate and duration of another epileptiform phenomenon were observed in a chronic model of temporal lobe epilepsy [13]. In this model, increased rate and increased duration of specific type of interictal activity, so-
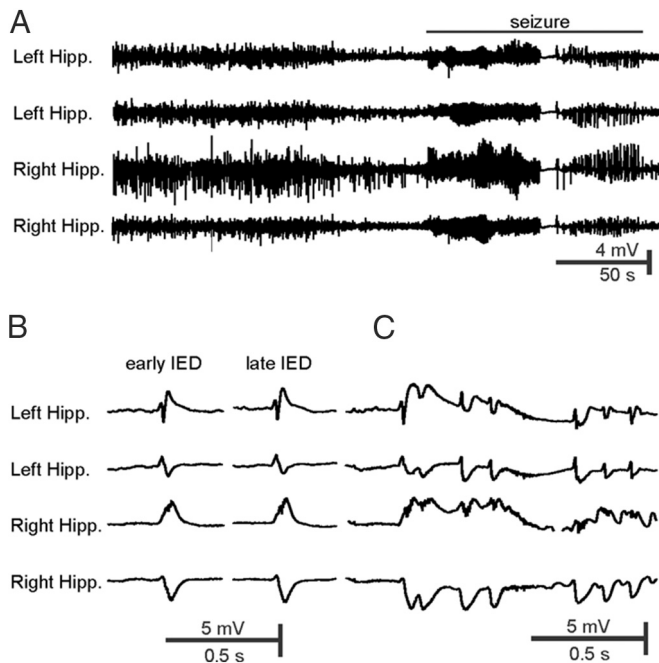
Fig. 3. IEDs and heralding spikes. A: Recording from the left and right hippocampi in the tetanus toxin model of temporal lobe epilepsy. Activity during the interictal period and a seizure. B: Interictal discharges during the early and late part of the interictal period. C: Hypersynchronous seizure onset pattern is characterized by the initial heralding spike. Note the similarity between the morphology and spatial extent of IED events and heralding spike.

called epileptic bursts, was observed with impeding seizure cluster. This represents an evidence that critical slowing is present on a longer time-scale, indicating the approach of the entire seizure cluster instead of individual seizures.

6. Conclusions

Interictal epileptiform discharge is a complex phenomenon that involves various cellular and network processes and displays multiple effects of brain dynamics. Recent studies show that the multifaceted nature of IEDs can also be explained from the dynamical perspective when the response to IED is primarily determined by the dynamical state of the epileptic networks. The combination of the neurophysiological basis of IED combined with the temporal dynamics and knowledge of the organization of the epileptic networks can provide meaningful and highly informative insight into the role of IEDs. Improved knowledge about IEDs and underlying dynamical routes to seizure can increase the clinical yield of the information provided by interictal discharges. For example, regions that increased IED rate ahead of seizure may be highly indicative of unstable brain tissue that may colocalize with seizure onset or epileptogenic zone and which should be considered for resection. Understanding IEDs from a dynamical perspective may also have crucial implication for the brain stimulation therapy. The stimulation delivered during the stable states may display seizure delaying effect whereas stimulation applied during unstable state may increase the probability of seizure occurrence.

Declaration of Competing Interest

The authors declare no competing interests.

Acknowledgment

References

[1] de Curtis M, Avanzini G. Interictal spikes in focal epileptogenesis. Prog Neurobiol 2001;63:541–67.
[2] Gibbs FA, Davis H, Lennox WG. The electro-encephalogram in epilepsy and in conditions of impaired consciousness. Arch Neurol Psychiatr 1935;34:1133–48.
[3] Rosenow F, Luders H. Presurgical evaluation of epilepsy. Brain 2001;124:1683–700.
[4] Janca R, Krsek P, Jezdik P, Cmejla R, Tomasek M, Komarek V, et al. The sub-regional functional organization of neocortical irritative epileptic networks in pediatric epilepsy. Front Neurol 2018;9.
[5] Alarcon G, Garcia Seoane JJ, Binnie CD, Martin Miguel MC, Juler J, Polkey CE, et al. Origin and propagation of interictal discharges in the acute electrocorticogram. Implications for pathophysiology and surgical treatment of temporal lobe epilepsy. Brain 1997;120(Pt 12):2259–82.
[6] Matsumoto H, Marsan CA. Cortical cellular phenomena in experimental epilepsy: interictal manifestations. ExpNeurol 1964;9:286–304.
[7] Johnston D, Brown TH. Giant synaptic potential hypothesis for epileptiform activity. Science 1981;211:294–7.
[8] Su H, Sochivko D, Becker A, Chen J, Jiang Y, Yaari Y, et al. Upregulation of a T-type Ca2+ channel causes a long-lasting modification of neuronal firing mode after status epilepticus. JNeurosci 2002;22:3645–55.
[9] Bernard C, Anderson A, Becker A, Poolos NP, Beck H, Johnston D. Acquired dendritic channelopathy in temporal lobe epilepsy. Science 2004;305:532–5.
[10] Yaari Y, Beck H. "Epileptic neurons" in temporal lobe epilepsy. Brain Pathol 2002;12:234–9.
[11] Shah MM, Anderson AE, Leung V, Lin X, Johnston D. Seizure-induced plasticity of h channels in entorhinal cortical layer III pyramidal neurons. Neuron 2004;44:495–508.
[12] Jensen MS, Yaari Y. Role of intrinsic burst firing, potassium accumulation, and electrical coupling in the elevated potassium model of hippocampal epilepsy. JNeurophysiol 1997;77:1224–33.
[13] Chang W-C, Kudlacek J, Hlinka J, Chvojka J, Hadrava M, Kumpost V, et al. Loss of neuronal network resilience precedes seizures and determines the ictogenic nature of interictal synaptic perturbations. Nat Neurosci 2018;21:1742–52.
[14] Karlocai MR, Kohus Z, Kali S, Ulbert I, Szabo G, Mate Z, et al. Physiological sharp wave-ripples and interictal events in vitro: what's the difference? Brain 2014; 137:463–85.
[15] Avoli M, Barbarosie M, Lucke A, Nagao T, Lopantsev V, Kohling R. Synchronous GABA-mediated potentials and epileptiform discharges in the rat limbic system in vitro. J Neurosci 1996;16:3912–24.
[16] Avoli M, de Curtis M. GABAergic synchronization in the limbic system and its role in the generation of epileptiform activity. Prog Neurobiol 2011;95:104–32.
[17] Perreault P, Avoli M. 4-Aminopyridine induced epileptiform activity and a GABA-mediated long-lasting depolarization in the rat hippocampus. J Neurosci 1992;12: 104–15.
[18] Hamidi S, D'Antuono M, Avoli M. On the contribution of KCC2 and carbonic anhydrase to two types of in vitro interictal discharge. Pflugers Archiv-European. J Physiol 2015;467:2325–35.
[19] Hamidi S, Avoli M. KCC2 function modulates in vitro ictogenesis. Neurobiol Dis 2015;79:51–8.
[20] Huberfeld G, Menendez de la Prida L, Pallud J, Cohen I, Le Van Quyen M, Adam C, et al. Glutamatergic pre-ictal discharges emerge at the transition to seizure in human epilepsy. Nat Neurosci 2011;14:627–34.
[21] Traub RD, Wong RK. Cellular mechanism of neuronal synchronization in epilepsy. Science 1982;216:745–7.
[22] Schwartzkroin PA, Futamachi KJ, Noebels JL, Prince DA. Transcallosal effects of a cortical epileptiform focus. Brain Res 1975;99:59–68.
[23] Prince DA, Wilder BJ. Control mechanisms in cortical epileptogenic foci. "Surround" inhibition. Arch Neurol 1967;16:194–202.
[24] Crowell RM. Projected effects in focal epilepsy. Neurology 1970;20:414.
[25] Ishijima B. Unitary analysis of epileptic activity in acute and chronic foci and related cortex of cat and monkey. Epilepsia 1972;13:561–81.
[26] Muldoon SF, Villette V, Tressard T, Malvache A, Reichinnek S, Bartolomei F, et al. GABAergic inhibition shapes interictal dynamics in awake epileptic mice. Brain 2015;138:2875–90.
[27] Sabolek HR, Swiercz WB, Lillis KP, Cash SS, Huberfeld G, Zhao G, et al. A candidate mechanism underlying the variance of interictal spike propagation. J Neurosci 2012;32:3009–21.
[28] Trevelyan AJ, Sussillo D, Watson BO, Yuste R. Modular propagation of epileptiform activity: evidence for an inhibitory veto in neocortex. J Neurosci 2006;26: 12447–55.
[29] Trevelyan AJ, Sussillo D, Yuste R. Feedforward inhibition contributes to the control of epileptiform propagation speed. JNeurosci 2007;27:3383–7.
[30] Dudek FE, Staley KJ. Seizure probability in animal models of acquired epilepsy: a perspective on the concept of the preictal state. Epilepsy Res 2011;97:324–31.
[31] Dudek FE, Staley KJ. The time course of acquired epilepsy: implications for therapeutic intervention to suppress epileptogenesis. NeurosciLett 2011;497:240–6.
[32] Williams PA, White AM, Clark S, Ferraro DJ, Swiercz W, Staley KJ, et al. Development of spontaneous recurrent seizures after kainate-induced status epilepticus. JNeurosci 2009;29:2103–12.
[33] Engel Jr J, Bragin A, Staba R, Mody I. High-frequency oscillations: what is normal and what is not? Epilepsia 2009;50:598–604.
[34] Jiruska P, Alvarado-Rojas C, Schevon CA, Staba R, Stacey W, Wendling F, et al. Update on the mechanisms and roles of high-frequency oscillations in seizures and epileptic disorders. Epilepsia 2017;58:1330–9.

[35] Jiruska P, Finnerty GT, Powell AD, Lofti N, Cmejla R, Jefferys JG. Epileptic high-frequency network activity in a model of non-lesional temporal lobe epilepsy. Brain 2010;133:1380–90.

[36] Jacobs J, Zijlmans M, Zelmann R, Chatillon CE, Hall J, Olivier A, et al. High-frequency electroencephalographic oscillations correlate with outcome of epilepsy surgery. Ann Neurol 2010;67:209–20.

[37] Jiruska P, Bragin A. High-frequency activity in experimental and clinical epileptic foci. Epilepsy Res 2011;97:300–7.

[38] Avoli M, de Curtis M, Kohling R. Does interictal synchronization influence ictogenesis? Neuropharmacology 2013;69:37–44.

[39] Barbarosie M, Avoli M. CA3-driven hippocampal-entorhinal loop controls rather than sustains in vitro limbic seizures. JNeurosci 1997;17:9308–14.

[40] Jensen MS, Yaari Y. The relationship between interictal and ictal paroxysms in an in vitro model of focal hippocampal epilepsy. AnnNeurol 1988;24:591–8.

[41] Librizzi L, de Curtis M. Epileptiform ictal discharges are prevented by periodic interictal spiking in the olfactory cortex. Ann Neurol 2003;53:382–9.

[42] Weiss SA, Alvarado-Rojas C, Bragin A, Behnke E, Fields T, Fried I, et al. Ictal onset patterns of local field potentials, high frequency oscillations, and unit activity in human mesial temporal lobe epilepsy. Epilepsia 2016;57:111–21.

[43] Perucca P, Dubeau F, Gotman J. Intracranial electroencephalographic seizure-onset patterns: effect of underlying pathology. Brain 2014;137:183–96.

[44] Mormann F, Andrzejak RG, Elger CE, Lehnertz K. Seizure prediction: the long and winding road. Brain 2007;130:314–33.

[45] Karoly PJ, Freestone DR, Boston R, Grayden DB, Himes D, Leyde K, et al. Interictal spikes and epileptic seizures: their relationship and underlying rhythmicity. Brain 2016;139:1066–78.

[46] Cook MJ, O'Brien TJ, Berkovic SF, Murphy M, Morokoff A, Fabinyi G, et al. Prediction of seizure likelihood with a long-term, implanted seizure advisory system in patients with drug-resistant epilepsy: a first-in-man study. Lancet Neurol 2013;12:563–71.

[47] Lopes da Silva F. Epilepsy as a disease of the dynamics of neuronal networks — models and predictions. In: Schelter B, Timmer J, Schulze-Bonhage A, editors. Seizure prediction in epilepsy: from basic mechanisms to clinical applications. WILEY-VCH Vrlag GmbH & Co.; 2008. p. 97–107.

[48] Lopes da Silva FH, Blanes W, Kalitzin SN, Parra J, Suffczynski P, Velis DN. Dynamical diseases of brain systems: different routes to epileptic seizures. IEEE Trans Biomed Eng 2003;50:540–8.

[49] Lopes da Silva FH, Blanes W, Kalitzin SN, Parra J, Suffczynski P, Velis DN. Epilepsies as dynamical diseases of brain systems: basic models of the transition between normal and epileptic activity. Epilepsia 2003;44:72–83.

[50] Scheffer M. Critical transitions in nature and society. Princeton: Princeton University Press; 2009.

[51] Jirsa VK, Stacey WC, Quilichini PP, Ivanov AI, Bernard C. On the nature of seizure dynamics. Brain 2014;137:2210–30.

[52] Saggio ML, Spiegler A, Bernard C, Jirsa VK. Fast-slow bursters in the unfolding of a high codimension singularity and the ultra-slow transitions of classes. J Math Neurosci 2017;7.

[53] Suffczynski P, Lopes da Silva FH, Parra J, Velis DN, Bouwman BM, van Rijn CM, et al. Dynamics of epileptic phenomena determined from statistics of ictal transitions. IEEE Trans Biomed Eng 2006;53:524–32.

[54] Scheffer M, Carpenter SR, Lenton TM, Bascompte J, Brock W, Dakos V, et al. Anticipating critical transitions. Science 2012;338:344–8.

[55] Jiruska P, Csicsvari J, Powell AD, Fox JE, Chang WC, Vreugdenhil M, et al. High-frequency network activity, global increase in neuronal activity, and synchrony expansion precede epileptic seizures in vitro. J Neurosci 2010;30:5690–701.

[56] Kalitzin S, Velis D, Suffczynski P, Parra J, da Silva FL. Electrical brain-stimulation paradigm for estimating the seizure onset site and the time to ictal transition in temporal lobe epilepsy. Clin Neurophysiol 2005;116:718–28.

[57] Freestone DR, Kuhlmann L, Grayden DB, Burkitt AN, Lai A, Nelson TS, et al. Electrical probing of cortical excitability in patients with epilepsy. Epilepsy Behav 2011;22 (Suppl. 1):S110–8.

[58] Dakos V, Scheffer M, van Nes EH, Brovkin V, Petoukhov V, Held H. Slowing down as an early warning signal for abrupt climate change. Proc Natl Acad Sci U S A 2008;105:14308–12.

[59] Meisel C, Kuehn C. Scaling effects and spatio-temporal multilevel dynamics in epileptic seizures. PLoS One 2012;7.

[60] Scheffer M, Bascompte J, Brock WA, Brovkin V, Carpenter SR, Dakos V, et al. Early-warning signals for critical transitions. Nature 2009;461:53–9.

[61] Kramer MA, Truccolo W, Eden UT, Lepage KQ, Hochberg LR, Eskandar EN, et al. Human seizures self-terminate across spatial scales via a critical transition. Proc Natl Acad Sci U S A 2012;109:21116–21.

[62] Dorn T, Witte OW. Refractory periods following Interictal spikes in acute experimentally-induced epileptic foci. Electroencephalogr Clin Neurophysiol 1995;94:80–5.

[63] de Curtis M, Librizzi L, Biella G. Discharge threshold is enhanced for several seconds after a single interictal spike in a model of focal epileptogenesis. Eur J Neurosci 2001;14:174–8.

[64] Lopes MA, Lee KE, Goltsev AV. Neuronal network model of interictal and recurrent ictal activity. Phys Rev E 2017;96.

7 Computational modeling allows unsupervised classification of epileptic brain states across species

Epilepsy patients need constant brain monitoring to detect the onset of seizures from changes in brain states. Visual inspection of intracranial EEG by experts is time-consuming and not scalable. Furthermore, there is inherent variability across patients that makes reliable automated classification challenging. Tools to quantify personalized brain states could thus enable tailored, responsive treatment strategies.

7.1 The contributions toward the progress of the field

Computational models can provide mechanistic insight into state transitions. The proposed methods classify brief EEG epochs into known epileptic brain state types in an unsupervised way without a necessity for individualized algorithm training in each patient. The classification works even between species without custom training. This demonstrates similarities between rodent and human manifestations of epileptic brain states through unsupervised cross-species classification.

Wendling neural mass model is a computational model that simulates the interaction between excitatory and inhibitory neuron populations in the hippocampus. By simulating the Wendling model with known parameters, multiple realizations of four epileptic brain state types (interictal, preonset, onset, ictal) were obtained. From these realizations, prototypical examples of these states were computed and represented as cluster centroids in feature space. The 11 signal features calculated from each 5-second segment were: mean, band power in 5 frequency bands, the distance between quantiles, spike count, variance, autocorrelation, and line length. The features capture aspects like oscillations, spikes, and signal complexity. After computing the same 11 features from 5s segments of new data (electrographic signals from a high-

potassium model of epilepsy in rat slices and intracranial EEG from temporal lobe epilepsy patients), essentially representing these in the same feature space as the four prototypical class templates, the classification is done using k-means approach (by finding the closest matching prototype). This classification was validated against expert marking. The centroids serve as the data-driven prototypes that can be matched to model-based types. The prototypes were directly used for classification.

The whole pipeline does not leverage other expert knowledge beyond final validation, the cross-species generalization makes the methods innovative. The work leverages a computational model to enable robust, generalizable automated EEG classification without supervision. The work addresses inherent constraints in patient EEG data availability and variability. The fact that unsupervised model-based classification transfers across species further validates the capability of the modeling framework in capturing consistent dynamical disease signatures.

7.2 The author's contributions

The author performed all *in vitro* experiments in brain slices perfused with the high-potassium solution.

7.3 Compliance with the thesis objectives

The study aims to find a tool enabling better personalized treatment. Signal features, including high-frequency activity, identified in previous works were essential in estimating distinct brain states in an unsupervised manner from EEG and local field potentials suggesting HFO activity is a fingerprint reflecting the brain network's state.

scientific reports

OPEN

Computational modeling allows unsupervised classification of epileptic brain states across species

Isa Dallmer-Zerbe[1,2], Nikola Jajcay[1,3], Jan Chvojka[2,4], Radek Janca[4], Petr Jezdik[4], Pavel Krsek[5], Petr Marusic[6], Premysl Jiruska[2] & Jaroslav Hlinka[1,3]✉

Current advances in epilepsy treatment aim to personalize and responsively adjust treatment parameters to overcome patient heterogeneity in treatment efficiency. For tailoring treatment to the individual and the current brain state, tools are required that help to identify the patient- and time-point-specific parameters of epilepsy. Computational modeling has long proven its utility in gaining mechanistic insight. Recently, the technique has been introduced as a diagnostic tool to predict individual treatment outcomes. In this article, the Wendling model, an established computational model of epilepsy dynamics, is used to automatically classify epileptic brain states in intracranial EEG from patients (n = 4) and local field potential recordings from in vitro rat data (high-potassium model of epilepsy, n = 3). Five-second signal segments are classified to four types of brain state in epilepsy (interictal, preonset, onset, ictal) by comparing a vector of signal features for each data segment to four prototypical feature vectors obtained by Wendling model simulations. The classification result is validated against expert visual assessment. Model-driven brain state classification achieved a classification performance significantly above chance level (mean sensitivity 0.99 on model data, 0.77 on rat data, 0.56 on human data in a four-way classification task). Model-driven prototypes showed similarity with data-driven prototypes, which we obtained from real data for rats and humans. Our results indicate similar electrophysiological patterns of epileptic states in the human brain and the animal model that are well-reproduced by the computational model, and captured by a key set of signal features, enabling fully automated and unsupervised brain state classification in epilepsy.

Despite decades of research, current approaches to epilepsy treatment remain unsuccessful in about a third of patients, and the mechanisms of the disease remain insufficiently understood[1]. It has been highlighted how epilepsies and seizures are highly heterogeneous[2,3] and how treatment responses vary not only across patients but also across time[4,5]. Therefore, the modern approach to epilepsy treatment, as well as medicine in general, aims to tailor interventions to the individual and their current needs in a closed-loop and data-driven manner[6–8].

Trying to explain (some of) the heterogeneity in epilepsy, current advances in epilepsy research study epilepsy as a dynamic disease[9]. It has been shown how patient-specific fluctuations in seizure likelihood on the scale from hours to days govern seizure emergence[2,10–15]. Moreover, varying levels of seizure likelihood could explain the variability in treatment responses to brain stimulation: The same stimulation, that helped prevent a seizure when delivered at low seizure likelihood, could trigger a seizure at high seizure likelihood[4,5], a phenomenon that can be explained by fundamental dynamical systems principles[16]. Similarly, the varying efficiency of epilepsy surgery to render a patient seizure-free was linked to the percentage of resected brain areas that, in retrospect, were identified to have the highest seizure likelihood[17–19]. Finally, the variable patterns of seizure transitions could be classified according to a fixed set of "dynamotypes"[20]. The brain dynamics underlying the fluctuations in seizure

[1]Department of Complex Systems, Institute of Computer Science, Czech Academy of Sciences, 182 00 Prague, Czech Republic. [2]Department of Physiology, Second Faculty of Medicine, Charles University, 150 06 Prague, Czech Republic. [3]National Institute of Mental Health, 250 67 Klecany, Czech Republic. [4]Department of Circuit Theory, Faculty of Electrical Engineering, Czech Technical University in Prague, 166 27 Prague, Czech Republic. [5]Department of Paediatric Neurology, Second Faculty of Medicine, Motol University Hospital, Charles University, 150 06 Prague, Czech Republic. [6]Department of Neurology, Second Faculty of Medicine, Motol University Hospital, Charles University, 150 06 Prague, Czech Republic. ✉email: hlinka@cs.cas.cz

likelihood can be viewed as a dynamical system, the state of which develops based on some intrinsic laws of motion and is additionally driven by some endogeneous or exogeneous noise or forces[21–24]. While the space of possible brain states is very high-dimensional and continuous, just a subset of possible states corresponds to (at least transitionally) stable and attracting solutions. Attraction and stability in this context refer to the tendency of the brain to remain in or approach those states, such as a ball rolling down a slope and moving slower or coming to rest inside a valley until reaching or being pushed into another valley. The other brain states, such as the ball's visited positions while rolling down the slope, are unstable and therefore are visited for a negligible amount of time only. Thus, the dynamics may be reasonably simplified by considering the brain state progression through a smaller, discrete set of distinct states (such as "resting state" and "seizure state") corresponding to the ball positions when the ball has come to or is close to rest.

In the last years, studying recorded brain activity to uncover the latent brain states and the time points of their transitions has gained considerable interest, not just in the field of epilepsy, but also, for example, in the study of sleep and wakefulness[25,26] and information processing[27,28]. Employed methods typically include clustering analysis of segmented data from functional magnetic resonance imaging (fMRI), scalp, or intracranial electroencephalography (EEG or iEEG). Adding to such data-driven approaches, dynamical systems theory allows to characterize the observed brain states and their transitions (e.g., by linking distinct dynamical patterns to "resting state" and "seizure state" and showing how a change in a model parameter can lead the system to switch between the states). As observable from the recorded time series, the state-specific dynamic patterns can be simulated using models (sets of ordinary differential equations) given an initial condition and, potentially, some realization of dynamical or observation noise. Changing model parameters, different activity patterns, such as resting, oscillating, or spiking behavior, can be reproduced via simulations. Furthermore, transitions between different patterns can be studied, providing mechanistic insight and the means to predict or even control the likelihood of certain transitions[29,30]. Thus, in epilepsy, dynamical systems theory has provided valuable mechanistic insight helping to characterize epileptic brain states and the different mechanisms that could govern seizure emergence[31–34]. Recently, dynamical brain models have further been introduced as tools to predict individualized treatment outcome and test beds for developing treatment strategies in general[8,30,35,36]; see Dallmer-Zerbe et al.[37] for a recent review. However, to date, no clinically available applications are explicitly contingent on dynamical systems theory or computational modeling. Thus, a bridge between theory and application is yet to be built.

This study aims to propose a model-driven classification of epileptic brain states using a well-known, biophysiologically realistic model of epilepsy dynamics[38,39]. In contrast to two recent studies[40,41], that also used a model-driven approach, the proposed classification procedure is built on a prototype comparison using different types of model-generated activity. As in our case, only the model output (prototypical time series) is used; the modeling environment can be easily replaced in the developed pipeline. Furthermore, we include a direct comparison of the model-driven classification strategy with a data-driven one and a comparison between a generalized and individualized classification strategy. Data samples in this study include hippocampal rat slices *in vitro* (high potassium model), as well as intracranial EEG recordings (iEEG) collected in the human hippocampus from patients with temporal lobe epilepsy (TLE).

Results

Types of brain state in epilepsy.
Wendling et al.[39] describe four types of brain state in epilepsy (interictal, preonset, onset, and ictal) that can be observed from hippocampal recordings from patients with TLE and are reproduced by their computational model. In this study, we simulate the four types of brain state in epilepsy using the Wendling model (Fig. 1A, B) and show that they match the types of brain state identified through clustering segmented data from in vitro rat local field potential (LFP) recordings (high-potassium model of epilepsy, Fig. 1C) and human iEEG recordings (Fig. 1D). The interictal type of brain state is characterized by random fluctuations around a constant mean voltage of recorded activity. The preonset type of brain state features occasional high amplitude spikes, while the onset type has high-frequency oscillations, typically in 15 to 40 Hz frequency bands. Finally, the ictal type of brain state shows ongoing rhythmic activity, typically in the range of 4 to 10 Hz. Note that in the rat LFP recordings (see Fig. 1C), the captured dynamics seemingly take place at a higher temporal scale, and thus there was no observed onset type brain state.

Automated brain state classification.
The proposed procedure for automated brain state classification from electrophysiological data is based on the four types of brain states in epilepsy and the comparison of each segment of data to the corresponding epileptic brain state prototypes. The prototypes are generated following five sub-steps (further elaborated below): data segmentation or simulation, feature calculation, principle component analysis, cluster analysis, and centroid labeling. The labeled centroids then serve as prototypes, and individual data segments are labeled according to the label of the most similar prototype, i.e., the closest centroid. Classification performance is assessed against visual labeling for real data segments or against the known type-specific model configuration for simulated data segments. It is assessed in the dataset used for prototype generation to evaluate individualized classification performance (Table 1 and Fig. 2), as well as in all other datasets for assessing the generalizability of the prototypes (Table 2 and Fig. 3). Data- and model-driven classification differ regarding the dataset used for prototype generation: in model-driven classification, the prototypes are generated based on simulated segments with type-specific model configuration (100 segments per type). In data-driven individualized classification, the prototypes are generated based on (all) data segments of a given rat or human. For assessing the generalizability of the data-driven classification, we use the prototypes obtained from the rat and human with the highest number of data segments to classify the data of all others. Notably, even the data-driven classification is model-informed in that the centroid labeling during prototype generation is always based on Wendling-type simulations. This way, the suggested data-driven approach is also wholly unsupervised
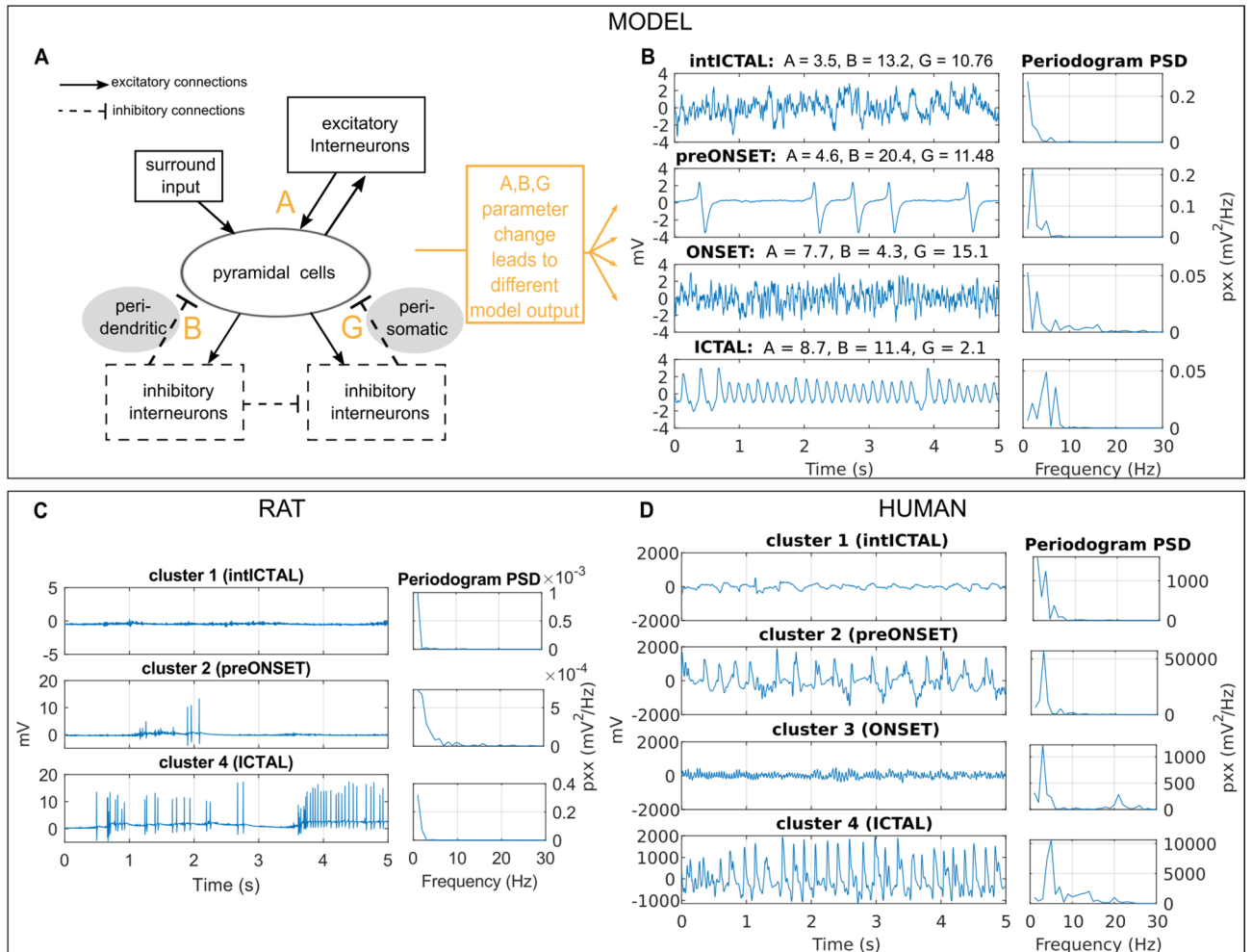
Figure 1. Types of epileptic brain state during epileptic transitions in the model, rat, and human electrophysiology. (**A**) The Wendling model[39] of neuronal population dynamics with two inhibitory interneuron populations, one communicating with the pyramidal cell population through somatic synapses (fast inhibition) and one through dendritic synapses (slow inhibition). The synaptic gain parameters A, B, and G control the amplitude of postsynaptic potentials of excitation, and slow and fast inhibition, respectively. (**B**) Under different model configurations of A, B, and G, the model output, the summed average postsynaptic potentials on pyramidal cells, resembles electrophysiological recordings during four distinct tissue states. (**C,D**) Randomly selected exemplary time series for each one of four clusters in rat 1 and human 1. Clusters are matched with the four types of brain state defined by Wendling so that cluster 1 is the interictal, cluster 2 is the preonset, cluster 3 is the onset, and cluster 4 is the ictal type of brain state (see Methods section). Rat data segments did not include onset type segments due to faster and more local dynamics.

(i.e., no visual expert assessment of data segments needed) and thus fully automatized while utilizing the mechanistic understanding of epileptic dynamics encoded in the well-established dynamical model.

Individualized, data-driven brain state classification is visually summarized in Fig. 2 for the rat and the human with the most recorded seizures (continuous recording in rat, concatenated in humans), and thus the highest number of data segments, respectively (rat 1 and human 1 in Table 1). After cutting the data into segments of five-second length (Fig. 2A), we calculate 11 signal features expected to indicate the current epileptic brain state. The features are chosen based on literature, where they have proven their utility to (a) differentiate between the four types of brain state in epilepsy in particular[39,42] or (b) to capture critical slowing during epileptic transitions[4,14] The features are: the signal mean, the average band power in different frequency bands (b0power: 0–0.5 Hz, b1power: 0.5–4 Hz, b2power: 4–12 Hz, b3power: 12–64 Hz, b4power: >64 Hz), two spike measures (alphdiff: distance between 0.05 and 0.95 quantile; spikeabs: spike count as the number of outliers based on Tukey 1.5 interquartile range threshold), as well as signal variance (sigvar), auto-correlation (autocorrel) at 5 ms lag, and line length (linelen). We find that feature values change over time and seem to be indicative of the current epileptic brain state, such that, for example, autocorrel typically drops at the onset, and b1power and spikeabs usually peak at the end of a seizure (Fig. 2B). Furthermore, it is apparent that the features behave similarly and thus overlap in the information they capture about seizure dynamics.
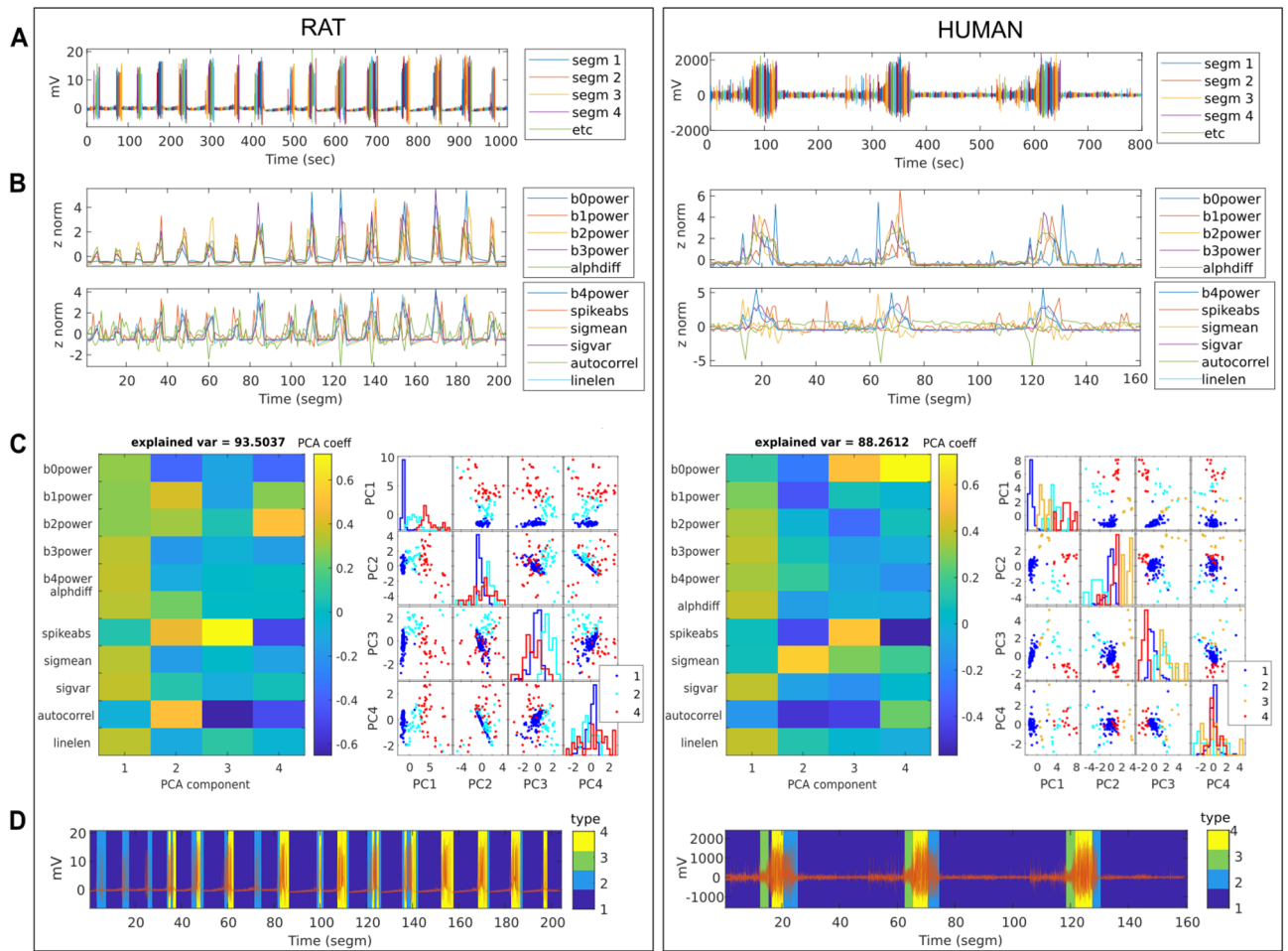
Figure 2. Individualized, data-driven brain state classification in rat 1 (left) and human 1 (right). (**A**) Continuous rat LFP and concatenated human iEEG seizure recordings are segmented into 5-s segments. (**B**) 11 signal features are calculated for each 5-s segment and displayed over time. Characteristic changes in feature values indicate the current brain state concerning seizure dynamics. (**C**) Dimensionality reduction from 11 features to four principle components (PC). Factor loadings for each of the features (left) show a shared contribution to PC 1 and main contributions to PC 2–4 by auto-correlation, spike count (spikeabs), and band power in slower frequencies (b0- to b2power ≤ 12 Hz). Cluster identity of each data segment (right, color-coded for type 1: interictal, 2: preonset, 3: onset, and 4: ictal) shows well-separated clusters in rat and human data, especially for PC 1. (**D**) Resulting data-driven brain state classification over time. Color code in the background of each data segment indicates which of the cluster centroids from data-driven clustering was closest to the segment's PCA-projected signal features. The brain state classification shows to identify time points of seizures and their transitions reliably. However, in the human data (right), Wendling-defined preonset type of brain state (type 2, light blue) is often detected during the transitions out of instead of into seizure.

	Model	Rat 1	Rat 2	Rat 3	Human 1	Human 2	Human 3	Human 4
Sensitivity	**0.99**	0.74	0.79	0.65	0.63	0.51	0.45	0.39
PPV	**0.99**	0.75	0.66	0.97	0.66	0.64	0.79	0.46
# segments	**400**	204	110	108	160	127	98	70
# prototypes	**4**	3	3	2	4	3	2	3

Table 1. Individualized classification performance for all datasets. . Model-driven classification, here applied to model data only, is marked in boldface. Generally, bigger datasets (higher # segments) had higher sensitivity, and more identified clusters matched the Wendling types (hence higher # types).
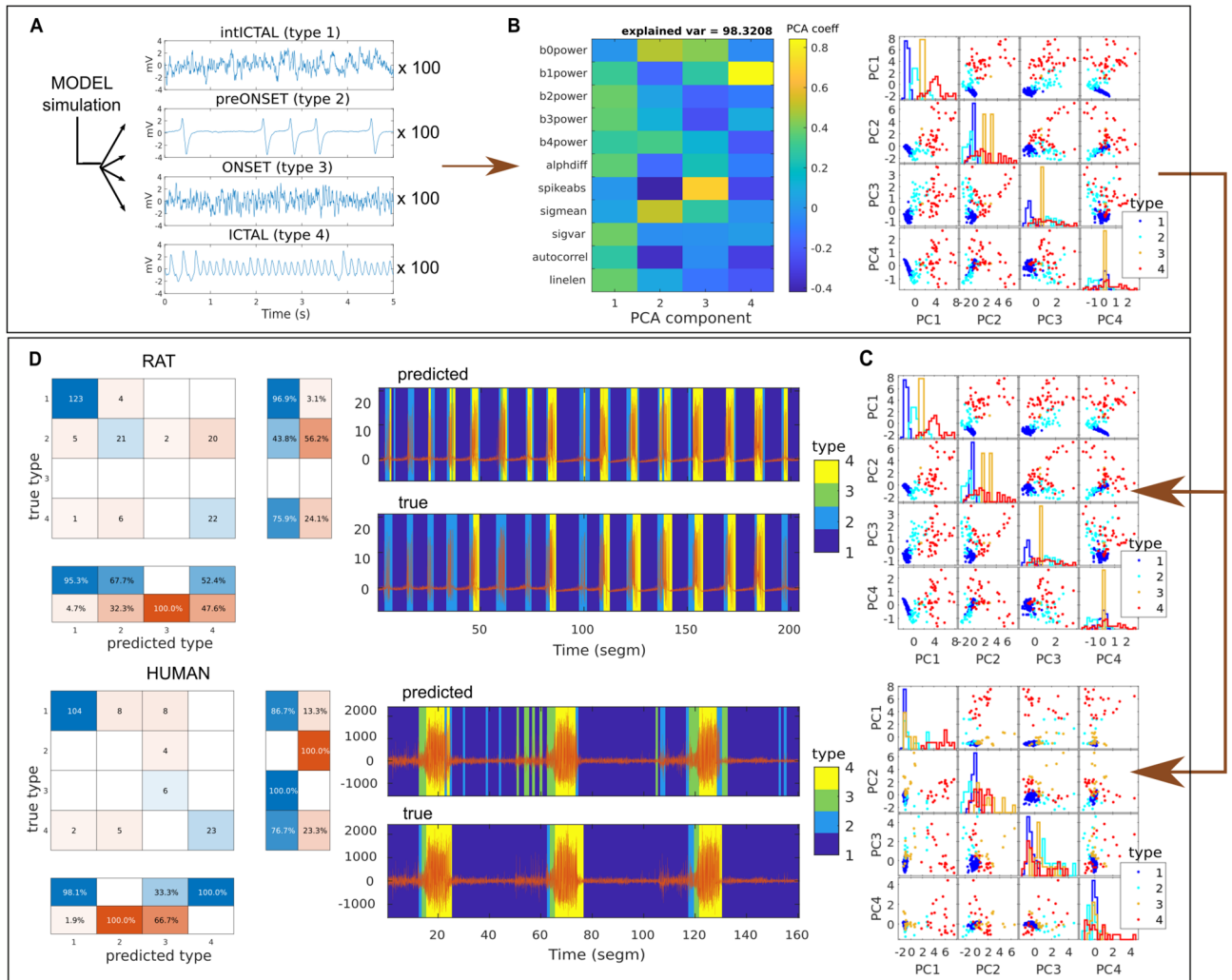
Figure 3. Generalized, model-driven brain state classification of real data segments. (**A**) Model simulation of different types of brain state in epilepsy. Due to noise, the model output varies slightly over the 100 iterations performed for each type of model configuration. (**B**) Cluster analysis on features calculated from the 400 simulated data segments. Feature loadings on the four components show very similar patterns to data-driven clustering (Fig. 2C, left). The four types (right, color-coded) form separated clusters with small overlaps of type 1 and type 2 due to varying amounts of spikes in the preonset segments (type 2). (**C**) Example rat (top) and human data (bottom) are projected into model-driven PC space and assigned a color-coded type label based on the closest model centroid. (**D**) The assigned label (predicted) is then compared to the visually obtained label (true). In the displayed dataset, classification performance (left) was especially good for interictal and ictal types of brain state and preonset type in rats; however, low for preonset type in humans.

	Model		Rat		Human	
Prototype origin	Sensitivity	PPV	Sensitivity	PPV	Sensitivity	PPV
Model-driven	**0.99****	**0.99****	0.77** ± 0.05	0.65** ± 0.11	0.56** ± 0.07	0.52** ± 0.05
Rat-driven	0.69**	0.81**	**0.76**** ± **0.04**	**0.70**** ± **0.10**	0.50** ± 0.08	0.61** ± 0.07
Human-driven	0.56 *	0.84**	0.62** ± 0.07	0.54** ± 0.09	**0.47**** ± **0.11**	**0.55**** ± **0.11**

Table 2. Generalizability of prototypes across different datasets. . The mean sensitivity and standard deviation of type-averaged sensitivity and PPV rates are shown across all dataset individuals. In the case of labeling data of a given species (values on diagonal, marked in boldface), the individual whose data were used to derive the brain state prototypes was excluded. Model-driven prototype origin led to the best results for sensitivity in all datasets and had better PPV than human-driven classification. Rat-driven classification had higher PPV in the rat and human datasets. All classifications had performance significantly above the chance level: ** significant with $p < 0.01$; * significant with $p < 0.05$.

To eliminate redundant information and thus help differentiate the epileptic brain state types based on the features, principle components analysis (PCA) was conducted, reducing the dimensionality from the 11 features to four principal components. The biggest part of captured information, PC 1, is shared among most features. Additional information is captured by power in lower frequency bands, spikeabs, and autocorrel, which in turn substantially contribute to PC 2–4 (Fig. 2C left panels). In the next sub-steps, the projected signal features (i.e., the PCA scores) for all data segments are clustered into four clusters, and the cluster centroids are matched with the Wendling-defined types (so that, e.g., the centroid of cluster 2 becomes the prototype for type 4: ictal), to obtain the labeled brain state prototypes. Figure 2C right panels shows that PC 1 reliably differentiates interictal (type 1) and ictal (type 4) state, while PC 2 helps to differentiate preonset (type 2) and onset (type 3) state. Moreover, human and rat-driven clustering show astonishing similarity, especially for the interictal state (across PCs) and ictal state (PC 1). Finally, for each data segment (dot in Fig. 2C right panel), we identify the labeled centroid (prototype) that is spatially closest in PC space, thus most similar, to predict the type label of each segment (color-coded in Fig. 2D). Predicted labels are then compared against visual data labels to obtain individualized sensitivity and positive predictive value (PPV) performance.

As Table 1 shows, individualized model-driven brain state classification performs best. In data-driven classification, individualized rat data classification performs better than individualized human data classification. Overall, higher classification performance is achieved in larger datasets, and more of the Wendling types match the clusters of observed brain states. Only in human dataset 1 does data clustering manage to identify all four types of brain states in epilepsy. Testing the mean sensitivity and PPV across datasets of each species for significance, we find that classification results are always highly significant ($p < 0.01$, for group level permutation testing against classification performance for Markov chain simulations, see Methods: Statistical Analysis), with $mean \pm STD$ sensitivity in the model: 0.99, rat: 0.73 ± 0.07, or human: 0.45 ± 0.15, and PPV in the model: 0.99, rat: 0.79 ± 0.16, or human: 0.56 ± 0.10.

Generalizability of prototypes across datasets in data- and model-driven brain state classification.

Using the four prototypes obtained from any dataset, we can also label data segments from other datasets based on the closest prototype, e.g., using rat-driven prototypes to label human data segments. Figure 3 visually summarizes generalized, model-driven brain state classification for rat and human data. After simulating data segments using different model configurations for each type of brain state (Fig. 3A) and calculating the signal features, PCA, clustering, and centroid labeling (Fig. 3B), feature vectors obtained from rat and human data segments can be projected into (and labeled in) the model-driven PC space (Fig. 3C). For performance assessment, the predicted segment label (predicted type) is then again compared against the visually assessed segment labeling (true type; Fig. 3D). For ease of visual comparison with Fig. 2, Fig. 3 displays the same data of the rat and the human with the longest recording (rat 1 and human 1). The same individuals are used for generalized, data-driven brain state classification. Classification performance across all individuals of another (or the same species, excluding the one individual used for prototype generation) for model-, rat- or human-driven prototype generation is shown in Table 2.

We find that model-driven brain state classification is generalizable and thus reliably detects the type of brain state in epilepsy in our rat and human dataset, with highly significant mean sensitivity and PPV rates across the different types of brain state (see Table 2, row 'model-driven'). Also, rat- and human-driven brain state classification (see row 'rat-driven' and 'human-driven') performed significantly above chance ($p < 0.01$ in rat and human datasets). While sensitivity was consistently highest for model-driven classification, rat-driven classification had higher PPV in both the rat and the human data set.

Comparing the mean sensitivity and PPV rates in rats and humans between the individualized and generalized classification strategies (Table 2 vs. Table 1), we find that for model-driven classification, the generalized approach achieved higher sensitivity, but lower PPV than the individualized approach (sensitivity: rat 0.77 > 0.73, human 0.56 > 0.45; PPV: rat 0.65 < 0.79, human 0.52 < 0.56). Also, rat- and human-driven classification showed the pattern of higher sensitivity but lower PPV in generalized vs. individualized (rat-driven classification in rat, sensitivity: 0.76 > 0.73, PPV: 0.70 < 0.79; human-driven classification in human, sensitivity: 0.47 > 0.45, PPV: 0.55 < 0.56).

Overall, the generalized, model-driven approach achieved the best mean sensitivity in both the rat and human data set (rat 0.77, human 0.56). The best mean PPV in the rat was achieved by the individualized, data-driven approach and in the human by using generalized rat-driven classification (rat 0.79 and 0.61, respectively).

Discussion

In this study, we propose epileptic brain state classification for data segments according to four types of brain state in epilepsy as described in Wendling et al.[39]. Notably, the prototypes for each type of brain state can be obtained from simulated, rat, or human data, respectively. Prototype generation included several sub-steps of data analysis, including feature calculation, principle component analysis, clustering, and centroid labeling (crucially, model-informed even during data-driven classification).

We find that the type of brain state of a given data segment was predicted significantly above chance for all datasets and strategies (model-driven vs. data-driven and individualized vs. generalized). Model-driven classification achieved higher sensitivity but lower PPV than data-driven classification, a pattern we commonly observed when comparing the generalized and individualized approaches. However, the model-driven approach not only generalized better to other datasets overall (Table 2) but achieved even higher sensitivity than using the same data to be also classified for prototype generation (individualized classification: Table 1). The classification of model-generated segments was particularly successful in terms of PPV. However, this might be partially ascribed to the homogeneous distribution of simulated segments between the four classes, which generally improves average

PPV compared to imbalanced classes. This is a general problem faced in real data, given the varying occurrence rate of the types. As proposed in this study, a model-driven approach has the natural advantage that the number of segments used for prototype generation is up to the experimenter. However, even in the imbalanced rat and human data, the achieved PPV was relatively high and significantly above the random classifier expectation.

The overall results of this study suggest that epilepsy dynamics manifest with consistent electrophysiological patterns across species well-captured by the Wendling model. For epilepsy diagnosis and treatment, this implies that brain state classification (1) is automatizable in an unsupervised and mechanism-enlightening manner, and (2) might not need to be tuned to the individual to achieve good classification results (especially to achieve high sensitivity), despite the substantial heterogeneity among patients. These implications will be discussed in the following, alongside a more detailed discussion of our findings.

Model-driven brain state classification is unsupervised and provides mechanistic insight. In recent years, significant advances have been achieved in the field of data-driven, automatized seizure detection for epilepsy (dealing with the classification of ictal against other states). Available seizure detection devices for EEG and non-EEG data have proven their efficiency primarily for tonic-clonic seizures[43,44]. Tracking epilepsy brain states over time, including transition states such as the preonset and onset type in this study, is a much more complex problem. Debates about the existence of a preictal brain state, as well as whether or not slow processes (like a successive loss of network resilience[4]) govern seizure emergence, are on-going[45,46]. Due to the mixed outcomes from the countless attempts to characterize and detect the preictal state, the research community has moved on to focus on detecting the so-called pro-ictal state, i.e., the state of increased seizure likelihood. Thus, our focus has shifted from trying to predict seizures deterministically towards seizure forecasting following a probabilistic approach[47]. As it has been shown, computational modeling, replicating different patterns of observed activity and providing means to test the mechanisms of their transitions, can serve as tools to fill in our gaps of understanding and better characterize current brain states[29,33]. We consider this study, the same as the work of Song et al.[40,41], an essential step on the way to making use of the advantages of modeling for modern brain state tracking for epilepsy, adding to the successes of data-driven strategies, instead of competing with them. Our results highlight that the model-driven approach can add to the data-driven strategy, achieving comparable or even better results than a data-driven approach. We demonstrate that a model can generate a set of "pure" prototypes (further elaborated below), which we believe lies at the heart of modeling: creating a highly simplified yet helpful representation of reality. Our results, in particular, support the usefulness of the four Wendling types of brain state for hippocampal recordings from TLE patients and the high potassium rat *in vitro* model. While the classification performance of real data in this study, overall, did not meet some of the seizure detection performances achieved in the literature, the achieved values in the range of 0.42 to 0.99 can be considered quite successful, given that the expected sensitivity in four-way classification in case of random assignments is 25%. It is important to note that the performance was not homogeneous across the states. As expected, it was typically the highest for the interictal and ictal states and lower for the transition types. This can be explained by the inherently heterogeneous nature of the segments corresponding to the transitions to and back from seizure. Furthermore, different types of seizures are preceded and followed by different types of brain states in epilepsy[20,31,35]. Thus, further studies are needed to extend our results beyond the four types of brain states and the narrow choice of epilepsy type and recording location in this study.

To eliminate redundant information and thus help differentiate the brain state types based on the features, principle components analysis (PCA) was conducted, reducing the dimensionality from the 11 features to four principal components. The biggest part of captured information, PC 1, is shared among most features. Additional information is captured by power in lower frequency bands, spikeabs, and autocorrel, which in turn substantially contribute to PC 2–4 (Fig. 2C left panels). In the next sub-steps, the projected signal features (i.e., the PCA scores) for all data segments are clustered into four clusters, and the cluster centroids are matched with the Wendling-defined types (so that, e.g., the centroid of cluster 2 becomes the prototype for type 4: ictal), to obtain the labeled brain state prototypes. Figure 2C right panels shows that PC 1 reliably differentiates interictal (type 1) and ictal (type 4) state, while PC 2 helps to differentiate preonset (type 2) and onset (type 3) state. Moreover, human and rat-driven clustering show astonishing similarity, especially for the interictal state (across PCs) and ictal state (PC 1). Finally, for each data segment (dot in Figure 2C right panel), we identify the labeled centroid (prototype) that is spatially closest in PC space, thus most similar, to predict the type label of each segment (color-coded in Fig. 2D). Predicted labels are compared against visual data labels for individualized sensitivity and PPV performance. We found the lower sensitivity of the data-driven classification might be a consequence of the limited amount of data segments to derive the prototypes (a problem that data-driven classifiers often face). Real data segments contain noise (produced by other ongoing brain processes, artifacts, and measurement noise) and segments of mixed type (e.g., first half onset, second half ictal type). This is one of the major reasons why data-driven classifiers typically require large, multi-center datasets and an appropriate time scale for data segmentation to identify reliable types of brain states. Data-driven prototypes of brain states that are identified via cluster analysis, thus, may be epileptic or tied to other brain processes taking place at the same time. Therefore, assuming that the modeled types of brain state capture relevant activity patterns of epileptic brain states, clustering model data has, by default, the advantage of providing somewhat "pure" type representatives instead of the more noise- and segmentation bias-prone clustering of real data. Thus, noise and segmentation bias most likely influenced the performance of data-driven classification in this study. That we did not find any onset type segments in the rat data could be an example. The captured dynamics in rat LFP recordings seemingly take place at a higher temporal scale (see Fig. 1). This could be attributed to (a) capturing neuronal activity from a more localized environment, i.e., from a few neurons instead of from thousands as recorded by the human iEEG macro-electrodes and (b) generally faster transitions between interictal and ictal states in the rat slice (see Fig. 2A

left panel, approximately one seizure per minute), than in the human intracranial recording (see Fig. 2A right panel, approximately one seizure per three hours; for plotting purposes inter-seizure interval is cut so that only 1 min before until 1 min after the seizure is kept). In the case of (b) segmentation bias might have played a role. Presumably, the 5-s interval for data segmentation was too long to contain mostly the high-frequency type of activity. Also, other choices in the pipeline could have influenced the results: for example, the chosen number of components of PCA kept for further analysis. We chose four components, as they contained more than 80% of variance for all datasets (88% in humans, 94% in rats, and 98% in model data). However, optimal thresholds are data-specific. Furthermore, overall, we worked with a limited sample size. Therefore, real data classification results might not be sufficiently robust. Overall, due to the outlined considerations, the performance of data-driven classification in this study could have been underestimated.

A significant practical advantage of the proposed model-driven approach, when compared to the data-driven approach, is that brain state labeling is achieved unsupervised, i.e., without the need for visually classified data to serve as ground truth for building the classifier. Visual labeling is a lengthy and cumbersome procedure requiring much clinical expertise, especially for classifying transition types of brain states. Thus, in this study, visual labeling was only used to validate the classification results so that even data-driven classification was partially model-informed and thus unsupervised. It is pretty remarkable that each data cluster in the human data (human 1) could be uniquely assigned one of the Wendling types and that in the rat data, where no onset type of brain state was present, the onset label was the only one not assigned to any of the clusters. This finding supports our main conclusion of consistent patterns in brain states in epilepsy across species. Yet, in shorter datasets, there were fewer type matches (Table 1). The different numbers of prototypes might have influenced the classification results. For example, in the rat data without onset type data, there were only three types of brain state to detect and sensitivity, increasing the chance level to assign a correct type label. On the contrary, classification performance was likely to be decreased in datasets where centroids were dropped because the same type label was given to two or more centroids.

Another vital advantage of the model-driven approach mentioned above is that it can add relevant mechanistic insight. In the employed model, the epileptic brain states are explained and linked in the mechanical framework of hippocampal excitation and inhibition levels. This is particularly relevant in the context of brain state tracking for the application of timing-specific intervention. There, defining the current brain state based on a specific balance in excitatory and inhibitory population dynamics (A, B, G parameters in the Wendling model) could have direct implications for the desired treatment effects (e.g., a reduction of peri-dendritic inhibition to achieve a transition from preonset type back to the interictal type of brain state). Classifying brain state according to four prototypes with given model parameters, as done here, is a more conservative approach than the one that was used by Song et al.[40,41], where the authors fit model parameters to individual data segments and infer brain states based on classifying the identified parameters. Our approach is more conservative in the sense that the specific model to generate the time series of prototypical activity for a given brain state is less relevant and, thus, can be more easily replaced (e.g., to obtain patient-specific prototypes from data-informed phenomenological models such as in[35,36]).

Model-driven brain state classification might help tackle patient-heterogeneity. The high heterogeneity among and within epilepsy patients and their seizures is one of the main challenges in epilepsy treatment, which has been suggested to be overcome by treatment approaches tailored to the individual patient and time point[6,7]. The proposed brain state classification approach provides a tool to assess the current brain state in a data-driven and, thus, time and patient-specific manner. We assessed the potential advantage of characterizing brain states, i.e., deriving prototypes, in a patient-tailored way over the generalizing approach, i.e., across-subject brain state classification. The individualized brain state classification had better PPV but worse sensitivity than the generalizing approach. Keeping in mind that sensitivity levels for the data-driven strategy might have been underestimated due to the limited sample size in this study and that the occasional smaller number of derived prototypes in the individualized approach might have influenced the results, we speculate that, especially when little data is available for a given patient (and a given type of brain state), the generalized approach might be preferable. The model-driven classification performed best among the different prototype datasets for the generalized approach. Conversely, generalized human-driven classification achieved the lowest performance in this study, suggesting that generalizing from one human to another might be problematic. Therefore, we propose that model-driven classification might better capture generalizable patterns and thus help overcome some of the observed patient heterogeneity in epilepsy. Note that the human dataset of this study was rather homogeneous, as it was recorded in the hippocampus from patients with hippocampal, temporal lobe epilepsy. Therefore, the presented results do not sufficiently address the patient heterogeneity due to the etiological background and varying locations of the epileptic focus. However, the types of brain state and model environment used here have been observed and applied outside of temporal lobe epilepsy[48,49] Future work is needed to assess the performance of the suggested approach to model-driven classification in bigger and more heterogeneous samples. Due to the chosen prototyping approach, the model and features are easily replaceable in the presented pipeline, which could thus be tailored to different patterns and types of brain states, if needed.

Conclusion

This study highlights the potential of model-driven brain state classification in epilepsy and provides a pipeline for unsupervised model- and data-driven classification based on prototype comparison. We are convinced that the potential of model-based approaches for clinical application is still on the verge of being explored. Future research for a potential clinical application of model-driven brain state classification includes optimization of

the performance of suggested procedures, a possible extension of the types of brain states, validation on a more extensive dataset, and a comparison with other machine learning schemes.

Methods

Study design. We compare the performance of epileptic brain state classification across different strategies (generalized classification: model-, human- and rat-driven; individualized classification: every individual for themselves) in three data sets (model, human, rat). The different employed strategies can be understood as treatment conditions. The outcome measures of this study are the sensitivity and PPV rate. They are assessed against the visual expert assessment of the data and statistically tested against the classification performance in 1000 realizations of a matching Markov Chain (permutation testing) per individual, which can be understood as the control condition in this study. Statistical testing was done on a group or individual level for generalized or individualized classification. The visual expert assessment was blinded to the predicted brain state of a given data segment. The experimental unit was a single rat or human. The sample size in this study was not calculated a priori but depended on the data available to us, fulfilling our data-specific selection criteria (see below). Table 1 shows the amount of data segments per individual.

Data. *Simulated data.* We simulate the Wendling neural mass model[38,39] of interacting populations in the hippocampus as implemented by Fietkewicz et al.[42] (customized code available at our GitHub repository), using the parameters listed in Table 3.

Changing additional parameters A, B, and G leads to different signal patterns in the model output representing the EEG signal. We simulate 100 segments of five seconds length at a sampling rate of 512 Hz for each type of brain state in epilepsy, given A, B, and G values from Wendling et al.[39]: interictal: A = 3.5, B = 13.2, G = 10.76; preonset: A = 4.6, B = 20.4, G = 11.48; onset: A = 7.7, B = 4.3, G = 15.1; ictal: A = 8.7, B = 11.4, G = 2.1.

Rat data. The data were obtained from three male Wistar rats (approximately 200 g) that underwent the following procedure. Before the experiment, animals were housed in an enriched environment in 12/12 h light and dark conditions. The health status of the animals was checked regularly. For the experiment, the animals were deeply anesthetized (ketamine 80 mg/kg, xylazine 25 mg/kg) and then decapitated. The brains were removed from the skull and placed into ice-cold, oxygenated protective solution sucACSF (containing mMol 189 Sucrose, 2.5 KCl, 0.1 $CaCl_2$, 5 $MgCl_2$, 26 $NaHCO_3$, 1.25 $NaH_2PO_4 \cdot H_20$, and 10 glucose). The brain was cut in the sagittal plane into slices of 350 μm thickness using a vibratome (Campden Instruments, Loughborough, UK). The hippocampus was cropped, and the CA3 area was cut off. The hippocampal slices were stored, at room temperature, in a holding chamber filled with "normal" ACSF consisting of (in mMol) 125 NaCl, 26 $NaHCO_3$, 3 KCl, 2 $CaCl_2$, 1 $MgCl_2$, 1.25 NaH_2PO_4, and 10 glucose, aerated with a humidified 95% O2–5% CO_2 mixture. After >60 min, slices were transferred to an oxygenated interface recording chamber (34 ± 1°C), constantly superfused with normal ACSF. Local field potentials were recorded using extracellular glass microelectrodes (diameter 10–15 μm) filled with ACSF. Signals were amplified (AC/DC Differential Amplifier Model 3000, A-M Systems, Inc., Carlsborg, Washington, USA) and digitized (Power1401, CED, Cambridge, England) with a sampling frequency of 10 kHz and stored using Spike 2 for further analysis. The slices were left for at least 10 min in the recording chamber to accommodate them. Then, the recording electrode was put on the stratum pyramidale. For spontaneous seizures to emerge, we increased the K+ concentration by adding KCl solution in large steps (1–3 mMol) until a total concentration of 6.5–7 mMol was reached. Then we increased the concentration further in small steps (0.2–0.5 mMol) until spontaneous seizure-like events occurred. The Ethics Committee of The Czech Academy of Sciences approved all experimental procedures. All methods were performed in accordance with the relevant guidelines and regulations, and the study is reported in accordance with ARRIVE (Animal Research: Reporting of In Vivo Experiments) guidelines. The data used in this study were chosen upon the occurrence of spontaneous seizure-like events up until the time point of stimulation, which was later applied to the slices for a different experiment. Recordings of Rat 1 included a total of 16 seizure-like events (Rat 2: 6, Rat 3: 7).

Human data. Intracranial EEG data were obtained from four patients recorded during their presurgical workup at Motol Epilepsy Center in Prague, Czech Republic, between 2009 and 2017. Data were recorded using macro depth electrodes (Dixi Medical or Ad-Tech) in the referential montage using Stellate Harmony (sampling frequency 1 kHz) or Natus NicOne (sampling frequency 512 Hz). The study was performed in accordance with the Declaration of Helsinki, ethical approval was granted by the Ethical Committee of Motol University Hospital, and written informed consent was obtained from all subjects. For this study, patients were retrospectively selected based on their type of epilepsy (temporal lobe epilepsy), that they had at least one resected channel in the hippocampus and had excellent surgery outcomes (Engel Ia 2 years after surgery). In those patients, data were selected from each recorded seizure, particularly the time interval ranging from one minute before the start to one minute after the end of the seizure, from a hippocampal and resected channel. iEEG contacts in hippocampal structure CA1 were identified by assigning MNI coordinates to the probabilistic cytoarchitectonic

Parameter	a	b	g	C	C1	C2,C7	C3,C4	C5	C6	Sigmoid v0, e0, r	Noise mean, std
Value	100	30	350	135	C	0.8 C	0.25 C	0.3 C	0.1 C	6, 2.5, 0.56	90, 30

Table 3. Model parameters used for simulations.

atlas using SPM Anatomy toolbox[50](*version 2.2c*), and the channel with the highest probability was selected for analysis. Individual patient characteristics are summarized in Table 4.

Data preprocessing and visual labeling. There was no data preprocessing, apart from centering the rat and human data around zero and inverting their polarity (to achieve consistency between rat, human, and model recordings). Furthermore, data were 50 Hz filtered to exclude line noise. Data were segmented into five-second segments, and for the rat and human data, each segment was assigned to one of the four Wendling types based on a visual assessment that took into account (1) the clinical marks of seizure on- and offset and (2) the order of brain state types (e.g., onset preceded ictal and was preceded by preonset). Figure 3D shows an example of visual assessment results. Visual labeling was not necessary for simulated data; for each segment, the used A, B, and G parameters—and thus the true type of brain state—was known.

Brain state classification procedure. Brain states are classified based on a prototype comparison procedure. The prototype generation follows these sub-steps: (1) feature calculation, (2) principle component analysis, (3) clustering analysis, and (4) centroid matching to Wendling types. Matched centroids then serve as prototypes, and any data segment can be classified by choosing the most similar of the prototypes. Code will have been made available at our GitHub repository at https://github.com/cobragroup/epileptic-brain-states by the publication date.

Feature calculation and normalization. We chose 11 signal features: signal mean, the average band power in range 0–0.5 Hz, 0.5–4 Hz, 4–12 Hz, 12–64 Hz, and >64 Hz, the distance between 0.95 and 0.05 quantile, spike count as the number of outliers based on Tukey 1.5 interquartile range threshold, signal variance, auto-correlation at 5 ms lag and line lengths; due to their demonstrated usefulness to differentiate between the specific four types of brain state in epilepsy considered in this study[39] and to characterize seizure transitions in general[4,14]. Features are calculated on each data segment separately and then z-normalized across all segments of a given individual or, in the case of the model, across all 400 simulated segments. Normalization is done to account for different scaling of the signal features.

Principle component analysis. For prototype generation, we aim to reduce the dimensionality by removing information that was shared among features. Therefore, we conducted the principal component analysis with four components, which always accounted for more than 80% of the variance in all datasets used for prototype generation (88% in humans, 94% in rats, and 98% in model data). To be able to project other data into the same PC space, PCA coefficients need to be stored.

Cluster analysis and centroid matching to Wendling types. In the next step of prototype generation, we cluster the PC data using *kmeans* algorithm to obtain cluster centroids which then serve as the prototypes for brain state classification. We choose four clusters of brain state, as our goal is to find clusters matching the four Wendling types. We then ask which of the four obtained clusters corresponds to which type of brain state (Fig. 4 "centroid matching"). We need to assign each cluster a unique type label to answer this question. For this, we use the model dataset, as in this dataset, the ground truth of the brain state type for each segment is known. Note that this step is done both in the model- and data-driven classification, as it solely matches the data-driven clusters with the Wendling-type brain state. Thus, in data-driven classification (Fig. 4A), real data is used to carry out the dimension reduction, clustering, and defining the prototypes as the centroids of the clusters, however, the model data is used to assign the four interpretable labels to the clusters. Therefore, for each segment of model data, z-normalized signal features are projected into the PC space of the prototype dataset. We then carry out a Voronoi tiling of the PCA space concerning the cluster centroids: to each centroid, we associate the region of all points, i.e., model data segments, that are closer to this centroid than to any of the remaining three centroids. Then the label for a given centroid is decided by voting among the model data segments within each region.

In some individuals, two of the centroids received the same label by this procedure; in this case, we kept only the prototype with the higher number of label-defining simulated segments, while the latter was dropped. Sometimes no model segment fell into the region defined by a centroid, again leading to omitting the centroid. Thus, in some individuals, we find fewer prototypes than four (marked as # types in Table 1).

Patient	Gender	Type of epilepsy	Age (epil. duration)	Rec. location (probability)	n seizures
Human 1[a]	Male	Left temporal	28 (8) years	CA1 (100%)	3
Human 2	Male	Left temporal	54 (28) years	CA1 (92%)	3
Human 3	Female	Left temporal	41 (23) years	CA1 (94%)	2
Human 4	Female	Right temporal	23 (4) years	CA1 (99%)	1

Table 4. Individual patient characteristics, as well as the recording location of the contact selected for this study, and the number of recorded seizures. . Recording location according to probabilistic cytoarchitectonic atlas (see text for details). [a]Human 1 was used for prototype generation in human data-driven brain state classification.
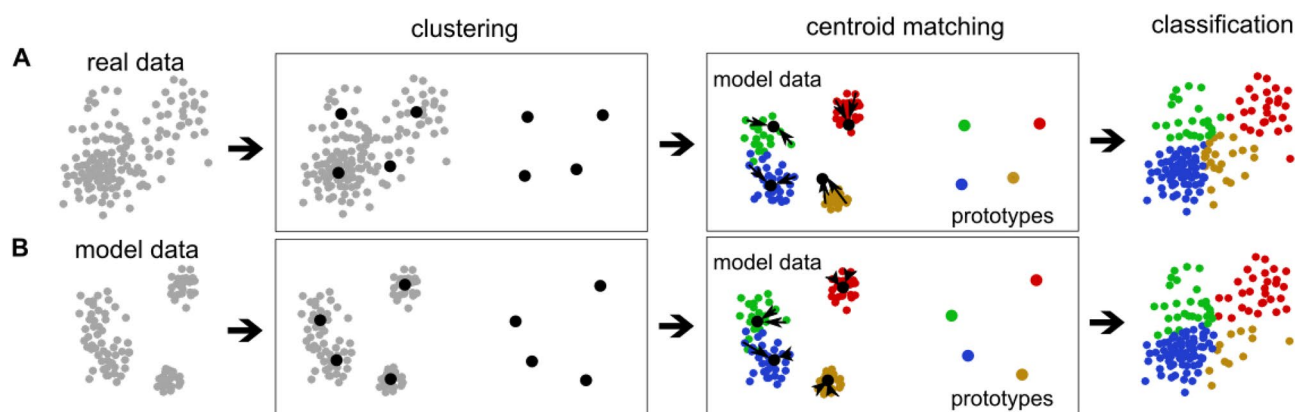
Figure 4. Brain state classification procedure. (A) Data-driven brain state classification. Real data segments (dots) are clustered to obtain centroids (black dots) labeled during centroid matching. Centroid matching is carried out via 'voting' among all closest model data segments, using their known type of brain state, given the model configuration used to generate them. The most commonly assigned model type becomes the new centroid label, indicated by color: interictal—blue; preonset—green; onset—yellow; ictal - red. Labeled centroids then serve as prototypes, and individual data segments are classified by identifying the closest prototype. In this example, the same dataset used clustering is classified for individualized classification. (**B**) Model-driven brain state classification of real data. Model data segments are clustered and labeled to obtain the model-driven prototypes. In this example, the obtained prototypes are used to classify the real dataset from (**A**), the same as for generalized classification.

Classification of a new data segment. Using the obtained prototypes (model, rat or human; colored dots in Fig. 4), we classify the type of brain state of any data segment by projecting its z-normalized feature values into the respective prototype dataset-derived PC space by multiplying them with the individual PCA coefficients and identifying the closest prototype centroid. That centroid's type label (color in Fig. 4) becomes the segment's label.

Statistical analysis of classification performance. For statistical analysis, we calculate the confusion matrix for predicted versus true type (see Fig. 3D) for each individual. Then, we calculate sensitivity and positive predictive value (PPV) before averaging across the four types of brain state as:

$$sensitivity = \frac{TruePositives}{TruePositives + FalseNegatives} \quad PPV = \frac{TruePositives}{TruePositives + FalsePositives}$$

Significance testing is done on the group level for each species (model, rat, or human) by comparing the group mean sensitivity or PPV against group mean sensitivity or PPV in 1000 surrogates (discrete-time, finite-state, time-homogeneous Markov chain simulations using the given data-specific true type transition matrix). For the model, the type transition matrix contains equal amounts of transitions for all types. Reported *p*-values correspond to the percentage of data realizations (including all surrogates and the single original data) that achieved the same or a higher sensitivity or PPV than the obtained group mean sensitivity or PPV, respectively.

Data availability
The datasets generated and analyzed during the current study are available from https://osf.io/8cdz5/.

Code availability
All data processing and analysis were conducted in Matlab version *R2021a* (Mathworks Inc., USA). Relevant code is publicly available at the COBRA group GitHub repository at https://github.com/cobragroup/epileptic-brain-states.

References
1. Billakota, S., Devinsky, O. & Kim, K.-W. Why we urgently need improved epilepsy therapies for adult patients. *Neuropharmacology* **170**, 107855. https://doi.org/10.1016/j.neuropharm.2019.107855 (2020).
2. Cook, M. J. *et al.* Human focal seizures are characterized by populations of fixed duration and interval. *Epilepsia* **57**, 359–368. https://doi.org/10.1111/epi.13291 (2016).
3. Pitkänen, A. *et al.* Advances in the development of biomarkers for epilepsy. *Lancet Neurol.* **15**, 843–856. https://doi.org/10.1016/S1474-4422(16)00112-5 (2016).
4. Chang, W.-C. *et al.* Loss of neuronal network resilience precedes seizures and determines the ictogenic nature of interictal synaptic perturbations. *Nat. Neurosci.* **21**, 1742–1752. https://doi.org/10.1038/s41593-018-0278-y (2018).
5. Jiruska, P., Powell, A. D., Deans, J. K. & Jefferys, J. G. Effects of direct brain stimulation depend on seizure dynamics: Brain Stimulation Depends on Seizure Dynamics. *Epilepsia* **51**, 93–97. https://doi.org/10.1111/j.1528-1167.2010.02619.x (2010).

6. Rosenow, F. *et al.* Personalized translational epilepsy research—Novel approaches and future perspectives. *Epilepsy Behav.* **76**, 13–18. https://doi.org/10.1016/j.yebeh.2017.06.041 (2017).

7. Nagaraj, V. *et al.* Future of seizure prediction and intervention: Closing the loop. *J. Clin. Neurophysiol.* **32**, 194–206. https://doi.org/10.1097/WNP.0000000000000139 (2015).

8. Falcon, M. I., Jirsa, V. K. & Solodkin, A. A new neuroinformatics approach to personalized medicine in neurology: The virtual brain. *Curr. Opin. Neurol.* **29**, 429–436. https://doi.org/10.1097/WCO.0000000000000344 (2016).

9. Moraes, M. F. D., de Castro Medeiros, D., Mourao, F. A. G., Cancado, S. A. V. & Cota, V. R. Epilepsy as a dynamical system, a most needed paradigm shift in epileptology. *Epilepsy & Behavior* **121**, 106838. https://doi.org/10.1016/j.yebeh.2019.106838 (2021).

10. Cook, M. J. *et al.* The dynamics of the epileptic brain reveal long-memory processes. *Front. Neurol.* https://doi.org/10.3389/fneur.2014.00217 *(2014).*

11. Karoly, P. J. *et al.* Circadian and circaseptan rhythms in human epilepsy: A retrospective cohort study. *Lancet Neurol.* **17**, 977–985. https://doi.org/10.1016/S1474-4422(18)30274-6 (2018).

12. Baud, M. O. *et al.* Multi-day rhythms modulate seizure risk in epilepsy. *Nat. Commun.* **9**, 88. https://doi.org/10.1038/s41467-017-02577-y (2018).

13. Kudlacek, J. *et al.* Long-term seizure dynamics are determined by the nature of seizures and the mutual interactions between them. *Neurobiol. Dis.* **154**, 105347. https://doi.org/10.1016/j.nbd.2021.105347 (2021).

14. Maturana, M. I. *et al.* Critical slowing down as a biomarker for seizure susceptibility. *Nat. Commun.* **11**, 2172. https://doi.org/10.1038/s41467-020-15908-3 (2020).

15. Schroeder, G. M. *et al.* Seizure pathways change on circadian and slower timescales in individual patients with focal epilepsy. *Proc. Natl. Acad. Sci.* **117**, 11048–11058. https://doi.org/10.1073/pnas.1922084117 (2020).

16. Pérez-Cervera, A. & Hlinka, J. Perturbations both trigger and delay seizures due to generic properties of slow-fast relaxation oscillators. *PLOS Comput. Biol.* **17**, e1008521. https://doi.org/10.1371/journal.pcbi.1008521 (2021).

17. Sinha, N. *et al.* Predicting neurosurgical outcomes in focal epilepsy patients using computational modelling. *Brain* **140**, 319–332. https://doi.org/10.1093/brain/aww299 (2017).

18. Goodfellow, M. *et al.* Estimation of brain network ictogenicity predicts outcome from epilepsy surgery. *Sci. Rep.* **6**, 29215. https://doi.org/10.1038/srep29215 (2016).

19. Laiou, P. *et al.* Quantification and selection of ictogenic zones in epilepsy surgery. *Front. Neurol.* **10**, 1045. https://doi.org/10.3389/fneur.2019.01045 (2019).

20. Saggio, M. L. *et al.* A taxonomy of seizure dynamotypes. *eLife* **9**, e55632. https://doi.org/10.7554/eLife.55632 (2020).

21. McKenna, T., McMullen, T. & Shlesinger, M. The brain as a dynamic physical system. *Neuroscience* **60**, 587–605. https://doi.org/10.1016/0306-4522(94)90489-8 (1994).

22. Izhikevich, E. M. *Dynamical Systems in Neuroscience: The Geometry of Excitability and Bursting* (The MIT Press, 2006).

23. Breakspear, M. Dynamic models of large-scale brain activity. *Nat. Neurosci.* **20**, 340–352. https://doi.org/10.1038/nn.4497 (2017).

24. Haken, H. & Haken, H. Modeling the brain. A first attempt: The brain as a dynamical system. in *Principles of Brain Functioning.* Vol. 67. 31–33. https://doi.org/10.1007/978-3-642-79570-1_4 (Springer, 1996).

25. Poulet, J. F. A. & Crochet, S. The cortical states of wakefulness. *Front. Syst. Neurosci.* **12**, 64. https://doi.org/10.3389/fnsys.2018.00064 (2019).

26. Nguyen, G. & Postnova, S. Progress in modelling of brain dynamics during anaesthesia and the role of sleep-wake circuitry. *Biochem. Pharmacol.* **191**, 114388. https://doi.org/10.1016/j.bcp.2020.114388 (2021).

27. La Camera, G., Fontanini, A. & Mazzucato, L. Cortical computations via metastable activity. *Curr. Opin. Neurobiol.* **58**, 37–45. https://doi.org/10.1016/j.conb.2019.06.007 (2019).

28. Michel, C. M. & Koenig, T. EEG microstates as a tool for studying the temporal dynamics of whole-brain neuronal networks: A review. *NeuroImage* **180**, 577–593. https://doi.org/10.1016/j.neuroimage.2017.11.062 (2018).

29. Kringelbach, M. L. & Deco, G. Brain states and transitions: Insights from computational neuroscience. *Cell Rep.* **32**, 108128. https://doi.org/10.1016/j.celrep.2020.108128 (2020).

30. Wang, Y., Hutchings, F. & Kaiser, M. Computational modeling of neurostimulation in brain diseases. in *Progress in Brain Research.* Vol. 222. 191–228. https://doi.org/10.1016/bs.pbr.2015.06.012 (Elsevier, 2015).

31. Lopes da Silva, F. *et al.* Dynamical diseases of brain systems: Different routes to epileptic seizures. *IEEE Trans. Biomed. Eng.* **50**, 540–548. https://doi.org/10.1109/TBME.2003.810703 (2003).

32. Kalitzin, S. *et al.* Epilepsy as a manifestation of a multistate network of oscillatory systems. *Neurobiol. Dis.* **130**, 104488. https://doi.org/10.1016/j.nbd.2019.104488 (2019).

33. Wendling, F., Benquet, P., Bartolomei, F. & Jirsa, V. Computational models of epileptiform activity. *J. Neurosci. Methods* **260**, 233–251. https://doi.org/10.1016/j.jneumeth.2015.03.027 (2016).

34. Bernard, C., Naze, S., Proix, T. & Jirsa, V. K. Modern concepts of seizure modeling. in *International Review of Neurobiology*. Vol. 114. 121–153. https://doi.org/10.1016/B978-0-12-418693-4.00006-6 (Elsevier, 2014).

35. Jirsa, V. K., Stacey, W. C., Quilichini, P. P., Ivanov, A. I. & Bernard, C. On the nature of seizure dynamics. *Brain* **137**, 2210–2230. https://doi.org/10.1093/brain/awu133 (2014).

36. Jirsa, V. K. *et al.* The virtual epileptic patient: Individualized whole-brain models of epilepsy spread. *NeuroImage* **145**, 377–388. https://doi.org/10.1016/j.neuroimage.2016.04.049 (2017).

37. Dallmer-Zerbe, I., Jiruška, P. & Hlinka, J. Personalized dynamic network models of the human brain as a future tool for planning and optimizing epilepsy therapy. *Epilepsia*. _eprint: https://onlinelibrary.wiley.com/doi/pdf/10.1111/epi.17690.

38. Wendling, F., Bartolomei, F., Bellanger, J. J. & Chauvel, P. Epileptic fast activity can be explained by a model of impaired GABAergic dendritic inhibition: Epileptic activity explained by dendritic dis-inhibition. *Eur. J. Neurosci.* **15**, 1499–1508. https://doi.org/10.1046/j.1460-9568.2002.01985.x (2002).

39. Wendling, F., Hernandez, A., Bellanger, J.-J., Chauvel, P. & Bartolomei, F. Interictal to ictal transition in human temporal lobe epilepsy: Insights from a computational model of intracerebral EEG. *J. Clin. Neurophysiol.* **22**, 343–356 (2005).

40. Song, J., Li, Q., Zhang, B., Westover, B. & Zhang, R. A new neural mass model driven method and its application in early epileptic seizure detection. *IEEE Trans. Biomed. Eng.* https://doi.org/10.1109/TBME.2019.2957392 *(2019).*

41. Song, J.-L. *et al.* Seizure tracking of epileptic EEGs using a model-driven approach. *J. Neural Eng.* **17**, 016024. https://doi.org/10.1088/1741-2552/ab2409 (2020).

42. Fietkiewicz, C. & Loparo, K. A. Analysis and enhancements of a prolific macroscopic model of epilepsy. *Scientifica* **1–10**, 2016. https://doi.org/10.1155/2016/3628247 (2016).

43. Beniczky, S. *et al.* Automated seizure detection using wearable devices: A clinical practice guideline of the International League Against Epilepsy and the International Federation of Clinical Neurophysiology. *Clin. Neurophysiol.* **132**, 1173–1184. https://doi.org/10.1016/j.clinph.2020.12.009 (2021).

44. Ulate-Campos, A. *et al.* Automated seizure detection systems and their effectiveness for each type of seizure. *Seizure* **40**, 88–101. https://doi.org/10.1016/j.seizure.2016.06.008 (2016).

45. Mormann, F., Andrzejak, R. G., Elger, C. E. & Lehnertz, K. Seizure prediction: The long and winding road. *Brain* **130**, 314–333. https://doi.org/10.1093/brain/awl241 (2007).

46. Kuhlmann, L., Lehnertz, K., Richardson, M. P., Schelter, B. & Zaveri, H. P. Seizure prediction—Ready for a new era. *Nat. Rev. Neurol.* **14**, 618–630. https://doi.org/10.1038/s41582-018-0055-2 (2018).

47. Stirling, R. E., Cook, M. J., Grayden, D. B. & Karoly, P. J. Seizure forecasting and cyclic control of seizures. *Epilepsia* https://doi.org/10.1111/epi.16541 (2021).
48. Westmoreland, B. F. The EEG findings in extratemporal seizures. *Epilepsia* **39**, S1–S8. https://doi.org/10.1111/j.1528-1157.1998.tb05121.x (1998).
49. Lopez-Sola, E. *et al.* A personalizable autonomous neural mass model of epileptic seizures. *J. Neural Eng.* **19**, 055002. https://doi.org/10.1088/1741-2552/ac8ba8 (2022).
50. Eickhoff, S. B. *et al.* A new SPM toolbox for combining probabilistic cytoarchitectonic maps and functional imaging data. *NeuroImage* **25**, 1325–1335. https://doi.org/10.1016/j.neuroimage.2004.12.034 (2005).

Acknowledgements

Author contributions

I.D.-Z. conceived the study, analyzed the data, and wrote the manuscript under the supervision of J.H. (and P.J.). N.J. helped with methods and conceiving the manuscript. J.C., R.J., P.J., P.K., P.M., and P.J. were responsible for data acquisition and management; J.H. is the principal investigator of this work. All authors reviewed the manuscript.

Competing interests

The authors declare no competing interests.

Additional information

Correspondence and requests for materials should be addressed to J.H.

Reprints and permissions information is available at www.nature.com/reprints.

Publisher's note Springer Nature remains neutral with regard to jurisdictional claims in published maps and institutional affiliations.

8 Long-term seizure dynamics are determined by the nature of seizures and the mutual interactions between them

8.1 The contributions toward the progress of the field

The study showed that seizures tend to cluster in time and are followed by seizure-free periods. Within these clusters, the time interval between the seizures increases while the seizures become progressively more severe and spread to other brain areas. The key novel idea expressed in the study is that the seizures themselves determine the long-term dynamics of the seizure clusters. The authors propose that the trajectory of the disease is governed, or at least substantially influenced, by the mutual interaction between seizures. Specifically, the changes in the ictal dynamics within the cluster can be attributed to the occurrence of non-convulsive and convulsive seizures. Each non-convulsive focal seizure makes the next seizure stronger and more severe via the kindling mechanism. During the cluster progression, the cerebral network undergoes functional reorganization that facilitates the recruitment of extra-hippocampal structures which manifests itself by a progressive increase in the proportion of convulsive seizures. Meanwhile, convulsive seizures decrease the probability of a subsequent seizure occurrence, increase the time between the seizures, and decrease the seizure duration. The cumulative effect of repeated convulsive seizures leads to cluster termination. Understanding the long-term seizure dynamics and mechanisms driving fluctuations in seizure susceptibility is crucial for improving the treatments for epilepsy. This knowledge will greatly improve our comprehension of seizure genesis, ultimately leading to better therapeutic approaches.

8.2 The author's contributions

The author was involved in experimental work, data analysis and contributed to the discussion.

8.3 Compliance with the thesis objectives

Although the study was not directly focused on the research of high-frequency oscillations, it suggested the existence of a similar relationship between HFOs between clusters and contributed substantially to a sense of new ideas and research questions. Specifically, the results of the study can stand as a basis for the following research. The study found that seizure clustering is marked by the spread of electrographic epileptiform activity outside of the limbic system and suggests that the cerebral network undergoes functional reorganization during the cluster. Under the reorganization, it is likely that the properties of HFOs recorded between the seizures will change. Further research could investigate the spatial distribution of HFOs during seizure clustering to determine whether HFO activity is also spreading to extra-hippocampal structures and how its properties change. These changes in time in different sites of the brain could be exploited, possibly revealing the mechanism of how HFOs are generated. Therefore, further research should focus on investigating the long-term fluctuations in interictal activity, particularly ripples and fast ripples, with respect to the seizure clusters.
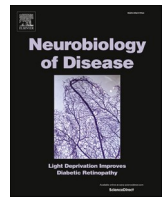
Long-term seizure dynamics are determined by the nature of seizures and the mutual interactions between them

Jan Kudlacek [a,b,c], Jan Chvojka [a,b,c], Vojtech Kumpost [b,c], Barbora Hermanovska [a,b], Antonin Posusta [b], John G.R. Jefferys [a], Matias I. Maturana [d,e], Ondrej Novak [a], Mark J. Cook [d], Jakub Otahal [b], Jaroslav Hlinka [f,g,*,1], Premysl Jiruska [a,b,**,1]

[a] Department of Physiology, Second Faculty of Medicine, Charles University, Prague, Czech Republic
[b] Department of Developmental Epileptology, Institute of Physiology of the Czech Academy of Sciences, Prague, Czech Republic
[c] Department of Circuit Theory, Faculty of Electrical Engineering, Czech Technical University in Prague, Prague, Czech Republic
[d] The Graeme Clark Institute & Department of Medicine, St Vincent's Hospital, The University of Melbourne, Melbourne, Australia
[e] Seer Medical, Melbourne, Australia
[f] Department of Nonlinear Modelling, Institute of Computer Science of the Czech Academy of Sciences, Prague 182 07, Czech Republic
[g] National Institute of Mental Health, Klecany, Czech Republic

ARTICLE INFO

ABSTRACT

The seemingly random and unpredictable nature of seizures is a major debilitating factor for people with epilepsy. An increasing body of evidence demonstrates that the epileptic brain exhibits long-term fluctuations in seizure susceptibility, and seizure emergence seems to be a consequence of processes operating over multiple temporal scales. A deeper insight into the mechanisms responsible for long-term seizure fluctuations may provide important information for understanding the complex nature of seizure genesis. In this study, we explored the long-term dynamics of seizures in the tetanus toxin model of temporal lobe epilepsy. The results demonstrate the existence of long-term fluctuations in seizure probability, where seizures form clusters in time and are then followed by seizure-free periods. Within each cluster, seizure distribution is non-Poissonian, as demonstrated by the progressively increasing inter-seizure interval (ISI), which marks the approaching cluster termination. The lengthening of ISIs is paralleled by: increasing behavioral seizure severity, the occurrence of convulsive seizures, recruitment of extra-hippocampal structures and the spread of electrographic epileptiform activity outside of the limbic system. The results suggest that repeated non-convulsive seizures obey the 'seizures-beget-seizures' principle, leading to the occurrence of convulsive seizures, which decrease the probability of a subsequent seizure and, thus, increase the following ISI. The cumulative effect of repeated convulsive seizures leads to cluster termination, followed by a long inter-cluster period. We propose that seizures themselves are an endogenous factor that contributes to long-term fluctuations in seizure susceptibility and their mutual interaction determines the future evolution of disease activity.

1. Introduction

Epilepsy is a chronic neurological disorder characterized by spontaneous recurrent seizures. From the patient's perspective seizures are usually unpredictable and random, occurring suddenly, with no apparent relationship to previous seizures. The unpredictability of seizures is a major debilitating factor that decreases the quality of life for

people with epilepsy (Cook et al., 2013; Fisher et al., 2000). Statistical analyses of patients' seizure diaries demonstrated non-random patterns in seizure distribution (Binnie et al., 1984; Milton et al., 1987; Balish et al., 1991; Tauboll et al., 1991; Bauer and Burr, 2001; Sunderam et al., 2007). One of the most important factors contributing to a non-random seizure occurrence is seizure clustering. Clinically, a cluster is defined as a closely grouped series of seizures or an overall increase in the patient's

* Corresponding author at: Complex networks and brain dynamics group, Institute of Computer Science, The Czech Academy of Sciences, Pod Vodarenskou vezi 271/2, Prague 182 07, Czech Republic.
** Corresponding author at: Department of Physiology, Second Faculty of Medicine, Charles University, Plzenska 130/221, CZ-15006 Prague 5, Czech Republic.
E-mail addresses: hlinka@cs.cas.cz (J. Hlinka), premysl.jiruska@lfmotol.cuni.cz (P. Jiruska).
[1] P. Jiruska and J Hlinka should be regarded as joint senior authors and joint corresponding authors.

typical seizure frequency (Haut, 2006). In patients with pharmacoresistant epilepsy, the prevalence of clustering ranges from 13 to 78% (Binnie et al., 1984; Milton et al., 1987; Balish et al., 1991; Tauboll et al., 1991; Bauer and Burr, 2001; Sunderam et al., 2007; Haut, 2006). Recently, the existence of a non-random seizure distribution was confirmed in studies in which intracranial EEG was recorded for months or years (Baud et al., 2018; Cook et al., 2014; Karoly et al., 2016). In these pivotal studies, nearly every patient displayed long-term rhythms in seizure probability, and in individual patients, even multiple rhythms (circadian, multi-day, multi-week, or multi-month) in seizure occurrence could be identified. Detailed analysis of long-term intracranial electrographic data revealed that the long-term fluctuations in seizure susceptibility were accompanied by changes in the dynamics of interictal discharges or specific signal properties (Baud et al., 2018; Maturana et al., 2020). The clinical observations are supported by data obtained from various chronic animal models of epilepsy, where seizure clustering is a common phenomenon. Clustering has been observed in models of temporal (Arida et al., 1999; Bajorat et al., 2011; Cavalheiro et al., 1991; Goffin et al., 2007; Pitsch et al., 2017; Mazzuferi et al., 2012; Grabenstatter et al., 2005; Williams et al., 2009), neocortical (Chang et al., 2018a), and generalized epilepsy, including genetic models.

Each patient or animal can experience multiple seizure types ranging from electrographic (asymptomatic seizures) or focal seizures with mild clinical correlates, to severe generalized seizures. The seizure type can change from one seizure to another, and the mechanisms and circumstances that are responsible for this fluctuation are unknown. However, it is now well established that detailed investigation of the long-term dynamics of the epileptic brain is one of the key steps in understanding seizure genesis and the emergence of various seizure types.

Whilst a myriad of mechanisms responsible for seizure initiation or transition to seizure have been identified (Blauwblomme et al., 2014), the cellular and network mechanisms underlying long-term fluctuations in seizure susceptibility, seizure clustering and clinical severity of seizures are not well understood. Seizure clustering can be associated with intercurrent illness or exogenous risk factors like drug withdrawal (Haut, 2006). In catamenial epilepsy, the seizure susceptibility is driven by changes in plasma levels of estrogens and progesterone (Herzog et al., 2004). In the majority of cases, the mechanisms responsible for endogenous fluctuations remain to be elucidated.

In this study, we explored long-term seizure dynamics and seizure clustering in the tetanus toxin (TeNT) model of temporal lobe epilepsy. The results demonstrate that fluctuations in seizure probability and seizure clustering are associated with functional reorganization of brain network properties. We show that the nature of past seizures, seizure severity, and network reorganization determine the brain propensity to seize and the evolution of disease activity.

2. Methods

2.1. Animals

Two groups of animals were used. The first group consisted of 11 adult male Sprague-Dawley rats weighing approximately 250 g. These animals were part of a study examining neurogenesis in the tetanus toxin model of temporal lobe epilepsy and the animals were implanted with wire-less telemetry (Jiruska et al., 2013a). The second group consisted of 9 Wistar rats weighing between 350 and 540 g. All animals were housed under standard conditions in a room with controlled temperature (22 ± 1 °C) and 12/12 h light/dark cycle. The animals had ad libitum access to food and water. All animal experiments were performed under the Animal Care and Animal Protection Law of the Czech Republic, fully compatible with the guidelines of the European Union directive 2010/63/EU or with the Animal Scientific Procedures Act (1986) of the United Kingdom and Institutional Ethical Review.

2.2. Surgery, electrode implantation and recording

In the first group, TeNT injection and electrode implantation were performed under generalized ketamine or isoflurane anesthesia. Small trephine openings were drilled symmetrically over both hippocampi at coordinates AP: −4.1 mm, L: ±3.9 mm in mm with respect to bregma (Paxinos and Watson, 1998). Using a Hamilton microsyringe and infusion pump (KD Scientific Inc., USA) 1 μl of TeNT (Sigma-Aldrich, UK) solution was injected into the stratum radiatum of the right dorsal hippocampal CA3 area (Jiruska et al., 2013a). TeNT solution contained 25 ng of TeNT in 1 μl of 0.05 M phosphate-buffered saline (PBS; Sigma-Aldrich, UK) and 2% bovine serum albumin (Sigma-Aldrich, UK). TeNT solution was injected at speed of 200 nl/min. The microsyringe was left in place for five minutes after the injection ended to avoid backflow along the injection track. Following the injection, silver ball electrodes were inserted into both openings epidurally over both cortices and fixed to the skull using dental acrylic. Electrodes were connected to single channel bipolar telemetric transmitters (Data Sciences International, s'Hertogenbosch, Netherlands), which were implanted subcutaneously over the dorsal aspect of the thorax and secured with sutures.

Following surgery, animals were housed in single cages and monitored by continuous electrocorticography starting on the 4th day until the 17th day. Electrocorticographic signals were recorded using Dataquest A.R.T. 4.3 acquisition system (Data Sciences International, s'Hertogenbosch, Netherlands) and sampled at 100 Hz. On day 17, animals were humanely overdosed with ketamine. This first group was part of a separate study focused on neurogenesis (Jiruska et al., 2013a).

In the second group, surgery was performed under generalized isoflurane anesthesia. Using a Hamilton 7001 syringe with a blunt needle and electronic infusion pump (KD Scientific Inc., USA) 1 μl of TeNT solution (Quadratech, UK) was injected into the stratum radiatum of the right dorsal hippocampal CA3 area, at coordinates AP: −4.1, L: ±3.9, D: −3.8 (Paxinos and Watson, 1998). The TeNT solution contained 10 ng of TeNT in 1 μl of 0.05 M phosphate-buffered saline (PBS; Sigma-Aldrich, UK) and 2% bovine serum albumin (Sigma-Aldrich, UK). Tetanus neurotoxin solution was injected at speed of 200 nl/min and the microsyringe was left in place for five minutes after the injection ended to avoid backflow along the injection track. Afterward, the animals were implanted with bipolar twisted electrodes bilaterally in the dorsal hippocampus and motor cortex. The electrodes were made from silver wire with a bare diameter of 120 μm, insulated by a 30 μm layer of PFA (A-M Systems, Inc., Carlsborg, Washington, USA). The two contacts of each electrode were 0.5 mm apart. The coordinates of hippocampal and cortical electrodes with respect to bregma were AP: −4.6, L: ±2.6, D: 3.3 and AP: 1.5, L: ±3.0, D: 1.5 respectively. Ground/reference stainless steel jeweler's screws were placed over the cerebellum.

Following a 5-day recovery period, the animals were subjected to video-EEG monitoring for at least three weeks. Two different recording setups were used. The Neuralynx setup consisted of a headstage unit gain amplifier HS-27 (Neuralynx, Bozeman, Montana, USA) and a Lynx-8 amplifier (Neuralynx, Bozeman, Montana, USA) set to a gain of 196, high-pass filter at 0.1 Hz and low-pass filter at 3 kHz. The signal was then digitized using a Power 1401 CE converter (Cambridge Electronic Design, Cambridge, UK) at the sampling frequency of 10 kHz and 16-bit resolution and recorded to a computer using Spike2 software (Cambridge Electronic Design, Cambridge, UK). The synchronized video was recorded by Spike2 using a USB webcam. Signals recorded using the Intan setup were amplified, analog-filtered and digitized by a RHD2132 headstage board (Intan Technologies, Los Angeles, California, USA). The digitized signals were transferred via swivel using the SPI bus to the RHD2000 evaluation board, which was connected to a computer via USB. The analog high-pass filter was set to 0.1 Hz and the low-pass filter to 1.7 kHz. The sampling frequency was 5 kHz and the resolution was 16 bit. Custom-made software was used for EEG recording. The synchronized video was recorded using a USB camera.

2.3. Identification of seizures and interictal epileptiform discharges

Recorded signals were exported, reviewed, and analyzed using Spike2 (Cambridge Electronic Design, Cambridge, UK) and custom made programs written in Matlab (Mathworks Inc., USA). The EEG recordings from the second group of rats were analyzed in the unipolar montage. In the examination of seizure occurrence, animals from both groups were pooled. Seizures were identified visually in the hippocampal EEG traces. If the presence of artifacts complicated identification of seizures, the visual analysis was combined with spectral analysis. Using fast Fourier transform, time-frequency maps were constructed and seizures were determined according to their characteristic spectral profiles (Cook et al., 2014; Schiff et al., 2000). To differentiate clearly short ictal discharges from interictal bursts (Chang et al., 2018b), only ictal discharges lasting more than 15 s were selected for subsequent statistical analysis. Seizures less than three minutes apart were joined into a single event. For each animal, we obtained a series of seizure onsets and durations.

In 9 animals, synchronized video recordings of the seizures were used to visually evaluate seizure behavioral severity using the Racine scale (Racine, 1972a). Then we separated seizures into non-convulsive (Racine stage 1–2) and convulsive (Racine stage 3–5) group for the subsequent analysis.

Interictal epileptiform discharges (IEDs) were detected in each channel using an automatic detector (Janca et al., 2015). Subsequently, we combined the detections from all four motor cortex channels into one series and detections from all four hippocampal channels into another series. Events in different channels closer than 0.2 s were considered one propagating IED.

2.4. Statistical evaluation of trends

The statistical evaluation of trends with respect to intra-cluster time was performed by the following procedure. Each cluster was divided into 10 time bins. We computed the mean of a given parameter in each time bin. We fitted a straight line to the means of the bins. The slopes of the fitted lines were subjected to the Wilcoxon signed-rank test to determine whether they were statistically significantly different from zero. Data are given as mean ± standard error of the mean followed by the median value in parentheses; mean ± SEM (median).

3. Results

3.1. Seizure profiles

All 17 rats from both groups developed spontaneous recurrent seizures (Fig. 1A,B) of varying behavioral intensity ranging from Racine 1 up to 5. Both groups presented a similar mean seizure frequency (0.54 vs. 0.53 seizure/h). Each animal experienced 152 ± 33 (109) seizures. The first seizure occurred on day 12 ± 1 (Arida et al., 1999). The average seizure duration was 81 ± 2 (Shapira et al., 1996) s. The mean inter-seizure interval (ISI) was 103 ± 9 (Hawkins and Mellanby, 1987) min. In 2/17 rats, long-term dynamics could not be studied, because the recording terminated prematurely due to the loss of the implant. In the remaining 15/17 rats, seizures occurred in visually discernible clusters (Fig. 1D). In addition to clusters, in three animals, we also recorded a > 10 day long period of moderate seizure incidence of 1.00 ± 0.29 (0.78) seizures per hour, towards the end of the recording. We checked whether the seizures could form a homogeneous Poisson process, which would imply an exponential distribution of ISIs. In all 15 rats, we confirmed a non-exponential distribution of ISIs ($p < 0.05$, χ^2 test); thus, the seizure profiles were not entirely random (Fig. 1C,D).

We defined a seizure cluster, based on visual investigation on the seizure profiles, as a group of at least 10 seizures separated by an ISI of no more than 12 h and lasting no more than 96 h (Fig. 1D). In three of the 15 rats, after the first inter-cluster period, we observed a long period
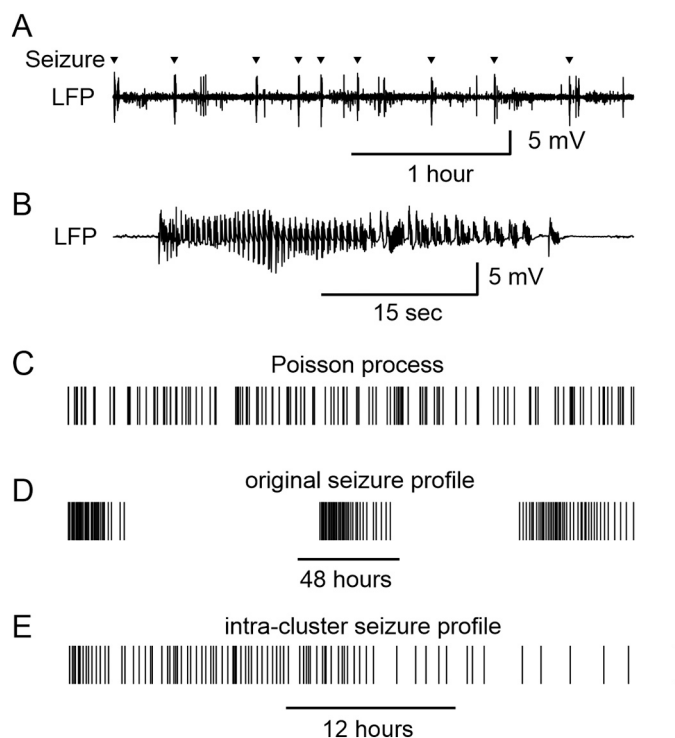

Fig. 1. Seizure clusters. (A) Four hours of hippocampal EEG containing nine seizures. (B) An example of ictal discharge. (C) Example of artificially generated completely random data, i.e. Poisson process. (D) Raster plot of the seizure times in a selected animal. It displays an accumulation of seizures into three clusters, interspersed with prolonged seizure-free inter-cluster periods. (E) During an individual seizure cluster, inter-seizure intervals progressively increase.

of moderate seizure incidence without the longer seizure-free intervals. One to three clusters were recorded per animal. In total, we identified 26 clusters. The mean cluster duration was 46 ± 3 (Howbert et al., 2014) hours and the mean inter-cluster period was 61 ± 10 (Jirsa et al., 2014) hours. The mean number of seizures in a cluster was 60 ± 6 (Krystal et al., 1998). The ISI duration within clusters was 46 ± 2 (Chang et al., 2018b) min.

3.2. Temporal distribution of seizures within the cluster

To find possible mechanisms responsible for clustering, we evaluated the seizure distribution in each cluster. We observed that ISIs increased with intra-cluster time (Fig. 1E, 2A). A regression line was fitted to the ISI duration versus the intra-cluster time. In 22/26 clusters there was a positive slope (Fig. 2B; $p < 0.001$, Wilcoxon signed-rank test). For visualisation of the population data, we divided each cluster into 10 equal time segments in which we evaluated the mean duration of the ISIs (Fig. 2C). We then graphically displayed the mutual relationship between the duration of a given ISI (ISI_n) and the next ISI (ISI_{n+1}) for each cluster (Fig. 2D). The results demonstrated that the durations of future ISIs are a function of past ISIs (Fig. 2D,E). Short ISIs are followed by short ISIs, which happens typically during the early parts of the cluster (Fig. 2D, cold colors). Meanwhile, long ISIs tend to be followed by long ISIs, dynamics that occur almost only during the terminal stages of the cluster (Fig. 2D, warmer colors). This is in line with the fact, that subsequent ISIs were correlated in 19/26 clusters (Spearman's correlation coefficient, $\rho > 0.3$, $p < 0.05$) which is evidence that seizures within these clusters are not a fully random (Poisson) process. The presence of interdependency between ISI durations suggests that seizures must be governed by a non-random underlying process. However, it is not clear whether this process is driven by endogenous changes in the
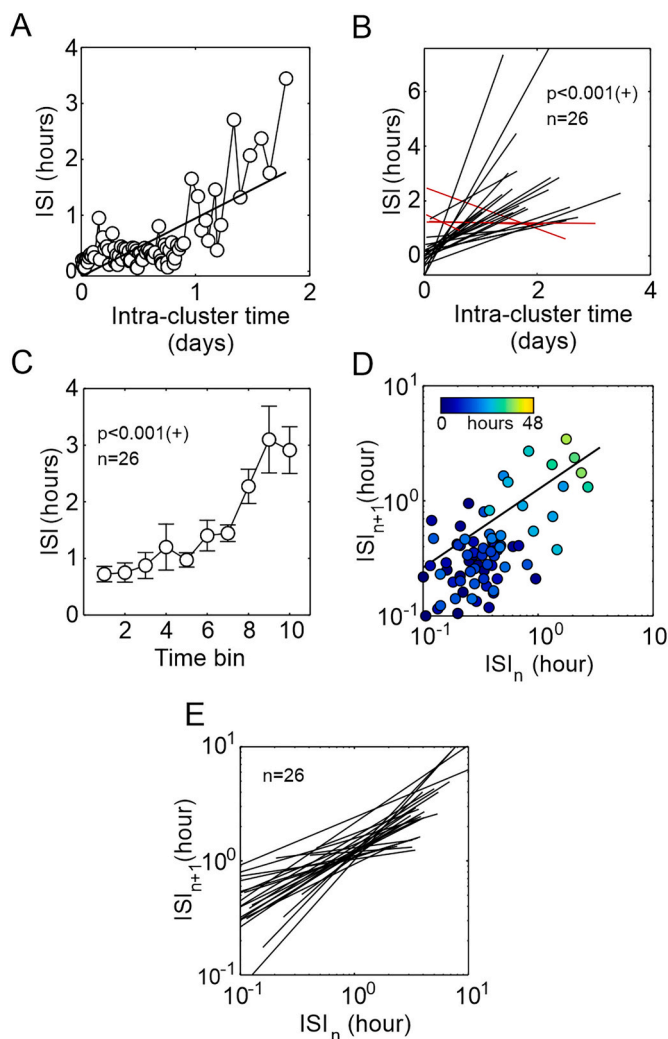
Fig. 2. Intra-cluster changes in ISIs. (A) An example of the temporal evolution of the ISIs during the course of the cluster. The duration of ISIs progressively increases with time. (B) The ISI data for each cluster was fitted with a regression line. Each line represents an individual cluster. Black color marks regression lines with a positive slope, while red lines have a negative slope. (C) Population statistics of ISI for all analyzed clusters. The x-axis represents evenly spaced time intervals from the beginning to the end of each cluster. (D) Scatter plot showing the duration of the nth and $n^{th} + 1$ ISI (ISI_n and ISI_{n+1}, respectively) within an example cluster (the time is color-coded). Thus, the future ISI_{n+1} is the function of the current ISI_n. Short ISIs occuring during the early stages of the cluster (cold colors) will also be followed by short ISIs, while long ISIs observed during the terminal stages of the cluster (warm colors) will be preferentially followed by ISIs with a long duration. (E) The scatter plot of each cluster was fitted with a regression line, showing that these relationships are observable in the majority of clusters.

epileptogenic tissue caused by the seizures per se or whether this process is external in origin. Therefore, in the next step, we explored in detail whether intra-cluster seizure properties could explain the seizure distribution pattern.

3.3. Changes in seizure properties during the cluster

Firstly, we evaluated whether the observed changes in ISI could be a consequence of seizure duration. With cluster progression, the seizure duration decreased, particularly during the terminal parts (Fig. 3A, B, *n* = 26 clusters, *p* = 0.007, Wilcoxon signed-rank test, see Methods). In the second group of animals (*n* = 9), we analyzed seizure severity and spread. Changes in ISI were paralleled by increasing behavioral severity
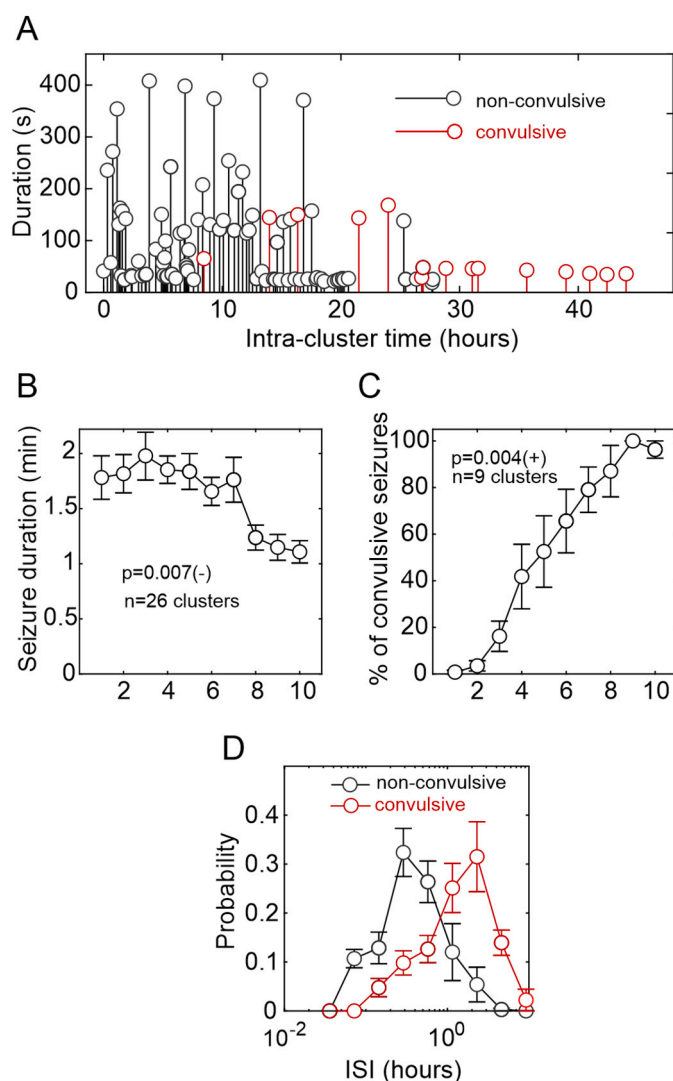
Fig. 3. Changes in seizure duration and severity during the clusters. (A) Stem plot demonstrating time-dependent changes in seizure severity and duration with cluster progression. The cluster starts with non-convulsive seizures of long duration. With cluster progression, the number of seizures with a convulsive component increases. The terminal parts are usually associated with Racine five seizures of short duration. (B) Population data demonstrate a decrease in seizure duration and an increase in seizure severity (C) throughout the course of the cluster. (D) Probability distribution of subsequent ISIs after non-convulsive and convulsive seizures. The distribution of ISIs after a convulsive seizure is shifted to the right, which indicates that severe seizures tend to be followed by longer ISIs.

of seizures, which was classified according to the Racine scale (Racine, 1972a). The cluster typically started with non-convulsive seizures (Racine 1–2) with a progressively increasing percentage of convulsive seizures (Racine 3–5) towards the end of the cluster (Fig. 3A,C; *n* = 9 clusters, *p* = 0.004, Wilcoxon signed-rank test, see Methods). Usually, the cluster terminated with multiple Racine stage 5 seizures. We then explored the relationship of seizure severity and subsequent ISI. The ISI probability distributions showed that non-convulsive seizures are followed by shorter ISIs (Fig. 3D). The mean duration of ISI was 0.53 ± 0.13 (0.39) hours after the non-convulsive seizures (*n* = 9 cluster ISI means) and 1.77 ± 0.18 (1.65) hours after convulsive ones (*n* = 9 cluster ISI means, *p* < 0.001, Wilcoxon signed-rank test).

The aggravation in behavioral seizure severity was associated with increased electrographic seizure spread. Since the seizures initiated in the hippocampal electrodes, similarly to other temporal lobe epilepsy

models (Bertram, 2009; Toyoda et al., 2013), the spatial spread of a seizure can be assessed using the power of the seizure EEG signal in the motor cortices (Fig. 4A,B). Convulsive seizures had higher signal power in the motor cortices compared to non-convulsive seizures ($n = 9$ cluster means, 0.13 ± 0.02 (0.13) mV^2 vs. 0.05 ± 0.00 (0.04) mV^2, $p < 0.001$, Wilcoxon rank-sum test). Temporal analysis showed that the power increases with the progression of the cluster (Fig. 5A,D; $n = 9$ clusters, $p = 0.004$, Wilcoxon signed-rank test, see Methods). In contrast, the hippocampal ictal signal power did not show any significant changes during the cluster course (Fig. 5C, $n = 9$ clusters, $p = 0.82$, Wilcoxon signed-rank test, see Methods).

The data suggest that with cluster progression, the cerebral network undergoes functional reorganization that facilitates the recruitment of extra-hippocampal structures and the spread of epileptiform activity outside the hippocampus. This suggestion is also supported by the analysis of interictal epileptiform discharges (IEDs). IEDs were generated in the hippocampus and motor cortex (Fig. 4C). IEDs in the motor cortices occurred both, in synchrony with, and independently of, hippocampal discharges, which points to the active involvement of the motor cortex in epileptiform activity. With cluster progression, the IED rate in the motor cortices significantly increased (Fig. 5B,F; $n = 9$ clusters, $p = 0.004$, Wilcoxon signed-rank test, see Methods), whereas in the hippocampi, no such trend was observed (Fig. 5 E; $n = 9$ clusters, $p = 0.359$, Wilcoxon signed-rank test, see Methods).

To assess whether convulsive seizures produce a more pronounced postictal depression, we computed signal power in 5-s periods after seizure offsets. The signal was high-pass filtered with a cut-off frequency
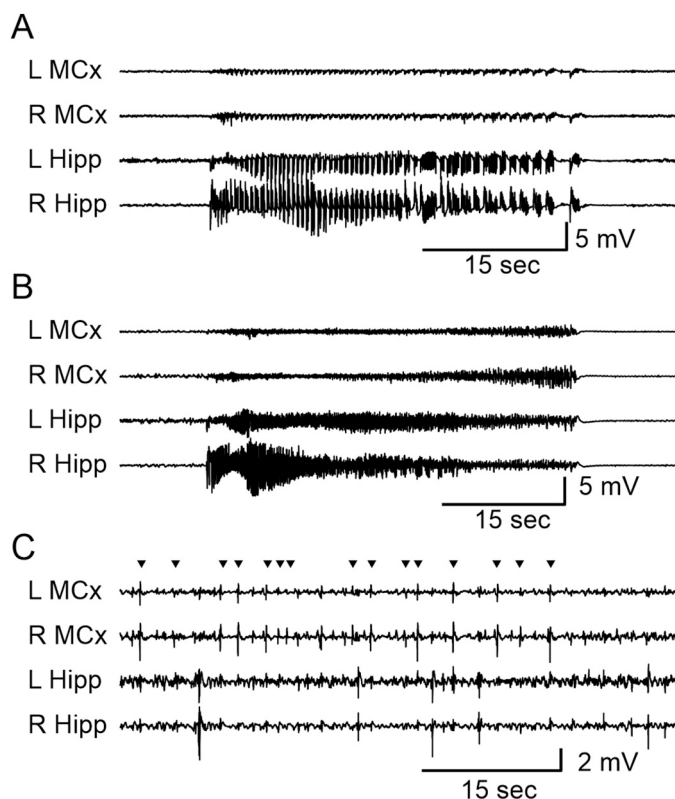
Fig. 4. Seizure spread and IEDs during the cluster. (A) An example of seizure activity recorded from the hippocampi (Hipp) and motor cortices (MCx) of both hemispheres during the early stages of the cluster. Note the low amplitude of the EEG signal in the motor cortex. (B) An example of a seizure during the terminal part of the cluster is characterized by enhanced involvement of motor cortices, which manifests as increased amplitude of ictal activity in each cortex. (C) Interictal recording during the late stages of the cluster. In the motor cortex, some IEDs are synchronous with the hippocampal ones whereas some are independent of the hippocampal activity (arrows).
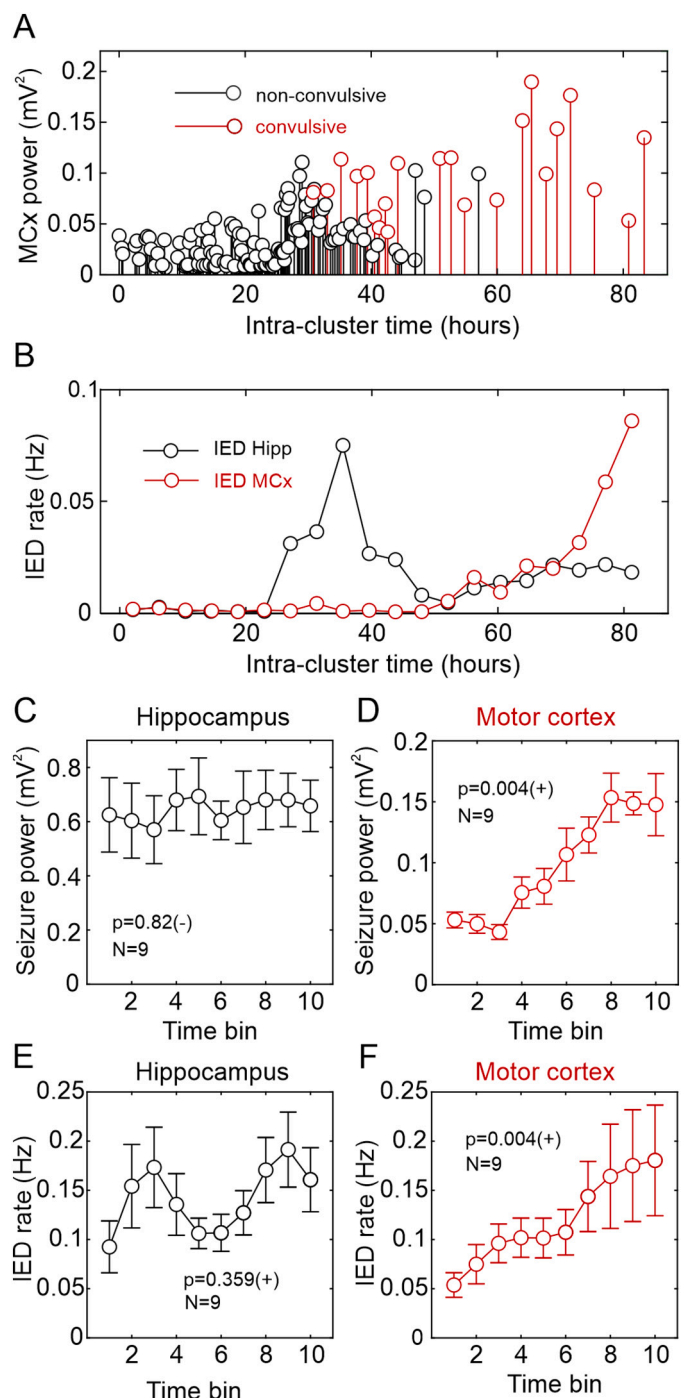
Fig. 5. Changes in seizure propagation and IED activity during the clusters. (A) Stem plot demonstrating the time-dependent evolution of the power of ictal discharge in the motor cortex (MCx) during the cluster. With cluster progression, the EEG signal power in the motor cortex and behavioral seizure severity increase, indicating enhanced seizure spread to extra-hippocampal structures. (B) An example of intra-cluster changes in the IED rate in the hippocampus and motor cortex. IED rate in the motor cortex increases with the approaching cluster termination. (C) Population analysis demonstrates that while the seizure power in the hippocampus did not change, it significantly increased in the motor cortex (D). (E) The IED rate did not change in the hippocampus. (F) The IED rate in the motor cortex progressively increased with cluster progression.

of 2 Hz prior to the power computation. Hippocampal and motor cortex channels were analyzed separately. In the hippocampus, postictal power was $0.016 \pm 0.004 \, (0.011) \, \text{mV}^2$ after non-convulsive seizures and $0.010 \pm 0.002 \, (0.009) \, \text{mV}^2$ after convulsive seizures ($n = 9$ cluster means, $p = 0.16$, Wilcoxon signed-rank test). In 6/9 clusters, the postictal signal power in the hippocampi was higher after non-convulsive seizures (Fig. 6A). In these clusters, we observed a decreasing trend of the hippocampal postictal power with intra-cluster time, which also dominates in the population data (Fig. 6B). In the motor cortex, signal power after non-convulsive seizures was $0.007 \pm 0.001 \, (0.006) \, \text{mV}^2$ while power after convulsive seizures was $0.008 \pm 0.002 \, (0.009) \, \text{mV}^2$ ($n = 9$ cluster means, $p = 0.57$, Wilcoxon signed-rank test). No changes in postictal power were observed with cluster progression (Fig. 6C).

4. Discussion

4.1. Long-term seizure dynamics

The growing body of evidence from experimental and clinical studies suggests that insights into long-term dynamics of seizures are critical for; 1) understanding the principles of ictogenesis, and 2) identification of the mechanisms that are driving the long-term fluctuations in seizure susceptibility. Long-term fluctuations in seizure probability or seizure clustering are present in both humans and animal models of chronic epilepsy, respectively. The period of fluctuations can range from a few days to weeks, months (Binnie et al., 1984; Balish et al., 1991; Bauer and Burr, 2001; Baud et al., 2018; Karoly et al., 2016; Maturana et al., 2020; Karoly et al., 2020) or even years (Griffiths and Fox, 1938). In humans, the analyses of seizure diaries demonstrate that seizure clustering is a common phenomenon (Milton et al., 1987; Balish et al., 1991; Tauboll et al., 1991; Bauer and Burr, 2001; Baud et al., 2018; Cook et al., 2014; Griffiths and Fox, 1938; Osorio et al., 2009; Fisher et al., 2015; Haut et al., 2005; Sillanpaa and Schmidt, 2008).

Recently, seizure-induced inhibition mechanism were explored in

Fig. 6. Impact of seizures on the post-ictal period. (A) Stem plot demonstrating the time-dependent evolution of the signal power of the post-ictal period in the hippocampus. In this cluster, note that a more prominent post-ictal suppression follows the convulsive seizures at the end of the cluster. (B) Time evolution of post-ictal power in the hippocampus and the cortex during the cluster (C).
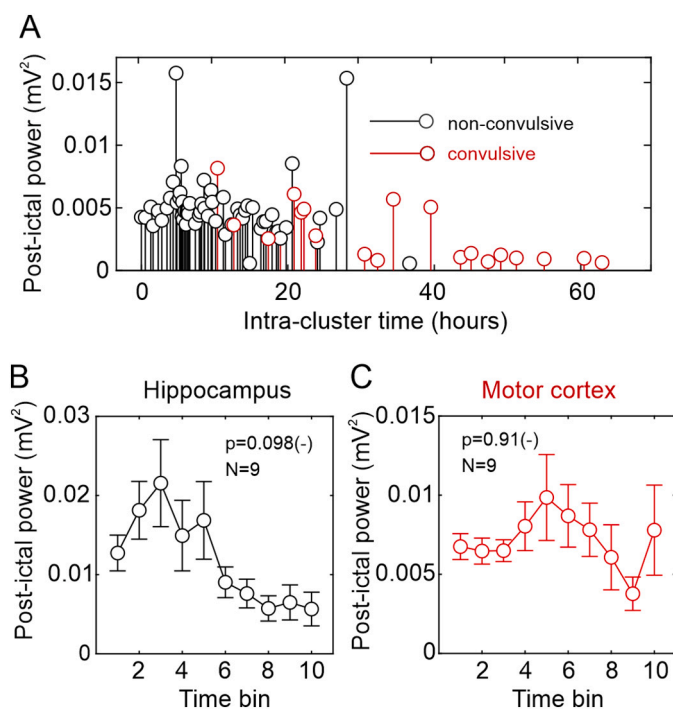
great detail using data from long-term intracranial recordings obtained from patients implanted with seizure prediction (Cook et al., 2013) or closed-loop stimulation devices (Baud et al., 2018). These recordings provided data about the real incidence of seizures, because a significant discrepancy exists between the number of electrographic seizures and number of seizures reported by patients (Cook et al., 2013). The analysis of detected electrographic seizures confirmed the existence of circadian and multidien cyclicity in seizure occurrence in nearly every patient. Also, the co-existence of multiple rhythms was identified, even in individual patients (Baud et al., 2018; Maturana et al., 2020). The subsequent studies showed that these rhythms could be tracked by analyzing biomarkers, such as interictal epileptiform activity or markers of dynamical stability derived from interictal EEG (Baud et al., 2018; Karoly et al., 2016; Maturana et al., 2020; Baud et al., 2019). Seizures preferentially occurred during specific (rising) phases of biomarker fluctuation and the combination of biomarker dynamics at multiple temporal scales was highly informative about the risk of seizure occurrence.

Long-term seizure fluctuations and clustering are also inherent to many chronic models of epilepsy in rodents. Seizure clustering is well documented in the pilocarpine (Arida et al., 1999; Bajorat et al., 2011; Cavalheiro et al., 1991; Goffin et al., 2007; Pitsch et al., 2017), kainic acid (Grabenstatter et al., 2005; Williams et al., 2009; Baud et al., 2019), hippocampal (Hawkins and Mellanby, 1987) and neocortical tetanus toxin models (Chang et al., 2018a), or in epilepsy induced by hypoxic-ischemic injury (Kadam et al., 2010). Seizures in dogs with naturally occurring epilepsy also tend to occur in clusters (Howbert et al., 2014; Gregg et al., 2020). Similar to human studies, the changes in seizure probability can be monitored. In the tetanus toxin model, the observed changes in brain stability were also indicative of the approaching period of seizure accumulation (Chang et al., 2018b).

4.2. Intra-cluster dynamics

In this study, we provide new data about cluster organization and how seizures themselves determine the long-term clustering dynamics. We propose that cluster evolution is an emergent phenomenon combining the well-known principles of kindling (Racine, 1972a; Goddard et al., 1969), the 'seizures-beget-seizures' theory, and the anti-seizure effect of generalized seizures (Mucha and Pinel, 1977; Handforth, 1982; Herberg and Watkins, 1966; Reisner, 2003; Fink, 1978). We showed that early parts of the cluster are characterized by the presence of non-convulsive seizures with short ISIs. The cluster progression is accompanied by increasing behavioral seizure severity, a gradual increase in the propagation of seizure activity and the involvement of extra-hippocampal regions. The progressive worsening of seizures and recruitment of extra-temporal structures into the epileptic activity are phenomena that were typically observed in the original kindling studies (Racine, 1972a; Goddard et al., 1969) and is in line with the 'seizures-beget-seizures' maxim. Note that the kindling studies showed that it was only the non-motor (focal) seizures that progressively decreased the seizure threshold (Stripling and Russell, 1989; Racine, 1972b).

On the contrary, the electrically induced seizures that were associated with a motor component (convulsive seizures, i.e. Racine 3–5) displayed an acute inhibitory effect on subsequent kindled seizures and increased the threshold for their induction (Mucha and Pinel, 1977; Herberg and Watkins, 1966). Interestingly, the inhibition lasted from one to two hours, which is similar to the ISI duration observed during the later parts of seizure clusters in our study. The inhibitory effect of generalized seizures was also demonstrated in experiments with maximal electroshock applied during the kindling (Handforth, 1982) and in humans who underwent electroconvulsive therapy (ECT) for pharmacoresistant depression (Reisner, 2003; Fink, 1978; Shapira et al., 1996; Green, 1960; Krystal et al., 1998). Thus, the ISI prolongation, which we observed in the second half of the seizure cluster, could be attributed to convulsive seizures emerging as a consequence of initial

kindling by focal seizures.

Previous studies have shown that the effect of convulsive seizures is cumulative. In the kindling model, the induction of repeated convulsive seizures by application of maximal electroshocks increased the threshold for elicitation of afterdischarges and led to a refractory period lasting several days (Mucha and Pinel, 1977; Handforth, 1982). The observed time course of the increased threshold for seizure induction is in good agreement with the presence of multiple convulsive seizures at the terminal parts of the cluster, followed by a long inter-cluster period. Therefore, we propose that the cumulative effect of repeated convulsive seizures led to a gradually increasing ISI and ultimately, resulted in cluster termination followed by a prolonged period of low seizure susceptibility that determined the duration of the inter-cluster period. A similar phenomenon was observed on a shorter time scale, at the level of individual seizures. Several studies demonstrated that seizure termination is characterized by large-amplitude bursts with a long interval between individual bursts and a high level of spatial synchronization (Jiruska et al., 2013b; Jirsa et al., 2014). Boido et al. showed that the inter-burst interval was associated with the refractoriness to burst induction (Boido et al., 2014). Each refractory period was determined by inhibitory synaptic transmission and also by seizure-induced non-synaptic and intrinsic mechanisms. The authors proposed that the bursts with high-amplitude have the capacity to induce a stronger and longer refractory period and that seizure termination occurs due to the cumulative effect of burst-induced anti-seizure mechanisms.

4.3. Mechanisms of seizure-induced inhibition

Several candidate mechanisms could be responsible for the long-term inhibitory effect of generalized seizures. The mechanism of seizure-induced inhibition is likely to be the same as that which terminates the seizure (Loscher and Kohling, 2010). One promising mechanism is the release of endogenous opioids that have an anti-seizure effect. Opioids are released into the cerebrospinal fluid after maximal electroshock seizures. Interestingly, when the cerebrospinal fluid was transplanted to the brain of naive animals, it increased seizure threshold and this effect could be blocked by the application of naloxone (Kryzhanovsky et al., 1989; Shandra et al., 1994).

Another promising neuromodulator with a long-term effect is neuropeptide Y (NPY). NPY targets 5 classes of receptors (Y1–Y5). In the hippocampus, the most abundant is Y2, which reduces excitation (Lado and Moshe, 2008). NPY was shown to inhibit electrically elicited seizures in rats (Woldbye et al., 1996) and coexpression of NPY with Y2 receptor was shown to decrease seizure frequency in epileptic rats (Melin et al., 2019). NPY expression is enhanced by recurrent seizures in various brain areas. Following kainate-induced status epilepticus, the NPY overexpression is maximal after 6–12 h, depending on the brain region. The NPY system is believed to represent another seizure-limiting factor (Loscher and Kohling, 2010; Lado and Moshe, 2008; Vezzani and Sperk, 2004) and could possibly also contribute to the prolongation of inter-seizure interval with seizure cluster progression and finally, cluster arrest. Another candidate mechanism of long-term inhibition is changes in the neurotransmitter receptor expression, for example, acetylcholine, GABA, or norepinephrin receptors (McNamara et al., 1980).

5. Conclusions

Deeper knowledge about long-term seizure dynamics and the driving factors will significantly contribute to our understanding of the complex mechanisms behind seizure generation. In this work, we suggested that fluctuations in seizure incidence are caused by the seizures themselves. Focal, non-convulsive, seizures at the beginning of the cluster act via positive feedback, contribute to cluster progression and aggravation of successive seizure activity. The subsequent occurrence of convulsive seizures has a negative feedback effect by progressively decreasing seizure rate and shifting the dynamics towards cluster termination,

followed by a long seizure-free period. Understanding the impact of seizures on long-term brain dynamics is an important prerequisite for improving seizure forecasting (Tauboll et al., 1991; Sunderam et al., 2007; Karoly et al., 2016), a research field, fortunately, experiencing a renaissance. Ultimately, identifying the key mechanisms responsible for seizure probability fluctuation and cluster termination is highly relevant for the development of more effective anti-seizure therapy (Loscher and Kohling, 2010).

References

Arida, R.M., Scorza, F.A., Peres, C.A., Cavalheiro, E.A., 1999. The course of untreated seizures in the pilocarpine model of epilepsy. Epilepsy Res. 34, 99–107.
Bajorat, R., Wilde, M., Sellmann, T., Kirschstein, T., Kohling, R., 2011. Seizure frequency in pilocarpine-treated rats is independent of circadian rhythm. Epilepsia 52, e118–e122.
Balish, M., Albert, P.S., Theodore, W.H., 1991. Seizure frequency in intractable partial epilepsy: a statistical analysis. Epilepsia 32, 642–649.
Baud, M.O., et al., 2018. Multi-day rhythms modulate seizure risk in epilepsy. Nat. Commun. 9, 88.
Baud, M.O., Ghestem, A., Benoliel, J.J., Becker, C., Bernard, C., 2019. Endogenous multidien rhythm of epilepsy in rats. Exp. Neurol. 315, 82–87.
Bauer, J., Burr, W., 2001. Course of chronic focal epilepsy resistant to anticonvulsant treatment. Seizure 10, 239–246.
Bertram, E.H., 2009. Temporal lobe epilepsy: where do the seizures really begin? Epilepsy Behav. 14 (Suppl. 1), 32–37.
Binnie, C.D., et al., 1984. Temporal characteristics of seizures and epileptiform discharges. Electroencephalogr. Clin. Neurophysiol. 58, 498–505.
Blauwblomme, T., Jiruska, P., Huberfeld, G., 2014. Mechanisms of ictogenesis. Int. Rev. Neurobiol. 114, 155–185.
Boido, D., Gnatkovsky, V., Uva, L., Francione, S., de Curtis, M., 2014. Simultaneous enhancement of excitation and postburst inhibition at the end of focal seizures. Ann. Neurol. 76, 826–836.
Cavalheiro, E.A., et al., 1991. Long-term effects of pilocarpine in rats: structural damage of the brain triggers kindling and spontaneous recurrent seizures. Epilepsia 32, 778–782.
Chang, B.L., et al., 2018a. Semiology, clustering, periodicity and natural history of seizures in an experimental occipital cortical epilepsy model. Dis. Model. Mech. 11.
Chang, W.C., et al., 2018b. Loss of neuronal network resilience precedes seizures and determines the ictogenic nature of interictal synaptic perturbations. Nat. Neurosci. 21, 1742–1752.
Cook, M.J., et al., 2013. Prediction of seizure likelihood with a long-term, implanted seizure advisory system in patients with drug-resistant epilepsy: a first-in-man study. Lancet Neurol. 12, 563–571.
Cook, M.J., et al., 2014. The dynamics of the epileptic brain reveal long-memory processes. Front. Neurol. 5, 217.

7

Fink, M., 1978. Efficacy and safety of induced seizures (EST) in man. Compr. Psychiatry 19, 1–18.

Fisher, R.S., et al., 2000. The impact of epilepsy from the patient's perspective I. Descriptions and subjective perceptions. Epilepsy Res. 41, 39–51.

Fisher, R.S., Bartfeld, E., Cramer, J.A., 2015. Use of an online epilepsy diary to characterize repetitive seizures. Epilepsy Behav. 47, 66–71.

Goddard, G.V., McIntyre, D.C., Leech, C.K., 1969. A permanent change in brain function resulting from daily electrical stimulation. Exp. Neurol. 25, 295–330.

Goffin, K., Nissinen, J., Van Laere, K., Pitkanen, A., 2007. Cyclicity of spontaneous recurrent seizures in pilocarpine model of temporal lobe epilepsy in rat. Exp. Neurol. 205, 501–505.

Grabenstatter, H.L., Ferraro, D.J., Williams, P.A., Chapman, P.L., Dudek, F.E., 2005. Use of chronic epilepsy models in antiepileptic drug discovery: the effect of topiramate on spontaneous motor seizures in rats with kainate-induced epilepsy. Epilepsia 46, 8–14.

Green, M.A., 1960. Relation between threshold and duration of seizures and electrographic change during convulsive therapy. J. Nerv. Ment. Dis. 131, 117–120.

Gregg, N.M., et al., 2020. Circadian and multiday seizure periodicities, and seizure clusters in canine epilepsy. Brain Commun. 2, fcaa008.

Griffiths, G., Fox, J.T., 1938. Rhythm in epilepsy. Lancet 232, 409–416.

Handforth, A., 1982. Postseizure inhibition of kindled seizures by electroconvulsive shock. Exp. Neurol. 78, 483–491.

Haut, S.R., 2006. Seizure clustering. Epilepsy Behav. 8, 50–55.

Haut, S.R., Lipton, R.B., LeValley, A.J., Hall, C.B., Shinnar, S., 2005. Identifying seizure clusters in patients with epilepsy. Neurology 65, 1313–1315.

Hawkins, C.A., Mellanby, J.H., 1987. Limbic epilepsy induced by tetanus toxin: a longitudinal electroencephalographic study. Epilepsia 28, 431–444.

Herberg, L.J., Watkins, P.J., 1966. Epileptiform seizures induced by hypothalamic stimulation in the rat: resistance to fits following fits. Nature 209, 515.

Herzog, A.G., et al., 2004. Frequency of catamenial seizure exacerbation in women with localization-related epilepsy. Ann. Neurol. 56, 431–434.

Howbert, J.J., et al., 2014. Forecasting seizures in dogs with naturally occurring epilepsy. PLoS One 9, e81920.

Janca, R., et al., 2015. Detection of interictal epileptiform discharges using signal envelope distribution modelling: application to epileptic and non-epileptic intracranial recordings. Brain Topogr. 28, 172–183.

Jirsa, V.K., Stacey, W.C., Quilichini, P.P., Ivanov, A.I., Bernard, C., 2014. On the nature of seizure dynamics. Brain 137, 2210–2230.

Jiruska, P., et al., 2013a. Dentate gyrus progenitor cell proliferation after the onset of spontaneous seizures in the tetanus toxin model of temporal lobe epilepsy. Neurobiol. Dis. 54, 492–498.

Jiruska, P., de Curtis, M., Jefferys, J.G., Schevon, C.A., Schiff, S.J., Schindler, K., 2013b. Synchronization and desynchronization in epilepsy: controversies and hypotheses. J. Physiol. 591, 787–797.

Kadam, S.D., White, A.M., Staley, K.J., Dudek, F.E., 2010. Continuous electroencephalographic monitoring with radio-telemetry in a rat model of perinatal hypoxia–ischemia reveals progressive post-stroke epilepsy. J. Neurosci. 30, 404–415.

Karoly, P.J., et al., 2016. Interictal spikes and epileptic seizures: their relationship and underlying rhythmicity. Brain 139, 1066–1078.

Karoly, P.J., et al., 2020. Forecasting cycles of seizure likelihood. Epilepsia 61, 776–786.

Krystal, A.D., Coffey, C.E., Weiner, R.D., Holsinger, T., 1998. Changes in seizure threshold over the course of electroconvulsive therapy affect therapeutic response and are detected by ictal EEG ratings. J. Neuropsychiatr. Clin. Neurosci. 10, 178–186.

Kryzhanovsky, G.N., Shandra, A.A., Godlevsky, L.S., Karganov, M.Y., 1989. Antiepileptic properties of cerebrospinal fluid after activation of the antiepileptic system of the brain. Epilepsia 30, 631–635.

Lado, F.A., Moshe, S.L., 2008. How do seizures stop? Epilepsia 49, 1651–1664.

Loscher, W., Kohling, R., 2010. Functional, metabolic, and synaptic changes after seizures as potential targets for antiepileptic therapy. Epilepsy Behav. 19, 105–113.

Maturana, M.I., et al., 2020. Critical slowing down as a biomarker for seizure susceptibility. Nat. Commun. 11, 2172.

Mazzuferi, M., Kumar, G., Rospo, C., Kaminski, R.M., 2012. Rapid epileptogenesis in the mouse pilocarpine model: video-EEG, pharmacokinetic and histopathological characterization. Exp. Neurol. 238, 156–167.

McNamara, J.O., Byrne, M.C., Dasheiff, R.M., Fitz, J.G., 1980. The kindling model of epilepsy: a review. Prog. Neurobiol. 15, 139–159.

Melin, E., et al., 2019. Disease modification by combinatorial single vector gene therapy: a preclinical translational study in epilepsy. Mol. Ther. Methods Clin. Dev. 15, 179–193.

Milton, J.G., Gotman, J., Remillard, G.M., Andermann, F., 1987. Timing of seizure recurrence in adult epileptic patients: a statistical analysis. Epilepsia 28, 471–478.

Mucha, R.F., Pinel, P.J., 1977. Postseizure inhibition of kindled seizures. Exp. Neurol. 54, 266–282.

Osorio, I., Frei, M.G., Sornette, D., Milton, J., 2009. Pharmaco-resistant seizures: self-triggering capacity, scale-free properties and predictability? Eur. J. Neurosci. 30, 1554–1558.

Paxinos, G., Watson, C., 1998. The Rat Brain in Stereotaxic Coordinates. Academic Press, Inc., San Diego, California 92101-4495, USA (pp. 474).

Pitsch, J., et al., 2017. Circadian clustering of spontaneous epileptic seizures emerges after pilocarpine-induced status epilepticus. Epilepsia 58, 1159–1171.

Racine, R.J., 1972a. Modification of seizure activity by electrical stimulation. II. Motor seizure. Electroencephalogr. Clin. Neurophysiol. 32, 281–294.

Racine, R.J., 1972b. Modification of seizure activity by electrical stimulation. I. After-discharge threshold. Electroencephalogr. Clin. Neurophysiol. 32, 269–279.

Reisner, A.D., 2003. The electroconvulsive therapy controversy: evidence and ethics. Neuropsychol. Rev. 13, 199–219.

Schiff, S.J., et al., 2000. Brain chirps: spectrographic signatures of epileptic seizures. Clin. Neurophysiol. 111, 953–958.

Shandra, A.A., et al., 1994. On the mechanism of antiepileptic peptides appearance in the cerebrospinal fluid. Brain Res. Bull. 35, 285–287.

Shapira, B., Lidsky, D., Gorfine, M., Lerer, B., 1996. Electroconvulsive therapy and resistant depression: clinical implications of seizure threshold. J. Clin. Psychiatry 57, 32–38.

Sillanpaa, M., Schmidt, D., 2008. Seizure clustering during drug treatment affects seizure outcome and mortality of childhood-onset epilepsy. Brain 131, 938–944.

Stripling, J.S., Russell, R.D., 1989. Twenty-four-hour post-seizure inhibition during limbic kindling requires seizure generalization. Neurosci. Lett. 99, 208–213.

Sunderam, S., Osorio, I., Frei, M.G., 2007. Epileptic seizures are temporally interdependent under certain conditions. Epilepsy Res. 76, 77–84.

Tauboll, E., Lundervold, A., Gjerstad, L., 1991. Temporal distribution of seizures in epilepsy. Epilepsy Res. 8, 153–165.

Toyoda, I., Bower, M.R., Leyva, F., Buckmaster, P.S., 2013. Early activation of ventral hippocampus and subiculum during spontaneous seizures in a rat model of temporal lobe epilepsy. J. Neurosci. 33, 11100–11115.

Vezzani, A., Sperk, G., 2004. Overexpression of NPY and Y2 receptors in epileptic brain tissue: an endogenous neuroprotective mechanism in temporal lobe epilepsy? Neuropeptides 38, 245–252.

Williams, P.A., et al., 2009. Development of spontaneous recurrent seizures after kainate-induced status epilepticus. J. Neurosci. 29, 2103–2112.

Woldbye, D.P., Madsen, T.M., Larsen, P.J., Mikkelsen, J.D., Bolwig, T.G., 1996. Neuropeptide Y inhibits hippocampal seizures and wet dog shakes. Brain Res. 737, 162–168.

9 Dissociation between the epileptogenic lesion and primary seizure onset zone in the tetanus toxin model of temporal lobe epilepsy

9.1 The contributions toward the progress of the field

This study provides important insights into the complex network organization of temporal lobe epilepsy (TLE) and the roles of different limbic structures in seizure initiation and propagation. By utilizing a non-lesional TLE model induced by tetanus toxin injection into the dorsal hippocampus, the authors were able to investigate the seizure onset and limbic structure recruitment without the confounding effects of widespread limbic damage seen in conventional TLE models. The findings reveal that seizures can initiate in any limbic structure, with a surprisingly high incidence of seizure onset in the ipsilateral and contralateral ventral hippocampi, despite the primary epileptogenic lesion being in the dorsal hippocampus.

9.2 The author's contributions

The author was involved in experimental work, performed part of the data analysis and contributed to the discussion and manuscript writing.

9.3 Compliance with the thesis objectives

HYP onset seizures are associated with discharge and high-frequency activity. The study suggests that HFOs may not always be localized to the primary epileptogenic lesion and can be generated by distant, interconnected limbic structures due to complex network interactions demonstrated in TLE. This has implications for the interpretation and clinical utility of HFOs in identifying the seizure onset zone. The ventral hippocampus was found to be the most common seizure onset zone, despite the primary lesion being elsewhere. The ventral hippocampus's increased excitability and susceptibility to disinhibition could make it a primary generator of HFOs in TLE.

Dissociation between the epileptogenic lesion and primary seizure onset zone in the tetanus toxin model of temporal lobe epilepsy

Jan Chvojka[1,2] (ORCID: 0000-0002-7957-858X), Jan Kudlacek[1] (ORCID: 0000-0001-5597-8709), Karolina Liska[1] (ORCID: 0000-0002-7228-6656), Aakash Pant[1] (ORCID: 0000-0002-9858-1186), John G.R. Jefferys[1] (ORCID: 0000-0003-0106-4412), Premysl Jiruska (ORCID: 0000-0003-4955-8577)[1]

Author affiliations:

1   Department of Physiology, Second Faculty of Medicine, Charles University, Prague, 15006, Czech Republic

2   Department of Circuit Theory, Faculty of Electrical Engineering, Czech Technical University in Prague, Prague, Czech Republic

Running title: Seizure onset in non-lesional TLE model

Keywords: temporal lobe epilepsy, hippocampus, entorhinal cortex, seizure onset, neural networks

Correspondence to:

Prof. Premysl Jiruska, M.D., Ph.D.

Department of Physiology

Second Faculty of Medicine

Charles University

Plzenska 311, Prague 5

CZ-15006, Czech Republic

Tel: +420257296202

Summary

Despite extensive temporal lobe epilepsy (TLE) research, understanding the specific limbic structures' roles in seizures remains limited. This weakness can be attributed to the complex nature of TLE and the existence of various TLE subsyndromes, including non-lesional TLE. Conventional TLE models like kainate and pilocarpine hinder precise assessment of the role of individual limbic structures in TLE ictogenesis due to widespread limbic damage induced by the initial status epilepticus. In this study, we used a non-lesional TLE model characterized by the absence of initial status and cell damage to determine the spatiotemporal profile of seizure initiation and limbic structure recruitment in TLE. Epilepsy was induced by injecting a minute dose of tetanus toxin into the right dorsal hippocampus in seven animals. Following injection, animals were implanted with bipolar recording electrodes in the amygdala, dorsal hippocampus, ventral hippocampus, piriform, perirhinal, and entorhinal cortices of both hemispheres. The animals were video-EEG monitored for four weeks. In total, 140 seizures (20 seizures per animal) were analyzed. The average duration of each seizure was 53.2±3.9 s. Seizure could initiate in any limbic structure. Most seizures initiated in the ipsilateral (41 %) and contralateral (18 %) ventral hippocampi. These two structures displayed a significantly higher probability of seizure initiation than by chance. The involvement of limbic structures in seizure initiation varied between individual animals. Surprisingly, only 7 % of seizures initiated in the injected dorsal hippocampus. The limbic structure recruitment into the seizure activity wasn't random and displayed consistent patterns of early recruitment of hippocampi and entorhinal cortices. Although ventral hippocampus represented the primary seizure onset zone, the study demonstrated the involvement of multiple limbic structures in seizure initiation in a non-lesional TLE model. The study also revealed the dichotomy between the primary epileptogenic lesion and main seizure onset zones and points to the central role of ventral hippocampi in temporal lobe ictogenesis.

Introduction

Epilepsy represents a cerebral network disorder where seizures emerge from complex interactions between the components of the epileptic network rather than from one specific brain region [1,2]. In temporal lobe epilepsy (TLE), the limbic structures and their connections with other brain areas represent the crucial components of the abnormal epileptic networks. The large interconnectivity of limbic structures plays a crucial role in physiological

functions, and limbic connectivity alterations represent a structural substrate contributing to high epileptogenicity and ictogenicity of the limbic system [3]. In TLE, the multiple limbic structures of both hemispheres become involved in the genesis of interictal and ictal activity. TLE is classified into various subsydromes in humans according to the level of involvement of individual limbic structures that also determine the outcome of epilepsy surgery [4,5]. The hippocampus is the most prominent limbic structure involved in TLE, and hippocampal sclerosis is one of the most common epileptogenic lesions and the most common source of seizures in TLE [6]. Seizure onsets can occur in entorhinal cortex, amygdala, or piriform cortex but less frequently than in the hippocampus [5]. The degree of involvement of individual limbic structures varies between patients but also within individuals. Human and animal studies demonstrate that multiple limbic structures can be involved in seizure genesis in the same patient or animals, and seizure onset can change in the long term [1, 7-9]. The high seizure onset variability explains why epilepsy surgery fails to provide seizure freedom in a significant proportion of patients with temporal lobe epilepsy. Non-lesional TLE is the most challenging form of TLE from the clinical perspective [10]. The absence of epileptogenic lesions in MRI (hippocampal or mesiotemporal lobe sclerosis, low-grade tumor) prevents the non-invasive identification of the plausible seizure onset zone. Therefore, patients with non-lesional TLE often undergo invasive exploration with intracranial electrodes to map the epileptic network and identify the most epileptogenic structures [11]. Despite advances in presurgical diagnostics, the success rate of post-surgical freedom remains less than optimal [10]. Experimental knowledge on the organization of TLE networks and the pathophysiology of TLE was obtained mainly from the status epilepticus models induced by pilocarpine or kainic acid models [12-17]. It is well documented that prolonged status epilepticus causes severe structural damage (cell loss, axonal sprouting, gliosis) affecting multiple limbic structures [13-16]. Multisite damage represents one of the disparities between human TLE and animal models and hinders the precise evaluation of individual limbic structure contributions to the TLE network [18].

The experimental model of non-lesional TLE induced by intrahippocampal injection of a minute dose of tetanus toxin (TeNT) is characterized by the absence of initial status epilepticus and the absence of severe cell loss or hippocampal sclerosis [19,20]. In this study, we took advantage of the unique nature of the TeNT model to explore the network organization and role of limbic structures in TLE ictogenesis. The results demonstrate that seizure can initiate in multiple limbic structures despite a localized epileptogenic lesion in the

dorsal hippocampus. Surprisingly, the most common seizure onset zones were the ipsilateral and contralateral ventral hippocampi, while the injected dorsal hippocampus played a minimal role in seizure initiation. Similarly to humans, the seizure onset varied between animals with various degrees of involvement of individual limbic structures in seizure genesis. The observed dichotomy between the primary lesion and principal seizure onset zone could be attributed to the ventral hippocampus's high endogenous epileptogenic potential and interconnectivity that may predispose the ventral hippocampus to generate seizures in response to distant lesions [21-24].

Materials and methods

TLE induction and electrode implantation

Seven adult male Wistar rats 250 – 400 g underwent implantation of multiple electrodes across the limbic structures, followed by long-term video-EEG monitoring. All experiments were performed under the Animal Care and Animal Protection Law of the Czech Republic, fully compatible with the European Union directive 2010/63/EU guidelines. The protocol was approved by the Ethics Committees of the Second Faculty of Medicine (Project Licence No. MSMT-31765/2019-4). Animals were housed in groups under standard and enriched conditions in a room with a controlled temperature (22 ± 1°C) and a 12/12 h light/dark cycle in open cages, enabling all but physical interaction.

Animals were anesthetized using 5% isoflurane in a plexiglass chamber. Then, the rat was fixed in the stereotaxic apparatus, and the anesthesia was maintained by 2.5% isoflurane, slowly decreasing to 1.5%. TLE was induced by injection of 10 ng of tetanus toxin (Quadratech Diagnostic Ltd, Epsom, UK, No #190A) to the right CA3 region of dorsal hippocampus at the coordinates AP -4.1 mm, L 3.9 mm from bregma and D 4.2 mm from the skull surface. Recording electrodes were implanted in the key structures of the limbic system using stereotaxic atlas [25], according to Table 1. Four animals had implanted additional electrodes in the dorsal hippocampal CA3 and subiculum, which were, however, not analyzed in this study (marked by gray shading in the table).

EEG recording and analysis

Following a 5-day recovery period, the animals were subjected to video-EEG monitoring for at least three weeks. Two different recording setups were used. The Neuralynx setup consisted of a headstage unity-gain amplifier HS-27 (Neuralynx, Bozeman, Montana, USA) and a Lynx-8 amplifier (Neuralynx, Bozeman, Montana, USA) set to a gain of 196, high-pass filter at 0.1 Hz and a low-pass filter at 3 kHz. The signal was then digitized using a Power 1401 analogue-digital converter (Cambridge Electronic Design, Cambridge, UK) at the sampling frequency of 10 kHz and 16-bit resolution and recorded to a computer using Spike2 software (Cambridge Electronic Design, Cambridge, UK). The synchronized video was recorded by Spike2 using a USB webcam. Signals recorded using the Intan setup were amplified, analog-filtered, and digitized by an RHD2132 headstage board (Intan Technologies, Los Angeles, California, USA). The digitized signals were transferred via swivel using the SPI bus to the RHD2000 evaluation board, which was connected to a computer via USB. The analog high-pass filter was set to 0.1 Hz and the low-pass filter to 1.7 kHz. The sampling frequency was 5 kHz, and the resolution was 16 bit. Custom-made software was used for EEG recording. The synchronized video was recorded using a USB camera.

Seizure onset detection and recruitment analysis

From each of the eight animals, we have chosen their first 20 seizures lasting > 10 s for detailed evaluation of electrographic seizure onset times. Seizures and seizure onsets were visually identified in each electrode using custom-written Matlab scripts (Mathworks Inc., USA). Seizure onset was defined as the earliest appearance of a persistent and profound change in EEG background activity that developed into clear ongoing seizure activity. Electrode with the earliest signal change was marked as a seizure onset (initiation) zone. The timing of seizure onset in each electrode was used to estimate the time delays of seizure propagation and limbic structure recruitment pattern. Seizure onsets time generated a 12x20 matrix (12 structures x 20 seizure onsets) from which propagation time delays and limbic structure recruitment plots were generated. We computed the "recruitment pathway" for each seizure onset as a vector of limbic structure ranking according to observed recruitment delays. Recruitment pathways were then compared to random pathways to assess significance.

Statistical analysis

Unless otherwise stated, all results and graphs are shown as mean ± s.e.m (median). All tests used level $\alpha = 0.05$ to determine the statistical significance. No data points were excluded. We did not implement any statistical approach to a priori define the sample size, but it corresponds to sample sizes that are generally used in this field of research.

Measured seizure onset frequencies were first compared to uniform frequencies using a one-way chi-square test, followed by an analysis of confidence intervals.

The PERMANOVA method of 10,000 iterations was used in the recruitment analysis to determine the statistical significance of dissimilarity between observed and random recruitment pathways. The dissimilarity was evaluated utilizing Kendall's Tau rank correlation as the distance metric. Recorded data and analytical tools used in this study are available from the corresponding author upon request.

Results

TeNT epileptic syndrome

All seven animals developed an epileptic syndrome characterized by recurrent spontaneous seizures (Fig. 1A). Seizures were behaviourally accompanied by staring, loss of awareness, and facial automatisms (sniffing, chewing; Racine scale 1-2) [26]. The seizure could progress further into a convulsive phase accompanied by motor phenomena ranging from forelimb clonus to rearing and ictal falling (Racine scale 3-5). A substantial number of seizures were electrographic without any apparent change in the animal's behavior. Wet dog shakes often followed the seizure termination. During the period between seizures, interictal epileptiform discharges of various morphologies were present in recordings.

Seizure onset analysis

In total, 140 seizures from seven male rats were analyzed. The average duration of each seizure was 53.2±3.9 s. The seizure onset pattern was characterized as hypersynchronous in all seizures (Fig. 1B). It manifested by initial high-amplitude discharge (heralding spikes), often with superimposed high-frequency oscillations. Spatially, the initial discharge occurred simultaneously in multiple limbic structures. Low-frequency, high-amplitude periodic spikes

followed the heralding discharge. Using the onset of the heralding spike, we determined the seizure onset in each recorded limbic structure. The analysis of seizure onset and time delays between each limbic structure recruitment into ictal activity allowed us to determine the major seizure onset structures and pattern of seizure propagation in this model of temporal lobe epilepsy.

The results showed that the seizure onset structure was not stable, and seizures could initiate between five to seven limbic structures in each animal, although with various proportions of initiation (Fig. 2 and 3A). On average, 55 ± 3 (55) % of seizures were initiated in the limbic structures of the right hemisphere (ipsilaterally to TeNT injection), while 45 ± 3 (45) % of seizures originated in the contralateral (left) limbic structures. The ipsilateral ventral hippocampus was the main seizure onset structure, with 41 ± 5 (40) % of seizures initiated in this structure (Fig. 3B, C). The proportion of ipsilateral ventral hippocampal seizure onsets varied from 30% up to 60% across the animals (Fig. 3A). Contralateral ventral hippocampus was the second most common seizure onset structure 18 ± 3 (20) % and was above chance levels (Fig 3B). The other limbic structures did not cross the significance of the random initiation threshold (Fig 3B). Surprisingly, only 6 ± 1 (5) % of seizures started from the injected right dorsal hippocampus. Dorsal and ventral hippocampi generated 75 ± 4 (75) % of all seizures (Fig 3B, C).

Seizure propagation and limbic structure recruitment

Because of the statistically significant difference ($p<0.001$, one-way chi-square test), we then focused on seizure onset propagation patterns of seizures generated only in ventral hippocampi. The ictal propagation maps of the right ventral hippocampal seizures (n=63 seizures) suggested that the seizure propagation pattern is consistent in each animal (Fig. 4 A-F) and across animals (Fig. 4 H). We determined the average propagation delay for each limbic structure to quantify the propagation pattern. We then ranked the recruitment of each structure (Fig. 5A). Entorhinal cortices and hippocampal subregions demonstrated the earliest recruitment. The average delay from the right ventral hippocampus of the right and left entorhinal cortex was 17 ± 3 (9) ms and 31 ± 4 (19) ms, respectively. The contralateral ventral and dorsal hippocampi were recruited into the seizure activity with a time delay of 29 ± 4 (18) ms and 50 ± 6 (29) ms. Surprisingly, the amygdalar complex wasn't amongst the structures with the fast recruitment. The average time delay to the ipsilateral amygdala was 44 ± 7 (23) ms, and the time delay to the contralateral amygdala was 70 ± 10 (46) ms. The results

confirmed the existence of consistent propagation pathways and a consistent sequence of limbic structures' recruitment. To statistically evaluate this observation, we compared the observed recruitment pattern with surrogate data of random recruitment (Fig. 5 B-D). The analysis demonstrated statistically significant dissimilarity between propagation pathways of seizures originating from the right ventral hippocampus (PERMANOVA, pseudo-F test statistic of 2.84, p-value of 0.011) compared to random recruitment. Propagation patterns (Fig. 4 I-P), average propagation delays (Fig. 6A), and limbic structure recruitment sequence (Fig. 6 B-E) of left ventral hippocampal seizures (n=28 seizures) demonstrated that they also followed the consistent paths and recruitment sequences (PERMANOVA, pseudo-F test statistic of 2.87, p-value of 0.015) that mirrored recruitment patterns of the right ventral hippocampus. The average propagation delay to the left and right entorhinal cortex was 12 ± 2 (10) ms and 29 ± 8 (21) ms, respectively. The contralateral ventral and dorsal hippocampi were recruited into the seizure activity with a time delay of 26 ± 8 (15) ms and 34 ± 6 (27) ms (Fig. 6 A).

Discussion

Temporal lobe networks

One of the reasons behind the unsatisfactory results of TLE surgery is that the temporal lobe epileptic network can be spatially extensive, and critical components of the network can differ in each subsyndrome [1,5,27-30]. TLE networks involve multiple structures of the limbic system, ranging from the hippocampus to entorhinal and perirhinal cortices [5,31,32], the amygdala, contralateral hippocampus, cingulate gyrus, and thalamic nuclei [8,33]. Animal models and human case studies show that in TLE, the seizure can initiate in any limbic structure, even in the same animal or patient, and often, seizures can have a diffuse multi-regional onset [8,9,34,35]. Such a complex network organization explains why the current surgical treatment of TLE, targeting primarily the hippocampus, results in seizure freedom for some patients and why seizures persist even after hippocampus resection in a substantial patient population. Significantly improving the outcome of epilepsy surgery relies on a better understanding of limbic network organization in appropriate models of these TLE subsyndromes [5].

In this study, we took advantage of a unique feature of the TeNT model of non-lesional temporal lobe epilepsy to explore how spatially limited lesion (unilateral dorsal hippocampal TeNT injection) affects limbic network ictogenesis. The TeNT model is a reliable model of acquired non-lesional TLE, although genetic models of TLE epilepsy with mild or absent hippocampal damage were also reported [36]. Results showed that single-site TeNT injection leads to widespread limbic network dysfunction. In our study, the network dysfunction manifested by multisite seizure onset that varied across animals. Although the seizures could initiate in any explored limbic structure, the ipsilateral ventral hippocampus played the central role and represented the primary seizure onset zone [37,38]. Past studies that sampled only dorsal hippocampal subregions have already demonstrated widely distributed abnormal network activity in the TeNT model that was manifested mainly by bilateral interictal activity [35]. Interictal epileptiform discharges were generated in both hippocampi in all animals, and interictal discharge rates were higher in the contralateral hippocampus in 40% of animals. Up to 27% of seizures originated from the contralateral dorsal hippocampus [35].

The involvement of multiple structures in our model was probably attributed to the functional changes rather than structural changes and cell damage observed in status epilepticus models of TLE [14,39]. Tetanus toxin cleaves two proteins, VAMP-1 and VAMP-2, critical for synaptic transmission [40]. The area of VAMP cleavage is spatially limited to the ipsilateral dorsal hippocampus, leading to the complete absence of spontaneous and evoked inhibitory postsynaptic currents and a significant reduction in excitatory postsynaptic currents [41,42]. The altered synaptic transmission can cause local hippocampal disinhibition and induce disinhibition in distant interconnected structures of limbic circuitry. A decreased excitatory drive from the injected dorsal hippocampus can be associated with reduced feedforward inhibition in a targeted area (entorhinal cortex, contralateral hippocampus). Alternatively, dorsal hippocampal toxin injection may affect long-range inhibition provided by hippocampal interneurons projecting to remote limbic structures [43,44]. This mechanism would explain the presence of entorhinal disinhibition in the chronic epileptic entorhinal cortex that maintains the local inhibition intact [45]. In this scenario, disinhibited distant structures may become active, if not dominant, components of the epileptic network that will substantially contribute to seizure genesis [46,47]. The ventral hippocampus represents a limbic structure (see below) that may be highly susceptible to disinhibition and become the primary seizure-generating structure.

The observed dissociation between the primary molecular lesion (TeNT injection site) and the major seizure onset zone was unexpected. Our results support the central role of the ventral hippocampus in the pathogenesis of seizures of temporal lobe (limbic) origin. Functional and structural differences between dorsal and ventral hippocampus are well determined, as well as higher epileptogenicity of the ventral hippocampus [48]. Similarly to humans, the rodent hippocampus is divided into functionally distinct regions along its longitudinal axis [49,50]. The rodent ventral hippocampus is homologous to the human anterior hippocampus, the most common seizure initiation site in temporal lobe epilepsy patients [51-56]. Animal models of TLE corroborate this observed intrinsic difference in ictogenicity of ventral and dorsal hippocampal poles, but the underlying cause remains to be fully elucidated.

Ventral and dorsal hippocampus differ in their synaptic input and output and were shown to activate different networks when seizing [57]. The dorsal hippocampus receives polymodal sensory information from the cortex, whereas the ventral hippocampus is more linked to subcortical structures, such as the amygdala and hypothalamus [21]. The trisynaptic circuit of the hippocampus remains conserved along its longitudinal axis, but the circuitry exhibits quantitative differences [24,58,59]. Injection of TeNT or kainic acid into the ventral hippocampus generates a seizure phenotype that is analogous to TLE in humans [12,41,49,60]. In another widely used model of epilepsy using systemic pilocarpine injections, the subsequent seizures were also generated in the ventral hippocampus [9,61]. At a cellular level, CA1 pyramidal neurons in the ventral hippocampus are more depolarized and fire action potentials in response to significantly smaller current injections than dorsal hippocampal neurons [22]. Increased neuronal excitability could result from expression profile differences between the dorsal and ventral hippocampus. In particular, increased ventral hippocampal pyramidal neuron excitability likely relates to the differences in NMDA receptors[24], A-type and KCNQ potassium channels [22,33], different subunit composition of voltage-gated sodium channels [62], and differences in adenosine signaling [63]. An imbalance of excitatory and inhibitory neuron populations might also explain the overall changes in excitability. The loss of GABAergic ventral hippocampal interneurons correlates with the seizure frequency in a mouse model of epilepsy [64]. Similarly, in humans, TLE is associated with more significant cell loss and hippocampal sclerosis in the homologous anterior hippocampal region [13,65]. Experimentally, local pharmacological suppression of the ventral hippocampal neurons [61] or transplantation of inhibitory neurons [66] successfully reduced the seizure frequency in the systemic pilocarpine model. The ventral

hippocampus also plays a pivotal role in TLE with dual pathologies cases where hippocampal sclerosis is associated with focal cortical dysplasia. It is hypothesized that the highly epileptogenic focal cortical dysplasia recruits the susceptible ventral hippocampus, becoming the primary seizure onset zone [6].

Conclusions

This study reveals the complex nature of TLE networks, highlighting the dissociation between the primary lesion and seizure onset zone that, in our observations, manifested as an unexpectedly central role of the ventral hippocampi in seizure initiation. These findings emphasize the importance of understanding the functional differences between the dorsal and ventral hippocampus and the need for a deeper understanding of the limbic network's organization in different TLE subsyndromes.

Acknowledgements

Funding

Competing interests

The authors report no competing interests.

References

1.	Bertram EH. Temporal lobe epilepsy: where do the seizures really begin? Epilepsy & Behav 2009;14(Suppl 1):32-37.

2.	Jefferys JGR, Jiruska P, de Curtis M, Avoli M. Limbic Network Synchronization and Temporal Lobe Epilepsy. In: Jasper's Basic Mechanisms of the Epilepsies, Noebels JL, Avoli M, Rogawski MA, Olsen RW, Delgado-Escueta AV (Eds.), National Center for Biotechnology Information (US), 2012, Bethesda (MD).

3.	Sutula T, Cascino G, Cavazos J, Parada I, Ramirez L. Mossy fiber synaptic reorganization in the epileptic human temporal lobe. Ann Neurol 1989;26(3):321-330.

4.	Bonilha L, Martz GU, Glazier SS, Edwards JC. Subtypes of medial temporal lobe epilepsy: influence on temporal lobectomy outcomes? Epilepsia 2012;53(1):1-6.

5.	Thom M, Mathern GW, Cross JH, Bertram EH. Mesial temporal lobe epilepsy: How do we improve surgical outcome? Ann Neurol 2010;68(4):424-434.

6.	Blümcke I, Coras R, Miyata H, Ozkara C. Defining clinico-neuropathological subtypes of mesial temporal lobe epilepsy with hippocampal sclerosis. Brain Pathol 2012;22(3):402-411.

7.	Bertram EH. Why does surgery fail to cure limbic epilepsy? Epilepsy Res 2003;56(2-3):93-99.

8.	Bertram EH, Zhang DX, Mangan P, Fountain N, Rempe D. Functional anatomy of limbic epilepsy: a proposal for central synchronization of a diffusely hyperexcitable network. Epilepsy Res 1998;32(1-2):194-205.

9.	Toyoda I, Bower MR, Leyva F, Buckmaster PS. Early activation of ventral hippocampus and subiculum during spontaneous seizures in a rat model of temporal lobe epilepsy. Pol J Pharmacol Pharm 2013;33(27):11100-11115.

10.	Téllez-Zenteno JF, Hernández Ronquillo L, Moien-Afshari F, Wiebe S. Surgical outcomes in lesional and non-lesional epilepsy: a systematic review and meta-analysis. Epilepsy Res 2010;89(2-3):310-318.

11.	Barba C, Barbati G, Minotti L, Hoffmann D, Kahane P. Ictal clinical and scalp-EEG findings differentiating temporal lobe epilepsies from temporal 'plus' epilepsies. Brain 2007;130(Pt 7):1957-1967.

12.	Cavalheiro EA, Riche DA, Le Gal La Salle G. Long-term effects of intrahippocampal kainic acid injection in rats: a method for inducing spontaneous recurrent seizures. Electroencephalogr Clin Neurophysiol 1982;53(6):581-589.

13.	Ekstrand JJ, Pouliot W, Scheerlinck P, Dudek FE. Lithium pilocarpine-induced status epilepticus in postnatal day 20 rats results in greater neuronal injury in ventral versus dorsal hippocampus. Neuroscience 2011;192:699-707.

14.	Pitkanen A, Schwartzkroin PA, Moshe SL. Models of seizures and epilepsy. Academic Press Inc (London), 1st edition, 2006, London, England.

15. Turski L, Cavalheiro EA, Czuczwar SJ, Turski WA, Kleinrok Z. The seizures induced by pilocarpine: behavioral, electroencephalographic and neuropathological studies in rodents. Pol J Pharmacol Pharm 1987;39(5):545-555.

16. Turski WA, Cavalheiro EA, Schwarz M, Czuczwar SJ, Kleinrok Z, Turski L. Limbic seizures produced by pilocarpine in rats: behavioral, electroencephalographic and neuropathological study. Behav Brain Res 1983;9(3):315-335.

17. Williams PA, White AM, Clark S, Ferraro DJ, Swiercz W, Staley KJ, Dudek FE. Development of spontaneous recurrent seizures after kainate-induced status epilepticus. J Neurosci 2009;29(7):2103-2112.

18. Sloviter RS. The neurobiology of temporal lobe epilepsy: too much information, not enough knowledge. C R Biol 2005;328(2):143-153.

19. Jefferys JG, Evans BJ, Hughes SA, Williams SF. Neuropathology of the chronic epileptic syndrome induced by intrahippocampal tetanus toxin in rat: preservation of pyramidal cells and incidence of dark cells. Neuropathol Appl Neurobiol 1992;18(1):53-70.

20. Jiruska P, Shtaya ABY, Bodansky DMS, Chang WC, Gray WP, Jefferys JGR. Dentate gyrus progenitor cell proliferation after the onset of spontaneous seizures in the tetanus toxin model of temporal lobe epilepsy. Neurobiol Dis 2013;54:492-498.

21. Bannerman DM, Sprengel R, Sanderson DJ, McHugh SB, Rawlins JNP, Monyer H, Seeburg PH. Hippocampal synaptic plasticity, spatial memory and anxiety. Nat Rev Neurosci 2014;15(3):181-192.

22. Dougherty KA, Islam T, Johnston D. Intrinsic excitability of CA1 pyramidal neurones from the rat dorsal and ventral hippocampus. J Physiol 2012;590(22):5707-5722.

23. Dougherty KA, Nicholson DA, Diaz L, Buss EW, Neuman KM, Chetkovich DM, Johnston D. Differential expression of HCN subunits alters voltage-dependent gating of h-channels in CA1 pyramidal neurons from dorsal and ventral hippocampus. J Neurophysiol 2013;109(7):1940-1953.

24. Papatheodoropoulos C, Moschovos C, Kostopoulos G. Greater contribution of N-methyl-D-aspartic acid receptors in ventral compared to dorsal hippocampal slices in the expression and long-term maintenance of epileptiform activity. Neuroscience 2005;135(3):765-779.

25. Paxinos G, Watson C. The Rat Brain in Stereotaxic Coordinates. Elsevier, 6th edition, 2007.

26. Racine RJ. Modification of seizure activity by electrical stimulation. II. Motor seizure. Electroencephalog Clin Neurophysiol 1972;32(3):281-294.

27. Avanzini G, Manganotti P, Meletti S, Moshé SL, Panzica F, Wolf P, Capovilla G. The system epilepsies: a pathophysiological hypothesis. Epilepsia 2012;53(5):771-778.

28. Holmes MD, Dodrill CB, Ojemann GA, Wilensky AJ, Ojemann LM. Outcome following surgery in patients with bitemporal interictal epileptiform patterns. Neurology 1997;48(4):1037-1040.

29. Jiruska P, de Curtis M, Jefferys JGR. Modern concepts of focal epileptic networks. Int Rev Neurobiol 2014;114:1-7.

30. Reid AY, Staba RJ. Limbic networks: clinical perspective. Int Rev Neurobiol 2014;114:89-120.

31. Avoli M, D'Antuono M, Louvel J, Köhling R, Biagini G, Pumain R, D'Arcangelo G, Tancredi V. Network and pharmacological mechanisms leading to epileptiform synchronization in the limbic system in vitro. Prog Neurobiol 2002;68(3):167-207.

32. Barbarosie M, Avoli M. CA3-driven hippocampal-entorhinal loop controls rather than sustains in vitro limbic seizures. J Neurosci 1997;17(23):9308-9314.

33. Levesque M, Salami P, Behr C, Avoli M. Temporal lobe epileptiform activity following systemic administration of 4-aminopyridine in rats. Epilepsia 2013;54(4):596-604.

34. Finnerty GT, Jefferys JGR. Investigation of the neuronal aggregate generating seizures in the rat tetanus toxin model of epilepsy. J Neurophysiol 2002;88(6):2919-2927.

35. Jiruska P, Finnerty GT, Powell AD, Lofti N, Cmejla R, Jefferys JGR. Epileptic high-frequency network activity in a model of non-lesional temporal lobe epilepsy. Brain 2010;133(Pt 5):1380-1390.

36. King JT Jr, LaMotte CC. El mouse as a model of focal epilepsy: a review. Epilepsia. 1989;30(3):257-65.

37. Kahane P, Landré E, Minotti L, Francione S, Ryvlin P. The Bancaud and Talairach view on the epileptogenic zone: a working hypothesis. Epileptic Disord 2006;8(Suppl 2):S16-26.

38. Rosenow F, Lüders H. Presurgical evaluation of epilepsy. Brain 2001;124(Pt 9):1683-1700.

39. Pitkänen A, Engel Jr J. Past and present definitions of epileptogenesis and its biomarkers. Neurotherapeutics 2014;11(2):231-241.

40. Schiavo G, Rossetto O, Benfenati F, Poulain B, Montecucco C. Tetanus and botulinum neurotoxins are zinc proteases specific for components of the neuroexocytosis apparatus. Ann N Y Acad Sci 1994;710:65-75.

41. Ferecskó AS, Jiruska P, Foss L, Powell AD, Chang W-C, Sik A, Jefferys JGR. Structural and functional substrates of tetanus toxin in an animal model of temporal lobe epilepsy. Brain Struct Funct 2015;220(2):1013-1029.

42. Jefferys JG. Chronic epileptic foci in vitro in hippocampal slices from rats with the tetanus toxin epileptic syndrome. J Neurophysiol 1989;62(2):458-468.

43. Chrobak JJ, Buzsáki G. High-frequency oscillations in the output networks of the hippocampal-entorhinal axis of the freely behaving rat. J Neurosci 1996;16(9):3056-3066.

44. Urrutia-Piñones J, Morales-Moraga C, Sanguinetti-González N, Escobar AP, Chiu CQ. Long-Range GABAergic Projections of Cortical Origin in Brain Function. Front Syst Neurosci 2022;16:841869.

45. Fountain NB, Bear J, Bertram 3rd EH, Lothman EW. Responses of deep entorhinal cortex are epileptiform in an electrogenic rat model of chronic temporal lobe epilepsy. J Neurophysiol 1998;80(1):230-240.

46. Empson RM, Jefferys JG. Synaptic inhibition in primary and secondary chronic epileptic foci induced by intrahippocampal tetanus toxin in the rat. J Physiol 1993;465:595-614.

47. Najlerahim A, Williams SF, Pearson RC, Jefferys JG. Increased expression of GAD mRNA during the chronic epileptic syndrome due to intrahippocampal tetanus toxin. Exp Brain Res 1992;90(2):332-342.

48. Fanselow MS, Dong H-W. Are the dorsal and ventral hippocampus functionally distinct structures? Neuron 2010;65(1):7-19.

49. Mellanby J, George G, Robinson A, Thompson P. Epileptiform syndrome in rats produced by injecting tetanus toxin into the hippocampus. J Neurol Neurosurg Psychiatry 1977;40(4):404-414.

50. Moser MB, Moser EI. Functional differentiation in the hippocampus. Hippocampus 1998;8(6):608-619.

51. Masukawa LM, O'Connor WM, Lynott J, Burdette LJ, Uruno K, McGonigle P, O'Connor MJ. Longitudinal variation in cell density and mossy fiber reorganization in the dentate gyrus from temporal lobe epileptic patients. Brain Res 1995;678(1-2):65-75.

52. Quesney LF. Clinical and EEG features of complex partial seizures of temporal lobe origin. Epilepsia 1986;27(Suppl 2):S27-45.

53. So N, Gloor P, Quesney LF, Jones-Gotman M, Olivier A, Andermann F. Depth electrode investigations in patients with bitemporal epileptiform abnormalities. Ann Neurol 1989;25(5):423-431.

54. Spencer SS. Neural networks in human epilepsy: evidence of and implications for treatment. Epilepsia 2002;43(3):219-227.

55. Spencer SS, Spencer DD. Entorhinal-hippocampal interactions in medial temporal lobe epilepsy. Epilepsia 1994;35(4):721-727.

56. Wennberg R, Arruda F, Quesney LF, Olivier A. Preeminence of extrahippocampal structures in the generation of mesial temporal seizures: evidence from human depth electrode recordings. Epilepsia 2002;43(7):716-726.

57. Duffy BA, Choy M, Lee JH. Predicting Successful Generation and Inhibition of Seizure-like Afterdischarges and Mapping Their Seizure Networks Using fMRI. Cell Rep 2020;30(8):2540-2554.e4.

58. Pandis C, Sotiriou E, Kouvaras E, Asprodini E, Papatheodoropoulos C, Angelatou F. Differential expression of NMDA and AMPA receptor subunits in rat dorsal and ventral hippocampus. Neuroscience 2006;140(1):163-175.

59. Sotiriou E, Papatheodoropoulos C, Angelatou F. Differential expression of gamma-aminobutyric acid--a receptor subunits in rat dorsal and ventral hippocampus. J Neurosci Res 2005;82(5):690-700.

60. Jefferys JGR, Ashby-Lumsden A, Lovick TA. Cardiac effects of repeated focal seizures in rats induced by intrahippocampal tetanus toxin: Bradyarrhythmias, tachycardias, and prolonged interictal QT interval. Epilepsia 2020;61(4):798-809.

61.	Buckmaster PS, Reyes B, Kahn T, Wyeth M. Ventral hippocampal formation is the primary epileptogenic zone in a rat model of temporal lobe epilepsy. J Neurosci 2022;42(39):7482-7495.

62.	Cembrowski MS, Wang L, Sugino K, Shields BC, Spruston N. Hipposeq: a comprehensive RNA-seq database of gene expression in hippocampal principal neurons. Elife 2016;5:e14997.

63.	Moschovos C, Kostopoulos G, Papatheodoropoulos C. Endogenous adenosine induces NMDA receptor-independent persistent epileptiform discharges in dorsal and ventral hippocampus via activation of A2 receptors. Epilepsy Res 2012;100(1-2):157-167.

64.	Wyeth M, Nagendran M, Buckmaster PS. Ictal onset sites and γ-aminobutyric acidergic neuron loss in epileptic pilocarpine-treated rats. Epilepsia 2020;61:856-867.

65.	Babb TL, Brown WJ, Pretorius J, Davenport C, Lieb JP, Crandall PH. Temporal lobe volumetric cell densities in temporal lobe epilepsy. Epilepsia 1984;25(6):729-740.

66.	Hunt RF, Girskis KM, Rubenstein JL, Alvarez-Buylla A, Baraban SC. GABA progenitors grafted into the adult epileptic brain control seizures and abnormal behavior. Nat Neurosci 2013;16(6):692-697.

Table legend

Table 1. Stereotactic coordinates of the implanted limbic structures. Units are millimeters. Positive values are rostral from bregma, while negative values are caudal from bregma. AP – anterio-posterior.

Figure legends

Figure 1. Seizure and seizure onset analysis. (A) An example of a seizure in the tetanus toxin model induced by the dorsal hippocampal TeNT injection. Seizure activity rapidly propagates across the limbic structures of both hemispheres. The seizure initiation displays features of hypersynchronous onset characterized by the initial high-amplitude discharge (heralding spike), often with superimposed high-frequency activity. Seizure terminates synchronously over the wide areas of both hemispheres. (B) The detail of seizure onset. The initial high-amplitude (hypersynchronous) discharge rapidly spread into the limbic structures of both hemispheres. The red lines mark visually determined seizure onset in each electrode. This seizure was initiated in the ipsilateral (right) ventral hippocampus. (C) Seizure onset and early ictal propagation analysis. The lines connect the limbic structures where the seizure activity propagates from the seizure onset structure (ventral hippocampus). The color coding reflects the propagation time. In this case, the propagation to the ipsilateral entorhinal cortex and contralateral ventral hippocampus is reflected by the hot color of the line endings. On the contrary, the propagation of ictal activity to piriform cortices of both hemispheres is slow, resulting in their late recruitment into the seizure. The cold color of the line endings reflects long propagation time and late recruitment. (D) The overlay of all seizure onsets (n=20) from one animal. In this animal, 30 % of seizures were initiated in the right ventral hippocampus, 30% in the left ventral hippocampus, 20% in the left dorsal hippocampus, 5% in the left entorhinal cortex, 10% in the right (injected) dorsal hippocampus, and 5% from the left perirhinal cortex. The white-red color coding of the limbic structure lable identifies the proportion of seizures initiated from the specific limbic structure. L – left hemisphere, R – right hemisphere, Pir – piriform cortex, Amy – amygdala, Prh – perirhinal cortex, DHip – dorsal hippocampus, VHip – ventral hippocampus, Ent – entorhinal cortex. The graph also displays the most common patterns and time delay of seizure propagation (parula color coding).

Figure 2. Seizure onset analysis in each animal. (A-G) The proportion of limbic structures involved in seizure initiation and propagation varies across the animals. Ventral and dorsal hippocampi and entorhinal cortices of both hemispheres were the most common structures triggering seizures. (H) Overlay and propagation of all 140 seizures from all animals. L – left hemisphere, R – right hemisphere, Pir – piriform cortex, Amy – amygdala, Prh – perirhinal cortex, DHip – dorsal hippocampus, VHip – ventral hippocampus, Ent – entorhinal cortex.

Figure 3. Limbic structures involved in seizure initiation. (A) The matrix displays a fraction/proportion of seizures initiated in a specific limbic structure in each animal (individual column). The number and proportion of limbic structures triggering seizures varies across animals. All animals had multiple seizure onset sites, but the ipsilateral ventral hippocampus represented the main seizure onset zone in most animals. (B) The mean proportion of seizure-initiating structures. The number designates the rank, while the star marks structures where the seizure initiation is significantly ($p<0.001$, one-way chi-square test) above the uniform distribution (vertical dashed line). Seizures initiated mainly in the ipsilateral ventral hippocampus, followed by the contralateral ventral hippocampus. (C) Schematics of a rat brain with the proportion of the individual structure involvement in seizure initiation (perirhinal cortex not shown). Asterix marks the tetanus toxin injection to the right dorsal hippocampus. L – left hemisphere, R – right hemisphere, Pir – piriform cortex, Amy – amygdala, Prh – perirhinal cortex, DHip – dorsal hippocampus, VHip – ventral hippocampus, Ent – entorhinal cortex.

Figure 4. Analysis of seizure pathway propagation for seizures originating from the right ventral hippocampus. (A-G) Pathways and time delays of seizure propagation for seizures initiating in the right ventral hippocampus in each animal. (H) Overlay of the seizure propagation patterns for all seizures initiated in the ipsilateral (right) ventral hippocampus (n=63). Maps show the consistent seizure recruitment/propagation pattern in each animal and across animals. (I-O) Recruitment pattern for seizures initiating in the left ventral hippocampus in each animal and across the animals (P). L – left hemisphere, R – right hemisphere, Pir – piriform cortex, Amy – amygdala, Prh – perirhinal cortex, DHip – dorsal hippocampus, VHip – ventral hippocampus, Ent – entorhinal cortex

Figure 5. Seizure pathway propagation and structure recruitment for seizures initiating in the right ventral hippocampus. (A) Average time delays show the recruitment sequence for seizures initiating in the right ventral hippocampus. The numbers mark the rank of the recruited structure. (B) Map of structure recruitment for one seizure starting in the right

ventral hippocampus. The numbers and color coding mark the rank of the recruited structure. (C) Map of random recruitment. (D) Recruitment maps of all 63 seizures initiating the right ventral hippocampus demonstrate the presence of a recruitment pattern. (E) An equal number of randomly generated recruitment maps without any recruitment pattern. L – left hemisphere, R – right hemisphere, Pir – piriform cortex, Amy – amygdala, Prh – perirhinal cortex, DHip – dorsal hippocampus, VHip – ventral hippocampus, Ent – entorhinal cortex.

Figure 6. Seizure pathway propagation and structure recruitment for seizures initiating in the left ventral hippocampus. (A) Average time delays show the recruitment sequence for seizures beginning in the contralateral ventral hippocampus. The numbers denote the rank of the recruited structure. (B) Map of limbic structure recruitment for a seizure originating in the left ventral hippocampus. The numbers and color coding mark the rank of the recruited structure. (C) Map of a random recruitment. (D) Recruitment maps of all 28 seizures initiating the left ventral hippocampus demonstrate the existence of a recruitment pattern. (E) Maps of all 28 randomly generated limbic structures recruitment display the absence of any recruitment pattern. L – left hemisphere, R – right hemisphere, Pir – piriform cortex, Amy – amygdala, Prh – perirhinal cortex, DHip – dorsal hippocampus, VHip – ventral hippocampus, Ent – entorhinal cortex.

Tables

Table 1.

Brain structure	AP	Lateral	Depth
Piriform cortex	0.2	4.2	8.2
Amygdala	-2.8	4.8	8.6
Perirhinal cortex	-2.8	6.2	7.4
Dorsal dentate gyrus	-4.6	2.6	3.3
Ventral hippocampus	-5.5	4.8	7.1
Entorhinal cortex	-8.0	5.0	7.0
Dorsal CA3	-4.1	4.2	4.4
Dorsal subiculum	-6.0	2.0	3.2

Figures

Figure 1.

Figure 2

Delay from seizure onset (ms)
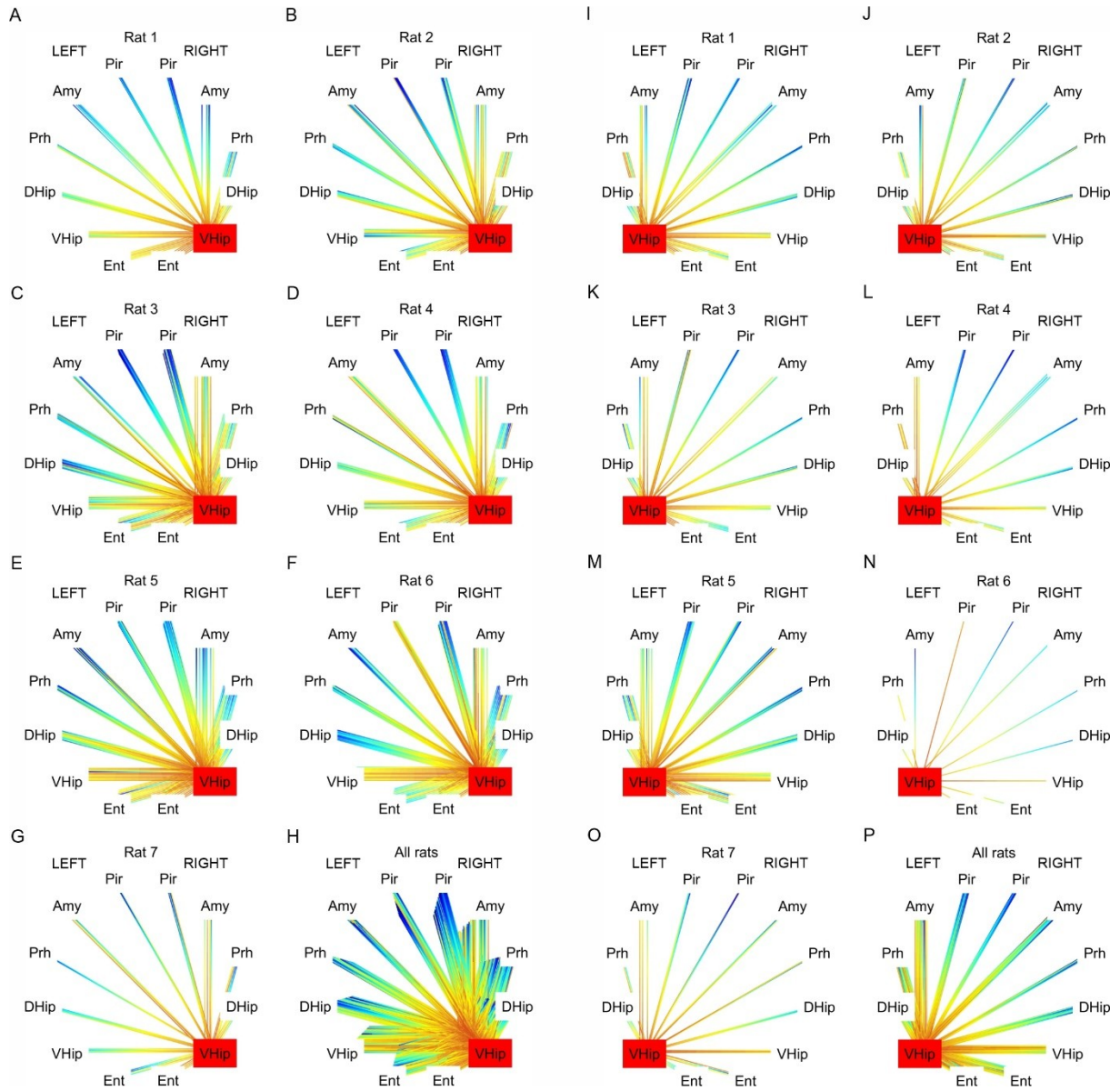0 .06 .12 .18 .24 0.3

Proportion of seizures (%)
0 20 40 60 80 100
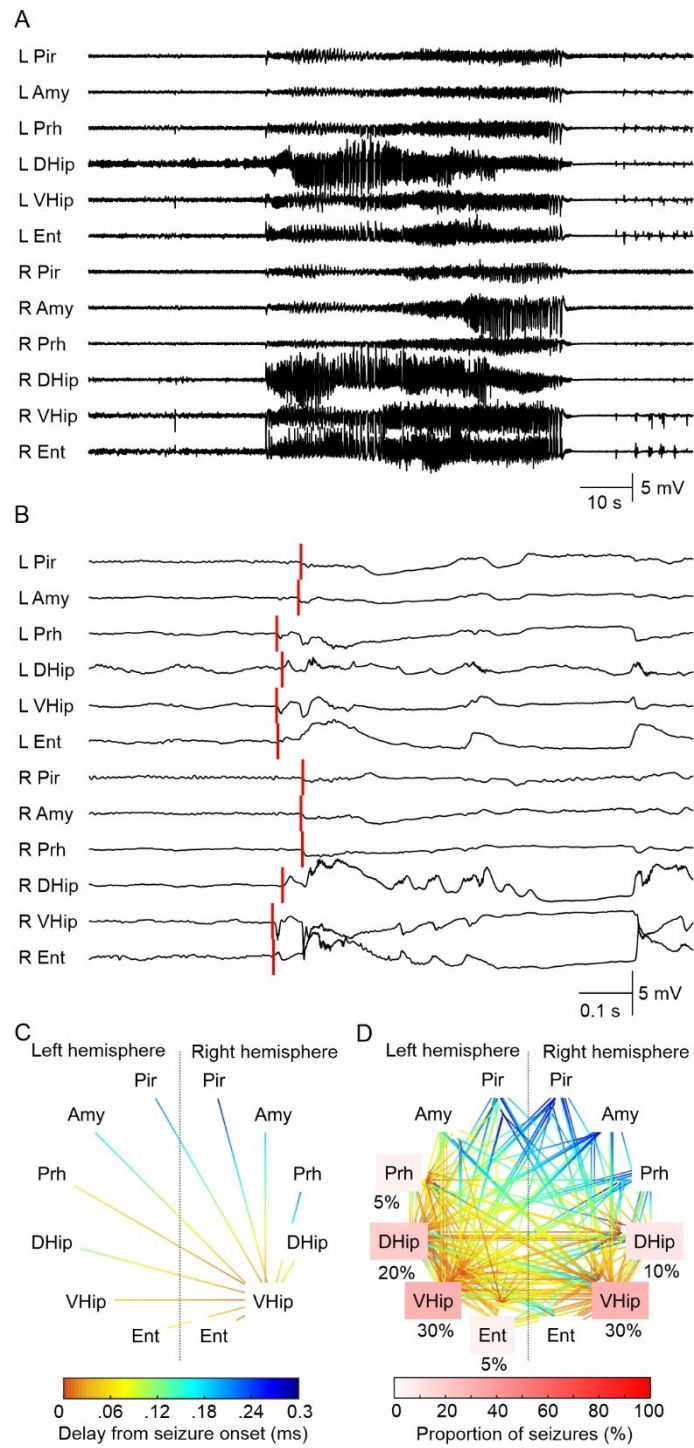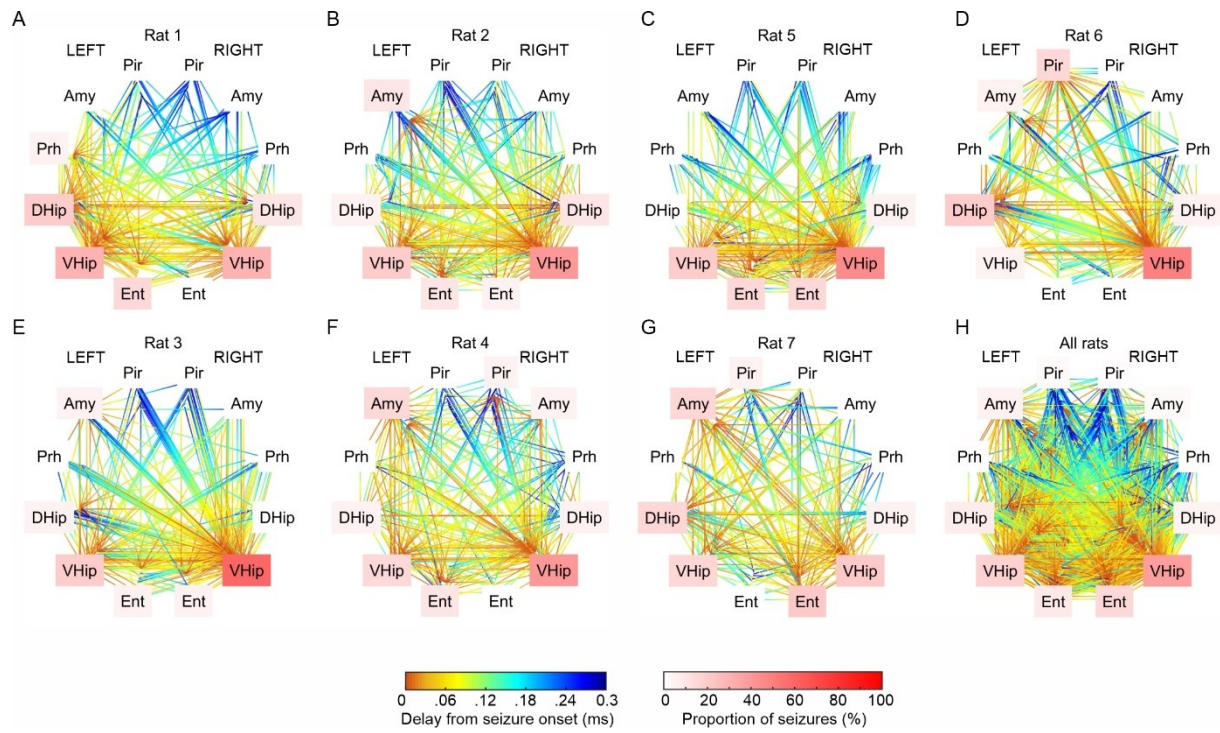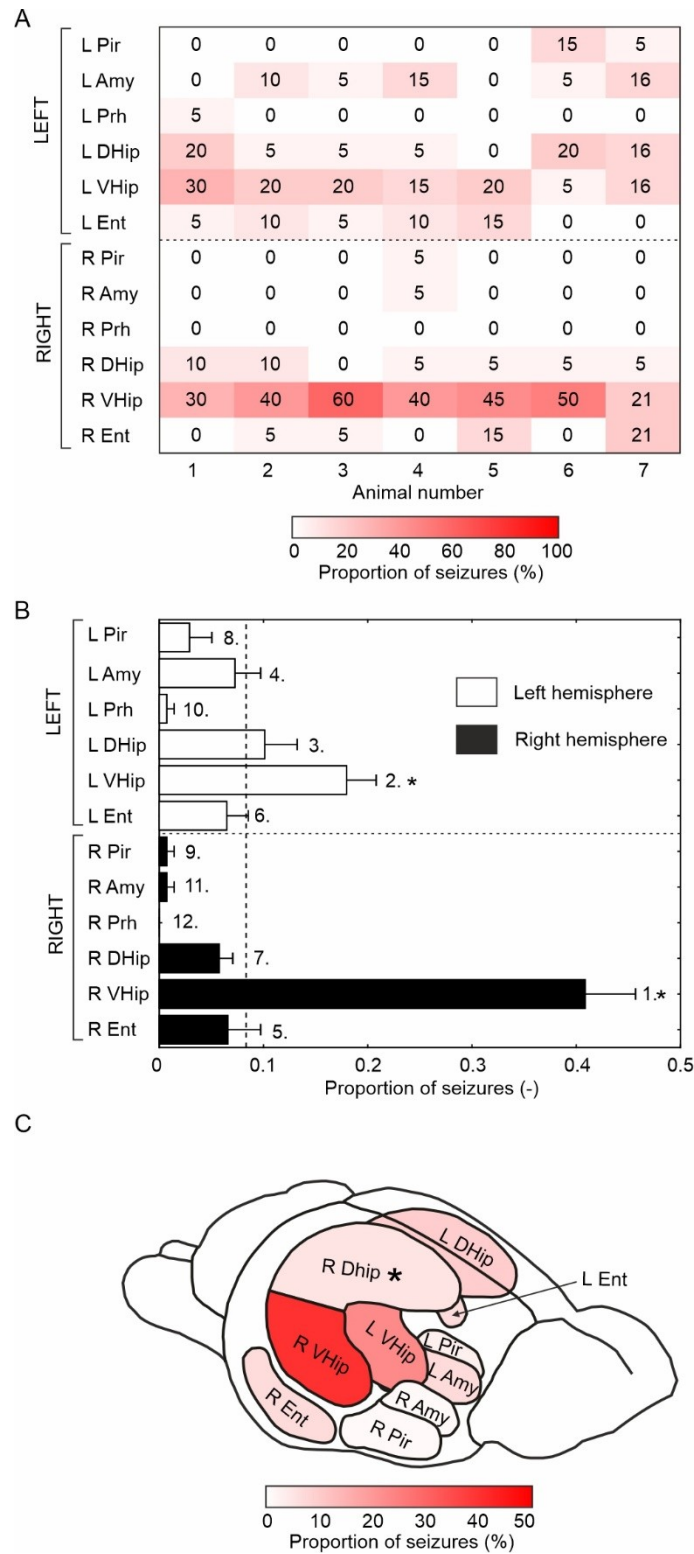
Figure 3

Figure 4

Figure 5
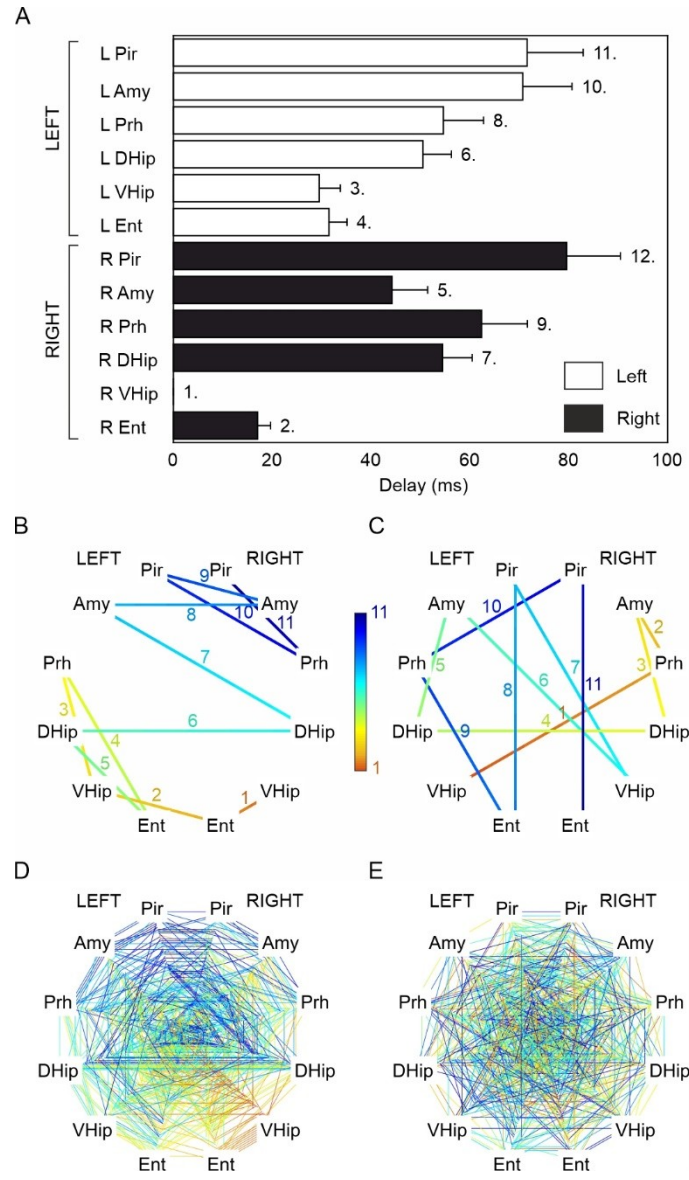
Figure 6
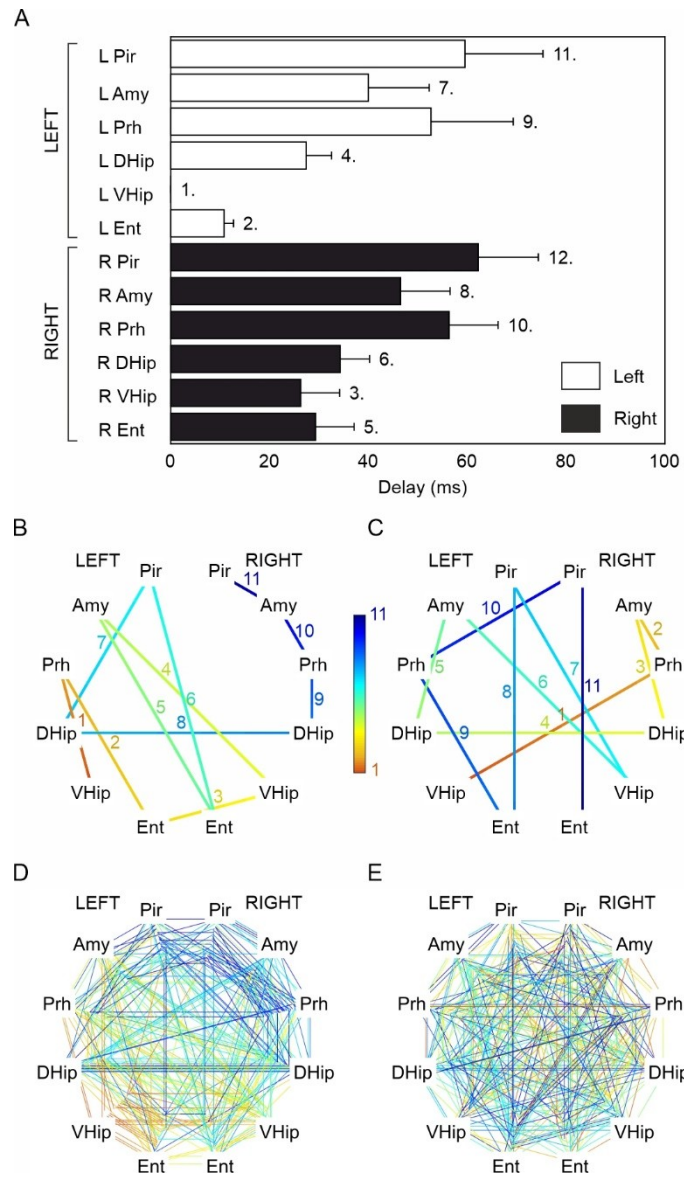
10 NeuroPorator: An open-source, current-limited electroporator for safe *in utero* gene transfer

10.1 The contributions toward the progress of the field

In utero electroporation (IUE) is a powerful technique for introducing genetic modifications in specific tissues of developing embryos, enabling the study of somatic mutations and their effects on brain development and neurological disorders. However, commercially available electroporators for IUE are often expensive and lack customizability. This study presents NeuroPorator, an inexpensive, open-design, and customizable electroporator optimized for safe IUE. NeuroPorator addresses the limitations of existing commercial electroporators and facilitates the adoption of IUE in various research laboratories because it is more affordable than comparable commercial ones, safe, easy to use, customizable, and capable of visualizing and storing the electroporation data. Safety is ensured by a current limiter that dynamically adjusts the voltage to constrain both applied voltage and current, preventing harmful insults to the uterus and embryos from excessive currents. NeuroPorator's functionality has been demonstrated by inducing FCD, a neurological disorder caused by somatic mutations, in mice through IUE.

10.2 The author's contributions

The author was responsible for the methodology of the NeuroPorator.

10.3 Compliance with the thesis objectives

The mouse model of FCD (Chvojka et al., 2024b) requires a somatic mutation to be introduced precisely into the lateral ventricle of a mouse embryo on a certain day through IUE. The IUE itself is a challenging method that necessitates a high degree of motor skill and precision. When not done properly, the animals either lack the required phenotype or die prematurely. Its open design and subsequent customizability allow targeting DNA delivery to specific brain regions and supporting modifications for techniques like tripolar electroporation, which is necessary to achieve low variability across the electroporated subjects. The development of NeuroPorator aligns with the thesis objectives by providing a device for genetic manipulation of embryos using the IUE. Without such a device, the study of neocortical HFOs in a highly relevant model of FCD would not be possible.

NeuroPorator: An open-source, current-limited electroporator for safe in utero gene transfer

Authors

Natálie Procházková[1]*, Minh-Thao Nguyenová[1]*, Monika Řehořová[1], Jan Kudláček[1], Jan Chvojka[1], Jakub Ziak[2, 4], Martin Balaštík[2], Jakub Otáhal[3], Přemysl Jiruška[1]†, and Ondřej Novák[1]†.

* NP and MTN should be considered joint first authors

† PJ and ON should be considered joint senior authors

[1] Department of Physiology, Second Faculty of Medicine, Charles University, Plzenska 311, 15000 - Prague, Czech Republic

[2] Laboratory of Molecular Neurobiology, Institute of Physiology, The Czech Academy of Sciences, Videnska 1083, 14200 - Prague, Czech Republic

[3] Department of Pathophysiology, Second Faculty of Medicine, Charles University, Plzenska 311, 15000 - Prague, Czech Republic

[4] Present address: The Solomon H. Snyder Department of Neuroscience, Johns Hopkins Kavli Neuroscience Discovery Institute, The Johns Hopkins School of Medicine, 725 North Wolfe St., Baltimore, MD 21205

Correspondence email: ondrej.novak@lfmotol.cuni.cz

Abstract

Background: Electroporation is an effective technique for genetic manipulation of cells, both *in vitro* and *in vivo*. *In utero* electroporation (IUE) is a special case, which represents a fine application of this technique to genetically modify specific tissues of embryos during prenatal development. Commercially available electroporators are expensive and not fully customizable. We have designed and produced an inexpensive, open-design, and customizable electroporator optimized for safe IUE. We introduce *NeuroPorator*.

Method: We used off-the-shelf electrical parts, a single-board microcontroller, and a cheap data logger to build an open-design electroporator. We included a safety circuit to limit the applied electrical current to protect the embryos. We added full documentation, design files, and assembly instructions.

Result: NeuroPorator output is on par with commercially available devices. Furthermore, the adjustable current limiter protects both the embryos and the uterus from overcurrent damage. A built-in data acquisition module provides real-time visualization and recordings of the actual voltage/current pulses applied to each embryo. Function of *NeuroPorator* has been demonstrated by inducing focal cortical dysplasia in mice.

Significance and Conclusion: The simple and fully open design enables quick and cheap construction of the device and facilitates further customization. The features of *NeuroPorator* can accelerate the IUE technique implementation in any laboratory and speed up its learning curve.

1. Introduction

Genetic manipulation of animals has brought unprecedented possibilities to model human diseases *in vivo.* Animal models, especially mice and rats, have been modified with various genes up to entire artificial transgene cassettes inserted to their genomes. Such lines of genetically modified animals usually carry germinal alteration, e.g. mutation, meaning the gene modification is present in all cells of the model animal. Many of these animal models have been successfully developed and established in preclinical research of a wide spectrum of diseases. However, it is increasingly recognized that the pathogenesis of various disorders can be attributed to somatic mutations occurring during early stages of embryonal development. The mutation then affects a limited number of cells (daughter cells), resulting in tissue mosaicism, affecting multiple parts of the organ. The specific gene, character, and embryonal timing of the mutation determine the severity of the phenotype. In neuroscience, recent genetic studies demonstrated that somatic mutations occurring during brain development are associated with various neurological conditions, such as malformations of the cortex (Lim et al., 2015) or brain tumors (Zhang et al., 2021), which are often related to epilepsy.

In contrast to breeding mouse lines with germinal mutations, where the mutation is hereditary to the offspring, modeling brain disorders due to somatic mutations require introducing the mutation in the naïve developing brain to mimic a spontaneous mutation occurring during the gestational period in humans.

Affecting a specific population of cells in a developing embryo can be achieved by a technique of *in utero* electroporation (IUE). The goal of electroporation is to deliver DNA into cells using an electric field. Transient electric fields form pores in the cell membrane, allowing charged DNA molecules to enter the cell. Electroporation was first introduced more than 40 years ago for transfecting mouse cell lines *in vitro* (Neumann et al., 1982; Potter et al., 1984). The technique had been modified for *in vivo* usage (Saito and Nakatsuji, 2001; Tabata and Nakajima, 2001) and successfully applied to study neuronal migration and various aberrations of brain development (Ackman et al., 2009; Bogoyevitch et al., 2012; Feliciano et al., 2011; Lim et al., 2015; Tsai et al., 2005).

In terms of special equipment, IUE requires platinum tweezer electrodes and a device that can generate and deliver a series of short electric pulses – mostly termed as electroporator. While both tools are commercially available, the electroporator comes at a substantially high price that can prevent many laboratories from taking advantage of the IUE method. Here, we present an alternative termed as *NeuroPorator*: A fully documented, open-design, easy-to-make electroporator that is affordable, largely configurable, and fits the parameters for IUE.

Our electroporator design comprises a current-limiting circuit to protect the embryos. Additionally, it includes a built-in data acquisition (DAQ) module that enables for real-time visualization and recording of the actual voltage and current applied during IUE to each embryo. *NeuroPorator* can be assembled within two days with only basic knowledge of soldering and almost no necessary knowledge of programming. In Supplementary materials, we have attached complete documentation with a detailed description of the manufacturing process, bill of materials, 3D models of all printable parts, documented and customizable Arduino code, and a parts layout for a printed circuit board (PCB) or solderless assembly. We have demonstrated routine usage of *NeuroPorator* in modeling a specific neurological disorder caused by localized somatic mutation – focal cortical dysplasia (FCD), which often manifests with epileptic seizures.

2. Material and methods

2.1. *NeuroPorator* design and hardware

NeuroPorator consists of three main parts – *Pulse generator*, *Current limiter*, and *Pulse recorder* modules. The source of energy in our design consists of five 9 V batteries connected in series to create a 45 V voltage source. Voltages of 30 V–45 V can be found as typical in literature for IUE (Baumgart and Baumgart, 2016; Saito and Nakatsuji, 2001; Tabata and Nakajima, 2001).

The *Pulse generator* module is based on an Arduino Uno Rev3 microcontroller (Arduino LLC, Italy) and a fast reed relay (figure 1(a)). The fast reed relay can be directly driven by an Arduino digital output (+5 V). The module produces precisely timed pulse trains. The Arduino board continuously senses a contact on the sustain pedal to trigger the predefined pulse sequence. This is sent to both the reed relay and a small active buzzer (figure 1(b)) for audio signaling of the pulse train. We provide a ready-to-use code sample for the microcontroller, including the default settings (five 50 ms pulses, 950 ms inter-pulse intervals), in the Supplementary material (*Default_code.ino*). The code was modified and uploaded to the board using Arduino Integrated Development Environment, Arduino IDE 2.0. The *Pulse generator* module connects voltage supply with the *Current limiter* module (figure 1(c)).
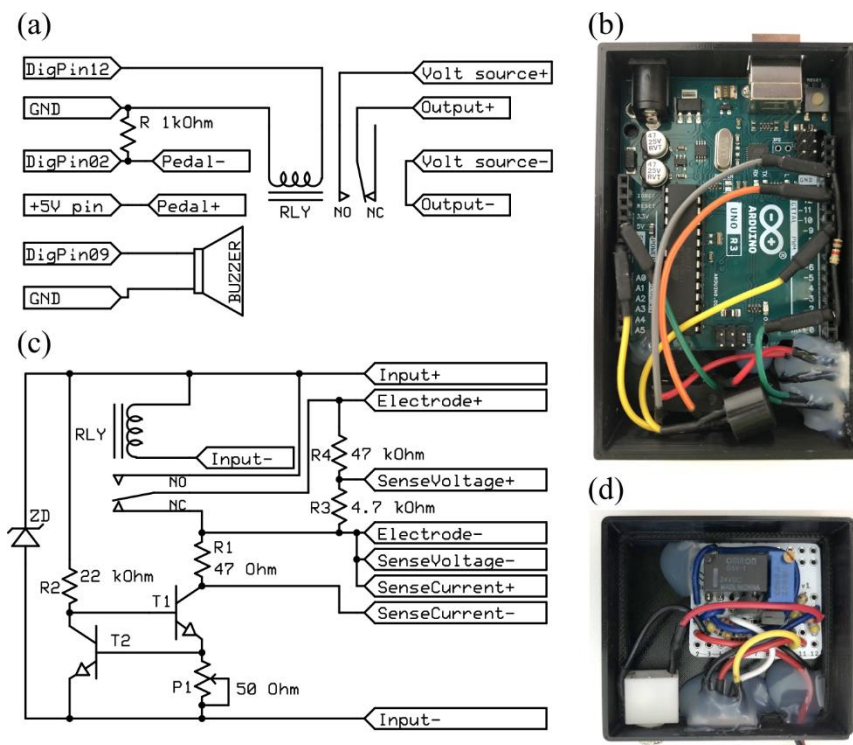
Figure 1. Circuit schemes and arrangement of the pulse-delivering *NeuroPorator* modules: (a) Circuitry of the *Pulse generator* module showing a fast reed relay driven by the Arduino Uno R3 digital pins. (b) Arrangement of the *Pulse generator* module in a 3D-printed case. (c) Circuitry of the *Current limiter* module with described input output points. (d) Arrangement of the *Current limiter* module.

The *Current limiter* serves as a module that dynamically adjusts its output voltage to keep output current below a predefined value. It includes one additional fast relay (G5V-1-DC24, Omron, Japan) that connects the pulses (NO pin of the relay) to the output during the high phase and short-circuits the output (the electrode contacts) during the low phase. The rated voltage of the relay is 24 V, but up to 48 V driving voltage is tolerated by the relay.

The current limitation mechanism is set by a combination of two transistors (T1, T2) and a potentiometer (P1). Transistor T1 is open when T2 is closed, as the voltage on T1 base is high. The voltage at the base

of T2 is given by the product of P1 resistance and the current through P1 that in series flows through the electrode. Once the electrode current rises, the T2 base voltage also rises, crosses the threshold (typically 0.6–0.7 V), and T2 opens. Once T2 opens, the voltage on T1 base drops as it is given by power supply voltage divided by R2 resistance (high) and T2 collector-emitter resistance (low for open transistor). T1 then closes. This mechanism sets this circuit to a steady state with the maximum current through T1 (and in series also through the electrode), governed by the P1 resistance as their product is kept under the T2 base threshold voltage. P1 resistance is adjustable (blue multiturn trimmer in figure 1(d)) to enable the setting of a maximum current. We incorporated a fast bistable relay that opens during the pulse and short-circuits the electrode pins between pulses to minimize capacitance-related artifacts, which would distort the pulse shape. Resistor R1 serves as a circuit protection and concurrently as a load of known resistance. The applied current can be monitored and calculated from the voltage (*SenseCurrent+*, *SenseCurrent-*) across R1. Resistors R4 and R3 constitute a voltage divider of substantially higher total resistance compared to the expected impedance at the electrode. The actual pulse voltage and shape is read out across R3 (*SenseVoltage+*, *SenseVoltage-*). Unwanted back-induction voltages generated at the relay coil during pulse ending are eliminated by a Zener diode (ZD). We provide three variants of PCB layouts made from off-the-shelf prototyping boards in the Supplementary materials (*Current limiter PCB layouts.pdf*).

 The aforementioned modules are accompanied by a third one—*Pulse recorder*—for which we use a commercially available system, USB-6001 (National Instruments, USA). It mainly serves to monitor and record the timing and amplitude of the pulses using a PC application (e.g. DAQExpress, National Instruments, USA). The module is connected to the *Current limiter* output through the *SenseCurrent* and *SenseVoltage* wires (figure 2).
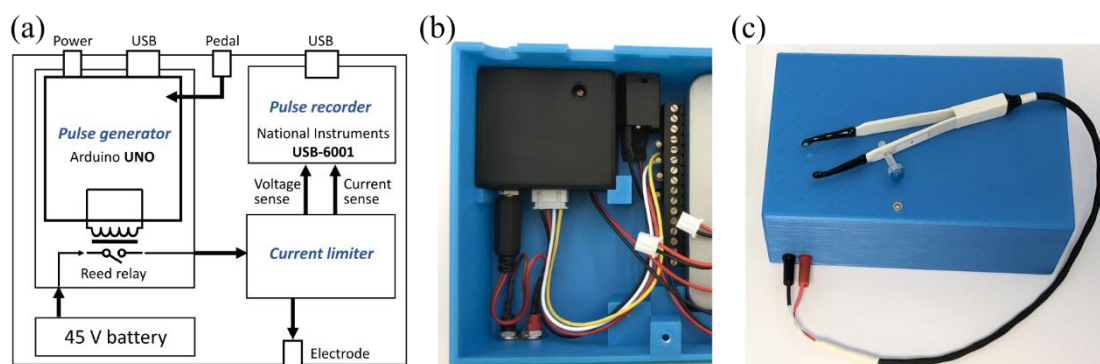
Figure 2. Arrangement of the *NeuroPorator* modules: (a) Block diagram of *NeuroPorator*, including an Arduino-based *Pulse generator*, analogue *Current limiter*, and a commercially available *Pulse recorder* (National Instruments USB-6001). The pulses are energized from five 9 V batteries connected in series. (b) Arrangement of individual modules inside the *NeuroPorator* box; here, the *Pulse generator* module has been removed. (c) Overall look of the presented electroporator together with CUY650P3 tweezer electrodes.

The *Pulse generator* and the *Current limiter* modules were assembled with solder and hot glue. Boxes for both modules and the main box were 3D printed with an FFF printer (Prusa i3 MK3S+, Prusa, Czech Republic). The 3D object files are attached as Supplementary materials in *.stl* and *.step* formats. Detailed assembly and setting instructions for all modules, connecting cables, and PCB variants are given in the Supplementary text and figures as well as the list of all necessary electronic parts (bill of material – *NeuroPorator_BOM.xlsx*). The whole process of assembling *NeuroPorator* is thoroughly described in Supplementary materials: *Assembly_instructions.pdf*.

### *2.2.* **Animals**

Mice used in this study were crossbreeds of an SST-IRES-Cre strain (Jackson Laboratory cat. number #018973), a PV-P2A-Cre strain (Jackson Laboratory, USA, cat. number #012358), or a VIP-IRES-Cre

strain (Jackson Laboratory cat. number #010908) and a flex-tdTomato reporter strain (Jackson Laboratory cat. number #007909). All strains were on a C57Bl/6J background except VIP-IRES-Cre strain, that was based on a mixed C57BL/6 x 129S4Sv background. Mice were kept under standard conditions in a room with controlled temperature (22±1 °C) and a 12/12 h light/dark cycle and *ad libitum* access to food and water.

2.3. *In utero* electroporation

Pregnant mice (day 14.5±0.5 post-fertilization) were anesthetized with isoflurane (5 % induction, 1.5 % maintenance). The fur on the abdomen was shaved off and a 1.5 cm incision was made in the middle of the abdomen to expose the muscle layer. A 1 cm-long laparotomy was performed in parallel with the *linea alba* to access the uterus. The exposed uterine horns were then placed on sterile gauze around the incision and frequently moistened with warm phosphate-buffered saline (PBS). To induce FCD and mark the transfection localization, embryos were injected with a plasmid mixture containing 3 µg/µl of expression plasmid CAG-mTOR$_{7280T>C}$-IRES-EGFP (SOVARGEN, Korea [1]), or its wild-type variant together with 1.5 µg/µl of expression plasmid CAG-EGFP, or CAG-iRFP (infrared fluorescent protein). Animals in one control group were electroporated with 1.5 µg/µl CAG-EGFP only. The expression plasmids were diluted in 2 ug/ml Fast Green (F7252, Sigma, USA) for visualization. Each embryo was injected into the left lateral ventricle using a pulled and beveled glass capillary (figure 3(a)). After each injection, forceps-type electrodes (3 mm, CUY650P3, Nepagene) were positioned on the head of the embryo, with the positive electrode facing the left side of the embryo's head, and electroporation of the plasmids was performed using *NeuroPorator* that delivered five 50 ms pulses with 950 ms inter-pulse intervals (figure 3(b)).
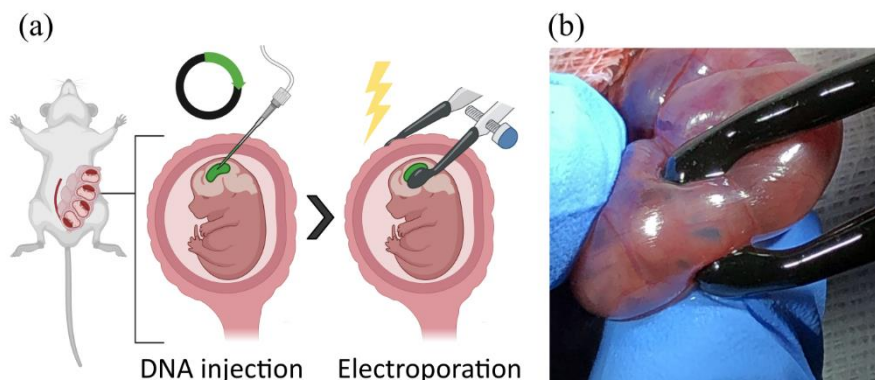
Figure 3. Basic principle of gene delivery through electroporation with focus on *in utero* conditions: (a) Outline of *in utero* electroporation of the brain. Each embryo is gently positioned in the uterus, a small volume of DNA solution is injected into embryo's brain ventricle through the uterine wall, and tweezers with platinum-plated electrodes are attached to the uterine wall, surrounding the embryo's head. Electrical pulses to transduce the targeted cells are delivered. (b) Real image of electroporation of previously injected embryo. The injected plasmid is visible as dark green substance in the lateral ventricle.

The applied voltage was 30–45 V (dynamically adjusted by the device) and the current limitation was set to 40 mA.

2.4. Electrode implantation and EEG recording

To evaluate the epilepsy phenotype induced by FCD, successfully electroporated pups (confirmed by fluorescence screening) were fostered and later implanted with recording electrodes and placed into a video-EEG monitoring chamber. Custom EEG connectors were prepared by soldering PFA-coated silver wires (AM Systems, Inc., USA, cat. no. 786000) to prefabricated connectors (TME Electronic Components, Poland, cat. no. DS1065-03-2*6S8BV). Animals were implanted with EEG electrodes at 8–10 weeks of age. The animals were anesthetized with isoflurane and their heads were fixed by a mouse gas anesthesia head holder (Kopf Instruments, USA, cat. no. 923-B). After exposing the dorsal skull, the exact position of GFP signal was assessed using a green bandpass filter (525/45 nm, Edmund Optics) attached to the surgical microscope and a 488 nm laser pointer (Sanwu, PRC). Using a high-speed microdrill (Osada Electric Co., Ltd., Japan, cat. no. OS-40) with 0.3 mm drilling bits, 2–6 holes were drilled through the skull carefully to avoid any damage to *dura mater*. At least one electrode was positioned directly over the FCD and one electrode to the mirror position in the contralateral skull area. Two holes were positioned over the cerebellum for grounding/reference electrodes. All electrode bare endings were placed on the surface of the dura, and the holes were covered with bone wax (SMI, Belgium, cat. no. Z046). Electrodes and the connector were attached to the skull using cyanoacrylate glue gel (Loctite, USA, cat. no. 1363589) accelerated with cyanoacrylate glue accelerator (Bob Smith Industries Inc., USA, cat. no. BSI-152).

After the surgery, animals were allowed to recover for five days and subsequently placed into the video-EEG recording chambers. All mice were individually video-EEG monitored for four weeks for 24 hours a day. Recorded electrographic activity was amplified, bandpass filtered (0.1 Hz–1.6 kHz), and digitized at 5 kHz using a 32-channel amplifier chip (Intan Technologies, USA, cat. no. RHD2132). Finally, EEG data were manually labeled for seizures using custom-made software in MATLAB 2019b (Mathworks Inc., USA).

2.5. Tissue clearing and microscopy

Animals were overdosed with a ketamine/xylazine intramuscular injection (120 mg/kg and 20 mg/kg, respectively) and intracardially perfused with cold saline followed by 4 % paraformaldehyde in PBS. Brains were explanted and postfixed overnight in 4 % paraformaldehyde, after which they were stored in 0.05 % sodium azide in PBS until they were processed according to the CUBIC clearing protocol (Susaki et al., 2015) for subsequent morphological imaging.

Images were taken using a custom-made two-photon microscope with a femtosecond laser (Chameleon Vision S, Coherent), an 8 kHz resonant scanner (LSK-GR08, Thorlabs), a 20x XLUMPLFLN water-immersion objective (Olympus), and two silicon photomultipliers (Hamamatsu). Cytoarchitecture of the fluorescently labeled tissue was recorded using sequential two-photon tomography (Ragan et al., 2012). In this procedure, a block of cleared tissue is embedded in agarose and glued to a vibratome inset. The brain was cut at a specific transversal position and moved to the two-photon microscope. The coronal section of the brain was mapped for fluorescence and tiled with an appropriate number of 800 μm-sided fields of view. At each field of view, the microscope took a fine 1200 μm-thick Z-stack, 2 μm step in Z, with 800 x 800 μm (2048 x 2048 pixels) X-Y field of view.

3. Results

Improved design to minimize the tissue damage

The current between the tweezer electrodes can flow through many ways (figure 4(a)). If the embryo is not positioned properly and the electrode is not compressed against the uterine wall, instead of the embryo's brain tissue, a large proportion of the current can flow through approximately four times more electrically conductive amniotic fluid (Pachi et al., 2001). However, all the current must flow through the uterine wall–electrode contacts. If an electroporator works only as a pulsed voltage source, the current flowing between the contacts of the electrode is inversely proportional to the impedance of the sample, but is not limited (figure 4(b), yellow). We incorporated current limiting circuitry to *NeuroPorator* to protect the uterus and embryos from excessive current (figure 4 (b), green).
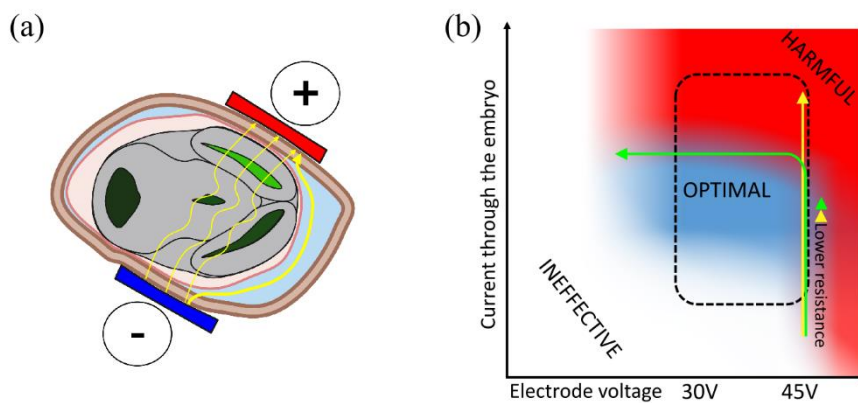
**Figure 4. Reasoning for optimal parameters for safe and effective IUE:** (a) Drawing of an embryo's head and electric current streamlines. Arrowheads are oriented in the direction of expected DNA movement. Current is induced by the electrode attached to the uterine wall. (b) Function principle of the current limiting feature of our electroporator in a current–voltage characteristic. Green and yellow curves are functions of one parameter—the impedance between contacts of the electrode (load). With a constant voltage (30–45 V)-delivering electroporator, voltage–current combinations can be found as points in a certain area, here depicted as a dashed line-rounded rectangle, depending on the load impedance. The yellow line represents a function of decreasing impedance for 45 V. With lower impedance, the current can easily reach harmful values. The *Current limiter* module of *NeuroPorator* does not let the curve continue straight and dynamically limits the voltage on the electrode to ensure that the maximum allowed current is not exceeded (green curve).

To assess the performance and safety of *NeuroPorator*, we have recorded the voltage and current delivered to mock samples of known resistance. We used resistors with values in range we observed during IUE. *NeuroPorator* was set to limit the current at 40 mA. Figure 5(a) shows the voltage and current recordings of pulses applied to 600 Ohm, 900 Ohm, and 1200 Ohm, respectively. Duration of pulses was set to 50 ms and the precise onset and offset edges of the pulses can be seen from the two zoomed pulses for different impedances (figure 5(a), inset). We measured and plotted the output voltage and current in figure 5(b) for resistors of 11 different values. For samples of high impedance (1200 Ohm and higher), the behavior of *NeuroPorator* is approximately Ohmic as the preset current limit cannot be reached and maximum voltage of the source is delivered. For lower impedances, e.g., 900 Ohm, 600 Ohm, *NeuroPorator* adjusts the output voltage to limit the current to the preset value.
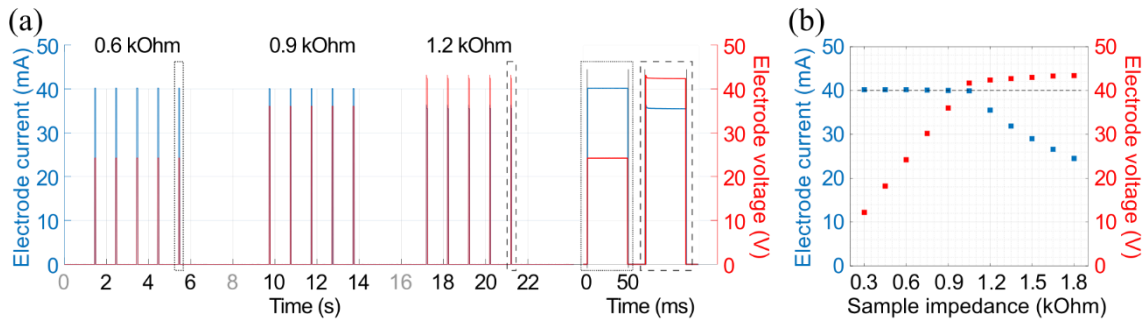
Figure 5. Performance of *NeuroPorator*: (a) Voltage and current pulses recorded at the testing load; the load consisted of 600 Ohm, 900 Ohm and 1200 Ohm resistors, respectively. The current limit was set to 40 mA. One pulse for a 600 Ohm load and one pulse for a 1200 Ohm load are zoomed in the inset. With low load impedance, the electrode voltage is being limited; with high impedance, the output voltage reaches the maximum voltage *NeuroPorator* can deliver. (b) Current limiting performance of *NeuroPorator* shown as the maximum recorded current and voltage pulses for various load values. The current limiter action can be seen from resistor samples of 1000 Ohm and below.

3.1. **Comparison to existing electroporators**

The parameters and features of *NeuroPorator* compared to commercially available electroporators and previously published custom-made electroporators are listed in Table 1.

Table 1. Comparison of the parameters between *NeuroPorator*, the commercially available electroporators, and the previously published custom-made electroporators. Abbreviations: HV, high-voltage; LV, low-voltage.

Machine, reference	Pulse design	Pulse time precision	Voltage settings	Current limiter	Readout/ recording	Approximate price
BTX ECM830	Rectangular pulses, unipolar, pulse trains	10 µs to 999 ms (1µs resolution)	5–500 V in 1 V steps	NO, short circuit safety protection	NO	$13,700
NEPAGENE NEPA21	Two types of pulses separately designable – HV poring pulse, LV transfer pulses, bipolar, pulse trains	0.05–99.9 ms (0.01 ms resolution)	0.1–300 V HV mode, 0.1–99.9 V LV mode (0.1 V resolution)	NO, short circuit safety protection	Display values	$24,000
Portoporator© (Schmitt et al., 2019)	Rectangular pulses, unipolar, Arduino-based; highly variable pulse trains	1 ms to 1000 ms, 1 ms step, <1 ms precision	400–600 V, (Cells in cuvette – oriented)	NO	NO	<$140
In utero electroporator (Bullmann et al., 2015)	Rectangular pulses, unipolar, single pulse	20 to 200 ms, precision ~10 %	Battery pack, 0–45V, 9 V step, or external source	YES, 125 mA safety and IUE protection	NO	<$50
NeuroPorator	Rectangular pulses, unipolar, Arduino-based; highly variable pulse trains	1 ms to 1000 ms, 1 ms step, <1 ms precision, inter-pulse short circuiting	Battery pack, 18–45 V, 9 V step	YES, easily adjustable, 1 mA–500 mA, <1 mA precision	Built-in USB module, displaying/ recording	~$550

NeuroPorator delivers rectangular unipolar pulses. This is also the case for most of the compared devices; the only one with variable bipolar pulses is NEPA21 (Nepagene). The pulse timing of

NeuroPorator is highly variable with comparable time precision to those declared by other electroporators. Some electroporators can deliver voltages for both *in utero* and *in vitro* electroporation (ECM830 by BTX), others are focused only on *in vitro* application (Portoporator©), and finally, there are electroporators with voltages primarily complying with the ranges for IUE, including *NeuroPorator*. The prominent advantages of *NeuroPorator*, which are absent in the compared devices, are the fully adjustable current limitation and the real-time displaying and recording of the voltage and current curves. Furthermore, it is possible to assemble the device in only two days and all necessary parts cost approximately $550.

3.2. Proof of *NeuroPorator* efficacy

NeuroPorator has been thoroughly tested in our laboratory for IUE of a plasmid-containing mutated mechanistic target of rapamycin (mTOR) gene to induce FCD—a very common cortical malformation (Crino, 2015). A specific point mutation (7280T>C) leads to a constitutively active protein and alters neuronal migration, growth, and proliferation [1]. Normally developed neocortex has a stereotypical cytoarchitecture, layered structure, and clear margins between the gray matter, consisting of cell bodies, and the white matter, made up of myelinated axons (figure 6(a)). If a plasmid (figure 6(a), top) is injected into a brain lateral ventricle in mouse embryos and electroporated at day E14.5, the plasmid primarily enters radial glia and newly formed neurons that should migrate into the upper layers of the cortex (layer 2/3 in mice). Plasmid containing only a control fluorescent protein EGFP (figure 6(a), left) leads to fluorescence-labeled layer 2/3 of the cortex (figure 6(b)). However, disrupting the mTOR signaling pathway using electroporation of mutated mTOR gene at day E14.5 leads to a dysplastic cortex with disrupted laminar structure, absence of clear borders between gray and white matter, ectopic neurons (figure 6(a), right, figure 6(c)), and abnormal neuronal phenotypes. These neurons (figure 6(d)) are characterized by enlarged somata, atypical dendritic branching, and abnormal connectivity. The FCD displays high endogenous epileptogenicity characterized by repeated spontaneous epileptic seizures (figure 6(e)).
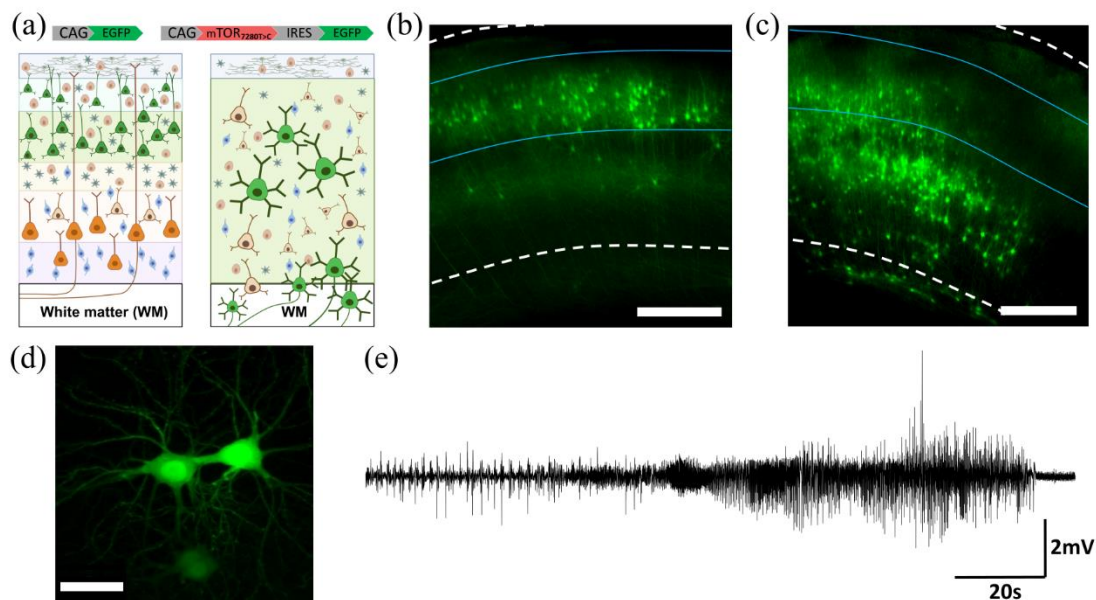
Figure 6. Performance of *NeuroPorator* in real mouse cortex: (a) Plasmids that were electroporated at day E14.5 included either a gene for constitutively active mTOR and a gene for enhanced green fluorescent protein or the fluorescent protein gene solely. Illustration of normal cortex with its stereotypical cytoarchitecture and layered structure (a, bottom left) and dysplastic cortex with smeared lamination and ectopic dysmorphic neurons (a, bottom right). (b) The cytoarchitecture of the cortex with almost all fluorescently labeled neurons migrated into layer2/3 after IUE with a control plasmid. (c) Dysplastic cortex with fluorescently labeled neurons throughout the gray and even the white matter after IUE with a plasmid carrying the mutated mTOR gene variant. (d) Dysmorphic neurons

with atypical dendritic branching and highly enlarged somata. E) Local field potential recording from the dysplastic cortex during an epileptic seizure. Legend: Scale bars correspond to 500 μm in (b), (c) and 50 μm in (d). WM = white matter. In (B), (C) white dashed lines depict the cortical surface and the gray matter / white matter border. Blue lines represent the approximate borders of layer 2/3 of the mouse somatosensory cortex.

Images and traces shown in figure 6 are based on the groups of mice prepared by Experimenter C (figure 7). The yield of the chosen FCD model of chronic epilepsy is relatively low. Out of 24 mice that were in utero electroporated with the mutated mTOR gene and that were later preselected based on their relatively large lesion, only 9 developed epileptic phenotype and spontaneous seizures captured at video-EEG monitoring (37.5%). None of the mice electroporated with sole EGFP plasmid showed any signs of epileptic activity.

We also evaluated *NeuroPorator* in terms of survival rate and success rate in the hands of three independent, experienced experimenters working on separate projects (figure 7).
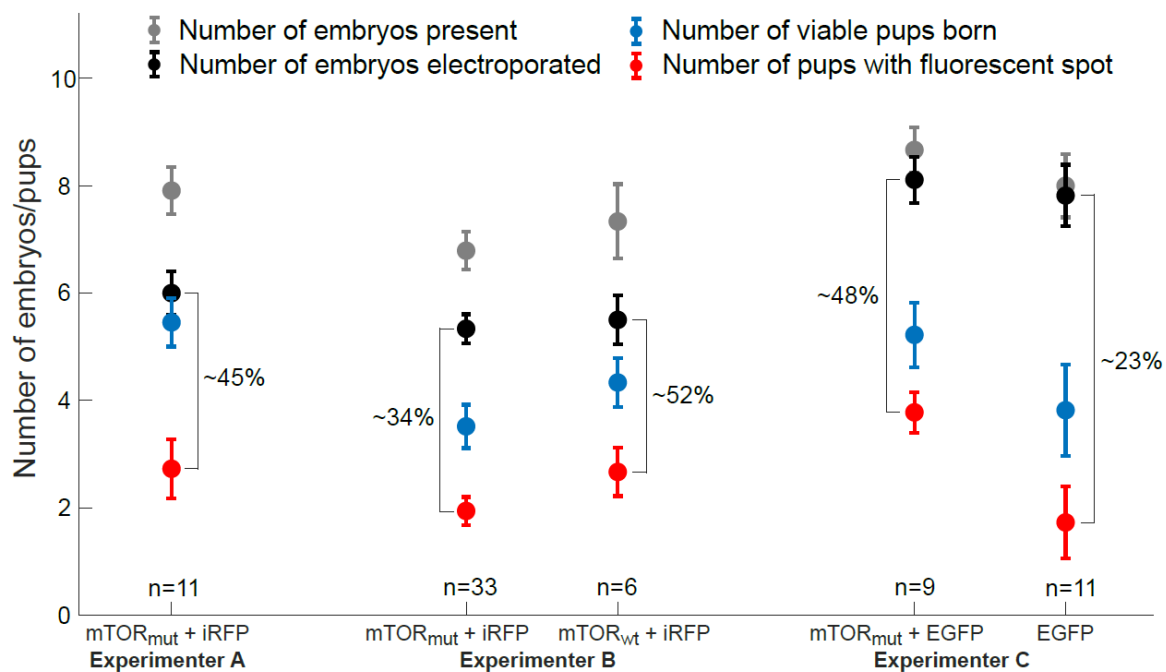
Figure 7. Evaluation of the survival rate and success rate of IUE using *NeuroPorator* by three different experimenters. In three separate projects, plasmids carrying a gene for two variants of mTOR, either wild-type (mTOR$_{wt}$) or mutated (mTOR$_{mut}$), were electroporated together with a plasmid carrying a gene for a fluorescent protein EGFP or iRFP. In one group, Experimenter C electroporated only plasmid with a gene for EGFP. The numbers below each graph denote the number of electroporated pregnant mice for the respective projects. For each group, mean fractions of successfully electroporated, viable pups, and electroporated embryos are shown. Error bars represent standard error of the mean (SEM).

We evaluated mean numbers of embryos found in each pregnant mouse, mean electroporated embryos, number of pups found one day after birth, and number of pups with a clearly observable fluorescent spot. Experimenters A and B mostly skipped the two embryos closest to the cervix. This is usually recommended to prevent complete abortion that can occur if those two embryos are damaged. Experimenter C followed such recommendation only partially. Mothers after the electroporation died only rarely. Out of the 70 mice described in figure 7, only two (<3%) mice died before or after the delivery. Experimenters A and C worked with mice on C57Bl/6J background. Experimenter B worked with crosses that were also partially based on 129S4Sv background; embryos/pups had one fourth of 129S4Sv background and mothers were either fully based on C57Bl/6j background (half of them) or were of mixed background C57BL/6 x 129S4Sv. Although many variables cannot be separated, our data

show that while using *NeuroPorator*, the mean success rate across various experimenters and different animal groups can be as high as ~40%.

4. Discussion

In this publication, we present a home-built electroporator, *NeuroPorator*, demonstrate its properties, and verify its functionality by inducing FCD through IUE. The main advantages of our proposed solution are safety, data recording, low price, adjustability, and an open design of the electroporator. In this section we discuss each of them in comparison to available products.

4.1. Safety

A successful electroporation of embryonal brain cells relies on creating the correct conditions for DNA to enter the cells. The strength of the pulsing field needs to be sufficient to create the pores in the membrane. However, the delivered energy must be minimized to prevent the tissue from heat and damage. The electrode is apposed directly to the uterine wall surrounding the head of the embryo (figure 3(b)). In case of a loose arrangement of the electrodes, uterus, and embryo (see figure 4(a)), which often happens, the resistance of the sample between electrodes can drop dramatically. If the voltage is kept constant in this case, the applied electric current increases. According to our experience, this can damage the uterine wall and lead to the complete abortion of all embryos. We added easily adjustable current limitation to protect embryos.

The commercially available electroporators are operated with chosen voltages, but the output current is not properly limited and is usually simply given by Ohm's law. Balancing all parameters of the procedure is difficult, since one of the crucial parameters, along with the mechanical manipulation with the uterus, is the sample (wrapped embryo) impedance. To prevent the excessive currents flowing through the uterine wall (yellow arrow in figure 4(b)), we applied an analogue current limiter to the output circuit of *NeuroPorator*. This limiter bends the current-voltage (I-V) curve by dynamically adjusting the voltage and ensures that the maximum current does not exceed the chosen value (green arrow). Constraining both applied voltage and current protects the uterus and embryo from harmful insults. The result in individual embryos can be either optimal or suboptimal and ineffective transfection, but not a complete abortion of all embryos due to uterine damage.

It is very difficult to exactly quantify the added safety and success rates in comparison with other groups. First, almost no groups publish such numbers. Second, a vast number of variables are involved. The success rate inter alia strongly depends on the experience level of the experimenter – whether the embryos are gripped enough, but not too much, whether the surgery is quick, whether the embryos are kept warm, whether the capillary is sharp and not broken, and other factors. Also, the mouse strain plays a big role. We mostly work with C57Bl/6J-based transgenic mouse strain and the presented electroporator was also evaluated in this strain. However, C57Bl/6J litter count is relatively small and C57Bl/6J females are known to not be very good mothers (Rennie et al., 2012). We showed that when using *NeuroPorator*, we achieved average success rate around 40%. As we also involved the pups that were probably eaten by their mothers and pups found dead because the absence of their mothers' lactation, the number would be probably substantially higher if we evaluated *NeuroPorator* in an outbred strain such as CD1 white mice.

4.2. Data recording and visualization

Direct visualization of the voltage and the current of the ongoing pulse trains is important for instant feedback and enables direct control of the procedure. It also facilitates learning of the procedure for lab workers starting with the method. Although commercially available electroporators display current and

voltage values in real time, *NeuroPorator* can record them throughout the whole operation. This feature allows the user to look back on each pulse train and relate them to IUE output.

4.3. Price and open design

Commercially available electroporators are debugged and reliable, however, they are also relatively expensive, most of them exceeding $10k in cost. In comparison, all material for assembling our device can be purchased for approximately $550. With the instructions attached in the Supplement, it can be assembled in two days with very basic equipment and soldering skills.

Higher price is the model case for the philosophy of Open Labware (Baden et al., 2015), that aims at making advanced laboratory devices more affordable. Recently, there were published two well-documented and designed custom-made open-source electroporators (Bullmann et al., 2015; Schmitt et al., 2019). However, the first of them, called Portoporator, is designed for electroporation of cells in cuvettes and thus operating at higher voltages. The second one (Bullmann et al., 2015) is designed directly for IUE and was shown to work properly. However, its versatility is somewhat limited, e.g., it does not enable pulse trains.

Our design offers high pulse train adaptability achievable with only minor adjustments of parameters in the provided code sample. Versatility of the code brings sub-millisecond time resolution, variable number and duration of the pulses, and variable inter-pulse intervals. The presented design can be easily further modified. With specific positioning of the bipolar electrode, the DNA can be targeted to selected brain areas such as cortex, hippocampus, striatum, and others (Kolk et al., 2011; Wang et al., 2012). This spectrum of targetable structures has been substantially broadened by introduction of tripolar electroporation (dal Maschio et al., 2012). *NeuroPorator* can be used as a source for tripolar electroporation with a proper external wiring of the electrodes.

In practice, we connect the Arduino board via a USB connector for both programming and power. However, it can be also powered from a sixth 9 V battery inside the *NeuroPorator* box, rendering the device independent of a power supply. Another modification can be done by altering the visualization module. If one does not need the real-time visualization and recording of the actually applied pulses, the data acquisition system can be disconnected and *NeuroPorator* can be fully independent and portable. The data acquisition system USB-6001 (National Instruments) is not too expensive, but if one wants to reduce the price of *NeuroPorator* even more, USB-6001 can be omitted. This would reduce the price down to ~$150. Alternatively, it is possible to design and add a visualization module to the device or an SD-card shield for data saving (e.g. *Assembled Data Logging shield for Arduino* for $15; Adafruit).

5. Conclusion

Here, we presented a fully documented open-design electroporator specially developed for *in utero* electroporation—*NeuroPorator*. Within the philosophy of Open Labware (Baden et al., 2015), the construction of *NeuroPorator* is easy and the material cost is low. We believe that by using very detailed documentation and assembly instructions, many laboratories will start using this device. *NeuroPorator* makes the technique of *in utero* electroporation more affordable and easier to implement.

Declaration of Competing Interest

None.

Data Availability

Data will be made available on request.

Acknowledgements

Contributions to the manuscript

Contributions to the manuscript using CRediT taxonomy. Natálie Procházková: Validation, Writing - Original Draft, Investigation. Minh-Thao Nguyenová: Conceptualization, Methodology, Validation, Writing - Original Draft. Monika Řehořová: Validation, Investigation. Jan Kudláček: Methodology. Jan Chvojka: Methodology. Jakub Ziak: Methodology. Martin Balaštík: Resources, Funding acquisition. Jakub Otáhal: Conceptualization, Funding acquisition. Přemysl Jiruška: Conceptualization, Writing - Original Draft, Supervision, Funding acquisition. Ondřej Novák: Conceptualization, Methodology, Software, Writing - Original Draft, Visualization, Supervision, Funding acquisition.

Ethical statement

This animal study was approved by Ethics Committee of the Second Faculty of Medicine—approval: MSMT-31765/2019-4. All experiments were performed under the Animal Care and Animal Protection Law of the Czech Republic, in line with the guidelines of the European Union directive 2010/63/EU.

References

Ackman JB, Aniksztejn L, Crépel V, Becq H, Pellegrino C, Cardoso C, Ben-Ari Y, Represa A. Abnormal Network Activity in a Targeted Genetic Model of Human Double Cortex. Journal of Neuroscience, 2009; 29: 313-27.

Baden T, Chagas AM, Gage G, Marzullo T, Prieto-Godino LL, Euler T. Open Labware: 3-D Printing Your Own Lab Equipment. Plos Biology, 2015; 13: 12.

Baumgart J, Baumgart N. Cortex-, Hippocampus-, Thalamus-, Hypothalamus-, Lateral Septal Nucleus-and Striatum-specific In Utero Electroporation in the C57BL/6 Mouse. Jove-Journal of Visualized Experiments, 2016: 11.

Bogoyevitch MA, Yeap YYC, Qu ZD, Ngoei KR, Yip YY, Zhao TT, Heng JI, Ng DCH. WD40-repeat protein 62 is a JNK-phosphorylated spindle pole protein required for spindle maintenance and timely mitotic progression. Journal of Cell Science, 2012; 125: 5096-109.

Bullmann T, Arendt T, Frey U, Hanashima C. A transportable, inexpensive electroporator for in utero electroporation. Development Growth & Differentiation, 2015; 57: 369-77.

Crino PB. Focal Cortical Dysplasia. Seminars in Neurology, 2015; 35: 201-8.

dal Maschio M, Ghezzi D, Bony G, Alabastri A, Deidda G, Brondi M, Sato SS, Zaccaria RP, Di Fabrizio E, Ratto GM, Cancedda L. High-performance and site-directed in utero electroporation by a triple-electrode probe. Nature Communications, 2012; 3: 11.

Feliciano DM, Su T, Lopez J, Platel JC, Bordey A. Single-cell *Tsc1* knockout during corticogenesis generates tuber-like lesions and reduces seizure threshold in mice. Journal of Clinical Investigation, 2011; 121: 1596-607.

Kolk SM, de Mooij-Malsen AJ, Martens GJ. Spatiotemporal molecular approach of in utero electroporation to functionally decipher endophenotypes in neurodevelopmental disorders. Frontiers in Molecular Neuroscience, 2011; 4.

Lim JS, Kim WI, Kang HC, Kim SH, Park AH, Park EK, Cho YW, Kim S, Kim HM, Kim JA, Kim J, Rhee H, Kang SG, Kim HD, Kim D, Kim DS, Lee JH. Brain somatic mutations in MTOR cause focal cortical dysplasia type II leading to intractable epilepsy. Nature Medicine, 2015; 21: 395-+.

Neumann E, Schaeferridder M, Wang Y, Hofschneider PH. GENE-TRANSFER INTO MOUSE LYOMA CELLS BY ELECTROPORATION IN HIGH ELECTRIC-FIELDS. Embo Journal, 1982; 1: 841-5.

Pachi A, De Luca F, Cametti C, Barresi S, Berta S. Use of electrical conductivity of amniotic fluid in the evaluation of fetal hung maturation. Fetal Diagnosis and Therapy, 2001; 16: 90-4.

Potter H, Weir L, Leder P. ENHANCER-DEPENDENT EXPRESSION OF HUMAN KAPPA-IMMUNOGLOBULIN GENES INTRODUCED INTO MOUSE PRE-B LYMPHOCYTES BY ELECTROPORATION. Proceedings of the National Academy of Sciences of the United States of America-Biological Sciences, 1984; 81: 7161-5.

Ragan T, Kadiri LR, Venkataraju KU, Bahlmann K, Sutin J, Taranda J, Arganda-Carreras I, Kim Y, Seung HS, Osten P. Serial two-photon tomography for automated ex vivo mouse brain imaging. Nature Methods, 2012; 9: 255-U48.

Rennie MY, Detmar J, Whiteley KJ, Jurisicova A, Adamson SL, Sled JG. Expansion of the fetoplacental vasculature in late gestation is strain dependent in mice. American Journal of Physiology-Heart and Circulatory Physiology, 2012; 302: H1261-H73.

Saito T, Nakatsuji N. Efficient gene transfer into the embryonic mouse brain using in vivo electroporation. Developmental Biology, 2001; 240: 237-46.

Schmitt MA, Friedrich O, Gilbert DF. Portoporator (R) : A portable low-cost electroporation device for gene transfer to cultured cells in biotechnology, biomedical research and education. Biosensors & Bioelectronics, 2019; 131: 95-103.

Susaki EA, Tainaka K, Perrin D, Yukinaga H, Kuno A, Ueda HR. Advanced CUBIC protocols for whole-brain and whole-body clearing and imaging. Nature Protocols, 2015; 10: 1709-27.

Tabata H, Nakajima K. Efficient in utero gene transfer system to the developing mouse brain using electroporation: Visualization of neuronal migration in the developing cortex. Neuroscience, 2001; 103: 865-72.

Tsai JW, Chen Y, Kriegstein AR, Vallee RB. LIS1 RNA interference blocks neural stem cell division, morphogenesis, and motility at multiple stages. Journal of Cell Biology, 2005; 170: 935-45.

Wang CL, Tang FL, Peng Y, Shen CY, Mei L, Xiong WC. VPS35 regulates developing mouse hippocampal neuronal morphogenesis by promoting retrograde trafficking of BACE1. Biology Open, 2012; 1: 1248-57.

Zhang YQ, Chen FJ, Donehower LA, Scheurer ME, Creighton CJ. A pediatric brain tumor atlas of genes deregulated by somatic genomic rearrangement. Nature Communications, 2021; 12: 17.

11 Conclusion

Since their discovery, the role of HFOs in various pathophysiological processes in epilepsy has been intensely studied. HFOs are now considered a marker of endogenous epileptogenicity, and the HFO analysis was introduced into the presurgical workup to better delineate the resection area (Frauscher et al., 2017). The early HFO occurrence following the precipitating injury was predictive of the future development of epilepsy (Jefferys et al., 2012). Therefore, HFOs are candidate markers of epileptogenesis. The presence of HFO at the seizure onset or changes in HFOs preceding the seizure initiation suggested that understanding the cellular and network mechanisms of HFOs could advance our understanding of the mechanisms responsible for seizure genesis (Jefferys et al., 2012; Jiruska et al., 2017). Although HFO research brought new and interesting observations, it raised also a lot of new questions. Some of these questions we aimed to address in our research. By conducting research into HFO, our results contributed to an improved understanding of the multiple aspects of HFOs, epilepsy brain dynamics, mechanisms of the transition to seizure, and long-term seizure dynamics.

The present work's first notable achievement was identifying HFOs in the highly realistic model of neocortical epilepsy due to FCD. We have brought experimental evidence that the epileptic neocortex can generate HFOs across a wide frequency range, including fast ripples. In the model of FCD, a highly epileptogenic lesion, we experimentally verified that HFOs provide localizing information about the location of the epileptogenic lesion and the seizure onset zone. This is valuable information for presurgical diagnosis. We found that spike-related gamma-ripples are a better marker of epileptogenic lesions than spikes alone. Spike-related fast ripples share the localization properties as well, but we think gamma-ripples are more valuable than fast ripples due to the simple fact that they can be recorded non-invasively from the scalp more easily (Zijlmans et al., 2017; Worrell and Gotman, 2011). The results are in agreement with findings from human studies on focal neocortical epilepsy (Park and Hong, 2019; Noorlag et al., 2022). Cai et al. (2021) demonstrated in a cohort of 25 patients with drug-refractory focal epilepsy who underwent a presurgical evaluation that "HFO-informed spikes" displayed lower localization error compared to conventional spikes, while pathological HFOs were superior to the HFO-informed spikes in predicting the resection-confirmed EZ (Cai et al., 2021). Our results regarding fast ripples are also in accordance with other studies reporting a preference

for fast ripples to appear before the peak of the spike signal, coinciding with the rising phase. This pattern was reported in human and animal models (Van Klink et al., 2016; Guth et al., 2021; Lévesque et al., 2011). This study supports past clinical and experimental observations that HFOs are good biomarkers of tissue epileptogenicity and can be used in the diagnostic workup of epilepsy surgery candidates to identify the most critical components of the epileptic network. We demonstrated another HFO aspect that is highly relevant for HFO utilization in the presurgical examination. We showed that the properties of physiological hippocampal HFOs are not affected by the application of levetiracetam and lacosamide, both common ASM. This is a feature that discriminates physiological HFOs from the pathological HFOs that are affected by anti-seizure medication. This information is relevant for presurgical diagnosis and increases the diagnostic yield of presurgical examination through the improved identification of pathological HFOs.

Do epileptic seizures start suddenly or are they preceded by detectable changes in the dynamics of brain activity? This is one of the key questions and research objectives of epilepsy research. From the patient's perspective, seizures are unpredictable and seemingly random. Observations of the long-term profiles of seizure occurrences have, however, disputed the view of seizures being poissonian, i.e. fully random (Baud et al., 2018; Kudlacek et al., 2021). The field of complex systems dynamics allowed us to explain such observations by providing original insights into the problem of seemingly random phenomena. Studies focusing on the dynamics of brain activity have shown that a seizure can be preceded by detectable changes in brain activity minutes to hours in advance (Litt et al., 2001; Mormann et al., 2003; Lehnertz et al., 2007; Maturana et al., 2020). Unfortunately, these studies focused only on the physical description of changes in electroencephalogram dynamics and did not provide information about the cellular and network mechanisms underlying these changes. We have shown that seizures are preceded by a change in the dynamics of individual neurons, whose activity extracellular recordings by an increase in high-frequency activity. Pre-ictal changes in HFO properties were indicative that the transition to seizure is not a random process but displays features of critical slowing that reflect a progressive loss of resilience of the neural networks to internal or external perturbation and slow recovery from them (Chang et al., 2018). These phenomena are also accompanied by fluctuations in extracellular potassium concentration and corresponding changes in direct current. We also demonstrated that the network's resilience demonstrates the response of the epileptic brain to perturbation. In a high resilience state, perturbations display a stabilizing effect, while perturbations occurring during a low resilience state have a destabilizing effect. This explains why interictal epileptiform can have a dichotomic effect on seizure genesis, i.e., anti-ictal and pro-ictal. Obtained observations are important not only for understanding the ictogenesis but also for the optimization of brain stimulation, which should take into account the current state of neural network resilience. Therefore, diagnostic tools that are able to determine the brain's dynamical state are of high importance for future disease-modifying stimulation therapies.

Although we have brought new discoveries about the role of HFOs and underlying mechanisms in epilepsy, there are still crucial aspects behind HFOs that should be addressed in future HFO research. The origins of epilepsy are diverse, with various pathways leading to its onset. Nonetheless, its defining characteristic—the presence of spontaneous epileptic seizures—remains consistent. Despite the vast differences in the proposed mechanisms driving HFOs, it's entirely within the realm of possibility that all theories of the cellular and network mechanisms of HFOs are valid, all manifesting by the same electrographic hallmark. From the therapeutic perspective, it is questionable whether targeting the HFO mechanisms will be beneficial. Efforts to control brain excitability in a precisely targeted, biocompatible manner either by focusing on the neurons themselves (Magloire et al., 2019; Snowball et al., 2019) or by improving the robustness of the extracellular space to support physiological conditions might prove more beneficial for the patients in the long term.

12 Future prospects

Despite increasing knowledge about HFOs, we still lack evidence about the exact cellular and network mechanisms of HFOs. To elucidate these mechanisms, we believe that more multi-modal and detailed research is needed. At the time of writing, experiments focused on elucidating the cellular mechanisms of HFO emergence are underway. These experiments rely mainly on patch-clamp and the latest state-of-the-art optophysiological techniques of *in vivo* calcium and voltage imaging. We believe that especially newly designed genetically-engineered voltage indicators combined with high-speed intravital microscopy will further advance our understanding of HFOs and provide seminal observations about HFO mechanisms.

High-frequency oscillations have sparked considerable interest in the epilepsy community. However, there is an ongoing debate about the quantification of their utility (Roehri et al., 2018; Frauscher et al., 2017). Although seizure-free patients show higher HFO-contained resection ratios compared to non-seizure-free patients after epilepsy surgery, the effect size is rather small (Frauscher et al., 2017). Large-scale prospective trials are currently ongoing (Jiruska, 2013). Apart from the obvious problem of incomplete EEG coverage and EEG source localization under particular geometric orientations, there are clear limitations in interpreting HFO recordings. We still struggle to reliably differentiate physiological HFOs from pathological ones (Roehri et al., 2018; Jacobs et al., 2018), while the physiological HFOs are not the only confounding factor. The resemblance between HFOs and the intracranial projection of muscle activity poses a unique challenge (Ren et al., 2019). Broadband characteristics and synchronicity between HFOs in different channels can be used to partially address such challenges, but such efforts are in no way standardized or common in clinical practice. Unstandardized recording in the presence of various confounding factors and a lack of personalization in subsequent analysis makes the utilization of HFOs particularly challenging (Worrell et al., 2012; Frauscher et al., 2017; Remakanthakurup Sindhu et al., 2020; Zijlmans et al., 2017; Barkmeier et al., 2012).

A general approach with promising results is to focus on a continuum, rather than on discrete HFO events (Mooij et al., 2020). This is valuable particularly if the data is scarce. Another recent study also supports the notion that the interest in localized HFO events is understandable, but suboptimal. High-frequency background activity (excluding HFOs) carries significant infor-

mation about the location of the EZ, with comparable or superior performance to the HFO rate (Stovall et al., 2021). Furthermore, the combination of HFO rate and signal features computed from high-frequency background activity yielded the best predictive performance. Nevertheless, the use of a detector remains important, but primarily to clean the EEG from artifacts rather than detecting HFOs (Ren et al., 2019). The current most valuable utility of HFOs lies in pre-surgical evaluation, but it is limited by various confounding factors such as the unknown geometric arrangement of the sources, physiological HFOs, and the laws of physics in general. Perhaps next-level multimodal neuroimaging tools could at least increase the informative value of HFOs in pre-surgical evaluation.

Pathological HFOs are inherent to the epileptic brain. They are considered markers of epileptogenicity. Surprisingly, no experimental study has tested whether HFOs really reflect epileptogenicity and what information HFOs provide about the underlying tissue excitability. We should consider the following question. If we had a magical device capable of measuring any epileptic brain variable, what is the single most important variable we should choose to measure? The answer I got from a prominent epileptologist may sound simple, but it captures the essence perfectly — cortical excitability (Baud, 2023). Therefore, future HFO research should primarily address what information HFOs provide about tissue excitability and epileptogenicity.

Bibliography

Ainsworth, M., Lee, S., Cunningham, M. O., Roopun, A. K., Traub, R. D., Kopell, N. J., and Whittington, M. A. (2011). Dual gamma rhythm generators control interlaminar synchrony in auditory cortex. *Journal of Neuroscience*, 31(47):17040–17051.

Alvarado-Rojas, C., Huberfeld, G., Baulac, M., Clemenceau, S., Charpier, S., Miles, R., de la Prida, L. M., and Le Van Quyen, M. (2015). Different mechanisms of ripple-like oscillations in the human epileptic subiculum. *Annals of Neurology*, 77(2):281–290.

Baker, G. A., Jacoby, A., Buck, D., Stalgis, C., and Monnet, D. (1997). Quality of life of people with epilepsy: a european study. *Epilepsia*, 38(3):353–362.

Barkmeier, D. T., Shah, A. K., Flanagan, D., Atkinson, M. D., Agarwal, R., Fuerst, D. R., Jafari-Khouzani, K., and Loeb, J. A. (2012). High inter-reviewer variability of spike detection on intracranial eeg addressed by an automated multi-channel algorithm. *Clinical Neurophysiology*, 123(6):1088–1095.

Baud, M. (2023). Personal communication.

Baud, M. O., Kleen, J. K., Mirro, E. A., Andrechak, J. C., King-Stephens, D., Chang, E. F., and Rao, V. R. (2018). Multi-day rhythms modulate seizure risk in epilepsy. *Nature Communications*, 9(1):88.

Behr, C., Lévesque, M., Ragsdale, D., and Avoli, M. (2015). Lacosamide modulates interictal spiking and high-frequency oscillations in a model of mesial temporal lobe epilepsy. *Epilepsy Research*, 115:8–16.

Blauwblomme, T., Dossi, E., Pellegrino, C., Goubert, E., Iglesias, B. G., Sainte-Rose, C., Rouach, N., Nabbout, R., and Huberfeld, G. (2019). Gamma-aminobutyric acidergic transmission underlies interictal epileptogenicity in pediatric focal cortical dysplasia. *Annals of Neurology*, 85(2):204–217.

Bragin, A., Benassi, S. K., Kheiri, F., and Engel Jr, J. (2011). Further evidence that pathologic high-frequency oscillations are bursts of population spikes derived from recordings of identified cells in dentate gyrus. *Epilepsia*, 52(1):45–52.

Bragin, A., Engel Jr, J., Wilson, C. L., Fried, I., and Buzsáki, G. (1999a). High-frequency oscillations in human brain. *Hippocampus*, 9(2):137–142.

Bragin, A., Engel Jr, J., Wilson, C. L., Fried, I., and Mathern, G. W. (1999b). Hippocampal and entorhinal cortex high-frequency oscillations (100–500 hz) in human epileptic brain and in kainic acid-treated rats with chronic seizures. *Epilepsia*, 40(2):127–137.

Bragin, A., Wilson, C. L., Almajano, J., Mody, I., and Engel Jr, J. (2004). High-frequency oscillations after status epilepticus: epileptogenesis and seizure genesis. *Epilepsia*, 45(9):1017–1023.

Bragin, A., Wilson, C. L., and Engel Jr, J. (2003). Spatial stability over time of brain areas generating fast ripples in the epileptic rat. *Epilepsia*, 44(9):1233–1237.

Brázdil, M., Pail, M., Halámek, J., Plešinger, F., Cimbálník, J., Roman, R., Klimeš, P., Daniel, P., Chrastina, J., Brichtová, E., et al. (2017). Very high-frequency oscillations: novel biomarkers of the epileptogenic zone. *Annals of Neurology*, 82(2):299–310.

Breton, V. L., Aquilino, M. S., Repudi, S., Saleem, A., Mylvaganam, S., Abu-Swai, S., Bardakjian, B. L., Aqeilan, R. I., and Carlen, P. L. (2021). Altered neocortical oscillations and cellular excitability in an in vitro wwox knockout mouse model of epileptic encephalopathy. *Neurobiology of Disease*, 160:105529.

Buzsáki, G. (1989). Two-stage model of memory trace formation: a role for "noisy" brain states. *Neuroscience*, 31(3):551–570.

Buzsáki, G. (2015). Hippocampal sharp wave-ripple: A cognitive biomarker for episodic memory and planning. *Hippocampus*, 25(10):1073–1188.

Buzsáki, G. and Chrobak, J. J. (1995). Temporal structure in spatially organized neuronal ensembles: a role for interneuronal networks. *Current Opinion in Neurobiology*, 5(4):504–510.

Buzsáki, G., Vanderwolf, C. H., et al. (1983). Cellular bases of hippocampal eeg in the behaving rat. *Brain Research Reviews*, 6(2):139–171.

Cai, Z., Sohrabpour, A., Jiang, H., Ye, S., Joseph, B., Brinkmann, B. H., Worrell, G. A., and He, B. (2021). Noninvasive high-frequency oscillations riding spikes delineates epileptogenic sources. *Proceedings of the National Academy of Sciences*, 118(17):e2011130118.

Cammarota, M., Losi, G., Chiavegato, A., Zonta, M., and Carmignoto, G. (2013). Fast spiking interneuron control of seizure propagation in a cortical slice model of focal epilepsy. *The Journal of Physiology*, 591(4):807–822.

Cannon, J., McCarthy, M. M., Lee, S., Lee, J., Börgers, C., Whittington, M. A., and Kopell, N. (2014). Neurosystems: brain rhythms and cognitive processing. *European Journal of Neuroscience*, 39(5):705–719.

Cepeda, C., Chen, J. Y., Wu, J. Y., Fisher, R. S., Vinters, H. V., Mathern, G. W., and Levine, M. S. (2014). Pacemaker gaba synaptic activity may contribute to network synchronization in pediatric cortical dysplasia. *Neurobiology of Disease*, 62:208–217.

Cepeda, C., Levinson, S., Nariai, H., Yazon, V.-W., Tran, C., Barry, J., Oikonomou, K. D., Vinters, H. V., Fallah, A., Mathern, G. W., et al. (2020). Pathological high frequency oscillations associate with increased gaba synaptic activity in pediatric epilepsy surgery patients. *Neurobiology of Disease*, 134:104618.

Chang, W.-C., Kudlacek, J., Hlinka, J., Chvojka, J., Hadrava, M., Kumpost, V., Powell, A. D., Janca, R., Maturana, M. I., Karoly, P. J., et al. (2018). Loss of neuronal network resilience precedes seizures and determines the ictogenic nature of interictal synaptic perturbations. *Nature Neuroscience*, 21(12):1742–1752.

Cheng, L., Xing, Y., Zhang, H., Liu, R., Lai, H., Piao, Y., Wang, W., Yan, X., Li, X., Wang, J., et al. (2022). Mechanistic analysis of micro-neurocircuits underlying the epileptogenic zone in focal cortical dysplasia patients. *Cerebral Cortex*, 32(10):2216–2230.

Chvojka, J., Kudlacek, J., Chang, W.-C., Novak, O., Tomaska, F., Otahal, J., Jefferys, J. G., and Jiruska, P. (2021). The role of interictal discharges in ictogenesis—a dynamical perspective. *Epilepsy & Behavior*, 121:106591.

Chvojka, J., Kudlacek, J., Liska, K., Pant, A., Jefferys, J., and Jiruska, P. (2024a). Dissociation between the epileptogenic lesion and primary seizure onset zone in the tetanus toxin model of temporal lobe epilepsy. *Physiological Research*.

Chvojka, J., Prochazkova, N., Rehorova, M., Kudlacek, J., Kylarova, S., Kralikova, M., Buran, P., Weissova, R., Balastik, M., Jefferys, J. G., et al. (2024b). Mouse model of focal cortical dysplasia type ii generates a wide spectrum of high-frequency activities. *Neurobiology of Disease*, 190:106383.

Cserpan, D., Gennari, A., Gaito, L., Lo Biundo, S. P., Tuura, R., Sarnthein, J., and Ramantani, G. (2022). Scalp hfo rates are higher for larger lesions. *Epilepsia Open*, 7(3):496–503.

Curot, J., Barbeau, E., Despouy, E., Denuelle, M., Sol, J. C., Lotterie, J.-A., Valton, L., and Peyrache, A. (2023). Local neuronal excitation and global inhibition during epileptic fast ripples in humans. *Brain*, 146(2):561–575.

Dallmer-Zerbe, I., Jajcay, N., Chvojka, J., Janca, R., Jezdik, P., Krsek, P., Marusic, P., Jiruska, P., and Hlinka, J. (2023). Computational modeling allows unsupervised classification of epileptic brain states across species. *Scientific Reports*, 13(1):13436.

Draguhn, A., Traub, R., Schmitz, D., and Jefferys, J. (1998). Electrical coupling underlies high-frequency oscillations in the hippocampus in vitro. *Nature*, 394(6689):189–192.

Dzhala, V. I. and Staley, K. J. (2004). Mechanisms of fast ripples in the hippocampus. *Journal of Neuroscience*, 24(40):8896–8906.

Engel, A. K., Fries, P., and Singer, W. (2001). Dynamic predictions: oscillations and synchrony in top–down processing. *Nature Reviews Neuroscience*, 2(10):704–716.

Engel, J., Pedley, T. A., and Aicardi, J. (2008). *Epilepsy: a comprehensive textbook*, volume 3. Lipsynaptic noisecott Williams & Wilkins.

Ferecskó, A. S., Jiruska, P., Foss, L., Powell, A. D., Chang, W.-C., Sik, A., and Jefferys, J. G. (2015). Structural and functional substrates of tetanus toxin in an animal model of temporal lobe epilepsy. *Brain Structure and Function*, 220:1013–1029.

Fink, C. G., Gliske, S., Catoni, N., and Stacey, W. C. (2015). Network mechanisms generating abnormal and normal hippocampal high-frequency oscillations: a computational analysis. *Eneuro*, 2(3).

Fisher, R. S., Cross, J. H., French, J. A., Higurashi, N., Hirsch, E., Jansen, F. E., Lagae, L., Moshé, S. L., Peltola, J., Roulet Perez, E., et al. (2017). Operational classification of seizure types by the international league against epilepsy: Position paper of the ilae commission for classification and terminology. *Epilepsia*, 58(4):522–530.

Foffani, G., Uzcategui, Y. G., Gal, B., and de la Prida, L. M. (2007). Reduced spike-timing reliability correlates with the emergence of fast ripples in the rat epileptic hippocampus. *Neuron*, 55(6):930–941.

Frauscher, B., Bartolomei, F., Kobayashi, K., Cimbalnik, J., van 't Klooster, M., Rampp, S., Otsubo, H., Höller, Y., Wu, J., Asano, E., Engel, J., Kahane, P., Jacobs, J., and Gotman, J. (2017). High-frequency oscillations: The state of clinical research. *Epilepsia*, 58(8):1316–1329.

Frauscher, B., von Ellenrieder, N., Zelmann, R., Rogers, C., Nguyen, D. K., Kahane, P., Dubeau, F., and Gotman, J. (2018). High-frequency oscillations in the normal human brain. *Annals of Neurology*, 84(3):374–385.

Fries, P. (2005). A mechanism for cognitive dynamics: neuronal communication through neuronal coherence. *Trends in Cognitive Sciences*, 9(10):474–480.

Fries, P. (2015). Rhythms for cognition: communication through coherence. *Neuron*, 88(1):220–235.

Gliske, S. V., Stacey, W. C., Lim, E., Holman, K. A., and Fink, C. G. (2017). Emergence of narrowband high frequency oscillations from asynchronous, uncoupled neural firing. *International Journal of Neural Systems*, 27(01):1650049.

Gnatkovsky, V., Librizzi, L., Trombin, F., and De Curtis, M. (2008). Fast activity at seizure onset is mediated by inhibitory circuits in the entorhinal cortex in vitro. *Annals of Neurology*, 64(6):674–686.

Grenier, F., Timofeev, I., and Steriade, M. (2001). Focal synchronization of ripples (80–200 hz) in neocortex and their neuronal correlates. *Journal of Neurophysiology*, 86(4):1884–1898.

Grenier, F., Timofeev, I., and Steriade, M. (2003). Neocortical very fast oscillations (ripples, 80–200 hz) during seizures: intracellular correlates. *Journal of Neurophysiology*, 89(2):841–852.

Grewe, B. F., Langer, D., Kasper, H., Kampa, B. M., and Helmchen, F. (2010). High-speed in vivo calcium imaging reveals neuronal network activity with near-millisecond precision. *Nature Methods*, 7(5):399–405.

Guth, T. A., Kunz, L., Brandt, A., Dümpelmann, M., Klotz, K. A., Reinacher, P. C., Schulze-Bonhage, A., Jacobs, J., and Schönberger, J. (2021). Interictal spikes with and without high-frequency oscillation have different single-neuron correlates. *Brain*, 144(10):3078–3088.

Höller, Y., Kutil, R., Klaffenböck, L., Thomschewski, A., Höller, P. M., Bathke, A. C., Jacobs, J., Taylor, A. C., Nardone, R., and Trinka, E. (2015). High-frequency oscillations in epilepsy and surgical outcome. a meta-analysis. *Frontiers in Human Neuroscience*, 9:574.

Hsieh, L. S., Wen, J. H., Claycomb, K., Huang, Y., Harrsch, F. A., Naegele, J. R., Hyder, F., Buchanan, G. F., and Bordey, A. (2016). Convulsive seizures from experimental focal cortical dysplasia occur independently of cell misplacement. *Nature Communications*, 7(1):11753.

Ibarz, J. M., Foffani, G., Cid, E., Inostroza, M., and de la Prida, L. M. (2010). Emergent dynamics of fast ripples in the epileptic hippocampus. *Journal of Neuroscience*, 30(48):16249–16261.

Isaacson, J. S. and Scanziani, M. (2011). How inhibition shapes cortical activity. *Neuron*, 72(2):231–243.

Jacobs, J., LeVan, P., Châtillon, C.-É., Olivier, A., Dubeau, F., and Gotman, J. (2009). High frequency oscillations in intracranial eegs mark epileptogenicity rather than lesion type. *Brain*, 132(4):1022–1037.

Jacobs, J., Wu, J. Y., Perucca, P., Zelmann, R., Mader, M., Dubeau, F., Mathern, G. W., Schulze-Bonhage, A., and Gotman, J. (2018). Removing high-frequency oscillations: A prospective multicenter study on seizure outcome. *Neurology*, 91(11):e1040–e1052.

Jefferys, J. G., De La Prida, L. M., Wendling, F., Bragin, A., Avoli, M., Timofeev, I., and da Silva, F. H. L. (2012). Mechanisms of physiological and epileptic hfo generation. *Progress in Neurobiology*, 98(3):250–264.

Jiruska, P. (2013). *The Significance of High-Frequency Oscillations in the Pathophysiology of Epilepsy and Their Clinical Application*. Habilitation thesis.

Jiruska, P., Alvarado-Rojas, C., Schevon, C. A., Staba, R., Stacey, W., Wendling, F., and Avoli, M. (2017). Update on the mechanisms and roles of high-frequency oscillations in seizures and epileptic disorders. *Epilepsia*, 58(8):1330–1339.

Jiruska, P., Csicsvari, J., Powell, A. D., Fox, J. E., Chang, W.-C., Vreugdenhil, M., Li, X., Palus, M., Bujan, A. F., Dearden, R. W., et al. (2010). High-frequency network activity, global increase in neuronal activity, and synchrony expansion precede epileptic seizures in vitro. *Journal of Neuroscience*, 30(16):5690–5701.

Kanazawa, K., Matsumoto, R., Imamura, H., Matsuhashi, M., Kikuchi, T., Kunieda, T., Mikuni, N., Miyamoto, S., Takahashi, R., and Ikeda, A. (2015). Intracranially recorded ictal direct current shifts may precede high frequency oscillations in human epilepsy. *Clinical Neurophysiology*, 126(1):47–59.

Kassai, H., Sugaya, Y., Noda, S., Nakao, K., Maeda, T., Kano, M., and Aiba, A. (2014). Selective activation of mtorc1 signaling recapitulates microcephaly, tuberous sclerosis, and neurodegenerative diseases. *Cell Reports*, 7(5):1626–1639.

Kucewicz, M. T., Cimbalnik, J., Matsumoto, J. Y., Brinkmann, B. H., Bower, M. R., Vasoli, V., Sulc, V., Meyer, F., Marsh, W., Stead, S., et al. (2014). High frequency oscillations are associated with cognitive processing in human recognition memory. *Brain*, 137(8):2231–2244.

Kudlacek, J., Chvojka, J., Kumpost, V., Hermanovska, B., Posusta, A., Jefferys, J. G., Maturana, M. I., Novak, O., Cook, M. J., Otahal, J., et al. (2021). Long-term seizure dynamics are determined by the nature of seizures and the mutual interactions between them. *Neurobiology of Disease*, 154:105347.

Kudlacek, J., Chvojka, J., Posusta, A., Kovacova, L., Hong, S. B., Weiss, S., Volna, K., Marusic, P., Otahal, J., and Jiruska, P. (2017). Lacosamide and levetiracetam have no effect on sharp-wave ripple rate. *Frontiers in Neurology*, 8:687.

Lehnertz, K., Mormann, F., Osterhage, H., Müller, A., Prusseit, J., Chernihovskyi, A., Staniek, M., Krug, D., Bialonski, S., and Elger, C. E. (2007). State-of-the-art of seizure prediction. *Journal of Clinical Neurophysiology*, 24(2):147–153.

Lévesque, M., Bortel, A., Gotman, J., and Avoli, M. (2011). High-frequency (80–500 hz) oscillations and epileptogenesis in temporal lobe epilepsy. *Neurobiology of disease*, 42(3):231–241.

Lévesque, M., Salami, P., Gotman, J., and Avoli, M. (2012). Two seizure-onset types reveal specific patterns of high-frequency oscillations in a model of temporal lobe epilepsy. *Journal of Neuroscience*, 32(38):13264–13272.

Li, L., Bragin, A., Staba, R., and Engel Jr, J. (2019). Unit firing and oscillations at seizure onset in epileptic rodents. *Neurobiology of Disease*, 127:382–389.

Lim, J. S., Kim, W.-i., Kang, H.-C., Kim, S. H., Park, A. H., Park, E. K., Cho, Y.-W., Kim, S., Kim, H. M., Kim, J. A., et al. (2015). Brain somatic mutations in mtor cause focal cortical dysplasia type ii leading to intractable epilepsy. *Nature Medicine*, 21(4):395–400.

Litt, B., Esteller, R., Echauz, J., D'Alessandro, M., Shor, R., Henry, T., Pennell, P., Epstein, C., Bakay, R., Dichter, M., et al. (2001). Epileptic seizures may begin hours in advance of clinical onset: a report of five patients. *Neuron*, 30(1):51–64.

Lopes da Silva, F. (2011). Computer-assisted eeg pattern recognition and diagnostic systems. *Niedermeyer's Electroencephalography: Basic Principles, Clinical Applications, and Related Fields, ed*, 6:1203–1225.

Löscher, W. (2020). The holy grail of epilepsy prevention: Preclinical approaches to antiepileptogenic treatments. *Neuropharmacology*, 167:107605.

Louis, E. D., Williamson, P. D., and Darcey, T. M. (1990). Chronic focal epilepsy induced by microinjection of tetanus toxin into the cat motor cortex. *Electroencephalography and Clinical Neurophysiology*, 75(6):548–557.

Magloire, V., Cornford, J., Lieb, A., Kullmann, D., and Pavlov, I. (2019). Kcc2 overexpression prevents the paradoxical seizure-promoting action of somatic inhibition. *Nature Communications*, 10(1225).

Magri, L., Cambiaghi, M., Cominelli, M., Alfaro-Cervello, C., Cursi, M., Pala, M., Bulfone, A., Garcìa-Verdugo, J. M., Leocani, L., Minicucci, F., et al. (2011). Sustained activation of mtor pathway in embryonic neural stem cells leads to development of tuberous sclerosis complex-associated lesions. *Cell - Stem Cell*, 9(5):447–462.

Marusic, P. (2018). Eeg misinterpretation in epileptology (oral presentation). In *Dolanské Dny*, Průhonice.

Marusic, P. (2023). Neuroscience. In *Scientific Conference under the Second Faculty of Medicine, Charles University*, Prague.

Maturana, M. I., Meisel, C., Dell, K., Karoly, P. J., D'Souza, W., Grayden, D. B., Burkitt, A. N., Jiruska, P., Kudlacek, J., Hlinka, J., et al. (2020). Critical slowing down as a biomarker for seizure susceptibility. *Nature Communications*, 11(1):2172.

Meikle, L., Talos, D. M., Onda, H., Pollizzi, K., Rotenberg, A., Sahin, M., Jensen, F. E., and Kwiatkowski, D. J. (2007). A mouse model of tuberous sclerosis: neuronal loss of tsc1 causes dysplastic and ectopic neurons, reduced myelination, seizure activity, and limited survival. *Journal of Neuroscience*, 27(21):5546–5558.

Mooij, A. H., Frauscher, B., Gotman, J., and Huiskamp, G. J. (2020). A skew-based method for identifying intracranial eeg channels with epileptic activity without detecting spikes, ripples, or fast ripples. *Clinical Neurophysiology*, 131(1):183–192.

Mormann, F., Kreuz, T., Andrzejak, R. G., David, P., Lehnertz, K., and Elger, C. E. (2003). Epileptic seizures are preceded by a decrease in synchronization. *Epilepsy Research*, 53(3):173–185.

Morris, G., Jiruska, P., and Powell, A. D. (2016). A new approach of modified submerged patch clamp recording reveals interneuronal dynamics during epileptiform oscillations. *Frontiers in Neuroscience*, 10:223358.

Mula, M. and Cock, H. (2015). More than seizures: improving the lives of people with refractory epilepsy. *European journal of neurology*, 22(1):24–30.

Naggar, I., Stewart, M., and Orman, R. (2020). High frequency oscillations in rat hippocampal slices: origin, frequency characteristics, and spread. *Frontiers in Neurology*, 11:528805.

Noorlag, L., van Klink, N. E., Kobayashi, K., Gotman, J., Braun, K. P., and Zijlmans, M. (2022). High-frequency oscillations in scalp eeg: A systematic review of methodological choices and clinical findings. *Clinical Neurophysiology*, 137:46–58.

O'Neill, J., Senior, T., and Csicsvari, J. (2006). Place-selective firing of ca1 pyramidal cells during sharp wave/ripple network patterns in exploratory behavior. *Neuron*, 49(1):143–155.

O'Neill, J., Pleydell-Bouverie, B., Dupret, D., and Csicsvari, J. (2010). Play it again: reactivation of waking experience and memory. *Trends in Neurosciences*, 33(5):220–229.

Park, C. J. and Hong, S. B. (2019). High frequency oscillations in epilepsy: detection methods and considerations in clinical application. *Journal of Epilepsy Research*, 9(1):1.

Perucca, E., Yasothan, U., Clincke, G., and Kirkpatrick, P. (2008). Lacosamide. *Nature Reviews Drug Discovery*, 7(12):973–975.

143

Perucca, P., Bahlo, M., and Berkovic, S. F. (2020). The genetics of epilepsy. *Annual Review of Genomics and Human Genetics*, 21:205–230.

Prochazkova, N., Nguyenova, M., Rehorova, M., Kudlacek, J., Chvojka, J., Ziak, J., Balastik, M., Otahal, J., Jiruska, P., and Novak, O. (2024). Neuroporator: An open-source, current-limited electroporator for safe in utero gene transfer. *Journal of Neuroscience Methods*.

Remakanthakurup Sindhu, K., Staba, R., and Lopour, B. A. (2020). Trends in the use of automated algorithms for the detection of high-frequency oscillations associated with human epilepsy. *Epilepsia*, 61(8):1553–1569.

Ren, S., Gliske, S. V., Brang, D., and Stacey, W. C. (2019). Redaction of false high frequency oscillations due to muscle artifact improves specificity to epileptic tissue. *Clinical Neurophysiology*, 130(6):976–985.

Roehri, N., Pizzo, F., Lagarde, S., Lambert, I., Nica, A., McGonigal, A., Giusiano, B., Bartolomei, F., and Bénar, C.-G. (2018). High-frequency oscillations are not better biomarkers of epileptogenic tissues than spikes. *Annals of Neurology*, 83(1):84–97.

Santana-Gomez, C. E., Engel Jr, J., and Staba, R. (2022). Drug-resistant epilepsy and the hypothesis of intrinsic severity: What about the high-frequency oscillations? *Epilepsia Open*, 7:S59–S67.

Scharfman, H. E. (2007). The neurobiology of epilepsy. *Current neurology and neuroscience reports*, 7(4):348–354.

Schevon, C. A., Trevelyan, A., Schroeder, C., Goodman, R., McKhann Jr, G., and Emerson, R. (2009). Spatial characterization of interictal high frequency oscillations in epileptic neocortex. *Brain*, 132(11):3047–3059.

Sheybani, L., van Mierlo, P., Birot, G., Michel, C. M., and Quairiaux, C. (2019). Large-scale 3–5 hz oscillation constrains the expression of neocortical fast ripples in a mouse model of mesial temporal lobe epilepsy. *Eneuro*, 6(1).

Shiri, Z., Manseau, F., Lévesque, M., Williams, S., and Avoli, M. (2016). Activation of specific neuronal networks leads to different seizure onset types. *Annals of Neurology*, 79(3):354–365.

Sirota, A. and Buzsáki, G. (2005). Interaction between neocortical and hippocampal networks via slow oscillations. *Thalamus & Related Systems*, 3(4):245–259.

Sirota, A., Csicsvari, J., Buhl, D., and Buzsáki, G. (2003). Communication between neocortex and hippocampus during sleep in rodents. *Proceedings of the National Academy of Sciences*, 100(4):2065–2069.

Sisodiya, S. (2004). Surgery for focal cortical dysplasia. *Brain*, 127(11):2383–2384.

Snowball, A., Chabrol, E., Wykes, R. C., Shekh-Ahmad, T., Cornford, J. H., Lieb, A., Hughes, M. P., Massaro, G., Rahim, A. A., Hashemi, K. S., et al. (2019). Epilepsy gene therapy using an engineered potassium channel. *Journal of Neuroscience*, 39(16):3159–3169.

Sohal, V. S., Zhang, F., Yizhar, O., and Deisseroth, K. (2009). Parvalbumin neurons and gamma rhythms enhance cortical circuit performance. *Nature*, 459(7247):698–702.

Staba, R. J., Frighetto, L., Behnke, E. J., Mathern, G. W., Fields, T., Bragin, A., Ogren, J., Fried, I., Wilson, C. L., and Engel Jr, J. (2007). Increased fast ripple to ripple ratios correlate with reduced hippocampal volumes and neuron loss in temporal lobe epilepsy patients. *Epilepsia*, 48(11):2130–2138.

Staba, R. J., Wilson, C. L., Bragin, A., Fried, I., and Engel Jr, J. (2002). Quantitative analysis of high-frequency oscillations (80–500 hz) recorded in human epileptic hippocampus and entorhinal cortex. *Journal of Neurophysiology*, 88(4):1743–1752.

Stacey, W. C., Krieger, A., and Litt, B. (2011). Network recruitment to coherent oscillations in a hippocampal computer model. *Journal of Neurophysiology*, 105(4):1464–1481.

Stacey, W. C., Lazarewicz, M. T., and Litt, B. (2009). Synaptic noise and physiological coupling generate high-frequency oscillations in a hippocampal computational model. *Journal of Neurophysiology*, 102(4):2342–2357.

Steriade, M., Nunez, A., and Amzica, F. (1993). Intracellular analysis of relations between the slow (< 1 hz) neocortical oscillation and other sleep rhythms of the electroencephalogram. *Journal of Neuroscience*, 13(8):3266–3283.

Stovall, T., Hunt, B., Glynn, S., Stacey, W. C., and Gliske, S. V. (2021). Interictal high frequency background activity as a biomarker of epileptogenic tissue. *Brain Communications*, 3(3):fcab188.

Strzelczyk, A., Reese, J. P., Dodel, R., and Hamer, H. M. (2008). Cost of epilepsy: a systematic review. *Pharmacoeconomics*, 26:463–476.

Tremblay, R., Lee, S., and Rudy, B. (2016). Gabaergic interneurons in the neocortex: from cellular properties to circuits. *Neuron*, 91(2):260–292.

Trinka, E., Cock, H., Hesdorffer, D., Rossetti, A. O., Scheffer, I. E., Shinnar, S., Shorvon, S., and Lowenstein, D. H. (2015). A definition and classification of status epilepticus–report of the ilae task force on classification of status epilepticus. *Epilepsia*, 56(10):1515–1523.

Uhlhaas, P. J. and Singer, W. (2006). Neural synchrony in brain disorders: relevance for cognitive dysfunctions and pathophysiology. *neuron*, 52(1):155–168.

Uhlmann, E. J., Wong, M., Baldwin, R. L., Bajenaru, M. L., Onda, H., Kwiatkowski, D. J., Yamada, K., and Gutmann, D. H. (2002). Astrocyte-specific tsc1 conditional knockout mice exhibit abnormal neuronal organization and seizures. *Annals of Neurology*, 52(3):285–296.

Van Klink, N., Frauscher, B., Zijlmans, M., and Gotman, J. (2016). Relationships between interictal epileptic spikes and ripples in surface eeg. *Clinical Neurophysiology*, 127(1):143–149.

Wang, X.-J. (2010). Neurophysiological and computational principles of cortical rhythms in cognition. *Physiological Reviews*, 90(3):1195–1268.

Weiss, S. A., Fried, I., Engel Jr, J., Sperling, M. R., Wong, R. K., Nir, Y., and Staba, R. J. (2023). Fast ripples reflect increased excitability that primes epileptiform spikes. *Brain Communications*, 5(5):fcad242.

Weiss, S. A., Lemesiou, A., Connors, R., Banks, G. P., McKhann, G. M., Goodman, R. R., Zhao, B., Filippi, C. G., Nowell, M., Rodionov, R., et al. (2015). Seizure localization using ictal phase-locked high gamma: A retrospective surgical outcome study. *Neurology*, 84(23):2320–2328.

Weiss, S. A., Staba, R. J., Sharan, A., Wu, C., Rubinstein, D., Das, S., Waldman, Z., Orosz, I., Worrell, G., Engel Jr, J., et al. (2021). Accuracy of high-frequency oscillations recorded intraoperatively for classification of epileptogenic regions. *Scientific Reports*, 11(1):21388.

White, A. R., Tiwari, D., MacLeod, M. C., Danzer, S. C., and Gross, C. (2020). Pi3k isoform-selective inhibition in neuron-specific pten-deficient mice rescues molecular defects and reduces epilepsy-associated phenotypes. *Neurobiology of Disease*, 144:105026.

Williams, A. J. and Sun, Q.-Q. (2019). Cortical layer and spectrotemporal architecture of epileptiform activity in vivo in a mouse model of focal cortical malformation. *Frontiers in Neural Circuits*, 13:2.

Worrell, G. and Gotman, J. (2011). High-frequency oscillations and other electrophysiological biomarkers of epilepsy: clinical studies. *Biomarkers in medicine*, 5(5):557–566.

Worrell, G. A., Jerbi, K., Kobayashi, K., Lina, J.-M., Zelmann, R., and Le Van Quyen, M. (2012). Recording and analysis techniques for high-frequency oscillations. *Progress in Neurobiology*, 98(3):265–278.

Wykes, R. C., Heeroma, J. H., Mantoan, L., Zheng, K., MacDonald, D. C., Deisseroth, K., Hashemi, K. S., Walker, M. C., Schorge, S., and Kullmann, D. M. (2012). Optogenetic and potassium channel gene therapy in a rodent model of focal neocortical epilepsy. *Science Translational Medicine*, 4(161):161ra152–161ra152.

Yang, W., Williams, A., and Sun, Q.-Q. (2020). Circuit mechanisms underlying chronic epilepsy in a mouse model of focal cortical malformation. *bioRxiv*, pages 2020–04.

Ylinen, A., Bragin, A., Nádasdy, Z., Jandó, G., Szabo, I., Sik, A., and Buzsáki, G. (1995). Sharp wave-associated high-frequency oscillation (200 hz) in the intact hippocampus: network and intracellular mechanisms. *Journal of Neuroscience*, 15(1):30–46.

Zijlmans, M., Jacobs, J., Zelmann, R., Dubeau, F., and Gotman, J. (2009). High-frequency oscillations mirror disease activity in patients with epilepsy. *Neurology*, 72(11):979–986.

Zijlmans, M., Jiruska, P., Zelmann, R., Leijten, F. S., Jefferys, J. G., and Gotman, J. (2012). High-frequency oscillations as a new biomarker in epilepsy. *Annals of Neurology*, 71(2):169–178.

Zijlmans, M., Worrell, G. A., Dümpelmann, M., Stieglitz, T., Barborica, A., Heers, M., Ikeda, A., Usui, N., and Le Van Quyen, M. (2017). How to record high-frequency oscillations in epilepsy: a practical guideline. *Epilepsia*, 58(8):1305–1315.

Zijlmans, M., Zweiphenning, W., and van Klink, N. (2019). Changing concepts in presurgical assessment for epilepsy surgery. *Nature Reviews Neurology*, 15(10):594–606.

13 List of publications

Chvojka, J., Prochazkova, N., Rehorova, M., Kudlacek, J., Kylarova, S., Kralikova, M., Buran, P., Weissova, R., Balastik, M., Jefferys, J.GR., Novak, O., Jiruska, P. (2024). Mouse model of focal cortical dysplasia type II generates a wide spectrum of high-frequency activities. *Neurobiology of Disease*. Jan;190:106383.

Kudlacek, J., **Chvojka, J.**, Posusta, A., Kovacova, L., Hong, S.B., Weiss, S., Volna, K., Marusic, P., Otahal, J., Jiruska, P. (2017). Lacosamide and Levetiracetam Have No Effect on Sharp-Wave Ripple Rate. *Frontiers Neurology*. Dec;21;8:687.

Chang, W.C., Kudlacek, J., Hlinka, J., **Chvojka, J.**, Hadrava, M., Kumpost, V., Powell, A.D., Janca, R., Maturana, M.I., Karoly, P.J., Freestone, D.R., Cook, M.J., Palus, M., Otahal, J, Jefferys, J.GR., Jiruska, P. (2018). Loss of neuronal network resilience precedes seizures and determines the ictogenic nature of interictal synaptic perturbations. *Nature Neuroscience*. Dec;21(12):1742-1752.

Chvojka, J., Kudlacek, J., Chang, W.C., Novak, O., Tomaska, F., Otahal, J., Jefferys, J.GR., Jiruska, P. (2021). The role of interictal discharges in ictogenesis - A dynamical perspective. *Epilepsy and Behaviour*, Aug;121(Pt B):106591.

Dallmer-Zerbe, I., Jajcay, N., **Chvojka, J.**, Janca, R., Jezdik, P., Krsek, P., ..., Hlinka, J. (2023). Computational modeling allows unsupervised classification of epileptic brain states across species. *Scientific Reports*, 13(1), 13436.

Kudlacek, J., **Chvojka, J.**, Kumpost, V., Hermanovska, B., Posusta, A., Jefferys, J.GR., ..., Jiruska, P. (2021). Long-term seizure dynamics are determined by the nature of seizures and the mutual interactions between them. *Neurobiology of Disease*, 154, 105347.

Chvojka, J., Kudlacek, J., Liška, K., Pant, A., Jefferys, J.GR., Jiruška, P. (2024). Dissociation between the epileptogenic lesion and primary seizure onset zone in the tetanus toxin model of

temporal lobe epilepsy. *Physiological Research*. (Accepted, in press)

Procházková, N., Nguyenová, M.T., Řehořová, M., Kudláček, J., **Chvojka, J.**, Ziak, J., Balaštík, M., Otáhal, J., Jiruška, P., Novák, O. (2024). NeuroPorator: An open-source, current-limited electroporator for safe *in utero* gene transfer. *Journal of Neuroscience Methods*. (Accepted, in press)